WELD QUALITY MONITORING AND DEFECT IDENTIFICATION IN FRICTION STIR WELDING PROCESS

Thesis submitted to

Indian Institute of Technology Guwahati

for the award of the degree

of

Doctor of Philosophy

by

Bipul Das

(126103001)

Under the supervision of

Dr. Sukhomay Pal

&

Dr. Swarup Bag

DEPARTMENT OF MECHANICAL ENGINEERING

INDIAN INSTITUTE OF TECHNOLOGY GUWAHATI

GUWAHATI 781039, ASSAM, INDIA

This thesis is dedicated to

My loving parents and wife

Department of Mechanical Engineering
Indian Institute of Technology Guwahati
Guwahati – 781039, Assam, India

CERTIFICATE

It is certified that the work contained in the thesis entitled "**WELD QUALITY MONITORING AND DEFECT IDENTIFICATION IN FRICTION STIR WELDING PROCESS**" submitted by **Mr. Bipul Das (Reg. No. 126103001)** to the Indian Institute of Technology Guwahati for the award of the degree of Doctor of Philosophy has been carried out under our supervision in the Department of Mechanical Engineering, Indian Institute of Technology Guwahati. The work has not been submitted elsewhere for the award of any other degree or diploma.

The thesis in our opinion, has reached the standard fulfilling the requirements for the award of degree of Doctor of Philosophy in accordance with the regulations of the Institute.

Dr. Sukhomay Pal
Associate Professor
Department of Mechanical Engineering
Indian Institute of Technology Guwahati
Guwahati – 781039
Assam, India

Dr. Swarup Bag
Associate Professor
Department of Mechanical Engineering
Indian Institute of Technology Guwahati
Guwahati – 781039
Assam, India

DECLARATION

I declare that,

a. The work contained in this thesis is original and has been carried out by me under the supervision of my supervisors.
b. The work has not been submitted to any other institute for any degree or diploma.
c. I have followed the guidelines provided by the institute in preparing the thesis
d. I have confirmed to the norms and guidelines given in the ethical code of conduct of the institute.
e. Whenever, I have used materials (data, theoretical analysis, figures) from the other relevant sources due credit has been given to them with proper citation in the text of the thesis and details in the references. Further, I have taken permissions from the competent authorities and copyright owners of the respective sources for the reproduction in the thesis.

Place: IIT Guwahati
Date: **Signature of the student**

ACKNOWLEDGEMENT

I start this by thanking almighty for keeping me healthy and giving patience throughout my research work. I wish to express my deep gratitude to all those who have helped me in various ways directly or indirectly during the tenure of my research work at Indian Institute of Technology Guwahati. In each step of the work was supported by many people and each one have played appreciable role. I am grateful to all of them and would like to express sincere thankfulness from the core of my heart.

I express my sincere gratitude and appreciation to my supervisors **Dr. Sukhomay Pal**, Associate Professor, Department of Mechanical Engineering, Indian Institute of Technology Guwahati and **Dr. Swarup Bag**, Associate Professor, Department of Mechanical Engineering, Indian Institute of Technology Guwahati for their valuable suggestions, expert guidance, patience, encouragement and support in every form offered to me during my research tenure at Indian Institute of Technology Guwahati. Their suggestions not only helped me to excel in the research work but also helped me in grooming my personal and profession life. I feel privileged for having such personalities as my supervisors during the research work at Indian Institute of Technology Guwahati. I pray to almighty for their good health and success and wish they reach greater heights with time.

I would like to express my sincere gratitude towards the doctoral committee formed at Department of Mechanical Engineering, Indian Institute of Technology Guwahati for monitoring the research work periodically. I would like to express my sincere thanks to the Chairman of the committee **Prof. S. K. Dwivedy**, Department of Mechanical Engineering for his sincere comments, discussion and suggestions that helped me to polish my research work. I would also like to express sincere thanks to the doctoral committee members **Dr. A. Banerjee**, Department of Mechanical Engineering and **Dr. I Kar**, Department of Electronics and Electrical Engineering, Indian Institute of Technology Guwahati for their valuable and encouraging comments, discussion and suggestions during the research work. I pray to almighty for great success of them.

It is my privilege to offer my sincere gratitude to **Prof. A. K. Dass**, Head of the Department of Mechanical Engineering and all the former respected Head of the Department for their selfless efforts in bringing world class facilities to the department, providing all necessary facilities for carrying out research work in the department and building a sporty and effective working environment in the department. I wish this department a great success in due course of time.

It is indeed a great opportunity to thank **Prof. P. S. Robi** and **Prof. U. S. Dixit**, Department of Mechanical Engineering for their valuable and expert comments offered to me during my research work.

My sincere thank to laboratory superintendents Mr. J. Basumatary, Mr. S. Sarma, Dr. D. Bordoloi, Mr. M. Dowarah, Mr. S. Ahmed, and the central workshop team Mr. N. K. Das, Mr. C. Banikya, Mr. M. Medhi, Mr. D. Chetry, Mr. N. Saikia, Mr. U. Gohain, Mr. D. Khaklary, Mr. M. Sarma, Mr. B. K. Choudhury for their help and support. I wish all of them a great life and success.

I would also like to express my sincere gratitude towards the team at Central Instrument Facility, Indian Institute of technology Guwahati for providing instrument facilities for conducting my research work at various stages.

I would like to thank my seniors Dr. B. Parida, Dr. D. Yaduwanshi and Dr. P. K. Sahu for their help and support during my research work. I would also like to thank my batch mate and friends Mr. U. K. Tarai, Mr. G. Bolar, Mr. C. Kumar, Mr. S. Agarwal, Mr. R. R. Behera, Mr. B. Das, Mr. K. Saikia, Mr. A. Garg, Mr. M. K. S. Sarkar, for their help and suggestion during my research work. I wish all of them good life and great success ahead.

I would like to express my sincere gratitude to all my teachers who mould me in every part of my life and helped me to excel in life.

The last but not the least I would like to express my sincere gratitude and thank to my parents Mr. A. K. Das and Mrs. A. Das, my in laws Mr. P. C. Das and Mrs. N. Das, my brother Mr. B. Das and my sister in law Dr. J. Mukherjee Das, my beloved wife Mrs. I. Das, my brother in law Mr. J. Das for their love, affection, support and motivation throughout my research tenure.

I may have missed some names in the above list and my sincere apologies are due in such inadvertent oversight.

Place: IIT Guwahati
Date: **Bipul Das**

ABSTRACT

Quality of welded components can be attributed with strength and presence of any internal or external defects in the welded joints. Posts welding destructive and non destructive evaluation techniques are available for quality assessment and defect identification. However, these techniques suffer from limitations pertaining to loss of usability of the component or high setup and operating investment. Alternatively real time monitoring of welded joints can help to decide the outcome of the process without the limitations prevailing with destructive and non destructive methods. The current research work develops methodologies to monitor weld quality and defect identification with real time information in friction stir welding (FSW) process. A total of sixty five welding experiments are performed over wide range of tool rotational speed, welding speed and shoulder diameter. During the experiments main spindle motor and welding motor current signals, tool rotational speed signal and temperature signal are acquired in real time. Apart from the above signals vertical force and torque signals are acquired with a strain gauge based measurement system developed in the present work. These signals are analyzed to extract useful features for monitoring of weld quality and identification of defects in friction stir welded samples.

Current signals are analyzed in time domain through computation of root mean square, variance, skewness and kurtosis as statistical features. Time frequency domain analysis is attempted through wavelet packet transform and a new energy-to-entropy ratio is developed for selection of suitable mother wavelet function. Using the computed signal features, artificial neural network (ANN) models and support regression (SVR) models are developed for prediction of ultimate tensile strength (UTS) of the joints. It is observed that the data driven models with signal features in the input space results in superior prediction performance compared to models with only process parameters in the input space. Vertical force signals are analyzed in time domain through computation of statistical features as computed for current signals. A new combined parameter is proposed for combining the statistical features of the force signal. The proposed combined parameter reveals an increasing trend with increase in UTS of the joints. Force signals are also analyzed with a proposed methodology combining wavelet packet transform and Hilbert-Huang transform. The instantaneous phase and instantaneous frequency computed from the analysis is very useful to identify defective welds. The signal features are further used for development of ANN and SVR models for prediction

of UTS of the joints. Interestingly with force signal also the models with signal features results in superior prediction performance compared to only process parameters. Torque signals are analyzed with discrete wavelet transform and statistical features namely dispersion, asymmetry and excess are computed from the decomposed signal. With these features a new defect index is developed for identification of defective welds. The features are further used for prediction of UTS of the joints using ANN and SVR models. The present research work is the first attempt in exploring the effectiveness of tool rotational speed signal in monitoring of FSW process. The rotational speed signals are analyzed using fractal theory. Higuchi's algorithm is implemented for computation of fractal dimensions and these are used for developing ANN and SVR models for prediction of UTS of the joints. Similar to the other models, in this case also the model with signal features has better prediction accuracy compared to model without signal features. The computed fractal dimensions also reveal the presence of defects in the welded samples. The present study also delivers a new methodology for identification of defects in the welded samples with real time temperature signal. Two new indicators namely absolute rate of change of temperature and wavelet based indicator are proposed for defect identification. Another contribution of the present study is the development of methodology for processing top surface images of the welded samples. Three methods based on fractal theory and wavelet transform are proposed for extraction of features from the images. The extracted features reveal an increasing trend with decrease in UTS of the joints. Overall the present research work is the collection of different methodologies developed with real time process signals and top surface images of welds for effective monitoring of the FSW process. The developed methodologies can be modified with little effort to be integrated to different hardware and software for successful implementation in actual industrial environment.

***Keywords*:** Friction stir welding; Monitoring; Weld quality; Defect detection; Fractal dimension; Wavelet transform; Hilbert-Huang transform; Current signal; Speed signal; Vertical force; Transverse force; Torque; Strain gauge; Image processinig

List of acronyms

AA	Aluminum alloy
ANN	Artificial neural network
BM	Base material
BPNN	Back propagation neural network
CWT	Continuous wavelet transform
DWT	Discrete wavelet transform
EMD	Empirical mode of decomposition
FD	Fractal dimension
FFT	Fast Fourier transform
FT	Fourier transform
FSW	Friction stir welding
HAZ	Heat affected zone
HHT	Hilbert-Huang transform
IMF	Intrinsic mode function
MSE	Mean square error
NZ	Nugget zone
RBF	Radial basis function
RBFNN	Radial basis function neural network
RMS	Root mean square
SD	Shoulder diameter
STFT	Short time Fourier transform
SVM	Support vector machine
SVR	Support vector regression
TMAZ	Thermo mechanically affected zone
TRS	Tool rotational speed
UTS	Ultimate tensile strength
WPT	Wavelet packet transform
WS	Welding speed
WT	Wavelet transform

List of Nomenclature

η	Learning rate for weight updated in BPNN
η_1	Learning rate for weight updated in RBFNN
η_2	Learning rate for center updated in RBFNN
η_3	Learning rate for Gaussian spread updated in RBFNN
α	Momentum coefficient for weight updated in BPNN
ε	Margin of SVR network
γ	Kernel parameter for kernel function in SVR
C	Cost function for SVR
L_I	Number of input neurons
L_H	Number of hidden neurons
L_O	Number of output neurons
O_i	Output of i^{th} output neuron
P	Total num of training patterns
Y_i	Input for i^{th} input neuron
$\sigma j(n)$	Center for RBF
$O_{jH}^{p}(n)$	Output from j^{th} hidden neuron at p^{th} training pattern for n^{th} iterations
$O_{kO}^{p}(n)$	Output from k^{th} output neuron at p^{th} training pattern for n^{th} iterations
$R_j^i(n)$	Output from j^{th} hidden neurons for i^{th} input pattern for RBFNN
$k(.,.)$	Kernel function
$MSE(n)$	Mean square error at n^{th} iteration
S	Skewness
σ^2	Variance
K	Kurtosis
μ	Mean
A_i	Approximation at i^{th} wavelet decomposition level
D_i	Detail at i^{th} wavelet decomposition level
GF	Gauge factor

List of Figures

List of Tables

Contents

Chapter 1

Introduction

1.1 Friction stir welding

Friction stir welding (FSW) since its development in the year 1991 (Thomas et al., 1991) has expanded to new dimensions and substantiated applications in a wide range of industrial sectors that include aerospace, automotive, railway and maritime industries (Gibson et al., 2014). It is a solid state joining process that does not involve melting of parent materials to be welded. The FSW process bears many attractive advantages over other welding processes and the most notable one is the ability to weld alloys that were earlier considered difficult to weld using fusion welding processes (Mishra and Ma, 2005). It is free from problems related to solidification such as formation of second phase particles, porosity, cracking and embrittlement etc. as experienced in fusion welding processes. Involvement of low temperature in joining process results in lower distortion and lower residual stresses. Other advantages of FSW process includes joining without the use of electrode and filler material, no loss of alloying elements etc. The major limitations of FSW process is the exit hole that remained at the end of the weld length. This hole has to be trimmed off from the welded component that leads to material loss and additional production processes. With the introduction of this method to the welding community newer possibilities with different light weight materials has been emerged. In FSW process various joint configuration is possible such as butt joint, lap joint, T-joint, fillet joint etc. making the process versatile for various application (Mishra and Ma, 2005). The FSW is also suitable for joining of dissimilar materials with appreciable difference in melting point as it does not involve

melting of parent materials (Sahu et al., 2016; Ji et al., 2017; Cioffi et al., 2015; Aval et al., 2015; Mohammadi et al., 2015). Although the joining of dissimilar materials with FSW process is limited by the formation of inter metallic compounds within the welds that deteriorate weld qualities.

The basic operating principle involved in FSW process is schematically represented in **Fig. 1.1** along with a typical FSW tool. In this process a rotating tool is plunged into a rigidly clamped work piece along the joining line. The tool is inserted to a specific depth called as plunge depth. The plunged tool is kept in that condition for a predefined time known as dwell time. Once the dwell time is over the rotating tool being plunged is traversed along the joining line up to the desired length. After the completion of the joint length the tool is retracted back and the welding is achieved. The heat required for joining the material is achieved through friction generated between the tool and work piece material. This heat increases the temperature and the material gets plasticized. The stirring action of the tool makes the flow of the plasticized material around the tool and on cooling the material gets joined. The frictional heat is aided by adiabatic heat generated due to the severe material deformation in the weld zone due to stirring action of the tool.

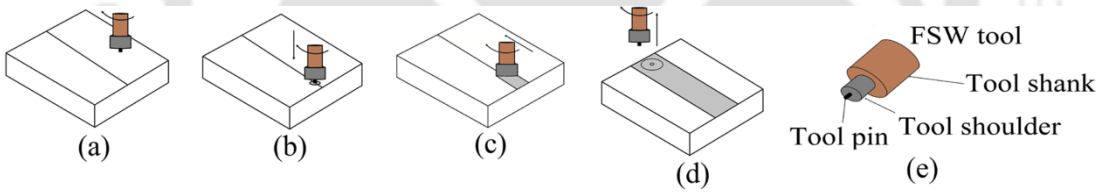

Fig. 1.1 Steps involved in FSW process (a) positioning of plate (b) tool plunge (c) tool travel (d) tool retraction (e) FSW tool

1.2 Motivation and preamble of the research work

The FSW process is a complicated system of interconnected factors that has dynamically changing behaviour. The quality of the weld is affected by tool rotational speed, welding speed, tool geometry among others. In welding applications quality is critical because in many cases it influences the lifetime of the product and safety issues. One of the measures that can be taken to assure the high quality of welded joints is to establish constant monitoring over the technological parameters and the needed output results including joint quality assessment and identification of internal defects. Real-time

monitoring allows avoiding defects and producing high quality joints. Theoretical knowledge is combined with the results of welding experiments of various real-time monitoring techniques. The study shows that relying on the conditions of the process a particular monitoring method may be suitable over another. The present study will help the weld quality designer and practitioner to choose suitable monitoring methods for FSW process.

The concept of real time monitoring in other welding and manufacturing processes has already gained significant attention (Zhu et al., 2017;Li et al., 2017; Ratnam et al., 2016; Sick, 2002; Pal et al., 2008) compared to FSW process. In these processes mostly sensor fusion technique is adopted for real time monitoring to evaluate the quality of the product. This includes acquisition of suitable signals and processing with effective processing techniques for impactful feature extraction. Realizing the need for monitoring methods in FSW process and conceptual aids from the published literature the present work is motivated to develop monitoring methodologies for FSW process with real time information. The study explores effectiveness of vertical force signal and torque signal and possibilities with tool rotational speed signal, main spindle motor and welding motor current signals for monitoring of FSW process. Among these signals current signals and speed signal will be tested for the first time for developing methodologies for weld quality monitoring. Suitable signal processing techniques are developed in time and time frequency domains in order to extract salient process information for quality assessment and internal defect identification. Apart from the signal processing based monitoring methods the study also attempts to deliver weld quality assessment method based on information extracted from top surface images of the welds. It is an effort first of its kind to correlate top surfaces of the welds with ultimate tensile strength (UTS) of the joints.

In the few attempts made for monitoring of FSW process researchers considers force signals with various signal processing techniques. Apart from the force signals main spindle motor and welding motor current signals may also contribute in order to capture process information. These two signals relate to two most influencing process parameters viz. tool rotational speed and welding speed in FSW process. Indirect monitoring of these two parameters might be influential in order to monitor the process. This study explores effectiveness of monitoring the process with information extracted from these signals. Time domain analysis and time frequency domain analysis with

wavelet packet transform (WPT) of the signals is performed through computing statistical features and data driven models are developed for prediction of weld quality specifically UTS of the joints.

Effectiveness of vertical force signals for monitoring of FSW process is explored through processing the signals with modified Hilbert-Huang transform (HHT) with WPT proposed in this study. A new indicator has been developed for identification of internal defects in FSW process with inconsiderable post processing time and effort. Later, data driven models are developed for modelling of UTS with appreciable accuracy. Torque signals acquired during the welding experiments are also analyzed in time frequency domain with discrete wavelet transform for efficient feature extraction. With the features an indicator has been proposed for reliable identification of internal defects in the welded samples. The two indicators developed one with vertical force signal and other with torque signal are both reliable and accurate and welding practitioners can choose depending on the their requirements and availability of information. The force and torque signals are acquired with a measurement setup developed in house with strain gauges. The developed setup is calibrated and tested for its reliability and accuracy. The setup is compared with commercially available piezoelectric based dynamometer and appreciable accuracy has been observed.

Apart from current, force and torque signals capability of tool rotational speed signal is also tested for monitoring of FSW process. The signal is selected owing to the fact that tool rotational speed being one of the most influencing process parameters in the process. Monitoring the parameter with real time signal might result in information that would be useful for understanding the process behaviour under the influence of factors that cannot be controlled during the process. Well established fractal theory has been implemented in order to extract salient signal feature in terms of fractal dimension of the signal. Later data driven models are developed for accurate modelling of FSW process. The computed FDs are also capable of delivering information for identification of defective welds. Another internal defect identification method based on real time temperature signals acquired during the process is developed and two novel indicators are computed from the extracted features. The developed features are as capable as that developed with vertical force and torque signal features.

The top surfaces of friction stir welded samples are characterized by semicircular rings which are reported to carry significant information regarding the process behaviour (Krishnan et al., 2002). The spacing between the consecutive rings provides an insight regarding the process behaviour and is presented as the combined output of tool rotational speed and welding speed. Hence, present study puts an effort in developing methodology for monitoring of FSW process with top surfaces images of the welds. The objective is to extract the information as depicted by semicircular rings present on the surface of the welded samples. Digital images of the top surfaces of the welded samples are captured and processed with two proposed fractal theory based methodologies. The computed fractal dimensions are then correlated to UTS of the joints and it is observed that intelligible correlation exists and can be presented as an indicator for monitoring weld quality. Later, the findings are compared with wavelet transform based image processing techniques that yields similar results as with the developed methodologies.

The developed methodologies will allow constant monitoring of the process without investing time and effort to monitor individual parameters with considerably less human intervention. The developed methodologies can be implemented for quality prediction of the welds with appreciable accuracy that will reduce post processing cost and time invested in production processes as well as accurate identification of defective welds with internal defects.

1.3 Objectives of the research work

The thrust of the present work is to develop methodologies for FSW process with real time process information for prediction of UTS and identification of defects. Effectiveness of main spindle motor and welding motor current signals, vertical force and torque signals and tool rotational are tested and evaluated for extraction of features that can be useful in prediction of UTS as well as defect detection. Apart from the real time signals top surface images of the welds are explored in monitoring the UTS of the joints which is an attempt made first of its kind. Along with the aforementioned signals temperature signals are also processed for developing methodologies for identification of internal defects. The objectives with which the current research work motivates and operated are outlined as follows.

- To design and develop a low cost force and torque measurement setup dedicated to FSW process.
- Exploring main spindle motor current and welding motor current signals in developing methodology for UTS prediction.
- Probing capability of vertical force and torque signals in effective monitoring of the process through accurate prediction of UTS of the joints.
- Presenting tool rotational speed signal as a competent option for modelling of UTS of the joints.
- To develop image information based weld quality monitoring approach.
- Identification of internal defects in the welded samples based on signal information.

1.4 Contribution of the thesis

- ✓ A strain gauge based low cost force and torque measurement setup has been developed dedicated to FSW process. The developed setup does not demand any alteration in the existing FSW machine for its integration.
- ✓ A process independent methodology has been developed and tested for selection of suitable mother wavelet function for WPT framework.
- ✓ A new signal processing technique is proposed by combining WPT and HHT to overcome the limitation of wide frequency band of first IMF in HHT. The proposed technique is applicable in FSW process monitoring.
- ✓ Impact and usefulness of top surface images of welds has been presented for monitoring of UTS of the joints which is an attempt made first of its kind.
- ✓ For identification of internal defects in the welded specimens defect index (DI) with features from torque signal, rate of change of temperature (R_cT) and wavelet based indicator (WBI) from temperature signals are the proposed performance indicators. The proposed indicators are found very effective for defects detection.

1.5 Organization of the thesis

The thesis comprises of eight chapters and highlight of each chapter is presented in the following.

Chapter 1 starts with the brief introduction of FSW process underlying its advantages and disadvantages and various applications. The motivation of the present study is also highlighted in this chapter with research objectives and contribution of the thesis.

Chapter 2 summarizes the research works carried out by other researchers in the field of FSW process. The chapter is divided into various sections starting from influence of process parameters, different techniques for signal processing and monitoring of FSW process, methods for identification of internal defects in the welded samples. The literature review reported in the chapter will guide through the gaps observed in the available work for the formulation of the research objectives for the present study.

Chapter 3 will showcase the experimental investigations carried for the present study. Selection of workpiece and tool material, selection of process parameters with suitable levels, design of experiments, and quality assessment of welded samples and demonstration of signal acquisition during the welding process are included in this chapter.

Chapter 4 demonstrates design and development of a robust and low cost force and torque measurement setup for FSW process. A strain gauge based setup has been developed and tested in real time during FSW process and the results are compared with commercially available and widely used dynamometers for mapping accuracy of the setup.

Chapter 5 includes the various signal processing techniques used in this study for useful extraction of signal features. Later part of this chapter demonstrates methodologies developed for prediction of UTS of the joints with machine learning based techniques and the signal features. The chapter demonstrates comparison of ANN models with SVR models to find out the best for accurate UTS prediction.

Chapter 6 is dedicated for representing the four methodologies developed for internal defect identification in the welded samples. Vertical force signal, torque signal, tool rotational speed signal and temperature signals are processed for feature extraction and the computed features are further processed for development of indicators for identification of defective welds.

Chapter 7 demonstrates an effort first of its kind to monitor quality of the friction stir welded samples with information extracted from top surface images of the welds. The

features of top surfaces in the welded samples are extracted with fractal theory and correlated to UTS of the joints.

Chapter 8 summarizes the present study and reported the findings of the research work. This chapter highlights contributions made from the thesis and outlines possible future research scopes of the present study.

Chapter 2

Literature Review

2.1 Introduction

The FSW process draws significant attention of researchers in the field of material joining across the globe since its introduction in the year 1991 (Thomas et al., 1991). The amount of research publications is exploding in this area with time and the count is still increasing. The process has gained immense exposure with the advantages of joining difficult to weld materials and free from defects those are inevitable in fusion welding processes. With increasing cutting edge research and development, lifts this process acceptable in many industrial sectors that include aerospace, automobile, railway, shipbuilding etc. Literature for FSW process has abundance in reporting effects of process parameters on FSW of different materials starting from aluminum (Park et al., 2017; Sun et al., 2017; Zapata et al., 2016; Ji et al., 2016; Dong et al., 2016; Guo et al., 2017; Aval, 2015), magnesium (Pan et al., 2016; Chen et al., 2015; Zhao et al., 2015; Mohammadi et al., 2015; Ni et al., 2014), steel of different grades (Li et al., 2017; Liu et al., 2017; Liu et al., 2016; Miura et al., 2016; Leitao et al., 2016), copper (Zhang et al., 2014; Bisadi et al., 2013; Khodaverdizadeh et al., 2012), composites (Salih et al., 2015; Oliveira et al., 2017; Bahrami et al., 2014; Cioffi et al., 2015; Palanivel et al., 2016) etc. Not only similar materials the FSW process has gained profound use in successful joining of dissimilar materials (Sahu et al., 2016; Ji et al., 2017; Cioffi et al., 2015; Aval et al., 2015; Mohammadi et al., 2015).

The survey of the available literature is carried out with the intention to ideate the research trend in line with the objectives of the present research work. This chapter is divided into various sections and sub sections to outline the salient results of the

reviewed literature. The literature review started with exploring the influence of process parameters on FSW process. In this regard section 2.2 is devoted to report results of various research works regarding the influence of tool rotational speed, welding speed and tool geometry on FSW process. The thrust area of this work is to develop methodologies for effective monitoring of FSW process. In this respect, the available literature are reviewed and reported in section 2.3. This is followed by literature review (section 2.4) of various signal processing techniques used in FSW as well as other welding and manufacturing processes for process monitoring. Various instruments used for measuring of force and torque signals during FSW process are reviewed and reported in section 2.5. This is followed by review of literature (section 2.6) for identifying various methods adopted and developed for identification of defects in FSW process. Various methods used for weld quality modeling is reviewed in section 2.7. Finally the observations are summarized in section 2.8 and gaps realized after reviewing the relevant literature are presented in section 2.9.

2.2 Process parameters

Material movement and plastic deformation involved in FSW process is relatively complex (Mishra and Ma, 2005). Welding parameters contribute significantly in governing material flow and temperature distribution in the weld, thereby influencing the microstructural evolution of material. In this section, published research articles are reviewed with the objective to figure out the most influencing process parameters in FSW process.

2.2.1 Tool rotational speed and welding speed

The working principle of FSW process includes plunging of a rotating tool up to a predefined depth called as the plunging depth and then traversing the plunged tool in rotating condition along the line of welding for achieving the desired weld. The heat required for plasticization of material is achieved through the frictional heat generated between the mating surfaces of tool and work piece. This heat is again aided by adiabatic heating due to plastic deformation of the material during the stirring action of the tool inside the work piece material. Thus, tool rotational speed is an important parameter in governing the heat generation or in other words temperature distribution in the weld. Apart from the tool rotational speed, welding speed governs the amount of heat deposited per unit weld length. This in turn regulates the temperature distribution along

the weld line which contributes towards microstructural evolution of the joints. Many researchers contribute towards investigation of effect of tool rotational speed, welding speed and tool geometry on FSW of different materials and produced suitable welding window for the selection of tool rotational speed for successful FSW.

Effects of tool rotational speed and welding speed on FSW of aluminum bronze joints were investigated by Zoeram et al. (2017). Use of lower tool rotational speed and welding speed was suggested to affect the joint mechanical and microstructural properties due to insufficient heat input. Joining of carbon nano tubes reinforced aluminum-copper-magnesium alloy was attempted by Zhao et al. (2017). The joints properties were evaluated under constant tool rotational speed with welding speed. With moderate range of welding speed the joints were reported to attain 87% of joint efficiency. Fracture and fatigue properties of friction stir welded samples were investigated with varying tool rotational speed and welding speed in the work by Moghadam and Farhangdoost (2016). The experiments were conducted over 2024 aluminum alloy and it was concluded that combination of high tool rotational speed and welding speed results in deterioration of fracture toughness of the joints. Defect formation, material flow behaviour and microstructural evolution of AA5456 aluminum alloy in FSW process was investigated in the work presented by Shirazi et al. (2015). The investigation results leads to the impression that combination of high tool rotational speed and welding speed results in turbulence in the material flow and leads to formation of internal defects. Effect of tool rotational speed and welding speed on UTS of the joints were investigated in the work by Liu et al. (2012). Results produced reflect a nonlinear behaviour of UTS with these two process parameters with increase up to a certain level of parameters and then following a decreasing trend. The effect of tool rotational speed and welding speed on vertical force was captured by Arora et al. (2010). The conclusions show an increase in vertical force with increase in welding speed and decrease in vertical force with increase in tool rotational speed. The effect of tool rotational speed and welding speed on peak temperature of welds was reported in Rajamanickam et al. (2009). The investigation reports that with increase in tool rotational speed peak temperature of the joins increases. However, effect of welding speed on peak temperature of the welds was reported to have less significant. Similar conclusive statement was also observed from the investigation carried out by Rezaei et al. (2011) during FSW of AA7075 aluminum alloy. Effect of welding speed at constant tool

rotational speed on average grain size at the NZ was investigated by Cavaliere et al. (2008). The investigation reported to observe decrease in grain size with increase in welding speed. Similar trend of decrease in NZ grain size with increase in welding speed was also reported by Zhang et al. (2015) in friction stir welded samples of high strength Al-Zn-Mg-Cu aluminum alloy. On the contrary Liu et al. (2013) observed increase in NZ grain size with increase in welding speed on FSW of AA6061 aluminum alloy. Effect of tool rotational speed and welding speed was also investigated for average NZ grain size by Sharma et al. (2012) for FSW of AA7039 aluminum alloy. The grain size at the NZ was found to have increasing trend with increase in tool rotational speed. Similar conclusion on size of grains at NZ of friction stir welded joints of AA7020 aluminum alloy was reported in Gafer et al. (2010) and Al-Jarrah et al. (2014). Mechanical properties of the joints viz. UTS, yield strength and percentage of elongation of the welded joints for AA2014 aluminum alloy were measured against various combination of tool rotational speed and welding speed by Aydin et al. (2012). All of these properties reported to display a nonlinear behavior with the process parameters. Similar nonlinear behaviour of mechanical properties of the joints was also reported in the work presented by Sakthivel et al. (2009) and Liu et al. (2011). Combination of high tool rotational speed and low welding speed were reported to result in internal defects in the welded samples that deteriorate the weld qualities. Similar nonlinear behaviour of UTS and percentage of elongation of the joints were reported by Hou et al. (2014) and Xu et al. (2009) for friction stir welded AA6061 and AA2219 aluminum alloys respectively. On the other hand Lim et al. (2004) reported to observe a linear behaviour of UTS and percentage elongation of the joints of AA6061 aluminum alloy with increase in tool rotational speed and welding speed. The effect of tool rotational speed and welding speed on micro hardness of welded samples of AA6082 aluminum alloy was investigated by Wan et al. (2014). The results showed that with increase in welding speed hardness of the joints followed an increasing trend. However, similar decisive conclusion was not reported with tool rotational speed. Efficiency of the joints produced from AA6061 aluminum alloy was reported to increase with increase in tool rotational speed and decrease in welding speed in the work reported by Cui et al. (2013).

The survey of literature on effect of tool rotational speed and welding speed on FSW process revealed that these two parameters have significant influence over the

process. These two parameters govern the process to achieve desired mechanical and microstructural properties of the joints.

2.2.2 Tool geometry

The tool geometry plays a critical role in material flow and in turn governs the traverse rate at which FSW can be conducted. An FSW tool consists of a shoulder and a pin as shown schematically in **Fig. 2.1**. The FSW tool has two primary functions: (a) localized heating, and (b) material flow. In the initial stage of tool plunge, the heating results primarily from the friction between pin and workpiece. Additional heating results from deformation of material during the plasticization. The tool is plunged till the shoulder touches the workpiece. The friction between the shoulder and workpiece results in the biggest component of heating. From the heating aspect, the relative size of pin and shoulder is important, and the other design features are not critical. The shoulder also provides confinement for the heated volume of material. The second function of the tool is to 'stir' and 'move' the material. The uniformity of microstructure and properties as well as process loads is governed by the tool design. Different researchers have carried out research to evaluate effect of tool geometry on FSW process and available literature are reviewed and presented as follows.

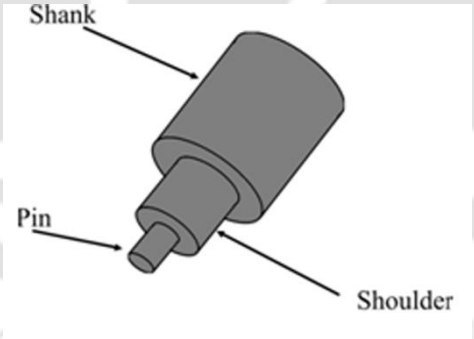

Fig. 2.1 Schematic representation of a conventional FSW tool

Tool geometry of FSW tool includes tool pin length, tool pin diameter, tool pin profile, shoulder diameter, shoulder profile. The parameters associated with the tool are schematically represented in **Fig. 2.1**. Out of various tool pin profiles developed in FSW process the most primitive one is the cylindrical profile. Various studies reported successful joining of different similar and dissimilar materials with this profile. Better mechanical properties, appreciable joint efficiency and microstructural properties were reported to observe with cylindrical pin profile in FSW process over various materials

(Mehta et al., 2017; Fujii et al., 2006; Boz and Kurt, 2004). Higher surface area and better mechanical contact with the plasticized materials around the tool pin during the welding process makes this profile one of the most suitable option for FSW process. The modification on the straight cylindrical pin is obtained through producing threads on the pin. Various threaded profiles has been investigated and reported in literature and many have confirmed successful joining with square thread profile (Imam et al., 2013; Elangovan and Balasubramanian, 2008; Sundaram and Murugan, 2010).Apart from the profile of the pin the other parameter associated with the tool that highly influence the FSW process is the geometry that includes shoulder diameter and shoulder profiles. The process of FSW process was investigated over various ranges and design of shoulder diameter. The common conclusions made in each contribution is the influence of shoulder diameter is maximum on FSW process (Scialpi et al., 2007; Leal et al., 2011; Rajakumar et al., 2011; Liu et al., 2008; Mehta et al., 2011). Shoulder diameter is mainly responsible for frictional heat generation between the rotating tool and the rigidly clamped workpiece material. This frictional heat softens the material around the tool and the stirring action of the tool help in plasticization of the materials. Thus contribution of shoulder diameter is observed to be more in heat generation during the process after tool rotational speed and welding speed. However, effect of pin diameter is found to be insignificant as reported by various researchers (Tozaki et al., 2007; Sharma et al., 2012; Mehta et al., 2017; DebRoy et al., 2012). The other parameter associated with FSW tool is the tool pin length. However, the available articles effect of tool pin length reported to be negligible compared to other parameters (Elangovan and Balasubramanian, 2008; Mishra and Ma, 2005; Gibson et al., 2014; Garg et al., 2017, Mehta and Badheka, 2016).

The survey on effect of tool geometry on FSW process provides the insight that straight cylindrical and square tool pin profile results in better mechanical properties compared to other tool pin profiles. Apart from the tool pin profile, shoulder diameter of the tool also plays significant role in FSW process. However, higher shoulder diameter might results in deterioration of joint quality. On the other hand tool pin diameter does not seem to have significant influence on FSW process.

2.3 Monitoring of FSW process

Monitoring can be defined as the procedure or method of observation of any physical process or phenomenon and acquiring valuable information. The performance

of the process can be evaluated continuously or periodically with the acquired information. Monitoring of a process involves two crucial steps: one is acquisition of valuable information through observation and the other one is the estimation or prediction of outcome from the acquired information. To have better control over the outcome of the process, the monitoring should be very effective to capture every possible change during the process. Process signals can be an effective option for detecting changes occurred during the process over time. Moreover, acquired signals give a more direct representation of the time dependent behaviour of the physical process. Monitoring a process over time can effectively reduce process faults, defects in the final product and can help in controlling the output quality in the desired level. FSW being an automated process monitoring the process over time would be useful in controlling the output as desired. Efforts made for development of methods for monitoring of FSW process are outlined in the following paragraphs.

Monitoring of FSW process with acoustic emission signals was reported in the work presented by Soundararajan et al. (2006). Fast Fourier transform (FFT), short time Fourier transform (STFT) and wavelet transform had been applied for processing of acoustic signals. The research work claimed that among the three signal processing methods adopted wavelet transform results in more information than FFT and STFT. Processing of acoustic emission signal with wavelet transform for monitoring of FSW process was also presented by Chen et al. (2003). The conclusions made leads to the impression that various defects formed during the FSW process have different signal band energy characteristics and the same can be an effective indicator for identification of defects in the welded samples. In the research work presented by Subramaniam et al. (2013) a signal frequency analysis based approach for monitoring of FSW process was presented with acoustic emission signal and Fourier transform. The chances of noise contamination with acoustic emission signal are high and the presented research work hardly describes the methods adopted for elimination of noise and extraction of suitable band in the desired frequency range.

Features extracted from force signals acquired during FSW process were presented as the indication for observing in-process gap between the mating surfaces by Yang et al. (2008).The presented results showed that with the gap present in the mating plates during the process the computed power spectral density would yield higher values. In an another attempt by Fleming et al (2008) force signals features based methodology

was proposed for identification of gap in welded samples. Possibilities of defect monitoring in FSW process using vertical force signal information was attempted by Kumari et al (2016). Continuous wavelet transform was implemented for analysis of the vertical force signals and it was reported that the developed methodology was able to detect defects in FSW process. However, the authors studied only surface level defects and did not extend the idea to identify internal defects those are more challenging in detection. Vertical and transverse force signals during FSW process were acquired and Fourier transform was implemented in order to develop defect monitoring method by Boldsaikhan et al. (2011). Artificial neural network based models were developed for classification of defective welds from defect free welds with signal information. Input electrical signatures of the driving motors in FSW system were captured and processed for monitoring of torque and transverse force during FSW process by Mehta et al. (2013).Monitoring of weld quality in terms of UTS of the joints was presented by Jene et al. (2008) with force signals features. Frequency spectrum of the force signals were reported to have significant information regarding process behaviour. It was reported that high frequency amplitudes in frequency spectra were observed for welds without any notable imperfections or defect.

Presence of defects in friction stir welded samples are attempted to monitor by Longhurst et al. (2016). The frequency information of current signal acquired from the main spindle motor of a FSW system is presented as the key feature for monitoring defect occurrence in the welded samples. The authors claimed that inclusion of void in the welded sampled would result in increase in frequency band of the signal. However, the authors did not emphasize on monitoring weld quality with the extracted signal features. Applicability of infrared thermography in online monitoring of FSW process has been presented by Serio et al. (2016). A new indicator termed as maximum heating slope value has been proposed to correlate tool rotational speed and welding speed during the process for monitoring the behaviour of the joining process. Imam et al. (2013) developed a methodology based on temperature distribution of friction stir welded joints for monitoring of the process. The study discloses that weld nugget zone temperature below 350 °C can result in formation of tunnel defect in joining 6063-T4 aluminum alloy. Image processing based monitoring of first mode metal transfer in FSW process is attempted by Sinha et al. (2008). Images of welds are captured to obtain image features in terms of grey level distribution, texture, pattern and contours. The authors

reported that the proposed methodology is effective and can be extended towards prediction of process parameters for unknown materials.

The survey of available literature provided the information that few works has been carried out for monitoring of FSW process. However, in other manufacturing processes monitoring has already gained significant attention. For instance, in the comprehensive review of turning operation over a decade by Sick (2002) around hundreds of literature on monitoring of the process is presented. In comparison to this the effort made for developing schemes for monitoring of FSW process is quite less. The demand of FSW process is increasing across various automated industrial sectors. In industry low cost, effective and reliable monitoring methods are useful for achieving the desired quality of the product. Monitoring schemes can help in decision making regarding the process outcome for the betterment of the process. The very less attempts made for monitoring of FSW process the current research work is motivated to develop effective methodologies for monitoring weld quality.

2.4 Signal processing techniques

Signals carry vital information regarding the process variability which can be enhanced further to produce decision making methodologies for efficient monitoring of the process. However, simply observing the signals may not end up with concrete evidences to understand the behaviour of the process. For this reason, the signals need to be processed to gather useful and salient information regarding the process. Processing of signals can be performed in time domain, frequency domain and time frequency domain. Time domain processing includes computation of statistical features from the signals. In frequency domain analysis fast Fourier transform and short time Fourier transform can be implemented for extraction of useful signal features. However, limitations with these methods lie in the assumption that the signal under consideration should be of stationary nature which is hard to achieve in actual conditions. Moreover, in frequency domain analysis time based information of the signals is lost that might be useful in many practical cases. Time frequency domain analysis solves the limitation of losing time information as in frequency domain analysis. It comprises of methods like wavelet transform, Hilbert-Huang transform, Gabor transform etc.

Fourier transform was applied to acoustic emission signals by Subramaniam et al. (2013) in FSW process. Effects of various pin profiles were investigated through computation of power spectral densities of the signals. Vertical and transverse force signals acquired during FSW process were analyzed in frequency domain by Jene et al. (2008). Fourier transform and short time Fourier transform were implemented as the signal processing tools. Frequency spectrum of the signals were computed and presented as the feature for monitoring variation of process with tool rotational speed and welding speed. Identification of automatic gap during FSW process was attempted through processing vertical force signal by Yang et al. (2008). Fourier transform was implemented for frequency domain feature extraction in terms of power spectral density of the signals. Fourier transform in gap detection in FSW process was also attempted by Fleming et al. (2008) with vertical force signals. Frequency domain features were computed in order to develop classification methodology for detection of gaps during the process. Processing of acoustic emission signal for monitoring of FSW process with Fourier transform, short time Fourier transform and wavelet transform was attempted by Soundararajan et al. (2006). It was concluded that among the three methods wavelet transform offers more valuable information regarding the process behaviour compared to others. Fourier transform as a signal processing signals was also implemented by Longhurst et al. (2016) for processing main spindle motor current signal. It was commented that inclusion of defects in FSW process show appreciable change in the frequency spectrum of the signal. Boldsaikhan et al. (2011) presented a methodology of defect detection in FSW process using Fourier transform of vertical and transverse force signals. It was commented that occurrence of defect in the welded samples bring notable change in frequency spectrum of the signals. The effect of tool wear on acoustic emission signal during FSW process was investigated by Zeng et al. (2006). The frequency domain analysis leads to the impression that characteristics of tool wear were evidential in acoustic signals. It was concluded that with the increase in the tool wear magnitude of the signals in frequency domain reduces indicating higher tool wear.

Despite the limitation and assumption with Fourier transform and short time Fourier transform many researchers have used these techniques for processing of signals acquired during FSW process. However, these methods results in loss in time information that might be useful in time dependent monitoring of FSW process. As a solution to the limitations with frequency domain techniques, time frequency domain

techniques are evolved with time. Wavelet transform is one of the most robust techniques for signal processing with retaining time and frequency information of the signal.

Wavelet transform was used by Chen et al. (2006) in processing of acoustic emission signal in FSW process. The study revealed that with the inclusion of defects in the welded samples wavelet energy signatures of the signals deviates from that of a defect free signal. In the work presented by Kumari et al (2016) continuous wavelet transform was used as signal processing technique for defect identification in FSW process. Vertical force signals were analyzed using continuous wavelet transform and features were computed for identification of surface level defects. However, the authors did not comment on selection of suitable mother wavelet function which is essential in effective decomposition of signal using wavelet transform. Kumar et al (2015) also attempted identification of surface level defects in FSW process using vertical force signal and discrete wavelet transform. Signal features were computed which later correlated to surface level defect information during the welding. In this work also the authors failed to mention about the selection procedure for suitable mother wavelet function and appropriate level of decomposition in wavelet transform. Although wavelet transform offers rich way of analyzing a signal in both time and frequency domain simultaneously, effort made in the field of FSW process is less. However, in other welding and manufacturing processes wavelet transform has gained significant use compared to FSW process (Liu et al., 2015; Bhat et al., 2015; Droubi et al., 2017; Chen et al., 2009; Praveen et al., 2013; Yang et al., 2016). Exploring the use of wavelet transform in developing monitoring methodology for FSW process would be an appreciable contribution of the current research work.

In signal information based monitoring of various other processes a relatively new time frequency domain technique known as Hilbert-Huang transform has gained significant attention(Lin and Chu, 2011, 2012; Law et al., 2012; Bin et al., 2012; Chen et al., 2012; He et al., 2013; Rado et al., 2014; Taralunga et al., 2015; Bakker et al., 2015; Liu et al., 2015; Li and Hao et al., 2015).The main advantage of Hilbert-Huang transform over wavelet transform is the ability to estimates subtle change in the frequency. Estimation of instantaneous frequency from wavelet transform is suboptimal because of frequency smoothening and wavelet transform assumes stationary frequency during the time span of wavelet function. Moreover, wavelet transform convolves a signal with a

predefined mother wavelet function to decompose a signal. The choice of wavelet function depends on the signal under consideration. On the other hand Hilbert-Huang transform does not require any convolution of the signal with a predefined basis function. These advantages of Hilbert-Huang transform makes it more robust than wavelet transform. Although there is no relevant literature found in FSW domain with Hilbert-Huang transform. Exploring Hilbert-Huang transform for processing of signals is FSW process might result in more useful information for developing effective monitoring scheme for the process.

Apart from Fourier transform and wavelet transform fractal theory is also a prospective technique for processing signals. The idea of extending the use of fractal dimension as an indicator to judge the quality of spot welding was proposed by Zhen et al. (2007). Defects in arc welding process was attempted to detect and characterize by Viera et al. (2008) through computing fractal dimensions from the current signals. Along with signal analysis, fractal dimension found its importance in analyzing images as well. Krivonosova et al. (2013) and Zhanfeng (2012) used images of welded specimens to compute fractal dimensions and thus proposed methods for the prediction of weld quality. In bio medical applications use of fractal theory as an effective signal processing technique has already been established (Parvinnia et al., 2014; Abhishekh et al., 2013; Paramanthan et al., 2008; Liu et al., 2005). In other processes fractal theory has found acceptances related to monitoring and control (Shoupeng et al., 2007; Shirong et al., 1999; Zhu et al., 2007; Yang et al., 2007; Kupkova et al., 2005; Tanaka et al., 2008). However, in FSW process monitoring use of fractal theory as a signal processing tool has not been attempted. Methodologies for monitoring of FSW process through processing signals with fractal theory can be an effective contribution of the present study. Potential of fractal theory as a tool for image processing is also established through various researchers (Ahammer, 2011; Li et al., 2009; Chappard et al., 2003; Risovic et al., 2008; Chen et al., 1989; Fortin et al., 1992).Similar attempts on monitoring of FSW process with images and fractal theory is not available and research in directive can be a valuable contribution.

The aforementioned survey of available literature fetched that researchers implemented Fourier transform, short time Fourier transform and wavelet transform as signal processing techniques in monitoring of FSW process. Although Fourier transform and short time Fourier transform have their own limitations such as lack of producing

time based information, lack of localization of events etc. Shortcomings with these two techniques were eliminated with the introduction of wavelet transform. However, use of wavelet transform in monitoring of FSW process is less compared to other manufacturing techniques. And the researchers reported to use wavelet transform without providing details on the selection of suitable mother wavelet function which plays influencing role in decomposition. Development of a method for selection of suitable mother wavelet function would be of great importance. The use of fractal theory for signal and image processing for monitoring of FSW process can also be attempted as it is lacking in the research trend.

2.5 Measurement of force/torque signals in FSW process

Appropriate design of FSW process demands real time measurement of process forces and torque experienced by the welding tool. By virtue of the simultaneous linear and rotary motion of the tool in the continuously deforming material imposes forces and torque on the welding tool (Mehta el al. 2013); measurement and control of which can be of great importance for controlling the outcome of the process.

A schematic representation of force and torque system associated with FSW process is shown in **Fig. 2.2**. When the rotating tool is plunged into the rigidly clamped work piece the material beneath the tool offers resistance to the tool. This resistance generates an upward reaction force known as plunge force or vertical force in FSW process. This force plays an important role as it governs the contact between the tool and work piece during the welding process. Along with vertical force another force experienced during FSW process is transverse force. As the rotating tool starts moving in the welding direction, material ahead of the tool offers resistance to the tool and it requires a force to overcome the resistance. This force is referred as transverse force or welding force. Along with these two forces, one more force is existent during the welding process, referred as lateral force. This force comes into existence due to the rigidity of the clamped work pieces during welding. Work pieces are rigidly clamped so that during plunging no gap is produced between the mating surfaces. In comparison with vertical and transverse forces, effect of lateral force in monitoring of FSW process is found to be less significant (Arora et al., 2012). Apart from these three forces, torque is also experienced in a FSW system (Mehta et al., 2013). Principal component in heating in FSW process is achieved by rotation of the tool (Mishra and Ma, 2005). To

achieve this rotation, torque is required to be applied to the tool. As the rotating tool is offered resistance by the material during the welding process, monitoring the torque during the process can yield salient information regarding the process outcome.

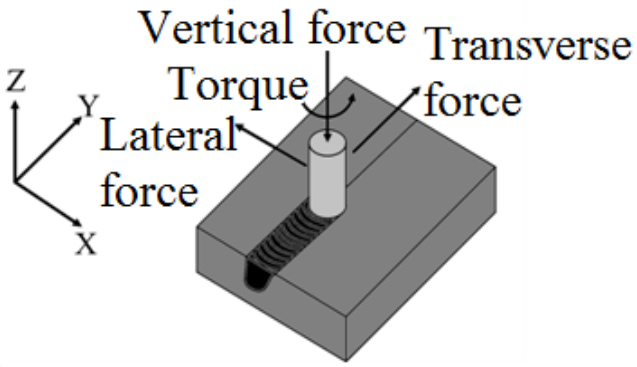

Fig. 2.2 Schematic of force/torque system associated with FSW process

Numerical modeling techniques (Mehta et. al., 2013) are available for estimation of force or torque in FSW process with limitations in its accuracy due to complex physics of the process, tool-workpiece interaction and unknown factors experienced during actual welding environment. Real time measurement of forces and torque can be achieved using load cells and multi-dimensional dynamometers (Jene et al., 2008; Kumari, 2016; Kumar, 2015; Astarita et al., 2014; Cavaliere et al., 2006).However, one of the limitations with the existing force measuring systems is the associated cost. Parida et al. (2015) appreciably compared cost of different available force measurement systems which reflects that the cost of measuring devices sometimes may be much higher than the welding machine (Mehta et al., 2013), which is not feasible for all users. Hence, researchers often motivated to develop their own measurement system for forces as well as torque.

An instrumented tool holder capable of measuring multi-dimensional forces in FSW process using strain gauges was developed by Blignault et al. (2008). Another tool based two-dimensional forces and torque measuring system was developed by Mitchell et al. (2002) using strain gauges. Different welding conditions demand different tool geometries with different dimensions. Moreover, breaking of tool and wear of the tool are possible in FSW process which brings the necessity of changing the tool. This brings limitations to the tool based force measurement systems as every time modification of the tool may not be a feasible option. Instead of tool based systems for force

measurement, welding fixture based system can be an effective alternate to overcome the limitations with tool based measurement systems. Efforts of developing fixture based force and torque measurement system in FSW process is not available. However, in milling, shaping and turning operations researchers attempted to develop strain gauge based setup for force measurement. Korkut (2003) and Yaldiz et al. (2007) developed a strain gauge based dynamometers for the measurement of forces during milling operation. Strain gauge based dynamometer was developed for measurement of forces during turning operation by Unsacar et al. (2006). Measurement of cutting forces during shaping operation was achieved with the dynamometer developed by Seker et al. (2003).

The literature review on measurement of force and torque reveals that researchers used various types of dynamometers. These dynamometers are known for its accuracy and reliability. However, the associated cost of these dynamometers is quite high and sometimes not affordable. On the other hand few researchers attempted to develop strain gauge based measurement setup for other manufacturing process. It is observed that strain gauges can be effectively used for the measurement of forces under static as well as dynamic working conditions. Moreover, the associated cost is also far less compared to other dynamometers. Hence, it would be appreciable to develop a fixture based forces and torque measurement setup with strain gauge for FSW process.

2.6 Defect identification in FSW process

The FSW process is found to be advantageous in many aspects compared to other fusion welding processes (Mishra and Ma, 2005; Gibson et al., 2014). Defects occurred in fusion welding processes such as porosity, lack of penetration, spattering of electrode material and defects related to solidification of joining material is out of question in FSW process. This makes the process free from defects commonly occurred in fusion welding processes. However, the FSW process suffers from defects occurred due to improper or sub-optimal selection of influencing process parameters.

Evaluation of welded samples for identification of defects can be achieved in terms of destructive as well as non-destructive techniques. Destructive testing methods include bend test, tensile test, fatigue test etc. These methods destroy the welded components that impede the use of the components. The non-destructive testing methods include visual testing, dye penetration testing, radiographic testing, eddy current testing,

ultrasonic testing etc. (Gibson et al., 2014). In these techniques the welded components do not lose its integrity and it can be effectively used if passed the test. The limitations with these testing methods are high initial investment and skilled operator for the processes.

Investigation of welding defects in AA5456 aluminum alloy friction stir welds was carried out by Chen et al. (2006). The defects were detected using mechanical sectioning method and observing the samples under optical microscope. Void defect and kissing bond defect were reported to occur in the friction stir welded samples by Cao et al. (2009) in magnesium alloy. Mechanical sectioning method was used for detection of defects in the welds followed by optical microscopy. Defects in friction stir welded magnesium alloy were also investigated by Zhang et al. (2006). They also reported formation of void and kissing bond defect in the welded samples. Mechanical sectioning method followed by optical microscopic observation for defect detection. Investigation of defect formation in friction stir welded 6013 aluminum alloy was carried out by Zhao et al. (2014). Tunnel defect and kissing bond are the two defect types reported to occur during the process. Mechanical sectioning method with optical microscopic technique was used for identification of defects. Liu et al. (2012) investigated the effect of tool rotational speed and welding speed on formation of void defect in FSW process. High tool rotational speed with low welding speed was reported to be the cause of void defects. In this study the defects were characterized by mechanical sectioning method. Voids and excessive flash were reported to occur in FSW of AA7075 aluminum alloy by Rezaei et al. (2011). They also reported that high tool rotational speed with low welding speed might be one of the reasons for voids in the welded samples. Macrostructure features of the joints obtained through mechanical sectioning of the joints were used for defect identification. Characteristics of kissing bond defect in friction stir welded AA1050 aluminum alloy were investigated by Sato et al. (2005). Improper heat generation due to low combination of tool rotational speed and welding speed were reported to be the possible cause of formation of kissing bond defect. Microscopic technique was used for identification of defects in the welded samples.

X-ray radiography and infrared thermography techniques were used by Saravanan et al. (2014) for identification of defects in friction stir welded joints. A methodology has been proposed based on radiography and thermography for identification of internal defects in FSW process. The study claimed that with the

developed method voids and micro pores can be detected with high accuracy. Signal features computed from vertical force signals acquired during FSW process were presented as indicator for identification of surface level defects by Kumari et al. (2016) and Kumar (2015). However, the method had not been tested for identification of internal defects in FSW process which is more challenging. Vertical force signal features based identification of worm hole defect in FSW process was also presented by Boldsaikhan et al. (2011). The authors concluded that with the inclusion of defect the frequency spectrum of the signals shows notable deviation than the spectrum for defect free welding cases. Effect of tool rotational speed and welding speed on defect formation of friction stir welded AA2014 aluminum alloy was investigated by Rajamanickam et al. (2009). The welded samples are tested using X-ray radiography for identification of defect. Rosado et al. (2010) proposed a non destructive testing method for identification of defects in FSW process. The authors developed a new type of eddy current probe for identification of internal defects in FSW process. The investigation reported that with the proposed methodology detection of defects with characteristics size of 60 μm would be possible. A methodology based on transient eddy current for defect identification in FSW process was presented by Smith (2005). Eddy current based conductivity measurements were performed for the estimation of flaws within the welded samples. Shen et al. (2011) summarized the possible use of available non destructive methods for identification of defects in FSW process. Besides a series of optical metallographic inspection the research work considered X-ray detection, ultrasonic C-scan technique, ultrasonic phased array inspection and fluorescent penetrating fluid inspection technique were tested for identification of defects. Effect of tool rotational speed, welding speed and plunging force on defect formation of FSW of die casting aluminum alloy was investigated by Kim et al. (2006). Three defect types were reported in the investigation. Mass of flash due to excess heat input, cavity or groove like defect due to insufficient heat input and cavity produced by abnormal stirring. X-ray radiography technique was used for identification of internal defects occurred during FSW process.

The above discussion on review of available literature for possible defects in FSW process and its detection leads to the impression that improper selection or sub-optimal range of process parameters are mainly responsible for defect generation. The welding parameters should be selected within the suitable welding window of materials for sound defect free welds using FSW process. The researchers concentrated mostly on

macrographs of welds for identification of defects using mechanical sectioning methods. However, few researchers concentrated on testing and developing non destructive methods for defect identification in FSW process although the effort is less. The tested or developed methodologies are limited for implementation in FSW process at every scale and needs further development of methods for reliable identification of defects in welded samples. One of the possible reasons that most of the researchers attempted conventional practices for identification of defect is the cost associated with the available non destructive testing equipment and further precise knowledge base for interpretation of results. Real time information contained in process signals can be extracted through suitable processing technique and features can be developed for defect identification in FSW process.

2.7 Data driven modelling techniques

The process of FSW involves complex physics and interaction among various process parameters is high. Understanding of FSW process behaviour against various combination of influencing process parameters can be achieved through various modelling approaches. Among these approaches mathematical modelling, regression based modelling and thermo mechanical modelling are available. Limitations with these approaches are that these consume notable computational time and often the reliability and accuracy are compromised. Physics based modelling of FSW process has gained significant attention among the research community to understand the process behaviour (Hasan et al., 2017; Xio et al., 2017; Shi et al., 2016; Tang et al., 2016; Zhu et al., 2016; Shu et al., 2015; Mehta et al., 2015). This approach is reliable but the time consumption is high. The interaction among various process parameters is difficult to accommodate and representation in terms of physics based mathematical models are difficult. Moreover, the assumptions made during the physics based modeling approaches are hard to realize in actual process environment. An alternative approach for modelling of FSW process is possible through data driven artificial intelligence techniques. Artificial neural network (ANN) and support vector machine (SVM) learning method has gained immense popularity. These models can deal with complex processes, high interaction of parameters and depends on data rather than physics based mathematical models. These models can handle non linear behaviour of the data and useful in representation of actual process behaviour compared to physics based modelling approaches. In this context few

literature are reviewed where researchers have attempted modelling of FSW process with various data driven modelling techniques.

An ANN model was developed by Buffa et al. (2012) for the estimation of microhardness and microstructure in friction stir welded samples. Local strain, strain rate and temperatures were used as the input for the development of the models. The estimated results showed that the developed neural network model results were in fair agreement with the experimental results. Prediction of peak temperature, width of heat affected zone and welding force were predicted with artificial neural network models by Shojaeefard et al. (2014). Tool rotational speed and welding speed were used as the input for the development of the neural network models. Feed forward neural network trained with back propagation algorithm was used with single hidden layer architecture. It was concluded that the developed neural network model was accurate in prediction of peak temperature, welding force and width of heat affected zone compared to experimental results. Effect of genetically optimized tool rotational speed and welding speed in FSW process were tested and modeled with artificial neural network models by Tansel et al. (2010). Five different neural network models were developed for the prediction of tensile strength, yield strength, percentage of elongation, hardness of nugget zone and hardness of heat affected zone. It was reported fair agreement between the measured quantities with the model predicted quantities with influence of parameters optimized using genetic algorithm. Fratini et al. (2009) attempted modelling of grain size in FSW process using artificial neural network approach. Local strain, strain rate, temperature and Zener-Holloman parameter were the input to the developed artificial neural network model. The most popular back propagation algorithm was used for the training of the model. The model estimated grain sizes showed appreciable match with the grain sizes measured experimentally. Weld height and width were predicted using artificial neural network approach by Pandya et al. (2014). Thickness of the plates, rolling direction, tensile strength and yield strength were selected as the process parameters for the development of the models. The neural network models were trained with back propagation algorithm. It was reported that the estimated parameters had fair agreement with experimental results. Dehabadi et al. (2016) attempted prediction of Vickers microhardness of friction stir welded samples with artificial neural network. The predicted results with the developed models when compared with results obtained from experimental investigation showed appreciable agreement.

Modelling of FSW process through data driven models with signal features were attempted by few researchers. In these models features extracted from real time signal information and process parameters are used as input. Various output characteristics of FSW process were modeled with the developed models. The use of artificial neural network in monitoring of FSW process was reported by Boldsaikhan et al. (2011). Vertical force and transverse force signals are acquired during FSW process and analyzed in frequency domain using Fourier transform. The frequency domain features were utilized in the development of artificial neural network model for classification of defective welds from defect free welds. The classification accuracy of the developed model showed the acceptability and reliability of the artificial neural network model in monitoring of FSW process. Misalignment detection and seam tracking was attempted by Fleming et al. (2009) in FSW process. General regression neural network was developed with axial force values as the input to the model for the estimation of tool offset position relative to the weld seam. An estimator was developed for detection of misalignment and tracking of weld seam in FSW process and it was concluded that the estimator was relatively accurate compared to the actual measured values. Comparison of modelling performance of response surface methodology and artificial neural network was reported by Lakshminarayanan et al. (2009). Tool rotational speed, welding speed and axial force values were considered as input for the development of artificial neural network model. The model was developed for the prediction of tensile strength of the friction stir welded joints. The comparison showed that the prediction performance of artificial neural network model is far better compared to response surface methodology.

Apart from the ANN models researchers have developed statistical models for the modelling of FSW process. Combinations of various process parameters were tested for the development of effective models to represent different output characteristics of the FSW process. Effect of tool rotational speed, welding speed, axial force, tool shoulder diameter, pin diameter and tool hardness were investigated by Rajakumar et al. (2010) through empirical modelling of FSW process. Statistical regression models were developed for prediction of average grain size at nugget zone and tensile strength of the joints. It was reported that the developed models yielded satisfactory prediction performance. Statistical models were also developed in a different work by Rajakumar et al. (2012) and effect of individual process parameters were investigated on tensile properties of the joints. It was reported that the developed models have fair agreement

with the experimental results. Hwang et al. (2008) attempted prediction of temperature during FSW process with the application of regression based models. Various regression models were developed and the results were compared with the results obtained from experimental investigation. Regression based models were developed by Bitondo et al. (2011) in order to predict vertical force and transverse force during FSW operation. Multiple models were developed with tool rotational speed and welding speed. The comparison of the predicted results with the experimental results showed that the developed models were accurate in estimation of vertical force and transverse force. Blignault et al. (2012) developed statistical models for the prediction of tensile strength using pin geometric information. Response surface methodology was the technique used for the modelling of tensile force during FSW process. The results of the developed model were reported to be in well correlation with the experimental results. Polynomial regression models were developed by Murugan et al. (2010) for the prediction of UTS and percentage of elongation of friction stir welded joints. Tool rotational speed, welding speed, tool pin profile and axial force were the input variables used for the development of the mathematical models. The developed models showed relatively higher percentage of prediction error but provided an insight to the implementation of regression based models in mathematical modelling of FSW process.

Apart from the ANN models researchers have attempted modelling of various other welding and other processes through SVM learning method (Koo et al., 2017; Shuangsheng et al., 2012; Gilan et al., 2012; Na et al., 2008; Lim et al., 2010; Pan et al., 2010; Zaidi, 2012; Wen et al., 2009). However, use of SVM in FSW process is not available in literature. The use of SVM in modelling of FSW process can be extended and real time information can be used for development of SVM models.

The survey of literature fetched that ANN modelling technique is popular followed by statistical models. In these models limited process parameters were used for modelling of the process. FSW process is governed by too many process parameters and modelling the process with few parameters may result in inadequate information regarding the process behaviour. However, it is difficult to consider all process parameters as it would increase the complexity in the experimentation. As an alternate, real time signals acquired during welding process can be useful. Signals carry vital information regarding the process and it retains combined effect of both controllable and uncontrollable parameters during the process. Extracting the signal information in terms

of signal features and developing data driven models with these can offer more reliable and accurate mean of modelling the FSW process.

2.8 Summary

The survey of available literature is carried out with the intention to develop prior knowledge about the process and to track the trend in the current research in FSW. The chapter is divided into various sections as per the interest of the present study. The observations made from the survey of literature boiled down to few conclusive remarks summarized as follows.

- Available literature in monitoring of FSW process is less compared to other manufacturing processes. The published research works mostly considers real time signals in monitoring various aspect of FSW process but missed to introduce weld quality monitoring. Thus scope remains in developing methodologies for monitoring of weld quality of the welded samples.
- In general it is observed that FFT is widely implemented for analysis of real time signals for monitoring of FSW process along with very limited use of WT. This further needs detailed investigation for wide implementation of WT in order to analyze real time signals acquired during FSW process. Apart from the regular signal processing methods it is observed that fractal theory is also capable of analyzing signals in time domain. However, this particular approach is not yet disclosed in FSW process monitoring with real time process signals. Exploring this would add a new avenue for monitoring FSW process that can be treated as the imperative contribution of the present study.
- Researchers mostly consider force signals acquired during welding process for monitoring of the FSW process but possibilities of other process signals such as current signals from main spindle motor and welding speed motor, tool rotational speed signal of the main spindle would also reveal salient information for developing effective monitoring methodology.
- It is observed that measurement and acquisition of force signals is mainly performed with costly and less flexible measurement systems that mostly include piezoelectric based dynamometers. On the other hand motivation is derived from the low cost effective dynamometers developed for milling and turning

operations with strain gauges for developing force and torque measurement system dedicated for FSW process.

- Despite being an automated process FSW yields various types of defects due to improper selection of suitable process parameters. The challenge is in their detection as all the defects are internal or subsurface. In spite of various nondestructive methods available for identification of internal defects researchers failed to use those methods and apparatus. One of the causes for adopting conventional destructive sectioning method for identification of defects in the welded samples over these nondestructive methods is the associated cost with the systems and prior expertise for interpretation of results. This area needs contribution in developing methods for identification of internal defects with real time signal information with reliability, accuracy, considerably less post processing time and requirement of no a priori knowledge for interpretation of results.
- Finally, various data driven modelling techniques used in FSW process is reviewed and it is observed that statistical regression modelling techniques, ANN models are quite popular among the researchers. However, various other nonlinear data driven modelling technique such as SVR is available with reasonably good prediction accuracy and implemented in monitoring of various other processes. This technique can be tested for its performance check over ANN models to comment on a more accurate modelling approach for weld quality prediction in FSW process.

2.9 Gaps in the literature

The review of available literature is carried out with the intention of finding the trend of current research works in FSW process. The review made realization of few gaps that can be attempted for enrichment of the FSW user and research community. The gaps observed during the review are listed below.

- The effort made for development of methodologies for monitoring of FSW process is less.
- The literature survey leads to the impression that use of sophisticated signal processing tools such as wavelet transform and Hilbert-Huang transform in FSW process is not attempted in great details.

- Selection of suitable mother wavelet function in wavelet transform framework is not discussed in details and further exploration is needed in this regard for FSW process.
- Measurement of force and torque is achieved through costly dynamometers and development of low cost measurement system for FSW process would be impactful.
- Identification of internal defects using process signal in friction stir welded samples is not attempted.
- Modelling of FSW process is mostly attempted through development of ANN models with process parameters in the input space of the models. Real time signal information can be tested for development of modelling approaches in FSW process.
- The use of ANN and statistical models populated the modelling of FSW process. More accurate modelling approach such as SVM is not tested for modelling of FSW process.
- Use of fractal theory for signal and image processing in FSW process is lacking and can be developed in the current research work.

Chapter 3

Experimental Investigation

3.1 Introduction

This chapter outlines materials selected for FSW experiments, methods used for testing of welded samples for measuring different weld quality attributes. Apart from the mechanical investigation this chapter also highlights different sensors and acquisition hardware used for signal acquisition during FSW. Tool rotational speed, welding speed and shoulder diameter is selected as the process parameters for the present study. After the selection of suitable levels for each parameter design of experiment matrix is formulated for conducting the welding experiments. After the completion of the experiments mechanical test samples are prepared from the welded samples for the measure of weld qualities such as ultimate tensile strength (UTS), yield strength and percentage of elongation. Details of different experimental procedures followed during the present research work are highlighted in the following sections.

3.2 Material for welding

The introduction of FSW process has revolutionized joining of light weight materials such as aluminum, magnesium, copper etc. those were earlier considered to be difficult to weld with fusion welding processes. Till then use of these materials mostly aluminum found extensive applications in industrial sectors. Researchers also found to motivate to consider aluminum at their first choice of materials for FSW process owing to its numerous advantageous uses in many industries. The present research work considers aluminum alloy of AA1100 series for conducting FSW operations. This grade of aluminum is considered as commercial grade and has extensive use in products like spun hollowware, fin stock, heat

exchanger fins, dials and name plates, cooking utensils, decorative parts, giftware, rivets and reflectors, and in sheet metal work. The material is received in plates having dimension of $1219\ mm \times 2438\ mm$ with 6 mm thickness. Welding work pieces are cut from the parent materials having dimension of $160\ mm \times 110\ mm \times 6\ mm$. Plates are friction stir welded in square butt joint configurations and edges of the work pieces are prepared with milling operation to meet the required dimensions and finish. The received material is tested under energy dispersive X-ray (EDX) emission method to find out the different components present in the base material. The composition of base material is shown in **Table 3.1**. Tensile coupons are cut as per ASTM E8M standard from the base material to evaluate UTS, yield strength and percentage of elongation. These values are further referred for the evaluation and comparison of weld qualities. Mechanical properties of base materials can be seen in **Table 3.1**.

Table 3.1 Mechanical properties and chemical composition of the base material

Mechanical properties	Chemical composition (wt %)
	Al: 99.3
Ultimate tensile strength: 119.8 MPa	Si: 0.2
Yield strength: 106 MPa	Zn: 0.2
Percentage of elongation: 17.1	Fe: 0.2
	Cu: 0.1

3.3 Tool materials and tool fabrication

Tool material plays an important role in FSW process. The precondition with the selection of tool material for FSW process is that the hardness of the tool material should be much higher than the hardness of the base material to be welded. For aluminum alloy it is observed that researchers mostly used H13 hardened steel (Leal et al., 2011; Tozaki et al., 2007; Zhang et al., 2012; Sharma et al., 2012) and stainless steel grade SS316 (Imam et al., 2013; Hao et al., 2013; Zhang et al., 2015) materials for fabrication of tool. As the materials selected for present research work is AA1100 with a hardness of 26 BHN, SS 316L with hardness of 143 BHN is selected which is sufficient for the welding operations. In literature

review chapter (chapter 2) various tool profiles have been discussed with their significant advantages and their affects on joint properties. However, among various profiles cylindrical tool with straight pin profile is most widely used in FSW process with reasonably good mechanical properties of the joints. Hence, it is decided to use the most primitive configuration of FSW tool for the present work. From the published literature and preliminary investigation with sufficient support of published literature (Sundaram et al., 2010; Kumar et al., 2008; Liu et al., 2008) it was observed that the pin length for successful FSW operations should be around 95% – 97% of the thickness of the base materials considered for welding. With this information in the present research work the length of the tool pin is kept fixed at 5.7 mm. The available literature (Rajakumar et al., 2011; Tozaki et al., 2007; Zhang et al., 2015) suggest that for successful joining the diameter of tool pin should be equal to the thickness of the plates considered for welding. However, literature with different combinations of plate thickness and pin diameter are also available. The present study considers the tool pin diameter to be 6 mm which is equal to the thickness of the welded plates. Another important FSW parameter associated with welding tool is the shoulder diameter of the tool. This determines the amount of heat generated during the welding process as the heat is generated due to friction between the work piece material and shoulder of the FSW tool. Owing to this shoulder diameter of tool is an influencing parameter for governing the heat input to the weld and in turn controlling the FSW process. Researchers have reported many profiles for shoulder (Mishra and Ma, 2005; Elangovan et al., 2008; Li et al., 2016) but the plain profile is widely used in FSW process. In the present work also the plain profile of shoulder is preferred over various profiles. This FSW parameter is varied in four levels for the investigation of its effect on joint qualities in the current research work. The FSW tool used in the present research work is schematically shown in **Fig. 3.1**.

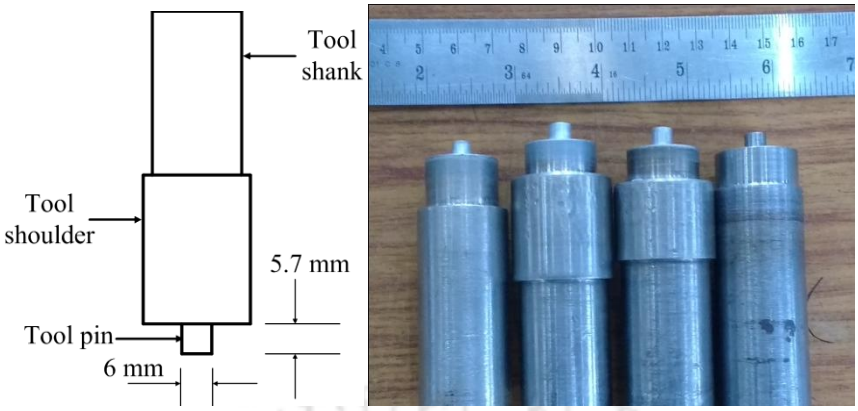

Fig. 3.1 Schematic representation of FSW tool with fabricated tools

3.4 FSW setup

In the present research work a milling machine is used for conducting the welding experiments. The choice of milling machine for FSW process is popular in research activities across the globe (Parida et al., 2011; Scialpi et al., 2007, Boz and Kurt, 2004; Elangovan et al., 2008; Kumar and Kailas, 2008; Record et al., 2007; Hwang et al., 2008; Movahedi et al., 2012; Aydin et al., 2012). In present scenario a vertical knee type milling machine is used for the welding process with modified fixture developed and fabricated in house for holding the work piece material during welding process. The vertical milling machine used in this work is shown in **Fig. 3.2** with the modified fixture developed in house for holding and aligning the work piece during welding. FSW process also required backing plate with low thermal conductivity and high structural rigidity. For this purpose mild steel plate with a thickness of 20 mm is used as backing in the present work. This will provide good thermal barrier to the work piece for controlled heat loss and high rigidity during the welding process. The milling machine has twelve steps in tool rotational speed (50, 65, 90,125, 175, 240, 325, 440, 600, 815, 1100, 1500 rev/min) and eight steps in welding speed (22, 36, 63, 98, 132, 200, 360, 550 mm/min). The main spindle motor has a power rating of 5.5 kW with maximum current rating of 19 A and feed motor has a power rating of 0.75 kW with maximum current rating of 5 A.

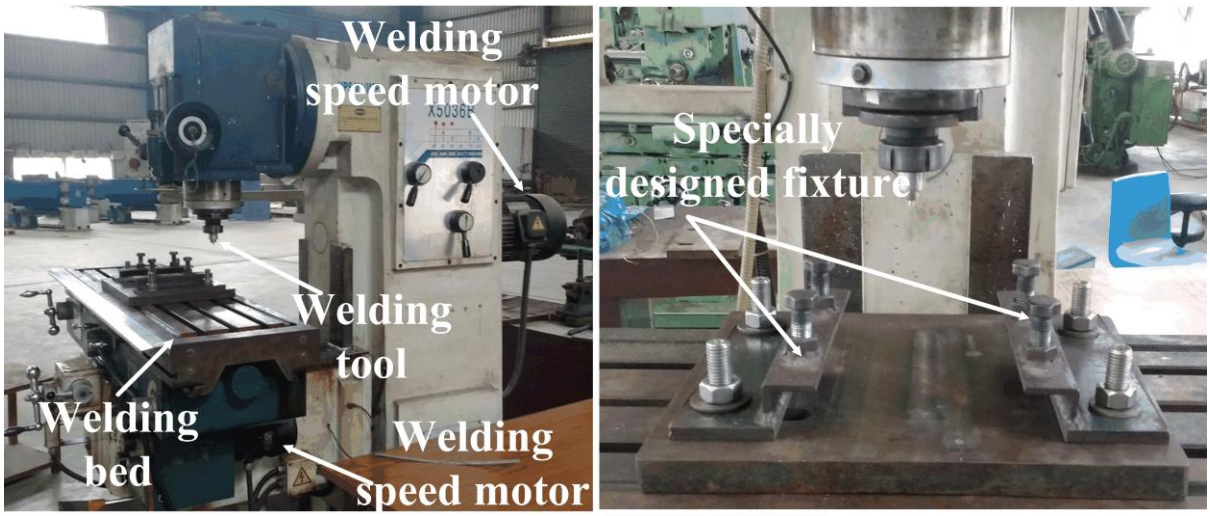

Fig. 3.2 FSW machine with specially designed fixture and backing plate

3.5 Selection of process parameters

Friction stir welding process is influenced by too many process parameters where selection of suitable combination of different parameters is important for successful welding. The effect of various process parameters is often investigated by measurement of different mechanical properties of the joints that include UTS, yield strength, percentage of elongation, bending strength, hardness of the joints. Apart from these mechanical properties weld dimensions are also sometimes used as the index for investigating the effect of process parameters on the welded joints. Microstructural investigation for measurement of grain sizes is also a key factor in estimating joint quality in FSW process. Various process parameters involved in FSW process is shown in **Fig. 3.3** for reference. However, from the preliminary investigation and information from the published literature it is observed that all the parameters do not have significant influence on qualities of the welded joints.

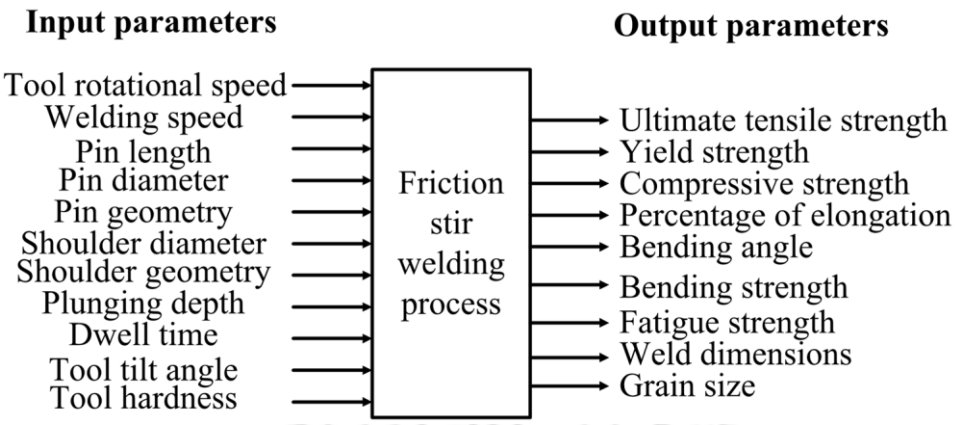

Fig. 3.3 FSW process with various process parameters

To select suitable process parameters for the present research work preliminary investigations are carried out and with suitable literature survey (Parida et al., 2014; Sahu et al., 2016, Kumar et al., 2008; Sharma et al., 2012) it is observed that among these parameters tool rotational speed, welding speed and shoulder diameter plays more significant role in FSW process. Hence, in this research work it is decided to consider these three parameters for conducting the welding experiments. After the selection of suitable process parameters suitable level of welding parameters are decided. Again with previous experience levels of tool rotational speed, welding speed and shoulder diameter are chosen so that it falls within the suitable welding window for FSW of AA1100 aluminum alloy. For each parameter four levels are selected for the formulation of experimental design matrix. The process parameters along with the level of each parameter are represented in **Table 3.2**. The rest of the parameters such as pin length, pin diameter, tool tilt angle, and plunge depth are kept constant as shown in **Table 3.3**. For three process parameters and four level of each parameter full factorial design approach result in 4^3, i.e., 64 welding experiments. One of the experiment is repeated which is selected randomly. All the experiments are performed randomly in order to minimize the experimental error or bias. The complete experimental design matrix is shown in **Table 3.4**.

Table 3.2 Process parameters with respective levels

Process parameters	Parameter levels			
	Level 1	**Level 2**	**Level 3**	**Level 4**
Tool rotational speed (rev/min)	600	815	1100	1500
Welding speed (mm/min)	36	63	98	132
Shoulder diameter (mm)	16	20	24	28

Table 3.3 Parameters with fixed level

Parameters	Value
Pin length	5.7 mm
Pin diameter	6 mm
Plunge depth	0.06 mm
Tool tilt angle	0°

Table 3.4 Complete design matrix for the present research work

Exp. No.	Process parameters		
	Tool rotational speed (rev/min)	**Welding speed (mm/min)**	**Shoulder diameter (mm)**
1	600	36	16
2	600	36	20
3	600	36	24
4	600	36	28
5	600	63	16
6	600	63	20
7	600	63	24
8	600	63	28
9	600	98	16
10	600	98	20
11	600	98	24
12	600	98	28
13	600	132	16
14	600	132	20

15	600	132	24
16	600	132	28
17	815	36	16
18	815	36	20
19	815	36	24
20	815	36	28
21	815	63	16
22	815	63	20
23	815	63	24
24	815	63	28
25	815	98	16
26	815	98	20
27	815	98	24
28	815	98	28
29	815	132	16
30	815	132	20
31	815	132	24
32	815	132	28
33	1100	36	16
34	1100	36	20
35	1100	36	24
36	1100	36	28
37	1100	63	16
38	1100	63	20
39	1100	63	24
40	1100	63	28
41	1100	98	16
42	1100	98	20
43	1100	98	24
44	1100	98	28
45	1100	132	16
46	1100	132	20
47	1100	132	24
48	1100	132	28
49	1500	36	16
50	1500	36	20
51	1500	36	24
52	1500	36	28
53	1500	63	16
54	1500	63	20
55	1500	63	24
56	1500	63	28
57	1500	98	16
58	1500	98	20
59	1500	98	24

60	1500	98	28
61	1500	132	16
62	1500	132	20
63	1500	132	24
64	1500	132	28
*65	1100	36	16

* is the repeated experiment of Exp. No. 33

3.6 Test sample preparation

The experiments are conducted as per the design matrix shown in **Table 3.4**. After the completion of the experiments test samples for mechanical and microstructural investigations are prepared. Test sample preparation and results obtained from these investigations are reported in the following paragraphs.

3.6.1 Mechanical testing

This group of test includes destructive testing of welded samples to measure different mechanical properties of the welds. The mechanical properties include UTS, yield strength and percentage of elongation of the joints produced against each welding experiments. One tensile test sample is prepared from the welded plates as shown in **Fig. 3.4**. ASTM E8M standard is adopted for the preparation of the tensile test samples. The gauge length of the samples is 50 mm. A hydraulically operated servo controlled universal testing machine (make: Instron; model: 8801) is used for the tensile testing with a constant progression of 1 mm/min. Tensile testing is carried out at room temperature and UTS, yield strength and percentage of elongation of the joints are measured and furnished in **Table 3.5** against each experimental condition. Stress strain curves for base material and welded samples with minimum and maximum UTS is shown in **Fig. 3.5**.

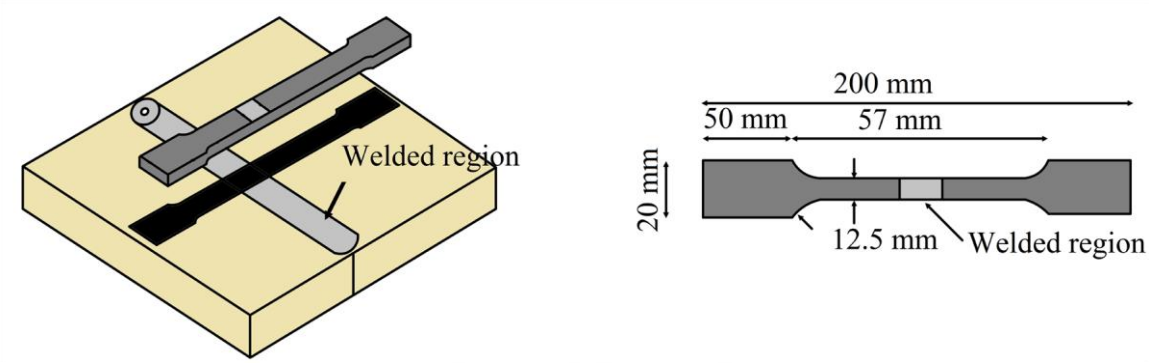

Fig. 3.4 Schematic of tensile test specimen

Table 3.5 Mechanical properties of the joints

Exp. No.	Ultimate tensile strength (MPa)	Yield strength (MPa)	Percentage of elongation
1	94.05	54.32	18.46
2	85.87	46.45	21.68
3	78.56	43.47	11.28
4	65.69	43.10	10.54
5	88.42	59.30	9.4
6	84.64	43.87	23.26
7	88.12	43.85	17.72
8	71.88	43.37	13.26
9	82.45	63.43	11.66
10	85.24	46.04	23.58
11	73.60	46.16	11.14
12	67.55	40.51	11.72
13	95.89	55.58	17.26
14	81.89	45.97	17
15	81.95	44.03	12.606
16	84.09	43.23	20.94
17	92.00	50.93	15.8
18	77.34	48.11	12.66

19	85.48	48.18	12.67
20	80.33	46.36	27.78
21	94.63	53.51	18.4
22	78.22	48.56	10.58
23	83.13	54.25	9.8
24	78.48	42.39	21.14
25	73.87	57.23	6.92
26	77.90	48.93	12.66
27	87.86	42.29	22.84
28	65.74	45.24	9.46
29	88.05	59.85	11.92
30	75.15	49.14	9.54
31	92.62	48.19	22.72
32	77.83	46.95	13.52
33	74.54	55.11	5.72
34	83.45	44.86	22.28
35	76.30	49.87	12.06
36	51.15	36.79	7.06
37	91.86	51.2	19.18
38	82.69	43.07	21.34
39	89.91	45.98	22.72
40	76.12	43.5	23.06
41	81.41	52.81	10.6
42	77.86	41.27	22.86
43	75.35	45.86	9.14
44	79.28	45.98	27.4
45	95.95	55.35	15.12
46	77.55	48.07	10.32
47	63.91	44.06	7.22
48	77.86	41.26	22.86
49	88.42	47.95	16.86

50	64.95	49.77	4.66
51	92.22	54.46	11.4
52	81.08	36.91	27.32
53	92.59	53.72	14.2
54	81.65	41.26	23.26
55	88.92	44.39	23.2
56	68.57	40.63	9.4
57	71.38	60.13	7.26
58	77.17	43.07	13.64
59	87.12	45.37	22.66
60	81.81	38.46	27.52
61	80.29	59.72	8.88
62	83.93	48.09	12.96
63	59.12	43.88	4.92
64	83.64	42.68	21.98
65	69.56	56.44	8.6

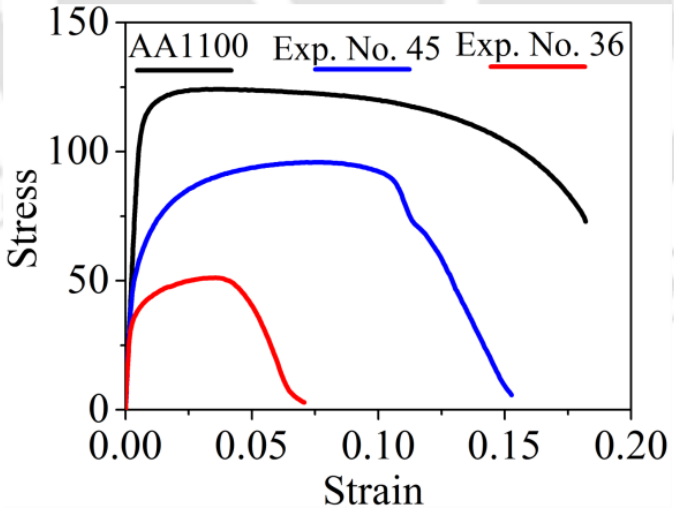

Fig. 3.5 Stress strain curve of welded joints versus base material

The tensile test specimens after the testing are shown in **Fig. 3.6**. The failure for specimen against Exp. No. 45 occurred outside the nugget zone (NZ) whereas the same for

Exp. No. 36 is within the NZ. The weld quality attributes measured from the welded samples are correlated to process parameters to investigate their effect on the weld qualities. **Figure 3.7** represents the variations of UTS, yield strength and percentage of elongation with tool rotational speed, welding speed and shoulder diameter. From the respective figures it is observed that none of the weld quality attributes intelligibly correlated with process parameters. Except few cases no definite conclusions can be drawn for the influence of process parameters on joint qualities.

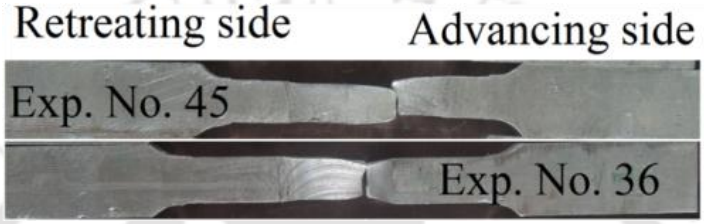

Fig. 3.6 Tensile specimens after tensile test

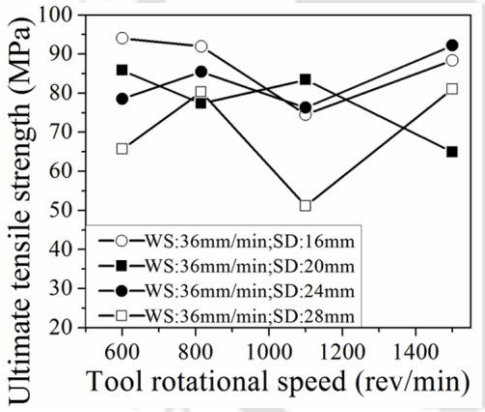

(a)

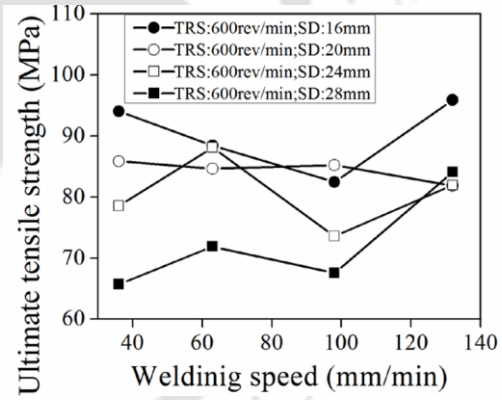

(b)

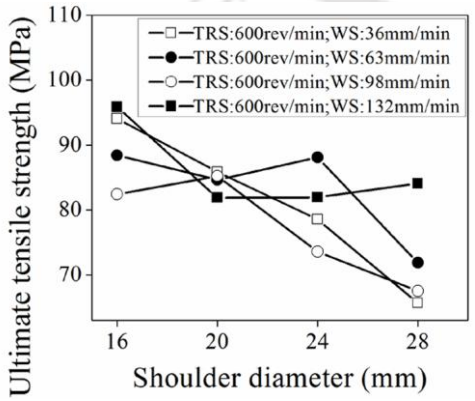

(c)

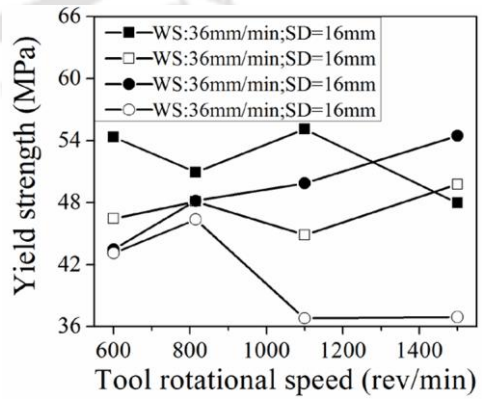

(d)

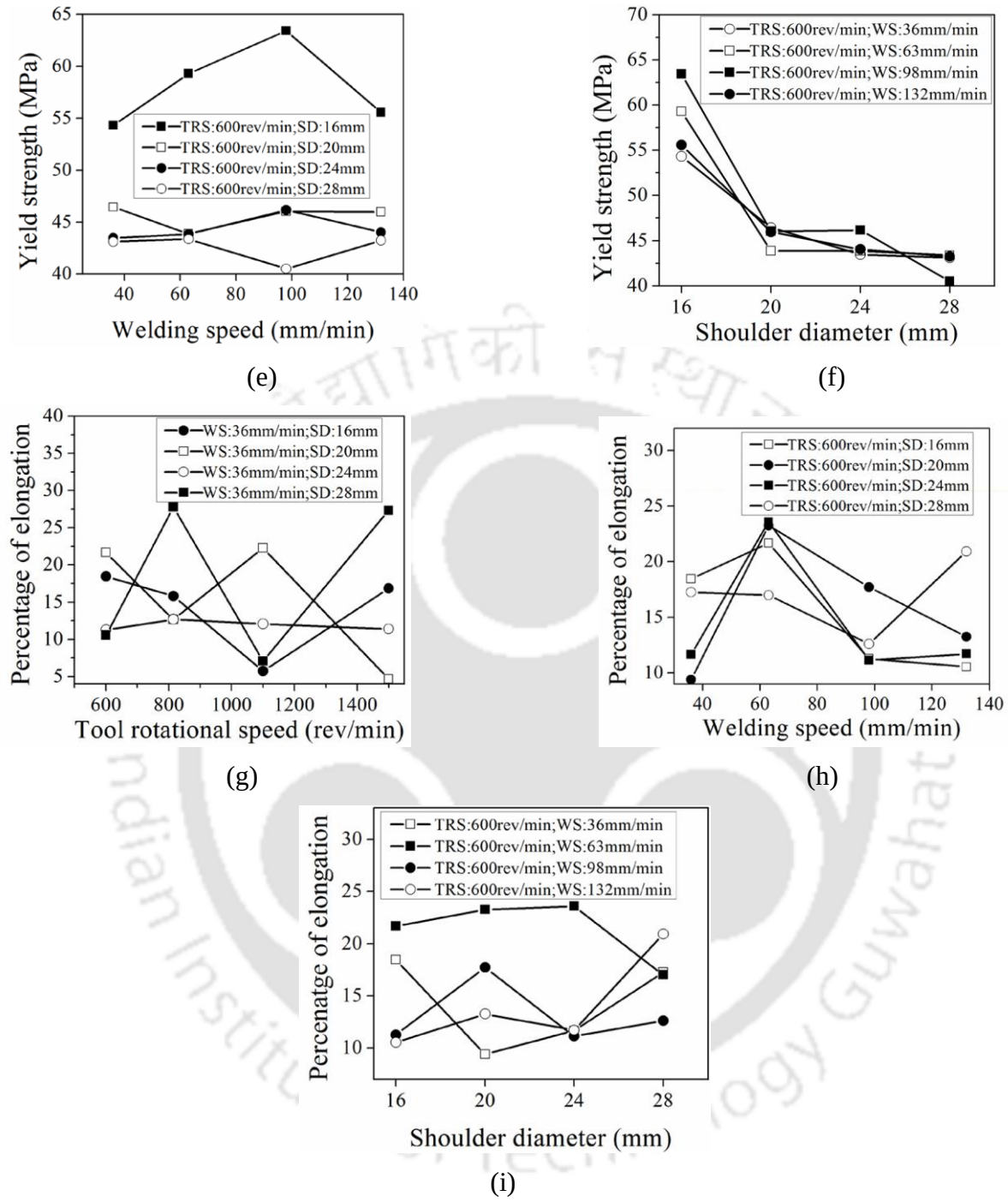

Fig. 3.7 Variation of (a) UTS with tool rotational speed (b) UTS with welding speed (c) UTS with shoulder diameter (c) yield strength with tool rotational speed (d) yield strength with welding speed (e) yield strength with shoulder diameter (f) percentage of elongation with tool rotational speed (g) percentage of elongation with welding speed (i) percentage of elongation with shoulder diameter

3.6.2 Hardness measurement

Test samples for the measurement of micro hardness of the welded samples are prepared with standard procedures. A Vickers's micro hardness testing equipment (make: Omni Tech) with a diamond shaped indenter is used for the measurement. The test is carried in 500 gf loading condition. Measurements are recorded after 2 mm interval from the weld centre line both towards advancing and retreating sides of the weld. The test sample prepared for hardness measurement is shown in **Fig. 3.8** along with the schematic of the process of measurement. Few representative cases are shown for the variation of microhardness in the welded samples in **Fig. 3.9**. From the hardness distribution it is observed that the hardness of weld zone is higher as compared to that of base material. This increase in micro hardness can be attributed due to finer grains at the NZ of the welded samples. Due to dynamic recrystallization in the NZ of the weld because of severe plastic deformation and heat generation due to friction grains at the NZ become finer than grains at the base material. From the comparison of the microhardness distribution of specimens against highest UTS and lowest UTS revealed that weld sample with lowest UTS have comparatively low microhardness values than sample with highest UTS.

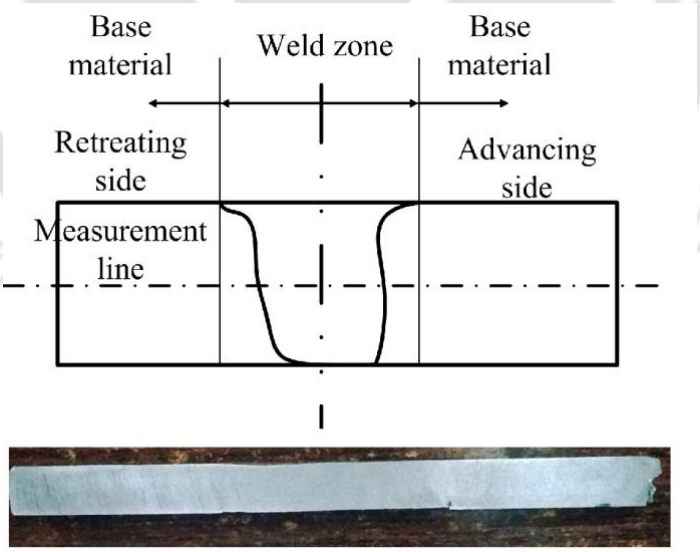

Fig. 3.8 Test sample for micro hardness measurement

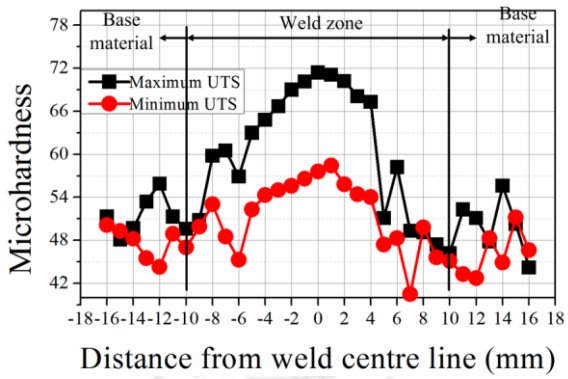

Fig. 3.9 Variation of microhardness

3.6.3 Microstructural investigation

For conducting microstructural investigation test specimens are cut from the welded specimens. The cut specimens are then prepared with standard procedures for the preparation of samples for microstructural observations by polishing with different grades emery papers (600, 800, 1200, 1500) and finally with velvet cloth for mirror like finish. Modified Keller's reagent (distilled water 190 mL, HNO_3 5 mL, HCl 3 mL and HF 2 mL) is used for etching purpose. The sample is dipped into the reagent solution for 15 seconds and then removed from the solution and cleaned with water. After drying the samples are observed under optical microscope (make: Carl Zeiss) at various magnification.

Friction stir welded samples is characterized by different metallographic zones as shown in **Fig. 3.10** such as NZ, thermo mechanically affected zone (TMAZ), heat effect zone (HAZ) and unaffected base material (BM). The NZ is characterized by very fine grains and the average grain size is much smaller than BM. This zone is under extensive effect of both mechanical deformation due to rotating tool and thermal effect due to heat generated during FSW process. During the welding process with combined effect of severe plastic deformation with sufficient heat the grains within NZ undergo dynamic recrystallization process and this result in relatively smaller grains compared to that of base material. Next to NZ is the TMAZ that is characterized by grains with size comparatively higher than NZ but smaller than BM. Apart from the NZ, TMAZ also experiences mechanical deformation and heat effect during the FSW process. However, the recrystallization effect is not as prominent as in NZ and the grains are relatively larger than NZ. Grains in the HAZ are comparatively

smaller than BM but relatively more than TMAZ and NZ. BM is not affected wither mechanically or thermally hence there is no alteration in the grain size and orientation. Microstructures of different metallographic zones of friction stir welded samples are shown in **Fig. 3.11**.

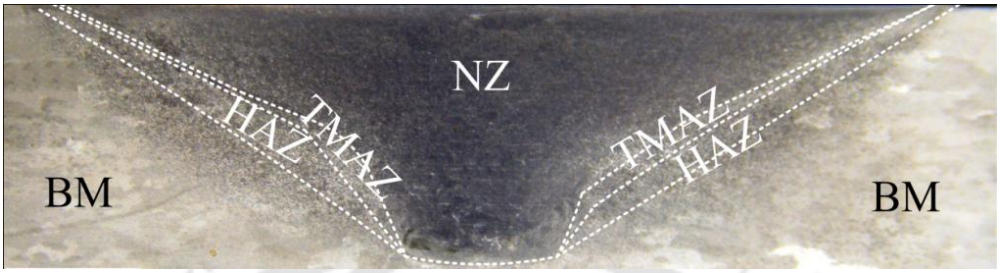

Fig. 3.10 Different metallographic zones in friction stir welded sample

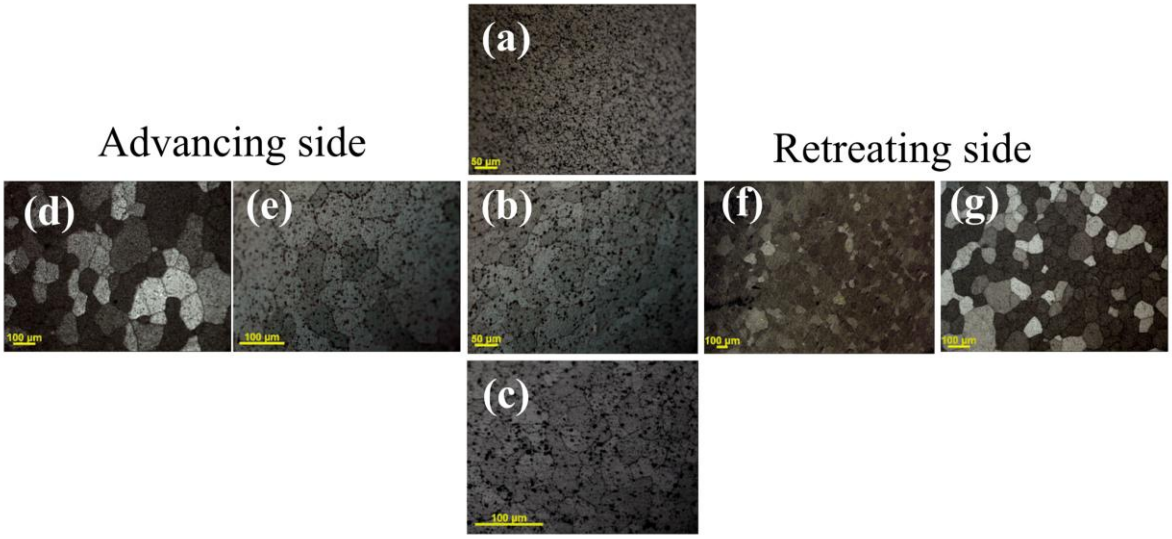

Fig. 3.11 Microstructure of friction stir welded sample (a) NZ at the top (b) NZ at the middle (c) NZ at the bottom (d) HAZ towards advancing side (e) TMAZ towards advancing side (f) TMAZ towards retreating side (g) HAZ towards retreating side

3.7 Signal acquisition

The primary objective of the present research work is to develop methodologies for monitoring of FSW process. In this respect information regarding the process is extracted through acquisition and processing of real time signals during FSW process. As process generated force signals are quite popular among researchers for monitoring of FSW process.

The present work apart from the force signals another few signals are also acquired and processed for effective monitoring of FSW process. These include current signals from motors responsible for generating tool rotational speed and welding speed, tool rotational speed signal of the main spindle where the welding tool is attached and voltage signal from the main spindle motor. Various sensors and data acquisition hardware used for acquisition of these signals are summaries in **Table 3.6**.

Table 3.6 Various sensors used for acquisition of signals during FSW process

Sl. No.	Sensor/Hardware		Specifications
1	Current sensor		Type: Hall Effect Make: Chauvin Arnoux Model: PAC 22 Accuracy: $\leq$ 1.5 % Range: 10 mA – 100 A
2	Current sensor		Type: Hall Effect Make: Tektronix Model: A 622 Accuracy: $\pm$ 3% Range: 50 mA – 100 A
3	Voltage sensor		Type: Differential Make: Metrix Model: MX 9030 Accuracy:$\pm$ 3% Range: $\pm$ 0.1 V $-$ $\pm$ 600 V
4	Tachometer		Type: Laser optical tachoprobe Make: Compact Instruments Model: A2108LSR Accuracy:$\pm$ 0.5% Range: 0 – 60000 rev/min Resolution: 1.5 mV
5	Force measurement setup		Type: Strain Gauge Make: Developed in house Accuracy: F_Z = 1.27 % F_Y = 1.06 % Torque = 0.96 % Range:

			F_Z = 15 kN F_Y = 5 kN T = 40 N-m
6	Data acquisition hardware	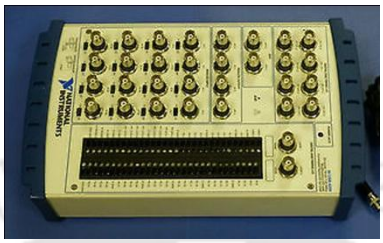	Type: Voltage measurement Make: National Instruments Model: NI-USB-6259 BNC Range: ±0.1 V - ± 10 V Max. sampling frequency: 1.25 MHz (single channel) 1.21 MHz (Multiple channel) Processor: 16-bit No. of input channel: 16

Information regarding FSW process to observe in process behavior is attempted through acquisition of seven real time signals integrating various sensors and data acquisition hardware as depicted in **Table 3.6**. To start with in **Fig. 3.12a-c** vertical force signal, transverse force signal and torque signal acquired using the developed force measurement setup is shown. The FSW process is characterized by four salient states during the process. This includes plunging of the rotating tool, dwell time, welding period and retraction of the rotating tool. All the stages have salient influence on the process and hence on the quality attributes of the joints. Effect of these four stages can be prominently seen in the vertical force signal as shown in **Fig. 3.12**. However, effects of these stages are not appreciably captured in the transverse force signal and torque signal as represented in the respective figure. In **Fig. 3.13** current signal acquired from main spindle motor is represented. This signal also bears the signature of salient stages occurred during FSW process as captured by vertical force signal. However, current signal acquired from the welding speed motor could not capture salient information regarding the welding stages occurred during FSW process. The full view of welding motor current signal is shown in **Fig. 3.14**. Tool rotational speed signal acquired with the non contact laser tachometer is represented in **Fig. 3.15**. From the respective figure it is observed that as like in vertical force signal and main spindle motor current signal salient stages involved in FSW process is

also captured by tool rotational speed signal. **Fig. 3.16** represents full view of voltage signal acquired during FSW process. This signal is found to be irrelevant in monitoring of FSW process as it does not capture any information regarding the welding process at any combination of process parameters. Hence, this signal is not processed further in this research work for developing methodologies for effective monitoring of FSW process.

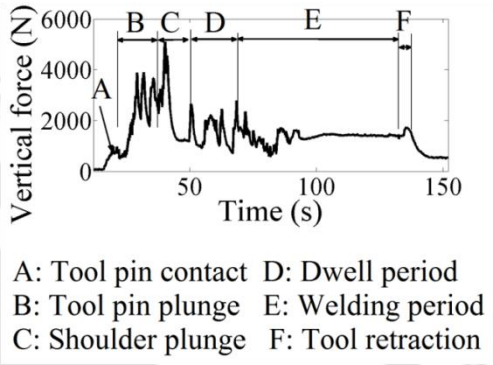

(a)

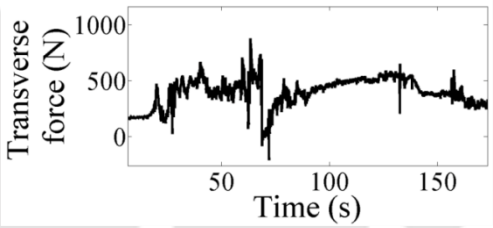

(b)

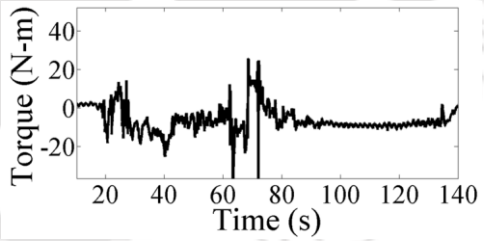

(c)

Fig. 3.12(a) Vertical force signal (b) transverse force signal (c) torque signal

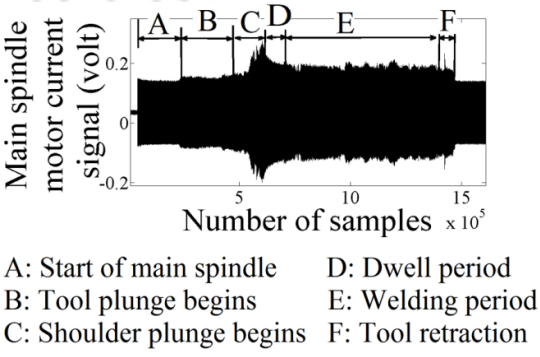

Fig. 3.13 Main spindle motor current signal

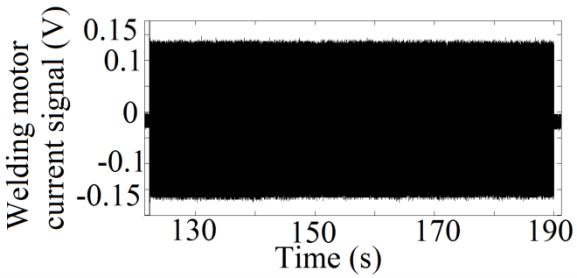

Fig. 3.14 Welding motor current signal

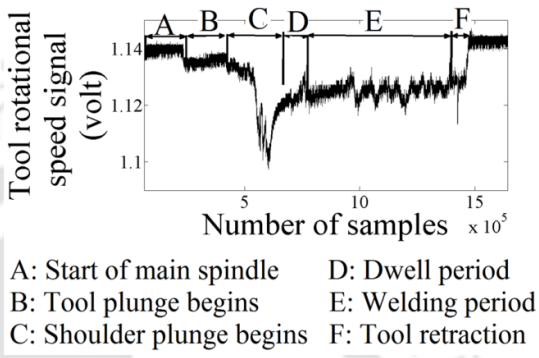

Fig. 3.15 Tool rotational speed signal

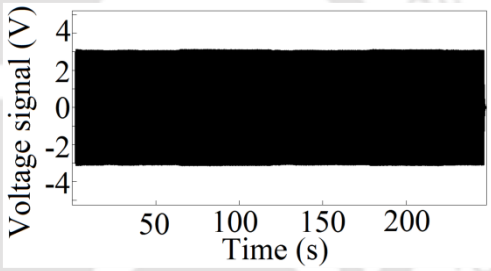

Fig. 3.16 Voltage signal from main spindle motor

3.8 Summary

This chapter outlines different procedures adopted for conducting the welding experiments along with different post processing steps for measurement of weld qualities of the welded samples. This chapter also highlights different sensors used in the current research work for real time acquisition of signals during FSW process. Out of seven process signals acquired during FSW process vertical force signal, transverse force signal, main spindle motor current signal and tool rotational speed signal found to have intelligible information regarding the in process behavior. The summary of the chapter is as follows.

- UTS, yield strength and percentage of elongation do not show any definite trend with tool rotational speed, welding speed and shoulder diameter.

- From microstructural investigation of the welds it is observed that grains at the NZ are finer compared to base material.
- Micro hardness distribution of the welded specimens revealed that hardness of weld zone is higher as compared to base materials. This increase in hardness can be attributed due to the finer grains at the NZ compared to base material.
- The visual observation of main spindle motor current signal and tool rotational speed signal brings the notion that these signals carry salient information regarding the process apart from vertical force signal. Efficient extraction of features from these two signals will lead to possible alternate for vertical force signal in monitoring the FSW process. Voltage signals of main spindle does not offer any intelligible information regarding the process as the acquired voltage is the line voltage.

Chapter 4

Design and development of force and torque measurement setup

4.1 Introduction

In the process of FSW three forces and torque system is experienced. These three forces are termed as vertical force or plunging force, transverse force and lateral force. Among these forces lateral force is found to be less significant in governing the process (Arora et al., 2012). Vertical force maintains the downward contact between the tool and the workpiece which is essential for generation of heat due to friction. This force is experienced by the tool in order to overcome the resistance offered by the workpiece material. Transverse force comes into existence due to movement of the tool along the welding line. The material ahead of the tool offers resistance to the tool and to overcome the tool applies a reaction force termed as transverse force. The direction of this force is perpendicular to the plane of vertical force. In the research of FSW, these two forces draw immense attention in understanding and controlling the process behavior. Apart from forces, FSW system also experience torque. This is the reaction force applied against the resistance offered by the material around the rotating tool. This in turn governs the rotation of the tool and has influence over welding process. In order to measure forces and torque various measurement systems are available with advantages and disadvantages. A detailed discussion on various force and torque measurement setup has been discussed in the literature review chapter (Section 2.5). The need for development of forces and torque measurement setup has been realized in FSW process witnessing the various limitations with the existing systems. One of the major limitations

of the available systems is high cost. Development of a low cost measurement system dedicated for FSW process without compromising the reliability and accuracy is one of the objectives for the current research work.

4.2 Design and construction of the developed setup

In Dynamometer design sensitivity, elasticity, rigidity and accuracy of measurement should be taken into consideration (Korkut at al., 2003). Selection of proper strain gauge is essential in accurate measurement of strains, which is correlated to measure the actual force (Younis and Kang, 2011). A metallic strain gauge consists of a very fine wire or, more commonly, metallic foil arranged in a grid pattern. This works on the principle that when a metallic wire changes its length, its resistance changes. This change in resistance is a quantitative index for the measure of the applied force. Strain gauge sensitivity is expressed in terms of gauge factor (GF). The GF can be quantitatively described as the ratio of the fractional change in the electrical resistance to the fractional change in the length or the strain experienced by the strain gauge (Ng and Wey, 1997). Mathematically, GF can be expressed by the relation represented in **Eq. 4.1**. Other relevant properties of the strain gauge used in this study are reported in **Table 4.1**.

$$GF = \frac{\Delta R/R}{\Delta L/L} = \frac{\Delta R/R}{\varepsilon} \quad (4.1)$$

where, L is the length of the wire and R is the resistance of the wire, ΔL and ΔR represents the change in L and R respectively.

Table 4.1 Variousproperties of strain gauge used for force measurement

Type	**Metal foil TT type**
Material	Constantan (55% copper, 45% Nickel)
Gauge length	10 mm
Resistance	350 Ω
Gauge factor	2.12
Specific resistance	500 nΩ.m
Maximum operating temperature	630℃
Ultimate elongation	1.0 %

Apart from the strain gauge, a force measurement setup contains ring member also referred as elastic members (Mitchel et al., 2002). These members provide a platform for attaching the strain gauges for the measurement of strain and hence the external force. In general, force measurement involves measurement of deflection with precise calibration between the applied force and the deflection produced by the application of the force (Karabay, 2007a). External force is actually experienced by these members and conveyed to the strain gauges attached to it. Selection of material and design of ring members should be based on rigidity, natural frequency, corrosion resistance, heat conductivity, deformation behaviour under loading conditions etc. Keeping these characteristics of the ring member, material for the members used is mild steel. Among various types of ring members, octagonal ring member satisfies the above criteria (Korkut, 2003; Yaldiz, 2007; Unsacar and Yaldiz, 2006; Karabay, 2007b). Therefore, bending type of octagonal ring is used as the ring members for attaching the strain gauges. The induced strain sensed by the strain gauge is converted to voltage output using Wheatstone bridge circuit formed by connecting different strain gauges.

Along with ring members, other parts of the developed force measurement setup are top plate, bottom plate, signal conditioning circuitry and acquisition hardware. Top and bottom plates are used to house and position the ring members with increased rigidity. The developed setup is capable of measuring two main forces (vertical and traverse) associated with FSW process along with torque. Design description of each component is given in the subsequent paragraphs followed by the finite element analysis of the ring member.

Top plate of the developed force measuring system is chosen to be 25 mm thick for high rigidity of the overall setup and to avoid permanent deformation during repeated welding operations. It is assumed that the top plate material is rigid and there is no elastic deformation of the material. The load experiences by the top plate will be completely transferred to the octagonal ring member. The thickness of the bottom plate is kept 10 mm as this will not affect the functioning of the developed setup. The other two dimensions of both top and bottom plates are 400 mm each. Mild steel is the material used for fabricating both top and bottom plates. Provisions on the top and bottom plates are made for mounting the ring members.

The bending type octagonal ring member selected in this study is schematically shown in **Fig. 4.1**. Dimension of each side of the octagonal ring is assumed to be 24 mm. The other design parameters of octagonal ring are the thickness and width of the ring. For designing the ring members it is assumed that the material is homogeneous and there is no plastic deformation of the material used for developing the ring members. Different combinations of design parameters are analyzed for its rigidity under different loading conditions using finite element analysis. After many trials, suitable design specifications are obtained for the octagonal ring and shown in **Fig. 4.1**. The analytical results are again verified by theoretical calculations for the thickness and width of the ring as available in relevant article (Beer et al., 2010) and found good match in the dimensions. With the dimensions obtained for ring member, stress values (for a maximum load of 10 kN in vertical direction and 5 kN in transverse direction) are computed as per the equations used by Korkut(2003). Computed stress values are within the safety limits of the material (mild steel) considered for the fabrication of ring members. Hence, the design for the ring member is safe for real time application. A total of four such octagonal ring members are fabricated to be used in the developed setup.

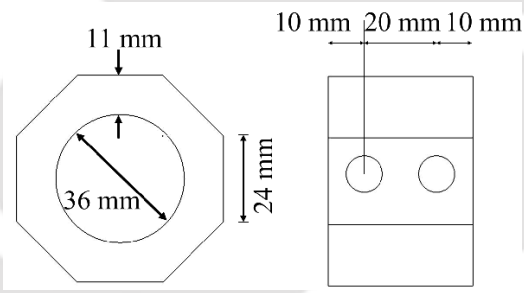

Fig. 4.1 Schematic of the octagonal ring member

4.3 Finite element analysis of the octagonal ring member

Finite element (FE) analysis is used to investigate the behavior of octagonal ring member under different loading conditions. This is firstly used to determine the optimal dimensions of the octagonal ring replicating the actual environment to be experienced by each member during welding operations. Secondly, FE analysis is carried out to find the optimal locations on the ring members for the attachment of the strain gauges. This analysis helped to study the effect of different loading conditions for its cross sensitivity on different faces of the ring members.

For the FE analysis, only one member is chosen and different loading environments are created in commercially available FE analysis package ABAQUS. The member with the obtained design dimensions is replicated in the software package and made to experience three different loading conditions viz. pure vertical force, pure transverse force and torque. The member is also analyzed under all these loading conditions collectively to investigate the behaviour under simultaneous exposure of forces and torque as experienced during actual welding condition. **Fig. 4.2** summarizes the results obtained from the FE analysis.

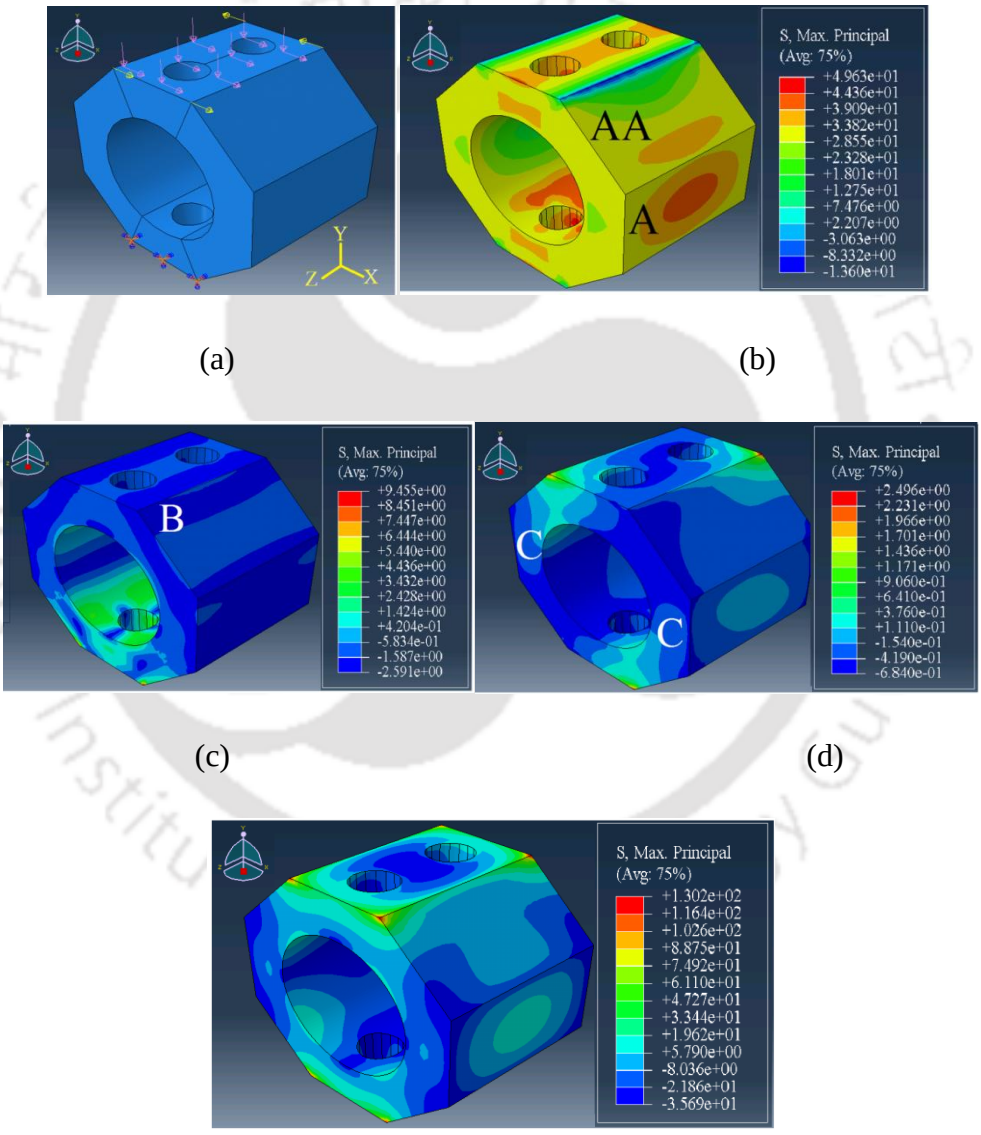

Fig. 4.2 FE analysis of the octagonal ring member (a) loading conditions (b) pure vertical force (c) pure transverse force (d) pure torque (e) all loads applied simultaneously

Behaviour of the octagonal ring member under pure vertical force is shown in **Fig. 4.2b** whereas direction of the applied force can be seen in **Fig. 4.2a**. A maximum of 5 kN force is applied to the ring member. From the respective figure, it is observed that maximum stress is generated near the provisions made for fixing the member to the top and bottom plate. But these regions are not feasible for attaching strain gauges, hence neglected. Next higher value of stress is observed in the face marked as 'A' in **Fig. 4.2b**. Due to the symmetry of the octagonal ring member, the face opposite to the face 'A' also experiences the same stress value. The maximum stress generated is 44.36 MPa. Apart from these two faces, the inner faces of the octagonal ring member also experience stress value of 28.55 MPa. Thus, these four faces of the ring member are selected for fixing the strain gauges responsible for the measurement of vertical force during welding operation. It is to note that the face marked as 'AA' also experiences appreciable stress values during vertical loading condition. This indicates the cross effect of the vertical force on the other faces, which are available for fixing strain gauges to measure other forces. This necessitates investigating the cross sensitivity effect of the forces on each other. However, the stress values generated on rest of the faces of the ring show lower values hence neglected for vertical force measurement.

A pure transverse force of magnitude 5 kN along x-direction (refer **Fig. 4.2a**) is applied to the octagonal ring member. The result of the analysis can be seen in **Fig. 4.2c**. It can be observed from the figure that as compared to the stress generated due to pure vertical force, stress generated due to pure transverse force is much lower. In this case also the maximum stress is generated near the holes kept for bolting the member to the bottom plate of the developed setup. This region is not feasible for mounting strain gauge and hence neglected. The next higher stress value is observed in the face marked as 'B' in **Fig. 4.2c**. This face experiences a stress value of -1.58 MPa. This face is selected for the installation of the strain gauges responsible for measuring transverse force.

Figure 4.2d represents the analysis result for pure torque condition. A maximum of 100 N-m torque is applied to the ring member about y-axis (refer **Fig. 4.2a**). In this analysis, the faces already selected for vertical and transverse force measuring strain gauges show higher stress values. Apart from these faces, faces marked as 'C' also shows considerable stress values. A maximum of -0.41 MPa is obtained from the analysis. Here also, these faces are highly affected during vertical force application but as no other feasible face is left for installation of strain gauge for measurement of torque,

these faces are selected for the strain gauges. Similar strategy as applied to adjust the effect of vertical force applied in transverse loading condition is applied to minimize the effect of vertical force in measurement of torque too.

All the three loading conditions viz. vertical loading, transverse loading and torque are simultaneously applied to the octagonal ring member to study its behaviour under combined loading as it will be experienced during actual welding condition. The result of the analysis is shown in **Fig. 4.2e**. It is observed from the figure that the faces selected for installation of strain gauges for measurement of vertical force, transverse force and torque show appreciable stress values but somewhat lesser than the pure loading conditions. This analysis gives an idea for the selection of faces in the ring members for the installation of strain gauges for accurate measurement of respective forces and torque. The faces so selected based on FE analysis for the measurement of vertical and transverse force as well as torque is in fair agreement with the faces justified by Karabay (2007b) in a similar ring member for similar loading conditions.

4.4 Strain gauge installation and orientation of ring member

Once the faces are selected for the installation of strain gauges, the respective faces are prepared for the installation. Installation of strain gauge requires special care so that it can sense the strain accurately. Selected faces of the octagonal ring member are mirror polished and cleaned to make it free from any oxides or other impurities. Then with industrial glue (Cyanoacrylate adhesive), strain gauges are fixed in the respective locations of the elastic member as indicated by the results from FE analysis. To protect it from the environment which may affect the gauge stability, silicon rubber coatings are applied above the strain gauges.

The strain gauges are installed in the respective faces of each member as shown in **Fig. 4.3a**. It can be seen from the figure that, strain gauges are distributed over all the members for the measurement of forces as well as torque. This distribution of the strain gauges is made keeping the orientation of the members in the developed system at particular arrangement as shown in **Fig. 4.3b**. This specific arrangement of octagonal members will make the developed setup independent of point of load application. Vertical force will affect all the members, so it is decided to install strain gauges for the measurement of vertical force in all four members in the feasible faces selected through FE analysis. Effect of transverse force would be more prominent in the members A and

C. So, strain gauges for measuring this force are mounted on the faces selected for transverse force. As per the arrangement, torque will also have effect on all the four members, so as like in vertical force, strain gauges for measuring torque is also distributed over all the four members. As can be seen from **Fig. 4.3a**, strain gauges indexed as 5, 6, 7, 8, 9, 10, 11, 12 are responsible for measurement of vertical force, 1, 2, 3, 4 are responsible for transverse force measurement and 13, 14, 15, 16 are responsible for torque measurement.

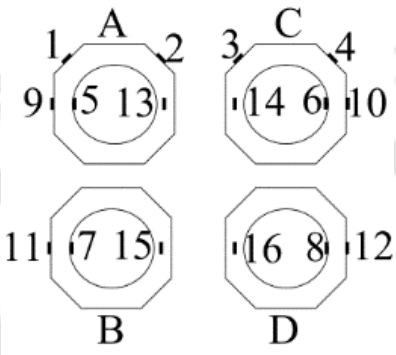

(a)

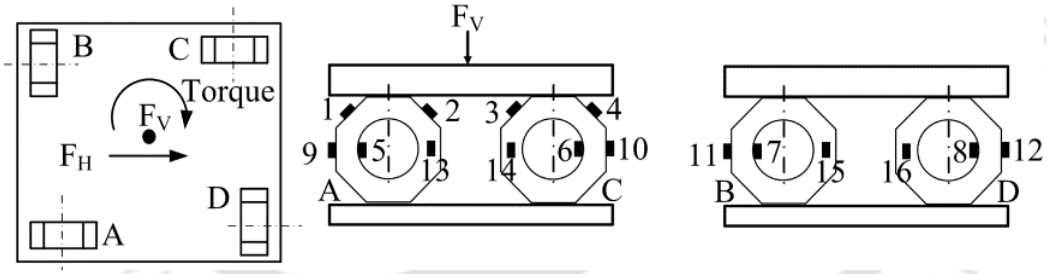

(b)

Fig. 4.3 (a) ring members with strain gauges (b) orientation of the ring members in the setup

The strain gauge arrangement as shown in **Fig. 4.3a** is connected to form Wheatstone bridge circuits for the conversion of measured strain values to voltage output. Using these circuits the measured strain by the strain gauges can be converted to voltage which can easily be acquired using data acquisition system in real time.

4.5 Data acquisition, amplification circuit and natural frequency of the setup

For measuring the force during actual FSW operations, force signals need to be acquired automatically with the help of necessary acquisition hardware and software. A

typical data acquisition system consists of transducer(s), signal conditioning circuitry and appropriate acquisition hardware for acquiring and storing the data into a digital computer. Strain gauges will act as transducers for the measurement of force signals. Signal conditioning system will amplify the circuit voltage to the range of the acquisition hardware. In the present study, dedicated data acquisition hardware (NI-USB-6259) is used for the measurement of voltage signals. This system has a resolution of 16-bit with maximum possible sampling frequency of 1.25 MHz and 16 analog input channels. It has maximum working voltage range of ±10 V. For interfacing a personal computer with the data acquisition hardware, MATLAB code was developed in house for storing and processing the data. Further, the signals acquired were filtered by developing a fifth order Butterworth filter in MATLAB environment with normalised cut off frequency of 0.001.

Amplifier increases the power of a signal using an external power supply (Gayakwad et al., 2005). The schematic of the developed amplifier circuit for the present case is shown in **Fig. 4.4.** The developed amplifier circuit works on ±5V dual power supply. As shown in the circuit, LM7805 is the voltage regulator used to supply +5V and LM7905 is used to supply -5V. Voltage regulators were used to supply uninterrupted and constant voltage supply to the amplifier IC and Wheatstone bridge circuit. INA122 PA was the amplifier IC used for the amplification. A gain resistor R_G can be varied in the **Eq. 4.2** to obtain different value of gain (G) for different level of amplification.

$$G = 5 + \frac{200k\Omega}{R_G} \qquad \textbf{(4.2)}$$

For the measurement of vertical and transverse forces and torque, individual amplifier circuits are fabricated. These circuits were kept in aluminium foil boxes to reduce the effect of surrounding noise. Moreover, electronic circuits are shielded using aluminum foil to minimize the noise due to electromagnetic interference, i.e., signal loss or gain is zero. From the FE analysis, issue of cross sensitivity due to one loading condition on other is witnessed. The effect of cross sensitivity is controlled by manipulating the overall gain of the respective circuits used for the measurement of vertical, transverse forces and torque. The R_G values are adjusted to obtain suitable gain for each amplification circuit so that cross effect of other loading directions can be minimized.

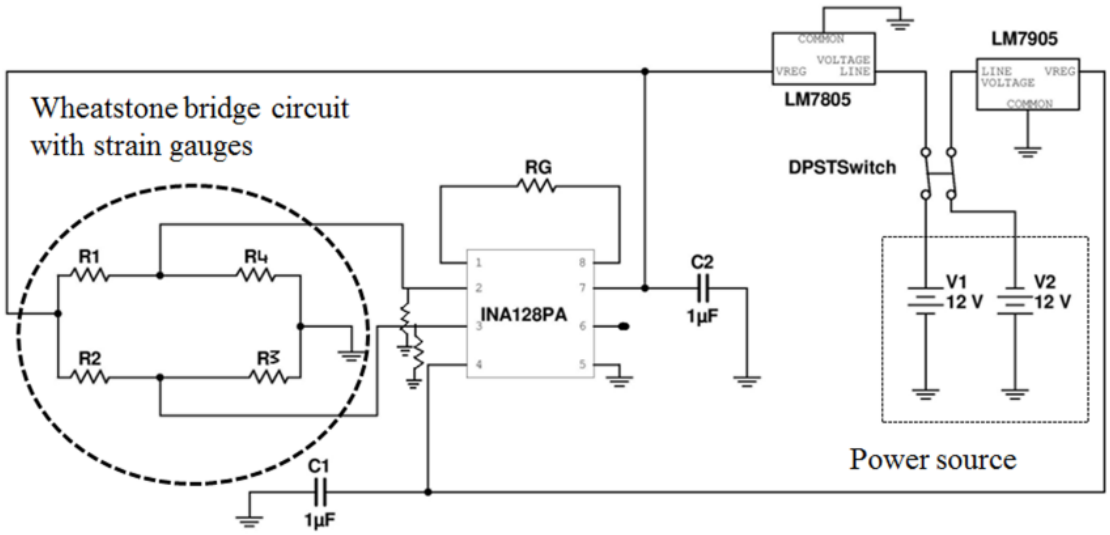

Fig. 4.4 Schematic of the amplifier circuit

Natural frequency of a system is the characteristics which can describe the performance of the system under dynamic operating conditions. The developed setup should have natural frequency at least four times the frequency of the machine tool (Korkut, 2003; Karabay, 2007b). Machine tool vibration frequency is related to the rotational speed of the spindle. The present setup can be treated as a mass supported by ring elements for analytical purpose. For a thin circular ring, the stiffness value K is given by the relation given as **Eq. 4.3**.

$$K = \frac{F_v}{\delta_v} = \frac{Ebt^3}{1.8r_1^3} \tag{4.3}$$

where, F_v is the vertical force applied, δ_v is the strain under load, E (≈ 210 GPa) is the elastic modulus of the material of the setup, b (≈ 40 mm) is the width, t (≈ 11 mm) is the thickness and r_1(≈ 18 mm) is the inner radius of the octagonal ring. Upon substitution of all the relevant data, we found out stiffness value $K$to be 1.065×10^9 N/m. Thus, the natural frequency of the developed setup can be computed using **Eq. 4.4** as follows

$$f_d = \frac{1}{2\pi}\sqrt{\frac{K}{m}} \tag{4.4}$$

where$m$ is the mass of the setup which is approximately 45 kg. This gives the natural frequency of the setup to be ~775 rev/s (~46457 rev min^{-1}). For the system to be stable, this frequency should be at least four times the frequency of the machine i.e., $f_d \geq 4\, f_m$,

where f_m is the frequency of the machine. So, using this f_m is found out to be ~11615 rev min^{-1}. Which is quite acceptable as the maximum spindle speed of the machine is 1500 rev min^{-1}. Moreover, from **Eq. 4.3** deformation δ_v under a load of 15 kN can be found as 0.014 mm. Maximum elongation limit of the strain gauge used is 1% of 10 mm i.e., 0.1 mm, which is more than the maximum elongation at a load of 15 kN, which is much higher than actual welding force.

4.6 Calibration and comparison of developed setup

Set of calibration experiments are performed using the developed force measurement setup to obtain a mathematical correlation between the acquired voltage and actual force/torque values. The setup is tested on a universal testing machine under a maximum vertical load of 15 kN and maximum transverse load of 5 kN in the steps of 0.5 kN. Against each loading condition, voltage output from the developed setup is recorded. From the recorded data, least square linear regression equations are obtained which will be used to convert the voltage data to the actual force/torque data. In order to verify the repeatability of the developed setup, each experiment is repeated three times and in each case the voltage output is found to be in the range of ±1%. Moreover, the developed setup is designed to be independent of point of load application. For testing this, known load on different point on the setup is applied and voltage values are recorded. The values so obtained are well within ±0.01% about the mean value when loaded at the center of the setup. Cross sensitivity imparts difficulties in immediate interpretation of the acquired data. In all the cases, the cross sensitivity are found to be less and hence ignored. All the data during calibration are acquired using the data acquisition system under MATLAB environment at sampling frequency of 10 kHz.

A known vertical force is applied to the developed setup and corresponding voltage output is recorded. The calibration curve for the applied vertical force versus the setup voltage output is shown in **Fig. 4.5** which also shows the effect of vertical force on transverse force and torque. Due to the vertical loading, cross sensitivity observed in transverse force is 0.01% and the same for torque is found to be 0.001%. This shows that the effect of vertical loading is not bringing appreciable change in transverse and torque measurement. The mathematical relation correlating the output voltage and actual vertical force is shown as **Eq. 4.5**. The coefficient of determination (R^2) found to be

0.99. Thus, this equation can be used for real time measurement of the force during actual welding operation.

$$Voltage(V) = 0.0907 \times Force(kN) - 0.0169 \quad \textbf{(4.5)}$$

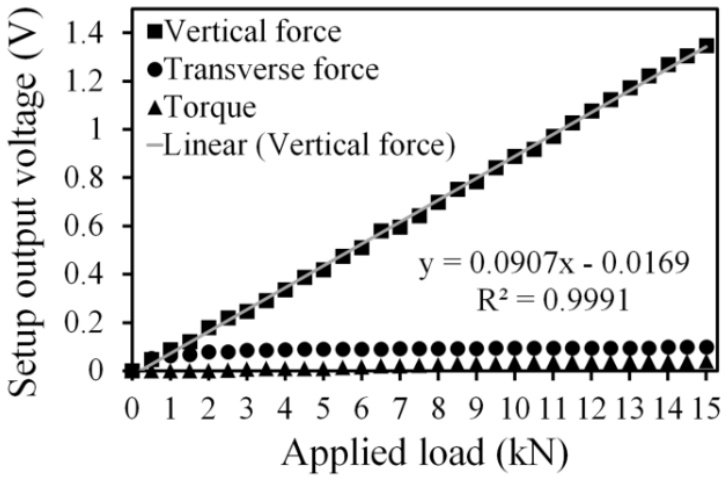

Fig. 4.5 Calibration result of vertical force with its cross sensitivity

The universal testing machine used for the calibration of vertical force cannot provide transverse force to the developed system directly. For this, the developed setup is kept at an angle of 30° with the horizontal base of the testing machine. To apply a maximum load of 5 kN in steps of 0.5 kN to the developed setup, from simple trigonometric calculations actual load values are computed that need to be applied by the universal testing machine. The acquisition procedure of voltage from the developed setup is same as used during vertical force calibration. The results of the calibration are given in **Fig. 4.6** and the mathematical correlation between the transverse force and acquired voltage is given in **Eq. 4.6**. Cross sensitivity of transverse loading on vertical force and torque are found to be 0.003% and 0.00034%. Thus, transverse loading is not affecting the other two measured quantity and the measurement is reliable. This is essential as during actual welding condition the setup will experience forces and torque simultaneously and should measure the individual component effectively.

$$Voltage(V) = 0.1385 \times Force(kN) + 0.0108 \quad \textbf{(4.6)}$$

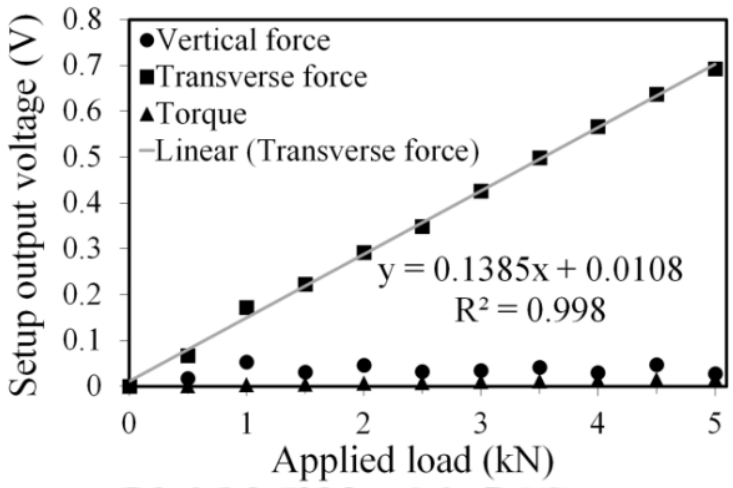

Fig. 4.6 Calibration result of transverse force with its cross sensitivity

The developed setup is calibrated for vertical and transverse force as described in the aforementioned paragraphs. But, the same approach cannot be implemented for the calibration of the torque due to the limitation in loading conditions and structure of the setup. Thus, torque is calibrated in the actual welding environment comparing the data with a piezoelectric device based dynamometer (make: Kistler; model: 9272) data. Five different experiments are performed by varying tool rotational speed and shoulder diameter which contributes most towards torque in welding. The calibration result is shown in **Fig. 4.7**. The dynamometer data is plotted against the voltage generated by the developed setup and linear regression analysis was carried out to find the best fit straight line (**Eq. 4.7**). The coefficient of determination obtained is 0.97 which is quite acceptable. The following equation is used to convert the setup voltage to actual torque for real time welding operation. As torque is calibrated in actual welding environment its cross-sensitivity cannot be tested as like in vertical and transverse loading conditions. To investigate its cross-sensitivity, manually a torque was applied to the setup keeping the bottom plate fixed to the base of the universal testing machine used for other calibration purpose. This is repeated many times and corresponding voltage output against vertical and transverse force is recorded. From all the cases, an average of 0.03% and 0.04% cross sensitivity is observed for vertical and transverse loading respectively.

$$Voltage(V) = -0.0028 \times Torque\ (Nm) + 2.7001 \qquad \textbf{(4.7)}$$

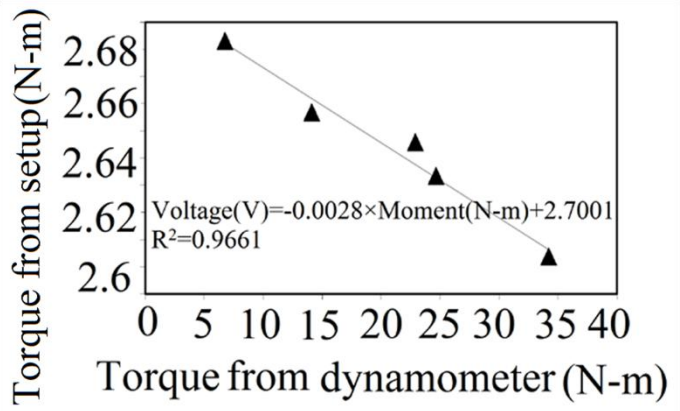

Fig. 4.7 Torque calibration curve

The developed setup is tested for two directional forces (vertical and transverse) and torque measurement with piezoelectric based dynamometer (make: Kistler; model: 9272). The testing arrangement is shown in **Fig. 4.8**. This system has a working range of – 5 to + 20 kN in vertical direction and ± 5 kN in other two directions with a range for torque as ± 200 N-m. The comparison results for the developed setup with the dynamometer are shown in **Fig. 4.9(a) – (c)**. From the figures, a good match in the trend as well as in the magnitude for all loading directions was observed. The accuracy of the developed force/torque measurement setup has been found to be 1.27%, 1.06% and 0.96% for vertical force, transverse force and torque measurement respectively. This is quite acceptable for implementation of the developed setup in real time force measurement during FSW process.

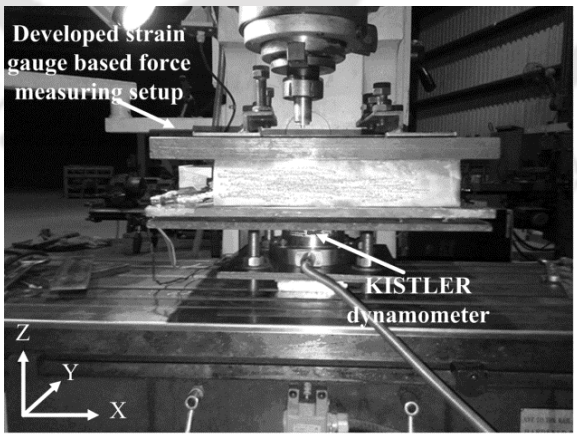

Fig. 4.8 Testing arrangements for comparison of developed setup and piezoelectric based dynamometer

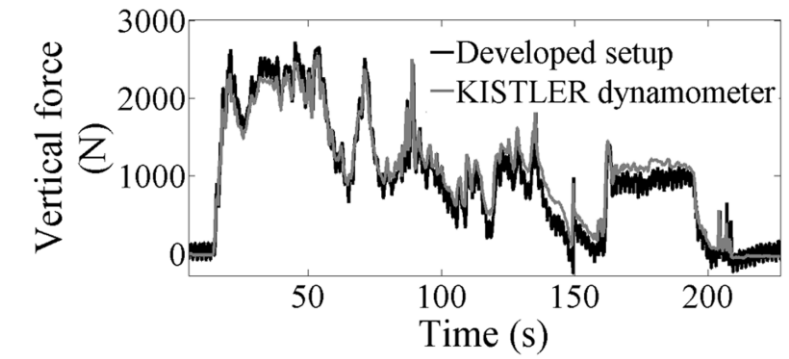

(a)

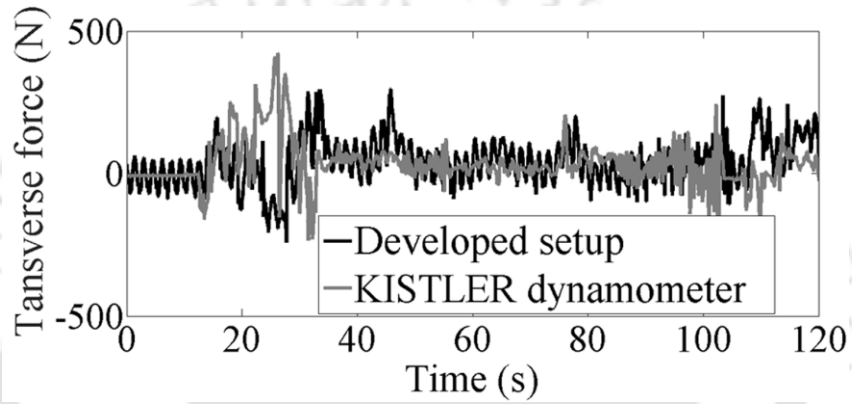

(b)

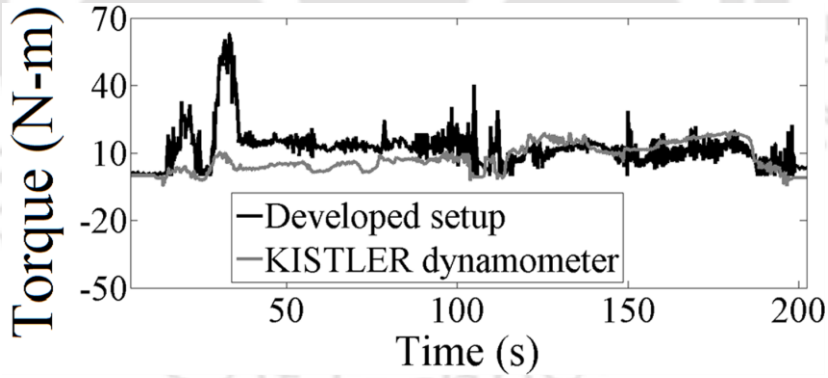

(c)

Fig. 4.9 Comparison plots between setup data and dynamometer data (a) vertical force (b) transverse force (c) torque

4.7 Real time welding results using the developed setup

The developed force measurement setup is tested for real time welding conditions. For conducting the welding experiments, a converted milling machine is

used. The reported results herewith is for tool rotational speed of 815 rev min^{-1}, welding speed of 98 mm min^{-1}, shoulder diameter of 16 mm and with a constant plunging depth of 0.12 mm. **Table 4.2** summarizes the results of the real time welding force data. Different force signals during actual welding operation are shown in **Fig. 4.10(a)–(c)**. The trend of the force and torque signals furnished in this research article found a fair agreement with the trends of the same signals reported in relevant articles (Su et al., 2013; Cavaliere et al., 2006; Trimble et al., 2012). The FSW process is characterized by few salient stages during welding process that includes pin plunge, shoulder plunge, dwell period and welding period. The vertical force signal as shown in **Fig. 4.10a** represents each stage effectively. In the signal initial 50 seconds represents idle time. A sudden increase in force magnitude is experienced after 50 seconds and it is due to the sudden contact of the pin of the rotating tool with the workpiece material. This increase continues till the pin plunges into the workpiece and the force magnitude rises up to around 2.5 kN. The continuous increase in the force magnitude is due to the resistance offered by the material in the tool. After this period a stable force period is seen characterized by the plunging period. In this period the force magnitude does not experience notable increase in force magnitude. During the plunging period considerable amount of heat is generated that soften the material around the tool and resistance offered by the material reduces and the reduction is characterized by sudden decrease in force magnitude up to 1.5 kN at around 150 seconds. After this period again a sudden rise in force magnitude is observed that continues up to around 4.5 kN. This sudden increase in force magnitude is attributed due to contact of tool shoulder with the workpiece. The diameter of shoulder is much higher compared to that of tool pin hence resistance offered is also higher resulting is peak force magnitude. This period continues till a drop is observed at around 200 seconds. Due to sufficient heat generated because of the friction between shoulder and workpiece materials gets soften and resistance reduced. This period is followed by dwell period of around 20 seconds signifies by further reduction in force magnitude due to adequate heat generation and sufficient material plasticization. This period is followed by welding period that is characterized by a stable force magnitude of around 4.3 kN on average. The starting of welding period at 220 seconds is characterized by a sudden increase in force magnitude of around 5 kN and is due to the sudden travel of rotating tool along the joint line. The end of welding period is characterized by continuous decrease in force magnitude due to retraction of the tool pin and reduces to zero at the point where the tool is completely retracted from the

workpiece. Thus, vertical force signal effectively capture each and every event occurred during the welding process. Unfortunately, torque signal does not offer such details as captured through vertical force signal.

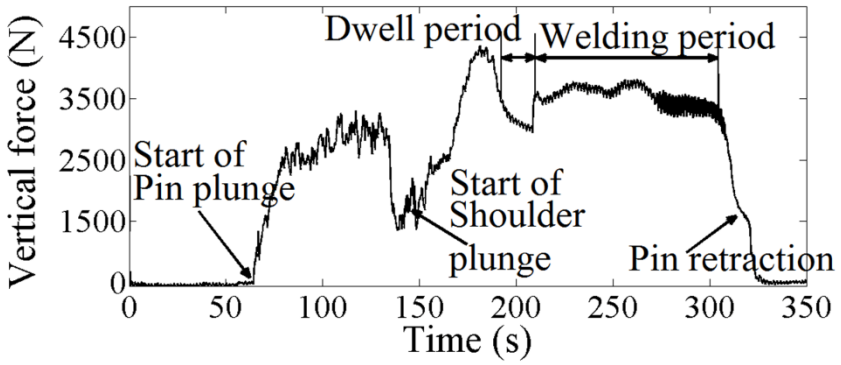

(a)

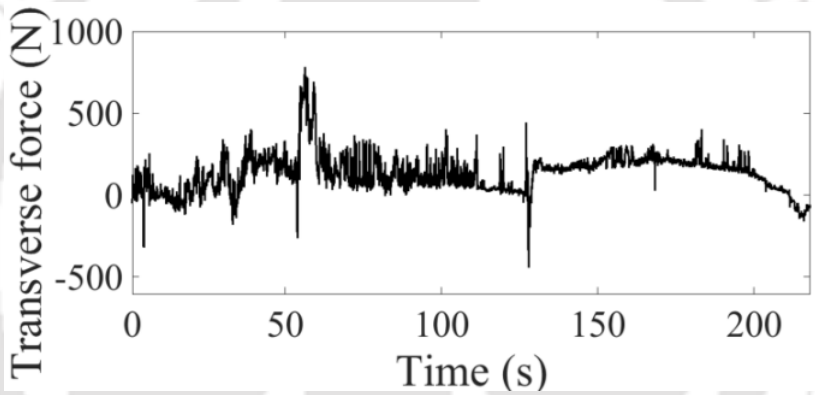

(b)

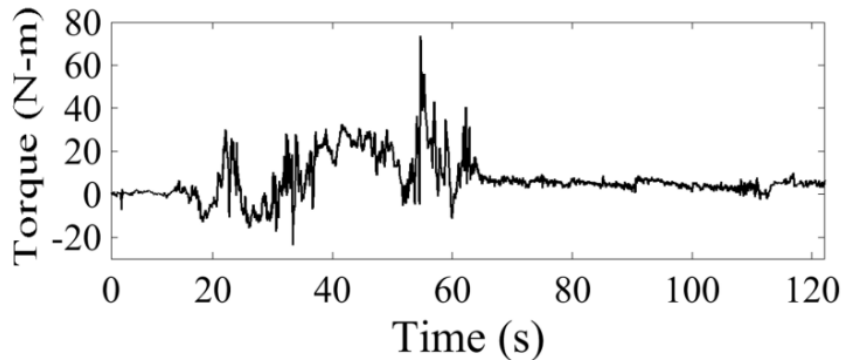

(c)

Fig. 4.10 Real time welding force data (a) vertical force (b) transverse force (c) torque

Table 4.2 Results from real time welding operation

Plunging force		Traverse force		Torque	
Output voltage (V)	**Maximum actual value (kN)**	**Output voltage (V)**	**Maximum actual value (kN)**	**Output voltage (V)**	**Maximum actual value (N-m)**
0.38	4.37	0.12	0.79	2.45	89.32

4.8 Summary

The chapter demonstrates the design and development of force and torque measurement system to be used for FSW process. The challenges faced for the measurement of forces/torque during FSW process due to simultaneous rotation and translation of the tool is overcome in this work by developing a welding fixture based measurement system. The developed system is calibrated and compared with standard available force measurement system for its accuracy and found appreciable match. The following are the major findings of the work presented in this chapter.

- The installation of the developed setup does not demand much alteration on the existing FSW machines as it is required for other existing measurement systems.
- Computed natural frequency of the developed setup suggests that the setup can be used in machines up to a maximum rotational speed of ~11,000 rev min^{-1}.
- The developed setup is capable of measuring forces and torque independent of point of application of load.
- Low cross sensitivity of the developed setup indicates the reliability in the measurement of individual forces and torque simultaneously.
- The accuracy of the developed setup is compared with the piezoelectric system based dynamometer and found an accuracy of 1.27%, 1.06% and 0.96% for vertical force, transverse force and torque measurement which is quite acceptable for real-time application.

Chapter 5

Signal features based monitoring of UTS

5.1 Introduction

The understanding of underlying physics of FSW process and influence of process parameters with dynamic characteristics leads to the impression of monitoring these parameters in real time. It is achievable with integration of various suitable sensors with FSW system and acquiring the sensor data in terms of process signals. It is believed that these signals can offer more realistic and accurate representation of process behaviour over time. Signal carries information that needs suitable representation for interpretation through machine intelligence. In the pursuit of achieving reliable monitoring of FSW process, few researchers have presented vertical force signal and acoustic emission signal as the real time information as discussed in chapter 2 (section 2.3). Different sensors integrated with FSW system in the present study are highlighted in chapter 3 (section 3.7). The signals are acquired with suitable sampling frequency integrating suitable acquisition hardware. The hardware used for acquisition of signals in the current research work is also demonstrated in chapter 3 (section 3.7). The survey of available literature (chapter 2, section 2.4) fetched that signals are processed mainly in time domain, frequency domain and time frequency domain for useful feature extraction. However, it is not guaranteed that the features will contribute towards direct monitoring of the underlying process and may show nonlinear behaviour with the process parameters. In this condition sometimes the features need to be fused with one another for better representation of the process information. Fusion of features can be achieved with machine learning techniques and the most popular is the artificial intelligence methods. These techniques are evolved to interpret data in a similar fashion to human intelligence of course with limited accuracy. The present study deals in extraction of

underlying information retained by main spindle motor and welding motor current signals, vertical force and torque signals and tool rotational speed signal acquired during FSW experiments. Implementing various signal processing techniques signal features are computed and presented to machine learning technique for feature fusion. This chapter highlights the signal processing techniques used in this study followed by fusion of features with ANN and SVR machine learning techniques for monitoring of UTS of the joints.

5.2 Time domain analysis

Time domain analysis is carried out with the signal being represented in time domain and mostly through computation of various statistical features. The computed statistical features describe the amplitude variations of the signals with respect to time. In the present work root mean square (RMS), skewness, kurtosis and variance are the four statistical features computed from different signals. The mathematical representations of these features are shown in **Eq. 5.1 – 5.4**.

$$RMS = \left[\frac{1}{N}\sum_{i=1}^{N} {s_i}^2\right]^{\frac{1}{2}} \tag{5.1}$$

$$S = \frac{\frac{1}{N}\sum_{i=1}^{N}(s_i - \mu)^3}{\left(\sqrt{\frac{1}{N}\sum_{i=1}^{N}(s_i - \mu)^2}\right)^3} \tag{5.2}$$

$$\sigma^2 = \frac{1}{N}\sum_{i=1}^{N}(s_i - \mu)^2 \tag{5.3}$$

$$K = \frac{\frac{1}{N}\sum_{i=1}^{N}(s_i - \mu)^4}{\frac{1}{N^2}(\sum_{i=1}^{N}(s_i - \mu)^2)^2} \tag{5.4}$$

where, S , σ^2 and K represents the skewness, variance and kurtosis respectively. $s_i$represents the data point in the signal and N represents the total number of points in the signal. μrepresents the mean of the data points of the signal. Although computing statistical features remain the most popular choice for feature extraction in time domain but sometimes it may fail to produce the exact correlation due to various external effects such as noise in the signal. In this case analyzing the signal in frequency domain may lead to more useful information with an observation for noises if present in the signal.

5.3 Frequency domain analysis

In the literature review for signal processing techniques used in FSW process it is observed that many researchers considered Fourier transform as the tool for processing signals in frequency domain. The following paragraphs outline the mathematical representation of Fourier transform.

5.3.1 Fourier transform

Fourier transform is a mathematical operation that decomposes a signal into its constituent frequencies. The original signal depends on time, and therefore is called the time domain representation of the signal, whereas the Fourier transform depends on frequency and is called the frequency domain representation of the signal. The term Fourier transform form refers both to the frequency domain representation of the signal and the process that transforms the signal to its frequency domain representation. A fast Fourier transform (FFT)(Cooley et al., 1967) is an efficient algorithm to compute the discrete Fourier transform (DFT) and it's inverse. Commonly, the FFT of a signal can be calculated by the following equation (Cooley et al., 1967).

$$S_k = \sum_{j=0}^{N-1} s_j e^{-2\pi i j k/N} \quad \textbf{(5.5)}$$

$$s_j = \sum_{k=0}^{N-1} S_k e^{2\pi i j k/N} \quad \textbf{(5.6)}$$

The result of DFT of N-point input time series is an N-point frequency spectrum, with Fourier frequencies k ranging from $-(\frac{N}{2} - 1)$ through zero or DC point to maximum frequency $\frac{N}{2}$.

The Fourier transform although found extensive implementation in signal processing have some serious limitations. The method is not applicable to non-stationary signals as it decomposes the signal from linear combinations of stationary signals which are time invariant sinusoids. Moreover, Fourier transform is not suitable to detect sharp

discontinuities occurred in the signal. The limitations with Fourier transform are somewhat relieved with the introduction of short time Fourier transform (STFT).

5.3.2 Short time Fourier transform

The limitations experienced in Fourier transform to localize event is relieved up to some extent with the introduction of windowed version of Fourier transform known as short time Fourier transform (STFT). In this approach original signal is segmented into many narrow time intervals (narrow enough to be considered stationary) and then applying the FFT algorithm to each segment. Each Fourier transform provides the spectral information of a separate time-slice of the signal, providing simultaneous time and frequency information. Short time Fourier transform can be expressed mathematically as follows:

$$STFT_f^{\omega}(t', \omega) = \int_t^{\cdot} [f(t).W(t - t')].e^{-2j\pi\omega t}\, dt \qquad (5.7)$$

Although the limitations with Fourier transform has been relieved by short time Fourier transform but it brings new challenges. First challenge is to select a suitable window function for segmenting the original time domain signal. Selection of suitable window function is crucial for efficient frequency spectrum containing all possible frequencies of the original signal. Second challenge is the selection of time lag for selection of width of the segmented signal. The narrower the segment in time domain the better would be the stationary assumption. However, narrower signals do not offer good localization in frequency domain. These limitations bring restriction in implementation of these two techniques in real time application of processing signals however; many have reported successful use of these two techniques. In due course of time new signal processing technique known as wavelet transform (WT) comes into existence and is free from limitations those were prominent in Fourier and short time Fourier transform.

5.4 Time frequency domain analysis

The inability of presenting detailed information of signals in frequency domain is the loss of time information. In many processes keeping a track of time dependent incidents captured through signals might be of interest for monitoring of the process. In this context time frequency domain analysis can offer suitable option for processing signals and acquiring useful information. Among the various time frequency domain

techniques WT and Hilbert-Huang transform (WT) is decided to implement in the present study. The following paragraphs outline the mathematical representation of these techniques.

5.4.1 Wavelet transform

WT is a time-frequency decomposition of a signal into a set of wavelet basic function. Wavelet analysis has proved its great capabilities in decomposing, denoising, and signal analysis which made the analysis of non-stationary signals achievable as well as detecting transient feature components as other methods were inept to perform since wavelet can concurrently impart time and frequency structures. Analysis with wavelets involves with breaking up a signal into shifted and scaled versions of the original (or mother) wavelet, i.e., one high frequency term from each level and one low frequency residual from the last level of decomposition. There are three categories of this transformation: continuous wavelet transform (CWT), discrete wavelet transform (DWT) and wavelet packet transform (WPT).

5.4.1.1 *Continuous wavelet transform*

A CWT is used to divide a continuous-time function into wavelets. Unlike Fourier transform, the CWT possesses the ability to construct a time-frequency representation of a signal that offers good time and frequency localization. The CWT of a time function $s(t)$ is given by following equation.

$$CT(a,b) = \int_{-\infty}^{\infty} s(t)\psi^*_{(a,b)}(t)dt \qquad \textbf{(5.8)}$$

where $\psi^*_{(a,b)}(t)$ is a continuous function in both the timedomain and the frequency domain called the mother wavelet and * represents operation of complex conjugate. $\psi^*_{(a,b)}(t)$can be expressed as:

$$\psi^*_{(a,b)} = \frac{1}{\sqrt{a}}\psi\left(\frac{t-b}{a}\right) \quad where\ a, b \in \mathbf{R}, a \neq 0 \qquad \textbf{(5.9)}$$

The main purpose of the mother wavelet is to provide a source function to generate the daughter wavelets which are simply the translated and scaled versions of the mother wavelet function. As seen in **Eq. 5.9**, the transform signal $CT(a,b)$ is defined on $a - b$ plane, which a and b are used to adjust the frequencyand the time location of the

wavelet in **Eq. 5.9**. A small $a$produces high-frequency wavelet when high frequency resolution is needed and the reverse is also true. The WT's superior time-localization properties stem from the finite support of the analysis wavelet: as b increases, the analysis wavelettransverses the length of the input signal, and an increases or decreases in response to changes in the signal's local time and frequency content. Finite support implies that the effect of each term in the wavelet representation is purely localized. This sets the WT apart from the Fourier transform, where the effects of adding higher frequency sine waves are spread throughout the frequency axis. One of the limitations with the CWT is that it quite a time consuming process due to finer sampling of scales. Thus, this technique is not implemented in the present study.

5.4.1.2 *Discrete wavelet transform*

In numerical and functional analysis, DWT is a wavelet transform for which the wavelet $\psi(a,b)$ is discretelysampled. In other words DWT can be understood as the discrete version of CWT. As with CWT, a key advantage it has over Fourier transforms is temporal resolution: it captures both frequency and location information (location in time). Usually, the DWT can be derived from discretization of CWT. The most common discretization is dyadic method:

$$DT(a,b) = \int_{-\infty}^{\infty} s(t)\psi^*_{(j,k)}(t)dt \qquad \textbf{(5.10)}$$

$$\psi^*_{(j,k)} = \frac{1}{\sqrt{2^j}}\psi\left(\frac{t - 2^j k}{2^j}\right) \qquad \textbf{(5.11)}$$

where, a and b are replaced by 2^j and $2^j k$ respectively (Daubechies, 1988; Mallat, 1989). An efficient way to implement this scheme using filters was developed by Mallat (1989).The original signal $s(t)$ passes through two complementaryfilters and emerges as low frequency called approximations and high frequency called details. The decomposition process can be iterated, with successive approximations being decomposed in turn, such that a signal can be broken down into many lower-resolution components.

5.4.1.3 *Wavelet packet transform*

The structure of WPT is similar to DWT. Both have the framework of multi-resolution analysis. The main difference in the two techniques is the WPT can simultaneously break up detail (D_i) and approximation (A_i) versions while DWT only breaks up as an approximation version. Therefore, the WPT have the same frequency bandwidths in each resolution and DWT does not have this property. The mode of decomposition does not increase or lose the information within the original signals. Therefore, the signal with great quantity of middle and high frequency signals can offer superior time-frequency analysis. The WPT suits signal processing, especially non-stationary signals because the same frequency bandwidths can provide good resolution regardless of high and low frequencies.

WPT decomposes a signal according to its frequency content. The high scale low frequency part is known as approximation and low scale high frequency part is termed as detail. A schematic decomposition tree with a signal sampling at 10 KHz up to third level is shown in **Fig. 5.1**. At first level the signal is decomposed to approximation and detail in the frequency band of 0-5 kHz and 5-10 kHz respectively. The approximation and detail are further decomposed to next level leading to frequency bands as 0-2.5 kHz, 2.5-5 kHz, 5-7.5 kHz and 7.5-10 kHz. Decomposing the approximation and detail further will lead to further reduction in frequency bands. The process is advantageous in the aspect that both low and high frequency content of the signals can be observed with various scales. This gives fidelity to breakdown a signal with respect to its frequency content and any anomaly in the signals can be viewed with respect to both frequency and time on decomposition.

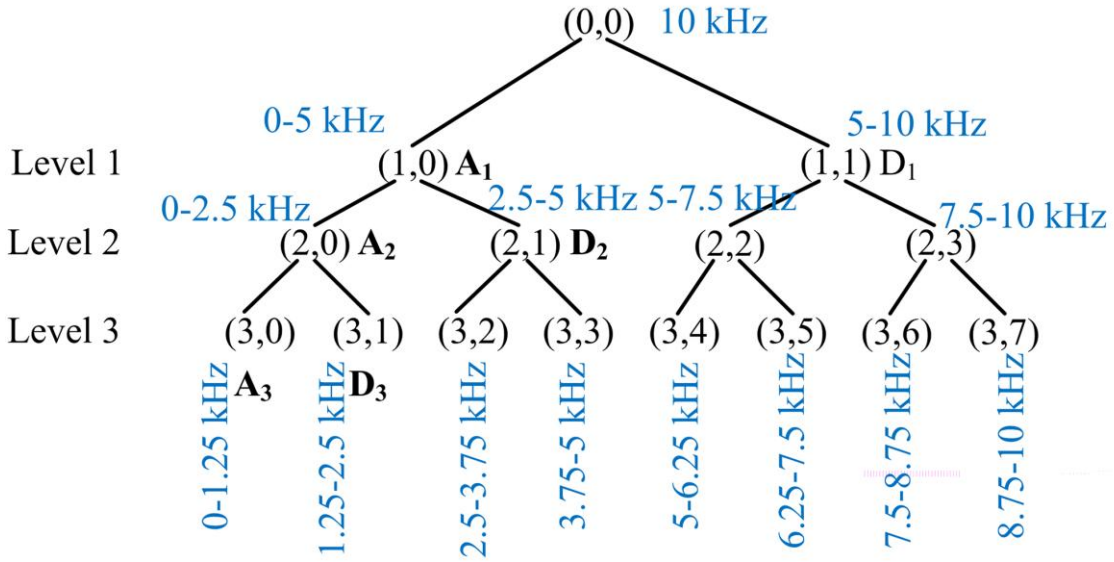

Fig. 5.1 Wavelet packet decomposition tree up to third level

In wavelet packet analysis a signal $s(t)$ can be represented as a sum of orthogonal wavelet packet function $W_{p,k,l}$ at different scales, oscillations and localisation.

$$s(t) = \sum_{p}\sum_{k}\sum_{l} C_{p,k,l} W_{p,k,l}(t) \tag{5.12}$$

where, $C_{p,k,l}$is the wavelet packet coefficients, which can be obtained by the following equation:

$$C_{p,k,l} = \int_{-\infty}^{+\infty} s(t) W_{p,k,l}(t) dt \tag{5.13}$$

and$W_{p,k,l}$generated from the base function

$$W_{p,k,l}(t) = 2^{p/2} W_k(2^p t - 1) \tag{5.14}$$

where, indices p, k, i are the scale, oscillation and the time localisation parameters respectively ($[(p,l)\, \epsilon\, Z^2\ and\ k = 0,1,2,\ldots\ldots 2^{p-1}]$). In general wavelet functions are defined by

$$W_{2k}(t) = 2^{1/2} \sum_{l} h_l W_k(2t - l) \quad \textbf{(5.15)}$$

$$W_{2k+1}(t) = 2^{1/2} \sum_{l} g_l W_k(2t - l) \quad \textbf{(5.16)}$$

where, h_l and g_l are the low pass and high pass filters. $W_0(t) = \phi(t)$ is the scaling function and $W_1(t) = \psi(t)$ is the wavelet function respectively. The discrete filters h_l and g_l are quadrature mirror filters associated with scaling function and wavelet function respectively.

Introduction of WT eliminates the limitations faced in Fourier transform or STFT by providing a time and frequency window for signal analysis with appreciable resolution in both time and frequency domain. However, in practice the process of WT suffers from few working limitations. In the WT framework number of optimum level of decomposition also play appreciable role in effective generation of signal features. The level of decomposition needs to be selected with care that high level may result in irrelevant or redundant signal information killing more time in processing. On the other hand low level of decomposition may result in improper signal processing and hence leading to non impactful signal features. In the present research work selection of suitable level of decomposition is achieved through Shannon entropy criterion as shown in **Eq. 5.17**. According to entropy criterion, a splitting is only of interest if the entropy of the parent packet is more than the total of the child packets. For computing the entropy values of each packet in the wavelet packet tree Shannon entropy method is used.

$$E(S) = -\sum_{k=1}^{N} {s_k}^2 \log({s_k}^2) \quad \textbf{(5.17)}$$

where, $E(S)$ is the Shannon entropy of the signal s and s_k is the k^{th} value of the signal. The entropies of all the packets at different levels are calculated using the above mentioned equation. In reference to the **Fig. 5.1** if the entropy value at node(2,0) is more than the total entropy of node (3,0) and (3,1) then only the splitting would be interesting and decomposition is preceded. Otherwise, that level can be treated as optimum level of

decomposition. The present work uses MATLAB software package to carry out WT on the acquired signals.

Another limitation in the application of WT is the selection of suitable mother wavelet function. The signal is scanned with this mother wavelet function at different scales by shifting and translating the mother wavelet function. The coefficient generated after the scanning of the signal under consideration significantly depends on the mother wavelet function. In practice there are many functions available for the selection and it is difficult to precisely select the most suitable function that will result in effective signal features. The present study developed a methodology for the selection of suitable mother wavelet function. The details of the proposed method are addressed in section 5.6.

5.4.2 Hilbert-Huang transform

HHT was introduced in the work by Huang (1971) and found intensified use in analysis of signals. This technique consists of two primitive stages: (i) empirical mode decomposition of signal and (ii) Hilbert analysis of the decomposed signal parts. Empirical mode of decomposition is used to decompose any complicated data in finite and so called intrinsic mode function (IMF) which admits well behaved Hilbert transform (Huang et al., 1971). This transform is based on local characteristics of the data on time scale, and is therefore adaptive in allowing the method to be applied on non-stationary processes. The second stage is to construct an energy-time-frequency distribution that lets us estimate the instantaneous frequency. The HHT represents an alternative to Fourier transform which has some critical limitations: the system must be linear and the data must be strictly periodic or stationary, the resulting spectrum having otherwise little physical meaning (Huang et al., 1971). On the other hand, HHT decomposes the data into a number of IMFs based on the direct extraction of the energy associated with various intrinsic time scales and computes the instantaneous frequency for each IMF, using the Hilbert analysis. In this way, any event can be localized in time and frequency domain. Moreover, the IMFs can be viewed as the basis for the complete and adaptive data expansion **(**Prah and Okine et al., 2008). The full energy-time-frequency distribution generated by HHT is an important tool for the analysis of the non-stationary data.

5.4.2.1 *Empirical mode of decomposition (EMD)*

EMD is used to obtain the IMFs which allow the identification of the instantaneous frequencies under the following assumptions: (i) at any point the mean value of the envelop determined by the local maxima and envelop determined by the local minima is zero, and (ii) the number of extrema and the number of zero crossings must be equal or differ at most by one (Huang et al., 1971). The computation of the IMF is fully data driven, they being obtained by decomposing the data (this process is called the shifting process) using the EMD algorithm which has the following steps:

(a) To find the local maxima and local minima of the given data;

(b) To construct the upper and lower envelopes by cubic spline interpolation of the local maxima and the local minima respectively;

(c) To find the number of zero crossings;

(d) For the first shifting process, the mean of the upper and lower envelopes, $m_1(t)$ is determined and subtracted from the signal $s(t)$ as given in **Eq. 5.18**.

$$P_1(t) = s(t) - m_1(t) \quad \textbf{(5.18)}$$

(i) If $P_1(t)$ satisfies the conditions of the IMF, then $P_1(t)$ is the first frequency and amplitude modulated oscillatory mode IMF.

(ii) If $P_1(t)$ does not satisfy the conditions of the IMF, then steps (a-c) are repeated for $P_1(t)$, thus $P_{1,1}(t)$ is obtained as follows

$$P_{1,1}(t) = P_1(t) - m_1(t) \quad \textbf{(5.19)}$$

The steps are iterative and after k cycles the IMF is obtained as given in **Eq. 5.20**

$$P_{1,k}(t) = P_{1,k-1}(t) - m_{1,k}(t) \quad \textbf{(5.20)}$$

Thus, first IMF component for the original data is obtained as $c_1(t) = P_{1,k}(t)$

(e) The obtained IMF is constructed from the original data leading to the residual component $r_1(t)$

$$r_1(t) = s(t) - c_1(t) \quad \textbf{(5.21)}$$

(f) $r_1(t)$ is now considered as the original data for the next cycle. The above steps are repeated n times, where n is the number of IMFs plus the residual $r_1(t)$. In order to guarantee that the IMFs so computed carry enough physical meaning, a stopping criterion is required and one is defined in (Huang et al., 1971). The so defined criterion is based on standard deviation computed from two consecutive shifting results.

$$SD = \sum_{t=0}^{T} \frac{\left|P_{1,k-1}(t) - P_{1,k}(t)\right|^2}{P_{1,k-1}(t)^2} \tag{5.22}$$

The data can be reconstructed from its IMFs as the following

$$s(t) = \sum_{i=1}^{n} c_1(t) + r_n(t) \tag{5.23}$$

5.4.2.2 *The Hilbert analysis*

The Hilbert transform is applied to each IMF, leading to the instantaneous frequency

$$y(t) = \frac{1}{\pi} P \int_{-\infty}^{+\infty} \frac{s(t)'}{t - t'} dt' \tag{5.24}$$

where, P indicates the Cauchy principal value which prevents a possible singularity at $t = \tau$ and $t = \pm\infty$ and $s(t)$ is an IMF. Then the analytical signal $z(t)$ is constructed as per **Eq. 5.25**.

$$z(t) = s(t) + iy(t) = a(t)e^{i\theta(t)} \tag{5.25}$$

with, $a(t) = \sqrt{s^2(t) + y^2(t)}$ and $\theta(t) = arctan\left(\frac{y(t)}{s(t)}\right)$

The instantaneous frequency is therefore obtained by$\omega(t) = \frac{d\theta(t)}{dt}$

Finally, the original data can be reconstructed as follows

$$s(t) = \sum_{i=1}^{n} a_i(t)e^{\int \omega c(t)dt} \tag{5.26}$$

The time-frequency distribution of the amplitude in **Eq. 5.26** is called the Hilbert transform (Huang et al., 1971). When the Hilbert transform is applied on $s(t)$, the magnitude is kept unchanged but the phase of all frequency components is shifted by $\frac{\pi}{2}$.

In the analysis of non-stationary signals, HHT found appreciable importance than other signal processing techniques (Prah and Okine, 2008). Even though, the shortcoming with HHT is that, the first IMF usually covers broad frequency range such that mono component conditions may be difficult to achieve. Once it occurs in actual signal processing this will lead to redundant signal features not correlating to actual process information. In the present study a modified HHT with WPT is proposed and presented in section 5.7 which is free from the aforementioned limitation.

5.5 Fractal theory

The concept of fractal dimension is not new in the field of science and engineering. This concept gained popularity in describing the complexity of the natural object in a more simplified manner. The use of fractal theory in signal processing is advantageous as implementation of it does not demand any a priori knowledge as like in WPT, HHT etc. Moreover, the output from the analysis is a single valued indicator and interpretation becomes fast and easy. Fractal theory does not demand any preprocessing of the signals and algorithms for estimation FD is hardly affected with noise contamination. The methods used in this study are explained in the subsequent paragraphs.

The estimated FD from various signals provides useful information to classify different welding periods and act as offline design tool to monitor the process. Fractal dimension in case of signals and curves can be defined as the space filling capacity of the signal or the curve. For planar curves, 1 to 2 is the range of FD (Katz et al., 1988). Many methods can be found in literature for determining FD of signals. Box counting method is most popular among researchers for determining FD of the signals. However, with box counting method the limitation is that the signals need to be sampled at very high rate. Higuchi's method (1988) for determining the FD is more robust and is more suitable for short segment time series data. The computation of FD depends upon measurement units used. If the measurements units are different, FDs will also vary. Katz's approach solves this problem by creating a general yardstick (Katz et al., 1988). Petrosian's algorithm is

another method for computing the FD of waveforms (1995).This method gives a quick estimate of the FD as compared to other methods.

5.5.1 Higuchi's algorithm

This algorithm was proposed by Higuchi (1988). This algorithm is best suited for finite length time sequence. Let consider a finite length time series sampled at regular interval as $S(1), S(2), S(3), \dots, S(N)$.

From the given time series a new time series is constructed as follows:

$$S_m^k; S(m), S(m+k), S(m+2k), \dots, S\left(m + \left\lfloor \frac{N-m}{k} \right\rfloor . k\right), \quad where\ m = 1,2, \dots, k \tag{5.27}$$

where, $\lfloor . \rfloor$ denotes the gauss' notation and both m and k are integers and m and k indicate the initial and interval time, respectively. For a time interval k, we get k sets of new time series. Now the length of the new curve is determined as follows:

$$L_m(k) = \frac{\left\{\left(\sum_{i=1}^{\left\lfloor \frac{N-m}{k} \right\rfloor} |S(m+i.k) - S(m+(i-1).k)|\right) \frac{N-1}{\left\lfloor \frac{N-m}{k} \right\rfloor .k}\right\}}{k} \tag{5.28}$$

The term $\lfloor \rfloor$ represents the normalization factor for the curve length of subset time series. Let the length of the curve for the time interval k is$\langle L(k) \rangle$, as the average value over $k$sets of $L_m(k)$. If $\langle L(k) \rangle \propto k^{-D}$, then the curve has a fractal dimension of D. In the curve of $ln(L(k))$ versus $ln(1/k)$, the slope of the least square linear best fit is the estimate of the FD.

5.5.2 Katz's algorithm

Katz (1988) proposed another algorithm for computing fractal dimension of waveform. Although this algorithm is slower than the other methods but the advantage is that it is derived from the original waveform, and eliminates the preprocessing step of creating a binary sequence as required for the algorithm as proposed by Petrosian (1995). The FD of a curve can be defined as:

$$D = \frac{log_{10}(L)}{log_{10}(d)} \tag{5.29}$$

where,L is the total length of the curve or sum of distances between successive points, and d is the diameter which defines the distance between the first point in the sequence and the point in the sequence which gives the farthest distance. Mathematically d can be expressed as

$$d = \max\left(distance(1,i)\right) \tag{5.30}$$

The FDs computed in this fashion depends on the measurement units used, so if the units are different then so as the FDs. Katz's method solves this issue by introducing a normalized distance parameter which is the average distance between successive points. Thus FD of a curve now becomes

$$D = \frac{log_{10}(\frac{L}{\underline{a}})}{log_{10}(\frac{d}{\underline{a}})} \tag{5.31}$$

where,$\underline{a}$is the average distance between successive points. Again defining a parameter n as $n = \frac{L}{\underline{a}}$ then FD of a curve can be expressed as which is the Katz's FD of a waveform.

$$D = \frac{log_{10}(n)}{log_{10}\left(\frac{d}{L}\right) + log_{10}(n)} \tag{5.32}$$

5.5.3 Validation of fractal dimension codes

The algorithms described above are used in this study to compute fractal dimension of signals acquired during FSW process. Code for each algorithm is developed using MATALB. All the developed codes are then tested for known waveform whose FD is known to check the proper functioning. In testing of the developed codes, fractional Brownian motion (with H = 0.5, 0.7, 0.95 and number of data points, N = 1024) waveforms as shown in **Fig. 5.2** is generated in MATLAB and the waveforms are used for estimating the FD using the developed codes. The comparison results for the computed fractal dimensions using the developed codes are listed in **Table 5.1**. It is observed that percentage error between the theoretical and computed fractal dimensions are reasonable and the codes can be implemented for real time applications.

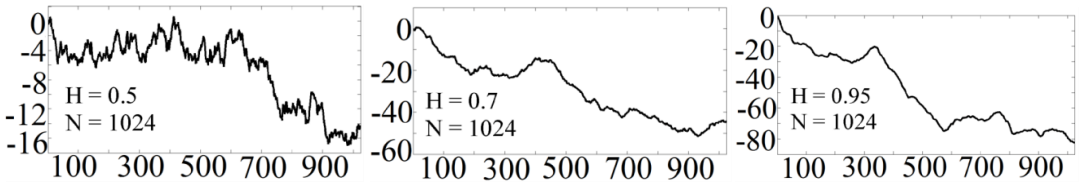

(a) (b) (c)

Fig. 5.2 Fractional Brownian motion curves with Hurst parameter (a) H = 0.5 (b) H= 0.7 and (c) H = 0.95

Table 5.1 Comparison between theoretical and estimated fractal dimensions

Algorithm	H = 0.5 Theoretical FD = 1.5		H = 0.7 Theoretical FD = 1.3		H = 0.95 Theoretical FD = 1.05	
	Estimated	% Error	Estimated	% Error	Estimated	% Error
Higuchi	1.51	-0.67	1.32	-1.53	1.05	0
Katz	1.49	0.67	1.28	1.53	1.06	-0.95

The signal processing techniques discussed in the aforementioned sections and subsections are utilized for processing of main spindle motor and welding motor current signals, vertical force and torque signals and tool rotational speed signal acquired during the welding experiments. The signals are processed in time domain and time frequency domain. Frequency domain analysis of the signals does not offer any intelligible information regarding the process behaviour. In the present study a total of five signals as mentioned above and four signal processing techniques are decided to implement for effective processing of signals. This results in twenty possible combinations for analysis of signals. However, it is not feasible that each signal processing techniques would result in effective processing of signals and the features extracted would be efficient in representing the process behaviour. Owing to this signals with different characteristics are processed with most suitable signal processing technique. Once the signal features are extracted those are fed to ANN and SVR models for fusion of features and for prediction of UTS of the joints.

5.6 Prediction of UTS with current signal features

The available research work on monitoring of FSW process mostly concentrates on acquisition and processing of force and acoustic emission signals. Among the reviewed literature Longhurst et al. (2016) attempted monitoring of FSW process with

main spindle motor current signal. However, in the reported work weld quality prediction with signal features was not attempted. Thus, this area needs further investigation for development of weld quality monitoring methodologies for FSW process with current signal features. The costs of current sensors are comparatively low as compared to that of acoustic emission and force/torque sensors which would be an added advantage.

In the present study current signals from main spindle motor and welding motor are acquired with hall effect sensors against the welding experiments as reported in chapter 3 (refer Table 3.6). At the outset of this chapter it is commented that signals can offer more reliable information regarding the process variation over dynamic nature of process parameters. The acquired signals against Exp. No. 33 and Exp. No. 65 are represented in **Fig. 5.3**. It is to note that these two experiments are conducted over same process parameters at same levels (refer Table 3.4, chapter 3). However, the time domain representation of the signals does not reflect similar behaviour of the process which substantiates to accept the dynamic nature of parameters. This in turn reveals the possibility of variation in process outcome under similar process parameters. A clear variation in magnitude of main spindle motor current signal can be seen. A closer observation of the signals as represented in the respective figure indicates that current magnitude against the Exp. No. 33 is less compared to that of Exp. No. 65. The current magnitude is proportional to rotational speed of the motor neglecting all the losses. This implies that low current magnitude represents less rotational speed for the respective experimental condition. The same can also be interpreted from the perspective of Exp. No. 65. It draws more current signifying more tool rotational speed. This can be due to the less plasticization of material around the rotating tool demanding high rotational speed to counter the material resistance. This shows an indirect method for monitoring the process for its proper functioning and thus the outcome of the process. This necessitates the processing of signals for effective features extraction to correlate with the process behaviour. The signals are processed in time domain, frequency domain and time frequency domain. Time domain analysis is carried out through computation RMS, variance, skewness and kurtosis from main spindle motor current signal. The same is not computed for welding motor current signals as the variation in time domain is less in comparison to main spindle motor current signal. In frequency domain analysis Fourier transform is performed on signals and in time frequency domain analysis current signals

are processed with WPT for effective feature extraction.WPT is selected due to its ability in decomposing signal for both low and high frequency content as described by approximation and detail part of wavelet packet tree. Observation of signals in both high and low frequency domains is expected to result in more suitable information regarding the process behaviour. The same is not achievable with DWT which only offer decomposition of low frequency component of the original signal leading to completely missing the high frequency information of the signals that might also carry useful process information.

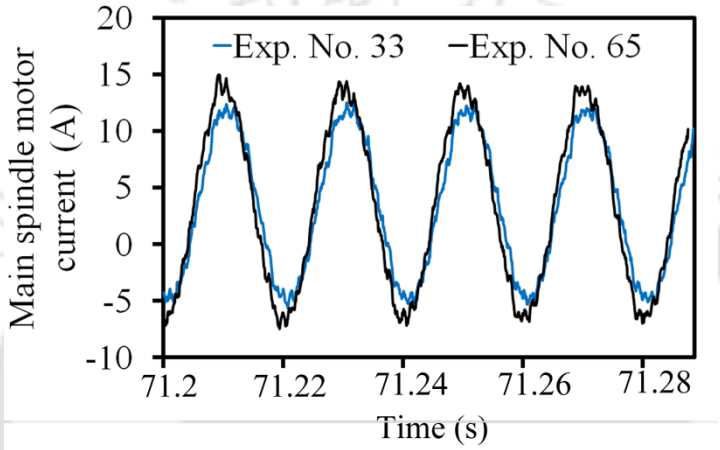

(a)

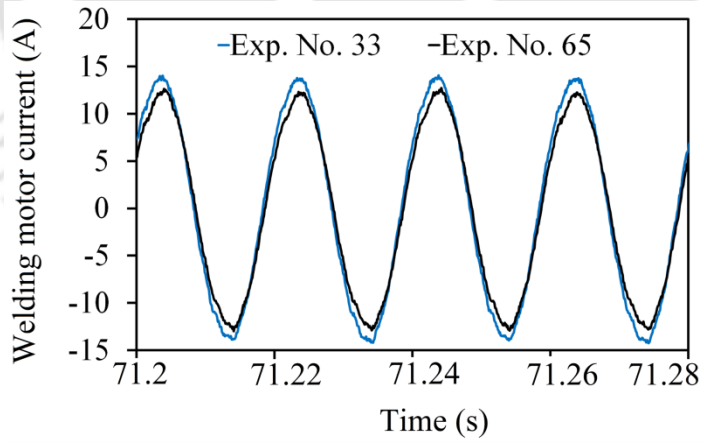

(b)

Fig. 5.3 Magnified view of (a) main spindle motor current signal (b) welding motor current signal

The computed statistical features from main spindle motor current signal are represented in **Table 5.2**. The statistical features against the repeated experiments

revealed that the variation in process parameters as reflected in amplitude of main spindle motor current signal is captured. It indicates that the features in time domain will provide salient information regarding the process behaviour. However, it is difficult to comment which feature is more informative among the four for prediction of UTS of the joints. Thus, the features are fused with the help of machine learning techniques ANN and SVR to predict the UTS of the joints irrespective of individual contribution of each feature. The model development and selection of respective model parameters with prediction performance are displayed in later part of this section.

Table 5.2 Time domain features for main spindle motor current signal

Exp. No.	RMS $\times 10^{-2}$	Variance $\times 10^{-3}$	Skewness $\times 10^{-3}$	Kurtosis
1	7.92	5.03	1.82	1.51
2	7.73	4.47	2.01	1.54
3	8.13	5.22	5.25	1.56
4	7.66	4.39	2.59	1.64
5	7.79	4.83	6.14	1.52
6	6.70	4.49	3.98	1.56
7	8.44	5.76	5.16	1.56
8	7.91	4.75	1.58	1.93
9	7.52	4.43	1.72	1.53
10	8.05	4.82	1.77	1.55
11	8.15	5.27	3.72	1.56
12	8.46	5.71	1.02	1.82
13	7.72	4.71	3.54	1.54
14	7.96	4.95	9.30	1.57
15	8.35	5.59	3.71	1.56
16	9.22	7.17	1.45	1.71
17	7.86	4.95	1.79	1.52
18	7.88	4.69	0.01	1.53
19	8.23	5.43	4.40	1.54
20	8.54	5.65	1.23	1.57
21	8.15	5.41	6.05	1.53

22	7.76	4.44	1.21	1.53
23	8.25	5.43	1.04	1.55
24	8.35	5.36	0.06	1.74
25	7.96	5.09	1.11	1.54
26	8.00	4.85	6.72	1.54
27	8.55	5.96	1.02	1.58
28	8.03	4.85	1.71	1.66
29	8.06	5.25	1.78	1.54
30	8.21	5.17	7.56	1.54
31	8.78	6.41	3.52	1.55
32	8.51	5.67	8.22	1.79
33	7.96	5.04	1.18	1.53
34	7.39	5.46	2.03	1.54
35	8.97	6.76	7.50	1.54
36	8.90	6.29	1.16	1.59
37	7.96	5.02	1.31	1.58
38	8.48	5.48	1.94	1.56
39	8.89	6.60	2.86	1.54
40	9.32	7.08	4.67	1.58
41	7.81	4.80	9.32	1.55
42	8.61	5.60	0.05	1.55
43	8.85	6.54	3.52	1.56
44	8.98	6.56	2.29	1.67
45	8.30	5.65	2.68	1.58
46	8.37	5.39	7.36	1.57
47	8.78	6.41	3.52	1.55
48	8.87	6.41	1.36	1.79
49	8.75	6.39	1.74	1.53
50	8.49	5.48	5.37	1.54
51	9.20	7.16	1.35	1.63
52	8.95	6.55	6.54	1.58
53	8.93	6.68	1.01	1.53
54	9.18	6.73	2.40	1.54

55	9.39	7.53	3.85	1.54
56	8.67	6.09	1.82	1.62
57	8.93	6.68	1.95	1.54
58	8.71	5.97	1.12	1.57
59	9.19	7.18	7.23	1.56
60	9.49	7.60	2.41	1.65
61	8.99	6.81	3.36	1.54
62	8.52	5.70	1.91	1.63
63	9.19	7.16	1.33	1.56
64	8.96	6.46	1.32	1.61
65	8.17	6.29	1.57	1.72

The time domain analysis of main spindle motor current signal is fruitful in the aspect of monitoring process behaviour. However, welding motor current signal failed to produce appreciable variation in time domain. Thus it is decided to analysis this signal along with main spindle motor current signal in time frequency domain with the intention of useful feature extraction. Prior to implement time frequency domain analysis; frequency domain analysis of current signals is carried out with fast Fourier transform (FFT) algorithm implemented with MATLAB software package (MATLAB 2017a). Frequency spectrum of main spindle motor current signal and welding motor current signal are obtained. Unfortunately, no appreciable information regarding the process behaviour can be extracted. Even the spectrum of signals against repeated experiments failed to produce any notable information for both the signals. As frequency domain analysis fails to produce notable information the present study is steered to analyze the signals with WPT for possible extraction of features. In order to implement WPT on a signal first step is to select suitable level of decomposition followed by selection of suitable mother wavelet function. However, adequate literature survey (chapter 2, section 2.4) fetches that no significant effort has been made for developing methodology for selection of suitable mother wavelet function. Hence, this study before implementing WPT in decomposition of current signal is motivated towards development of methodology for selection of suitable mother wavelet function. The developed methodology is compared with already proposed methodology and found that the present methodology is independent of process and depends only on the signal. Later,

this methodology is applied for effective selection of mother wavelet function and signal features in time frequency domain are computed.

Signal analysis is started with selection of suitable level of decomposition. The selection of suitable level of decomposition is achieved as per the **Eq. 5.17**and the relevant approach presented in sub section 5.4.1.3. In the family of wavelet, there are many wavelet functions available like, Haar, Daubechies, Symlet, Coiflet etc. known as mother wavelet functions. All these functions have different characteristics and to analyze any signal, specific selection of mother wavelet need to be made for effective extraction of useful features from the signals. In this study, a new method is proposed to obtain the suitable mother wavelet. The method proposed is based on a ratio of energy of the signal to the entropy of different wavelet packets as expressed in **Eq. 5.34**.

$$\text{Energy} - \text{to} - \text{entropy ratio}_{\text{i}} = \left(\frac{\text{E}}{\text{En}}\right)_{\text{i}} \tag{5.34}$$

$$E_S = \sum_{n=-\infty}^{\infty} |S(n)|^2 \tag{5.35}$$

where, i represents the family of the wavelet functions selected for the analysis, E_S represents the energy of the original signal calculated as per **Eq. 5.35** and En represents the entropy calculated as per **Eq. 5.17** of the decomposed wavelet packets using the selected mother wavelet functions.

Energy of a signal represents the information carried by the signal. Entropy of the decomposed wavelet packets at a particular level of decomposition reflects the amount of disorder in the signal which can be viewed as a measure of uncertainty regarding the information contained in the signal. Hence, wavelet function which fetches lower entropy values at selected level of decomposition should be preferred. The proposed ratio will represent the process information retained by signals as it deals with the original signal information in terms of energy and minimum entropy which reflects the uncertainty in the original signal. For the selection of suitable mother wavelet function, the one with maximum ratio should be considered. Here, for both main spindle motor and welding motor current signal this ratio is calculated using 44 different mother wavelet functions for each signal. The mother wavelet function with the maximum ratio of energy to entropy is considered as the best mother wavelet. All the acquired signals against each experiment are tested using the proposed method for finding the appropriate

mother wavelet function. **Figure 5.4** represents the ratio of different wavelet functions for main spindle motor and welding motor current signal against Exp. No. 45 which is the case of maximum UTS value. From the analysis, it is found that symlet19 and db20 are the best mother wavelets for main spindle motor and welding motor current signals, respectively. The proposed methodology is developed using MATLAB software package (MATLAB 2017a).

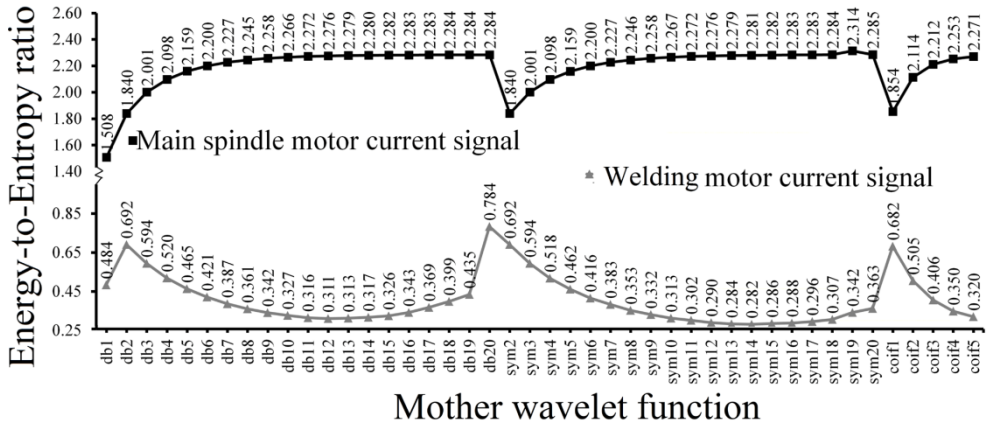

Fig. 5.4 Variation of computed ratio with mother wavelets for main spindle motor current signal and welding motor current signal

The result obtained using the proposed method is compared with two existing methods namely, root mean square difference (RMSD) between the original signal and the reconstructed signal from the wavelet packet tree (Ngui et al., 2013) and correlation coefficient between the wavelet packet coefficients and monitored quantity (Pal et al., 2011). The wavelet with the least RMSD and high correlation coefficient among the considered wavelet functions are considered as the best mother wavelet. **Figure 5.5** shows the RMSD of main spindle motor and welding motor current signal, respectively. Interestingly, this analysis also provides the same result as symlet19 and db20 to be the best mother wavelets for main spindle and welding motor current signals, respectively. **Figure 5.6** represents the results of the method based on correlation coefficient between the average RMS values of the wavelet coefficients and UTS of the joints.

The two methods selected for the comparison of the results from the proposed method although give the same results, but suffer from few limitations. The method based on RMSD of the original and the reconstructed signal is actually performing a noise reduction of the original signal. Once the original signal is decomposed, it is

filtered through the wavelet filters. Here, the chances of losing valuable process information are high. It is suggested that mother wavelet function which gives the least RMSD is suitable for decomposition. But it does not guarantee that the selected mother wavelet function can effectively extract the signal information that contains the valuable information of process variations. The selected mother wavelet can be a better candidate for noise elimination from the original signal.

The other method used for the comparison suggests finding a correlation coefficient between the average root mean square values of the wavelet packets with the parameter that is monitored using the signal information. Here, the value of the parameter monitored depends on the accuracy of the measurement procedure adapted and is process dependent. This is not suitable for approaches that concentrate to extract information contained in a signal. The selection from this approach depends on the accuracy of measurement of the parameter being monitored and can be hindered due to many external factors. Hence, selection of mother wavelet based on this approach may contain redundancy in the information extracted from signal. On the other hand the proposed method based on the ration of the energy of the original signal to the entropy of the decomposed wavelet packet does not suffer from above mentioned limitations. It purely depends on signal information which can detect characteristics of the process being monitored with signals without process interference. Thus, the proposed method can be a suitable alternate approach for the selection of mother wavelet function for effective decomposition of signals.

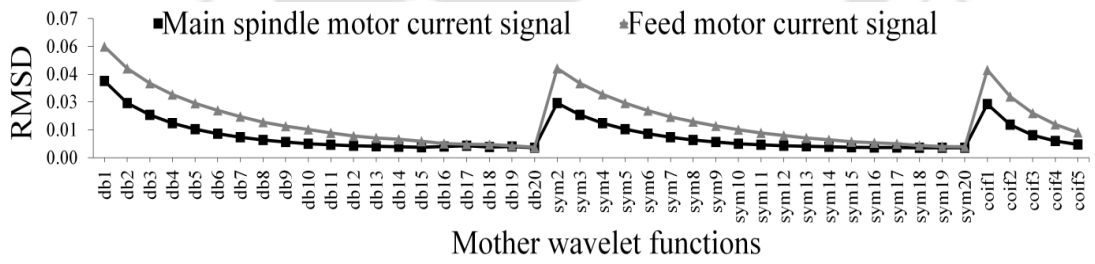

Fig. 5.5 Variation of computed root mean square difference values with mother wavelet functions for main spindle motor current signal and welding motor current signal

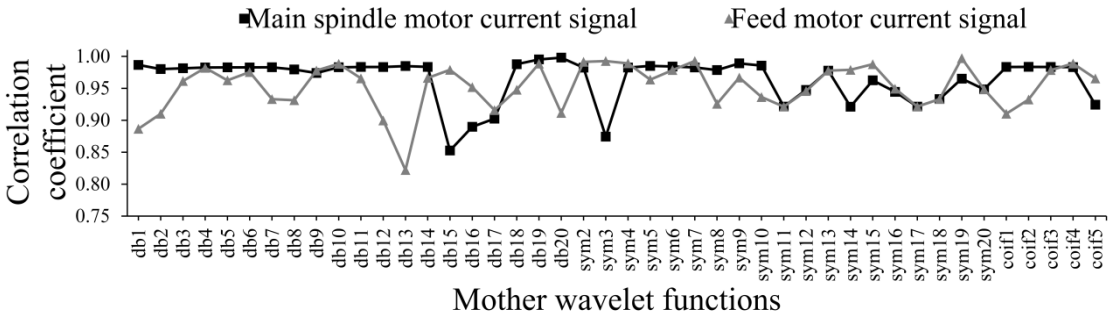

Fig. 5.6 Variation of correlation coefficient with mother wavelet functions for main spindle motor current signal and welding motor current signal

The decomposed wavelet packets at a particular level of decomposition carry the information retained by original signal. Hence, first the optimum level needs to be selected. In this study, Shannon entropy criterion is used for this purpose. Once the optimum level is found, each signal is decomposed to the optimum level of decomposition with different mother wavelet functions and the ratio against each signal is computed using **Eq. 5.34**. This is repeated for each acquired signal and an array consisting of ratios for each signal is obtained for each mother wavelet function. From this array, the mother wavelet function which yield maximum ratio is considered as the best mother wavelet. Then, the signals are decomposed to the optimum level using the best mother wavelet function. For the present study, Symlet 19 and Daubechies 20 are the best mother wavelet functions obtained for main spindle motor current signal and welding motor current signal, respectively.

Wavelet packet coefficients are extracted using the WPT for each signal and a list is obtained containing the signal features. From the wavelet packet analysis, a total of 192 (64 for main spindle motor current and 128 for welding motor current signals) features are obtained. However, it is very difficult to handle such a large number of features and it is not essential too, that all these features would be equally effective for modeling the weld quality. Moreover, multiple features may contain same information. To extract the most appropriate features for both the signals, data reduction method is essential. In this study, principal component analysis (PCA) is chosen as data reduction technique and to find out most eligible features from the available 192 features.

PCA is mathematically defined (Humberstone et al., 2012) as an orthogonal linear transformation that transforms a number of (possibly) correlated variables into a (smaller) number of uncorrelated variables called principal components. The first

principal component accounts for the greatest statistical variability and second greatest variance represented by the second component respectively and so on. PCA is theoretically the representation of the optimum transform for the given data in least square terms. The idea of PCA lies in calculating the eigenvectors and eigen values of the covariance matrix of the data and is efficiently calculated by singular value decomposition. These eigenvectors describe an orthonormal basis that is effectively a rotation of the original Cartesian basis. Each principal component is a linear combination of the original variables. All the principal components are orthogonal to each other, so there is no redundant information. The principal components as a whole form an orthogonal basis for the space of the data (Humberstone et al., 2012).

The percentage variability explained by the first ten components for the main spindle motor and welding motor current signals are shown in **Fig. 5.7**. It is observed that, in case of main spindle motor current signal features, first five components account for the 99.87% variability of the entire data set whereas the percentage variability of the rest of the components is only 0.13%. So, first five components are chosen as the features for the case of main spindle motor current signal. In case of welding motor current signal, out of first fourteen components, first four components represent 99.81% of total variability leaving the rest for the other components. Thus, first four components are judged to be effective feature space to represent the information contained in the welding motor current signal and are treated as the features for further analysis. Thus, a total of nine signal features are extracted from main spindle motor and welding motor current signals for further analysis. The selected features are then fed to ANN and SVR based data driven models for prediction of UTS of the joints.

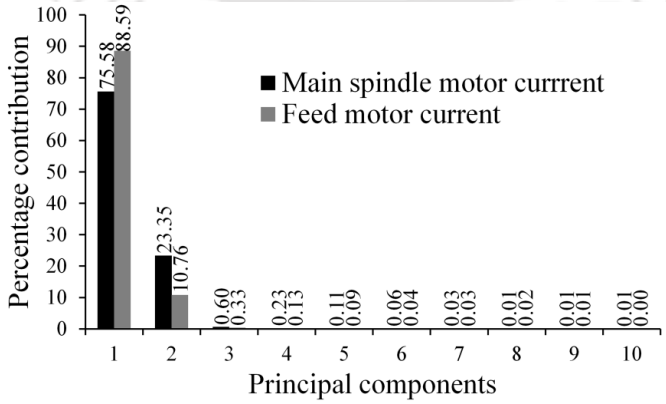

Fig. 5.7 Percentage contribution of principle components for wavelet packet features of main spindle motor and welding motor current signals

The computed signal features in time domain and time frequency domain are further used for developing data driven models for modelling of weld quality in FSW process. For this ANN and SVR are used as the modelling techniques. Detail mathematical representation of ANN and SVR is added in Appendix I and Appendix II, respectively. The outputs from both the modelling techniques are compared to find out the most suitable technique for accurate prediction of UTS of the joints with signal features.

Two SVR models are developed in this study for modelling of UTS of the joints. One model contains only time domain signal features and the other contains process parameters along with signal features. To find the optimum network parameters, the value of C is varied in the range of 1 to 100 in steps of 1.Whereas, γ and ε values are varied in the range of 1 to 10 in steps of 0.01 and 0.01 to 0.1 in steps of 0.001 respectively. From the grid search method, optimum set of C and γ are found to be 90 and 0.06, respectively, when the input space of the model contains signal features along with the process parameters. On the other hand, optimum set of C and γ values for the model when the input space contains only the process parameters are 60 and 0.07, respectively. Optimum values of ε are found to be 0.003 and 0.006 for the models, respectively. The models are trained using 58 data sets and remaining 7 data sets are used for testing the developed models. Prediction performance of the developed models is shown in **Fig. 5.8**. Output predictions of the developed models for the testing cases are listed in **Table 5.3**. From the table it is observed that absolute average percentage error of 2.15% and 6.03% are obtained from the models. Moreover, it is demonstrated that inclusion of signal features in the model input space, increases the prediction accuracy by 64% which indicates that signal features in the input space of the model can be quite effective to accurately predict the quality of the weld. The prediction performance of the SVR model is compared with performance obtained from ANN models to find the better candidate for accurate prediction of weld quality.

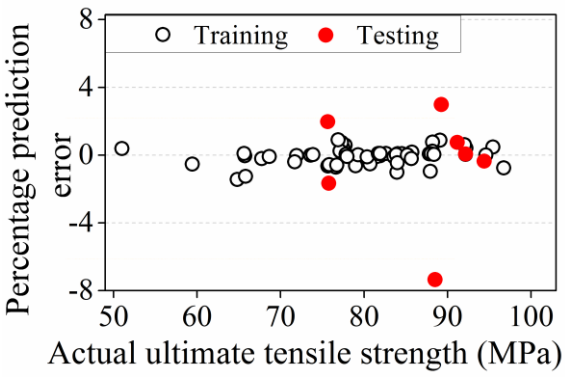

(a)

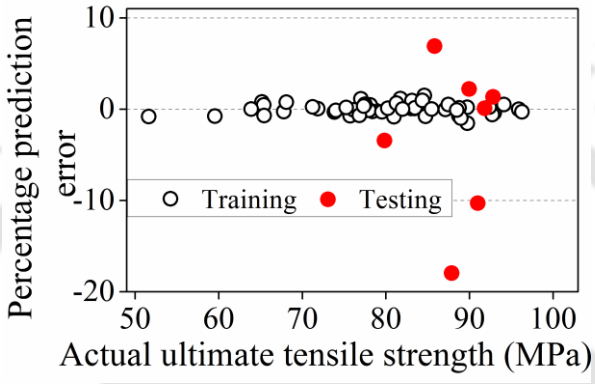

(b)

Fig. 5.8 Performance of support vector regression model (a) with signal features (b) without signal features

Table 5.3 Performance of SVR models with time domain features

Exp. No.	Actual UTS (MPa)	Predicted UTS (MPa)			
		Without signal features	% Error	With signal features	% Error
33	74.54	87.87	-17.88	75.77	-1.65
58	77.17	79.83	-3.44	75.64	1.98
1	94.05	92.82	1.31	94.38	-0.35
17	92	89.95	2.23	89.25	2.98
37	91.86	91.79	0.08	91.16	0.71
51	92.22	85.82	6.93	92.15	0.08
9	82.45	90.99	-10.36	88.50	-7.33
	Average absolute percentage error		**6.03**		**2.15**

A standard multi-layer feed forward neural network trained using back propagation algorithm; known as back propagation neural network (BPNN) and a radial basis function neural network (RBFNN) are developed to model the UTS of the welded samples. Computer programs for ANN models are developed using the C programming language. As neural networks are prone to overfitting the data, validation datasets are used to monitor the behaviour of the network so that it does not move towards overfitting (Pal et al., 2010). In general, it is found that around 15% of datasets are used for validation, 10% are used for testing the developed neural network model (Wang et al., 2008). Remaining datasets are used for training the network. Among the full factorial datasets, 48 and 10 patterns are selected randomly for training and validating the models, respectively. Data set used for testing the SVR model is used for testing the developed neural networks. Similar to that of SVR model development BPNN models are also developed with only process parameters and process parameters along with signal features.

The prediction performance of BPNN model depends on the architecture of the network, learning rate (η) and momentum coefficient (α). The number of neurons in the hidden layer is varied from 5 to 39 in steps of 1. Learning rate is varied in between 0.1 to 1 in the steps of 0.04 and momentum coefficient is varied in between 0.01 to 1 in the steps of 0.01. Initial weight values are chosen randomly between ±0.9 and the bias values at the input layer is taken as 0 and that for hidden and output layer as 1.0 respectively. All the inputs and output variables are normalized between 0.1 and 0.9 which ensures that the back propagation algorithm does not drive some of the connections weights to infinity and thus slow down the training (Haykin, 2003; Jang et al., 2004). The activation functions for both the hidden and output layers neurons are log-sigmoid. The objective of the training is to minimize the mean square error (MSE) by updating the weights through gradient descent method (Haykin et al., 2003).

The best network architecture from the optimization framework is found to be 7-21-1 with η=0.7 and α=0.41 with signal features and the process parameters in the input space. In the network architecture 7 represents total number of input neurons, 21 represents number of hidden neurons and 1 represent number of output neuron. The comparison between the actual UTS values and BPNN predicted UTS values are shown in **Fig. 5.9**. In the figure it is reflected that out of 64 number of patterns, only six predictions deviate from the ± 5% error line and among which, only two are from the

testing data set. The absolute average percentage error for the testing cases is 4.89%. The best BPNN model with only process parameters at the input space is found out to be 3-27-1 with $\eta = 0.84$and $\alpha = 0.61$. The average absolute prediction error for testing cases is found to be 8.57%.

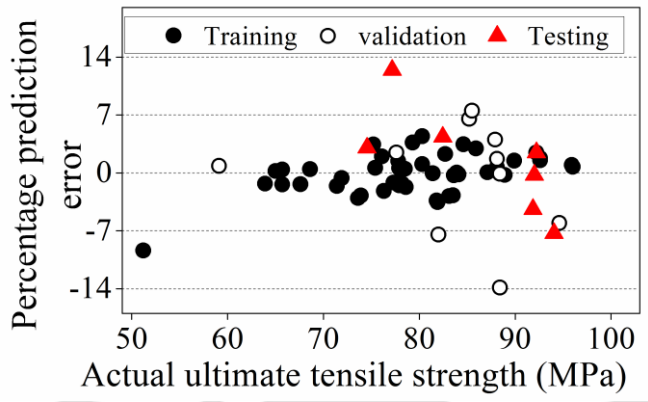

Fig. 5.9 Prediction performance of BPNN model

RBFNN are different than BPNN in the way that it has some special activation functions in the hidden layers called as the radial basis functions. Detail description of training algorithm for RBFNN model is added in Appendix I. Number of hidden layer neurons is varied from 5 to 29 in steps of 1 to find out the optimal network structure. Learning rate for updating weights is varied in the interval of 0.1 to 1 in steps of 0.04 and that for center updation and Gaussian functions spread updation were varied in the interval of 0.01 to 1 in steps of 0.04 respectively. The data set used for development of BPNN model is implemented for the development of RBFNN model.

The best RBFNN is found to be 7-7-1 with 0.46, 0.05 and 0.05 as learning rate for weight, center and spread updating, respectively, with signal features along with the process parameters in the input space. In **Fig. 5.10**, comparison between the actual UTS and RBFNN predicted UTS is shown. Compared to BPNN prediction, the prediction of RBFNN is inferior and out of 64 datasets, 23 predictions are out of ± 5% error line. The absolute average percentage error for the testing cases is 6.33%. The best RBFNN model with process parameters at input space is found out to be 3-11-1 with 0.54, 0.07 and 0.05 as learning rate for weight, center and spread updating, respectively. The average absolute prediction error for testing cases is found to be 9.90%.

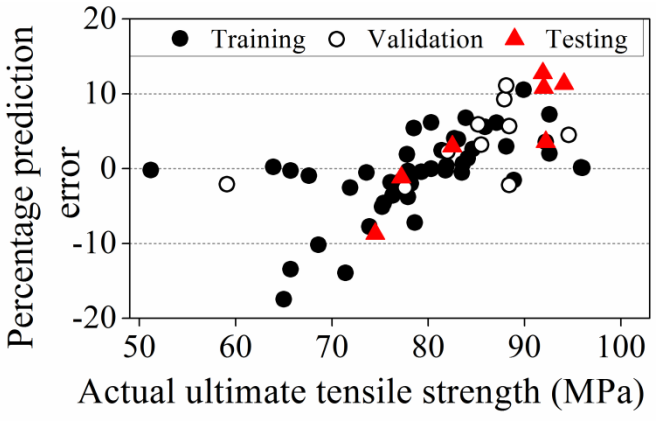

Fig. 5.10 Prediction performance of RBFNN model

The prediction performance of SVR, BPNN and RBFNN models developed are compared and comparative analysis is presented in **Fig. 5.11**. From the figure it is observed that, SVR model performance for prediction of UTS is better than ANN models. An improvement of 55% is experienced in SVR model prediction accuracy when compared with BPNN model predictions. When compared with RBFNN predictions, there is an improvement of 70% in prediction of SVR model. This implies that SVR models, coupled with current signal features can lead to more accurate predictions of UTS of friction stir welded joints and can be implemented in real time in-process monitoring of FSW process.

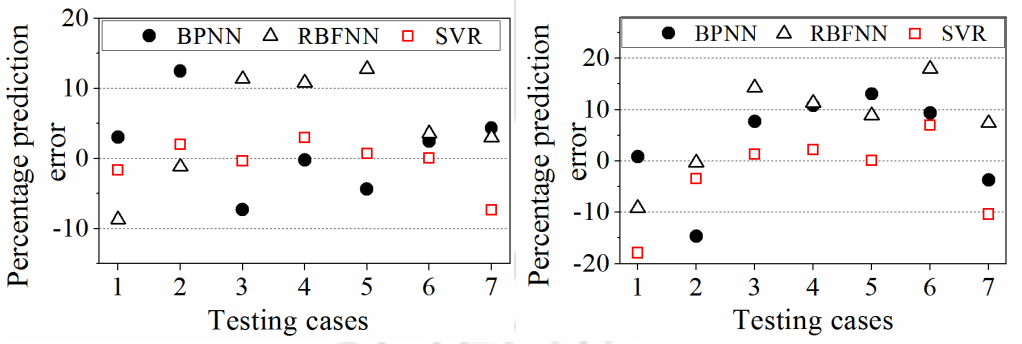

(a) (b)

Fig. 5.11 Comparison of SVR and ANN model performance (a) with time domain signal features (b) with only process parameters

To develop a comparative analysis with the weld quality modelling performance with time domain features, weld quality modelling with ANN and SVR is also attempted for time frequency domain features. The signal features computed with WPT for main

spindle motor current signal and welding motor current signal are reduced to nine features with PCA. These features along with process parameters are used for the development of data driven models for prediction of UTS of the joints.

Similar to the SVR model developed with time domain features of current signal, model with time frequency domain features is also developed. Out of 65 patterns 58 patterns are selected for training of the model and remaining 7 patterns are selected for testing of the developed model. The SVR parameters C, γ and ε are selected in the same range as the previous SVR model. Grid search algorithm is applied for selection of optimum values for C, γ and ε as 94, 1.85 and 0.004 respectively. The prediction performance of developed SVR model is presented in **Fig. 5.12**. The average absolute percentage error is found to be 1.55%. Moreover, from the figure it is observed that the testing errors are well within $\pm 2\%$ range and signifies that SVR model is quite accurate for prediction of UTS with time frequency domain signal features as well.

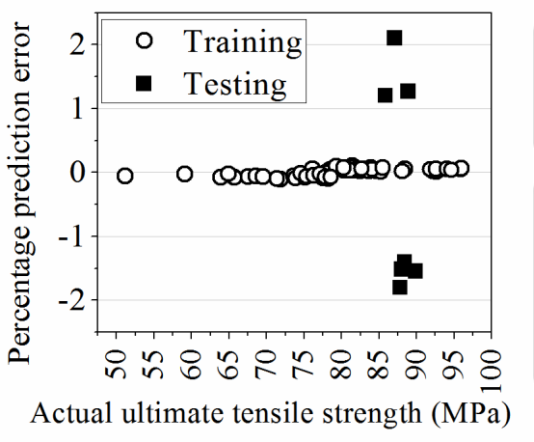

Fig. 5.12 Performance of SVR model with time frequency domain features

Comparison of SVR prediction performance is made through developing BPNN and RBFNN models for the prediction of UTS of the welded joints. Numbers of hidden neurons for BPNN are varied in between 5 to 39 in steps of 1. Learning rate (η) and momentum coefficient (α) for weight updation are varied in between 0.1 to 1 and 0.01 to 1 in steps of 0.04, respectively. Initial weight values are chosen randomly between ±0.9 and the bias values at the output layer is taken as 0 and that for input and hidden layers as 1.0. All the inputs and output variables are normalized between 0.1 and 0.9. The activation functions for both the hidden and output layers neurons are log-sigmoid. The optimum number of hidden neuron is selected based on the minimum of the sum of

training and validation MSE. Optimum hidden neuron, learning rate and momentum coefficient are found out to be 19, 0.62 and 0.53, respectively. Thus the optimum network structure of the developed BPNN model for UTS comes out to be 12-19-1 with η=0.62 and α=0.53. The prediction performance of the developed BPNN model is shown in **Fig. 5.13**. Absolute average percentage error for the testing cases for UTS is 5.87%. The performance of the developed BPNN model is inferior to that of SVR model. It indicates that SVR model can be effectively used for prediction of UTS of the joints.

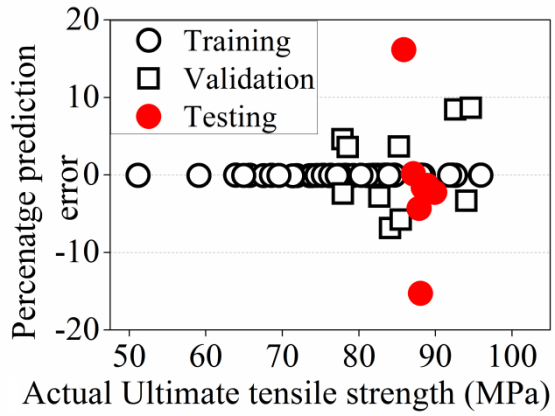

Fig. 5.13 Prediction performance of BPNN model

Another ANN model developed is the RBFNN model. In finding the optimal network parameters for RBFNN model, different combinations of number of hidden neurons, learning rate for weight updation, center updation and Gaussian function spread updation are tried and based on the minimum of sum of training and validation MSE criterion optimum parameters are obtained. Numbers of hidden neurons are varied in between 5 to 40 in steps of 1. Learning rate for updating weights is varied in between 0.1 to 1 in steps of 0.04. Learning rate for center and spread updation are varied in between 0.01 to 1 in steps of 0.4.

Based on the minimum MSE criterion, optimum number of hidden neurons for UTS prediction is found to be 15. The optimal network structure for UTS modeling found to be 12-15-1 with 0.9, 0.05 and 0.05 to be the optimum learning rates for weight, center and spread updation, respectively. Scatter plot for the comparison of predicted versus actual values of UTS is shown in **Fig.5.14**. Average absolute prediction error for the testing cases for UTS is 19.08%. It is observed that RBFNN performance in prediction of UTS is inferior compared to SVR and BPNN models. The prediction

performance of the developed models is shown in **Table 5.4**. The comparative analysis indicates that SVR model outperforms prediction of UTS of the joints with time frequency domain features compared to the developed ANN models.

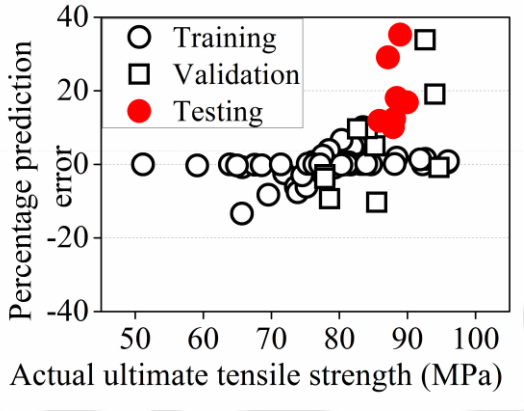

Fig. 5.14 Prediction performance of RBFNN model

Table 5.4 Comparison between BPNN, RBFNN and SVR predicted ultimate tensile strength with time frequency domain features and process parameters

Exp. No.	Actual UTS (MPa)	BPNN model		RBFNN model		SVR Model	
		Predicted UTS (MPa)	% error	Predicted UTS (MPa)	% error	Predicted UTS (MPa)	% error
39	89.91	91.94	-2.25	74.76	16.84	91.302	-1.55
59	87.12	86.99	0.14	61.77	29.09	85.291	2.10
2	85.87	71.99	16.16	75.71	11.83	84.839	1.20
29	88.05	101.51	-15.28	77.15	12.37	89.387	-1.52
27	87.86	91.67	-4.33	78.95	10.13	89.448	-1.81
55	88.92	90.13	-1.32	57.55	35.27	87.793	1.27
49	88.42	89.87	-1.64	72.45	18.05	89.668	-1.41
Absolute average percentage error			**5.87**		**19.08**		**1.55**

The analysis of current signals acquired during welding experiments leads to the impression that features computed can be effective in modelling of UTS of the joints in FSW process. Among the three data driven models developed namely BPNN, RBFNN

and SVR, the later outperforms in terms of prediction accuracy. This establishes SVR to be best for UTS prediction with current signals. Among the features computed in time domain for main spindle motor current signal and in time frequency domain for main spindle motor and welding motor current signals the later results in more accurate prediction of UTS of the joints. The objective of monitoring of FSW process with real time signal processing is carried forward through investigation of vertical force signal, torque signal and tool rotational speed signal as discussed in the following sections.

5.7 Prediction of UTS with vertical force signal features

There are three forces experienced during FSW process as discussed in the literature review chapter (section 2.5). Among the three forces it is observed that vertical force plays an important role in governing the FSW process compared to other two forces. Real time measurement of vertical force will lead to better monitoring of FSW process. The measurement setup developed in the current research work (discussed in chapter 4) is used for acquisition of real time vertical force signals. For conducting the welding experiments design matrix reported in experimental investigation chapter (chapter 3) is used. Vertical force signals are acquired against each experiment and processed for extraction of salient signal feature.

Vertical force signals acquired against the repeated experiments (Exp. No. 33 and Exp. No. 65 as reported in Chapter 3) are shown in **Fig. 5.15**. It is to note that these two experiments are conducted over same level of process parameters (refer **Table 3.4,** chapter 3). The signals against the experiments do not show similar trend and magnitude. The variation of the signals for the welding period (indicated by a red rectangular box in the figure) fetches that anomaly occurred during the process. The undulations in the signal against Exp. No. 65 are due to abnormal material flow around the welding tool during the welding process (Morisada et al., 2015). This brings the notion that even though process parameters remain constant variation in the welding process is possible due to the dynamic natures and interaction of process parameters. This variation in the process as captured by vertical force signals needs further exploration for effective correlation with the process behaviour. Extraction of useful information regarding the process behaviour vertical force signals are processed through time domain analysis, frequency domain analysis and time frequency domain analysis. Time domain analysis is carried out by computing statistical features as root mean square (RMS), skewness and

kurtosis. Frequency domain analysis is performed with discrete Fourier transform and time frequency domain analysis is performed with wavelet packet transform and Hilbert-Huang transform.

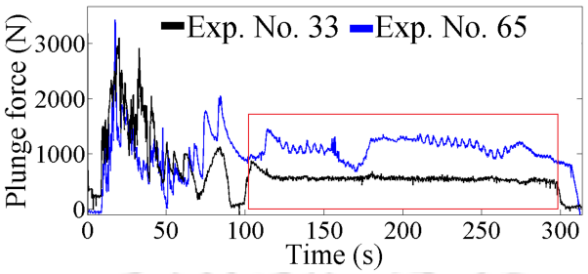

Fig. 5.15 Vertical force signals against Exp. No. 33 and Exp. No 65

RMS, skewness and kurtosis computed from vertical force signal are correlated to UTS of the joints. Unfortunately, no decisive correlation is observed from the analysis. Hence, a new parameter is developed in this work by combining the statistical features. The combined parameter (CP) is calculated as per the **Eq. 5.36**. This parameter is then correlated to UTS of the joints. **Figure 5.16** represents the correlation in graphical form. It can be observed that, with the increase in CP; UTS of the joints found to follow an increasing trend. Thus, the proposed combined parameter can be an effective indicator for monitoring the quality of the welds in terms of UTS of the joints.

$$\mathrm{CP} = \log_{10}\left[\frac{\mathrm{RMS} \times \mathrm{kurtosis}}{\mathrm{skewness}}\right]^{0.5} \quad \textbf{(5.36)}$$

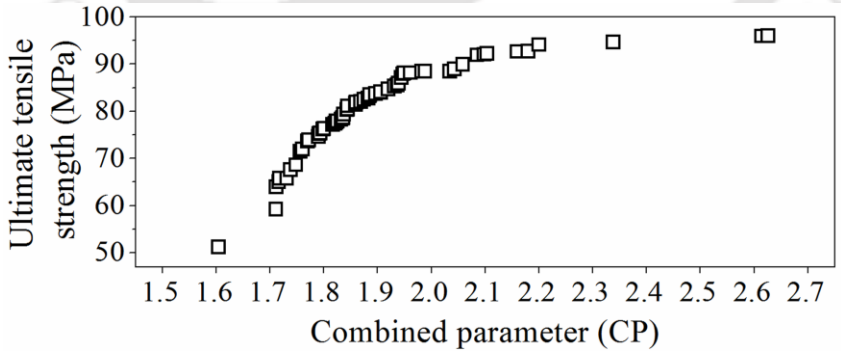

Fig. 5.16 Variation of proposed combine parameter for vertical force with ultimate tensile strength

Prior to the analysis in time frequency domain the signals are initially analyzed with FFT algorithm with MATLAB software package for conducting frequency domain

analysis on the signals. Unfortunately the frequency spectrum does not provide any notable information regarding the process behaviour. This necessitates for further investigation with time frequency domain analysis. Successful implementation of WPT in analysing current signals motivates the study to further explore it for vertical force signal analysis. Apart from wavelet packet transform HHT is also explored for analysis of vertical force signals.

In WPT, selection of suitable mother wavelet function plays an important role in efficient decomposition of signals. The selection of mother wavelet function is made as per the energy-entropy criterion discussed in section 5.6.3. The computed ratio for vertical force signals are shown in **Fig. 5.17**. From the figure it is observed that *db10* mother wavelet function is more suitable for the decomposition. With this mother wavelet function signals are decomposed up to third level. At the third level of decomposition eight wavelet packets are obtained. The RMS of the wavelet packets are computed for each signals acquired during welding as shown in **Eq. 5.37**. This is presented as the effective features for the force signals.

$$WPC = RMS[RMS(WP_i)], \qquad i = 1,2,\dots,8 \tag{5.37}$$

where, WPC are the extracted feature for vertical force signal, WP_i are the respective wavelet packets obtained from wavelet packet decomposition at third level and RMS represents the root mean square operation. In **Fig. 7.5** variations of WPC with respect to UTS of the joints is shown. From the figure it is evidential that with UTS, WPC follow an increasing trend. This indicates that wavelet packet features computed from vertical force signals is competent towards development of UTS prediction methodology. These features along with the proposed statistical indicator and considered process parameters are fed to SVR and BPNN models for prediction of UTS of the joints. In the analysis of vertical force signals another signal processing technique implemented is HHT.

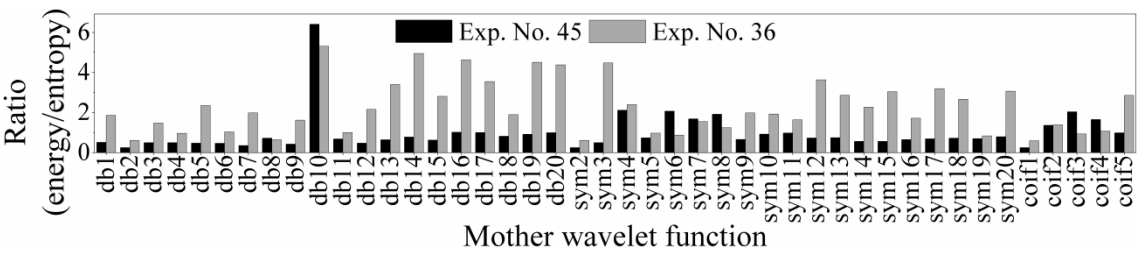

Fig. 5.17 Variation of energy to entropy ratio of the vertical force signal with mother wavelet functions.

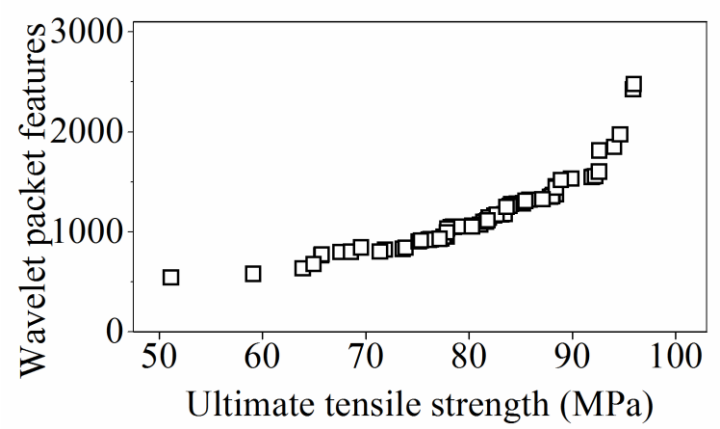

Fig. 5.18 Variation of wavelet features with ultimate tensile strength

In the analysis of non-stationary signals, HHT found appreciable importance (Lin et al., 2012). However, the shortcoming with HHT is that, the first IMF usually covers broad frequency range such that mono component conditions may be difficult to achieve (Lin et al., 2012). Moreover, observing signal in wide frequency band may result is redundant information. On the other hand, WPT decomposes a signal into sub-bands with low and high frequency content through which visualization of signals in different frequency bands is possible. This advantage of WPT is carry forward to reduce the limitation with HHT and a combined WPT-HHT approach is presented in this work. The flow chart of the proposed methodology is given in **Fig. 5.19**. The wavelet packets as computed in the WPT of vertical force signals as represented in aforementioned paragraphs are presented to HHT algorithm developed with MATLAB software package. However, it is not guaranteed that all the wavelet packets may be useful for further investigation. Thus an efficient method is required to select the suitable mother wavelet function. A signal energy based criterion is introduced to find the most suitable wavelet packet that can be a better candidate for HHT. The implemented energy criterion is given in **Eq. 5.38**.

$$E_{\%}^{i} = \frac{E_{wp}^{i}}{E_{s}} \times 100 \qquad \textbf{(5.38)}$$

where, $E_{\%}^{i}, E_{wp}^{i}, E_{s}$ are percentage energy, energy of the wavelet packets ($i = 1,2,\ldots,8$) and energy of the signal, respectively. From **Eq. 5.38**, energies of the packets are computed and the one with the maximum energy is further processed by HHT. The packet with maximum energy content is rich with signal information and due to limited

frequency band HHT will result in fine frequency resolution. Next, the selected packet is fed to HHT algorithm and respective IMFs are obtained. The respective IMFs are further processed with Hilbert transform to compute the instantaneous phase angles of the signals. The RMS of the amplitude of IMFs and instantaneous phase angles along with CP and WPC are fed to BPNN and SVR models for prediction of UTS of the joints.

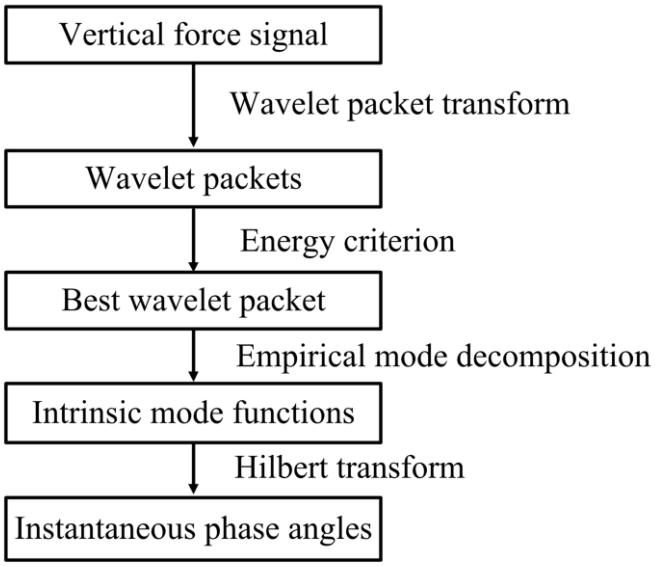

Fig. 5.19 Flow chart for combined WPT-HHT analysis

Modelling of weld quality with signal features is attempted with the development of SVR and BPNN models. Mathematical descriptions of these two methods are given in Appendix I and Appendix II. Tool rotational speed, welding speed, shoulder diameter, CP, WPC, instantaneous phase angles and RMS of amplitude of decomposed IMFs from WPT-HHT are selected as the input to the SVR and BPNN models. For the selection of optimum value of SVR parameters,C,γ and ε grid search algorithm is implemented. The range of these parameters are varied as 1 to 100 in steps of 1 for C, 1 to 10 in steps of 0.01 for γ and 0.01 to 0.1 in steps of 0.001 for ε. From the grid search algorithm the optimized parameters are found to be 97, 1.47 and 0.005 for C, γ and ε, respectively. Training and testing of the SVR model is achieved through minimization of MSE. Similarly, parameters that effect performance of BPNN model viz. learning rate (η), momentum coefficient (α) and number of neurons in the hidden layer are selected based on minimum MSE criteria. The range of η, α and number of hidden layer neurons are varied in the range of 0.1 to 1 in steps of 0.04, 0.01 to 1 in steps of 0.04 and 5 to 30 in steps of 1 respectively. For training the SVR model out of 65 patterns 50 are selected as training patterns and remaining 15 patterns are selected as testing patterns which is again

used for testing of BPNN model. For developing BPNN model out of 50 remaining patterns 10 patterns are selected for validation and remaining patterns are used for training of the model. The optimum BPNN network found out to be 7-27-1 with $\eta = 0.9$ and $\alpha = 0.85$. After the development of the models percentage prediction error values between the actual UTS and models predicted UTS are computed as per **Eq. 5.39**.

$$\%\ error = \frac{Actual\ value - predicted\ value}{Actual\ value} \times 100 \qquad (\mathbf{5.39})$$

where, actual value is the value obtained from the experimental investigation and predicted value is the value obtained from the SVR/BPNN model prediction. The prediction results for the testing patterns are shown in **Table 5.5** and the prediction performance of the developed models are compared in scatter diagrams as represented in **Fig. 5.20**. From the table and the figures it is observed that signal features combined with process parameters leads to an accurate UTS prediction SVR model with accuracy of 99.55%. The same for the BPNN model is found out to be 98.42% which is 1.13%less compared to SVR model.

Table 5.5 Prediction results for the testing cases

Exp. No.	Actual ultimate tensile strength (MPa)	SVR predicted ultimate tensile strength (MPa)	% error	BPNN predicted ultimate tensile strength (MPa)	% error
59	87.12	87.34	-0.25	86.27	0.98
9	82.45	82.18	0.33	81.96	0.59
40	76.12	76.77	-0.85	74.46	2.18
60	81.81	81.24	0.70	81.67	0.17
32	77.83	77.38	0.58	78.27	-0.57
7	88.12	88.62	-0.57	85.89	2.53
45	95.95	95.78	0.18	94.36	1.66
36	51.15	51.37	-0.43	47.66	6.81
61	80.29	79.82	0.59	80.81	-0.64
6	84.64	84.48	0.19	83.13	1.79
13	95.89	95.55	0.35	94.52	1.43
3	78.56	78.74	-0.23	78.03	0.68
31	92.62	92.07	0.59	93.91	-1.39
42	77.86	77.61	0.32	78.22	-0.46

2	85.87	85.35	0.61	84.29	1.85
Average absolute percentage error			**0.45**		**1.58**

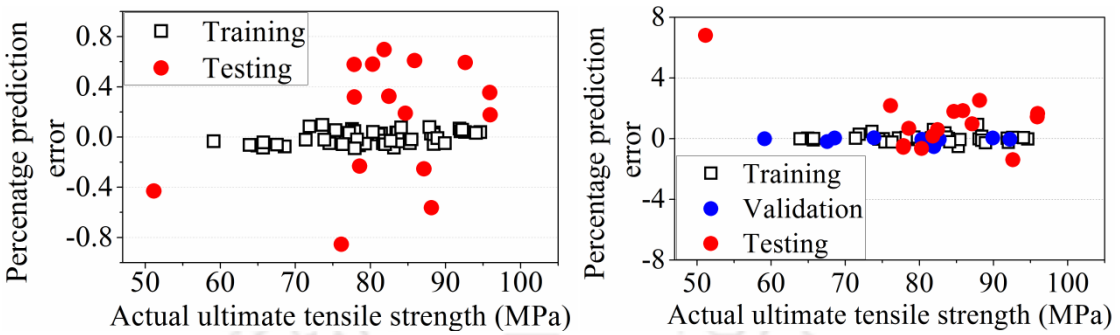

(a) (b)

Fig. 5.20 Scatter diagrams for the comparison of actual versus predicted ultimate tensile strength (a) SVR model (b) BPNN model

The influence of vertical force signal in monitoring of FSW process has been presented in the preceding section. The study delivers a new combined methodology based on WPT and HHT that is free from limitation existent with HHT. The computed signal features are fused with SVR and BPNN models for prediction of UTS of the joints. As like in the case of current signal features, in this case also SVR outperforms prediction of UTS over BPNN model.

5.8 Prediction of UTS with torque signal features

A methodology for extracting suitable information from vertical force signal for monitoring of FSW process has been presented in the preceding section. Apart from the vertical force another parameter that eventually governs the process is the associated torque. The associated torque is the result to overcome the resistance offered by the material around the rotating tool. Thus torque is the combined outcome of tool rotational speed and welding speed as these two governs the amount of material plasticization in the weld zone around the tool. As like in case of vertical force, real time measurement of torque can also offer to observe the process under the effect of both controllable and uncontrollable parameters. The influence of torque in monitoring of the process is identified and reported by Mehta et al., (2013). It was observed from the results presented that monitoring the torque behaviour of the process can be observed. However,

the work did not extends the concept in developing methodology for FSW process monitoring or rather more specifically monitoring of weld quality. This study is devoted for developing methodology for monitoring of FSW process through analyzing torque signals. In the literature review section it is realized that effort for developing methodologies for monitoring of FSW process with force signal is relatively more compared to torque signal which is almost nonexistent.

Real-time torque signals are acquired using the developed force/torque measurement setup (chapter 4) during the FSW process and analyzed in time domain through statistical features and time frequency domain through DWT. The torque signals are filtered before further processing. Fifth order Butterworth high pass filter is used in MATLAB software package for noise reduction. The cut off frequency of the filter is decided based on the frequency spectrum of the raw signal. The filter has eliminated the high frequency content of the signal which mostly represents noise part (Arora et al., 2012), the similar approach as applied in analysis of current signals with WPT is not attempted in this part of the study as decomposition of high frequency part will not be useful. The time frequency domain analysis of torque signals is achieved with DWT that offers decomposition of the signals on the low frequency band. The methodology of torque signal processing is represented schematically in **Fig. 5.21**. Apart from the UTS modelling the features computed are further developed for computing a combined indicator for identification internal defects in the welded samples which will be discussed in chapter 6.

Torque signals acquired during the repeated experiments (Exp. Nos. 33 and 65, Table 3.4, chapter 3) are shown in **Fig. 5.22**. From the figure it is indicative that even though the experiments are performed over same parameter setting, the torque signals are deviating. This deviation in the process is supported by the difference obtained in the UTS of the welded samples (Table 3.5, section 3.6, and chapter 3). Hence, relying on process parameters will not guarantee the desired outcome and quality modelling based only on process parameters might result in inaccurate decisions. The deviation in the torque data reveals its capability to compete with the existing monitoring indicators such as vertical force signal and acoustic signal in FSW process. The torque signals acquired during welding are analyzed in time domain and time frequency domain. Time domain analysis is carried out through computation of four statistical features as D_x, S_x and E_x.

Time frequency analysis of signal is attempted with DWT. The same statistical features are computed from decomposed signals with DWT.

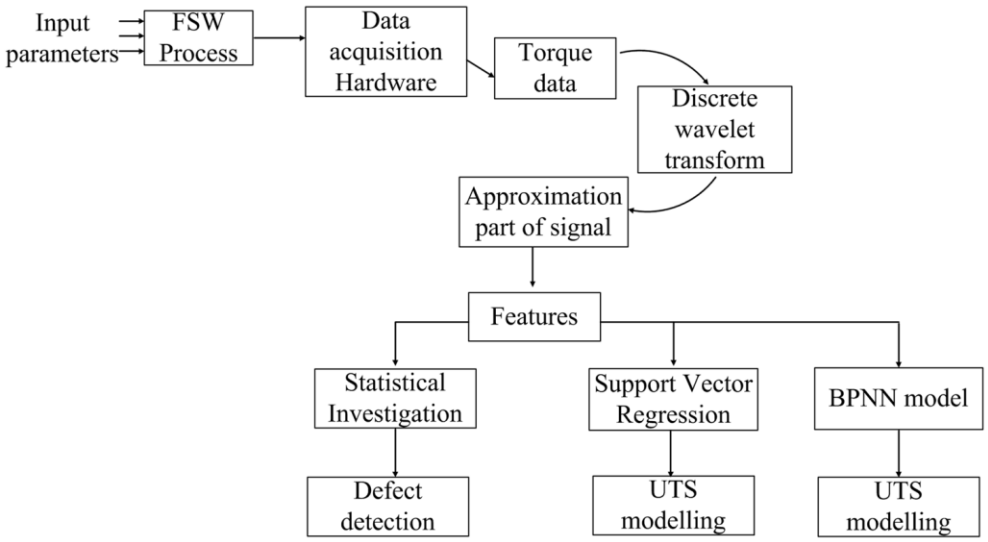

Fig. 5.21 Schematic representation of the methodology developed for analysis of torque signal

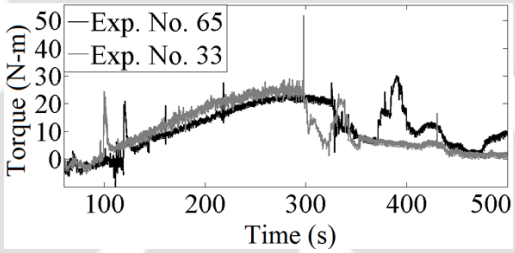

Fig. 5.22 Torque signals against repeated experiments

Interestingly from the computed statistical features viz. D_x, S_x and E_x in time domain no notable information can be fetched regarding the process behaviour. Moreover, the computed features failed to contribute effectively in identification of internal defects in the welded samples. Hence, in the study it is decided to perform time frequency analysis to extract more useful information from torque signals. The DWT on torque signals are performed up to fourth level of decomposition using Daubechies fifth order (db5) mother wavelet function as available in MATLAB software package. This particular wavelet function is chosen after comparing 24 different mother wavelet functions. Against each wavelet function, correlation coefficient is computed for the signal against the experiment that yields maximum UTS (Exp. No. 45). The correlation coefficients are displayed in **Fig. 5.23**. From the figure it is observed that db5 is the best

for the analysis of the torque signals. Decomposition of real-time torque signals against experiments with maximum UTS (Exp. No. 45) and minimum UTS (Exp. No. 36) using DWT is displayed in **Fig. 5.24**. To find out the contribution of the details of the decomposed signals Fourier transform is performed on the details part of the signals. For this, most widely used fast Fourier transform algorithm is applied. From the analysis of the details, it is observed that there is no significant peak in the frequency spectrums of the signals. Rather, it is observed that amplitude is distributed all over the frequencies even for the narrowest frequency band which is at the fourth level in wavelet decomposition. Thus, it is believed that details part mostly contains the noise information and hence, in this study only approximation parts are further analyzed to compute the statistical features.

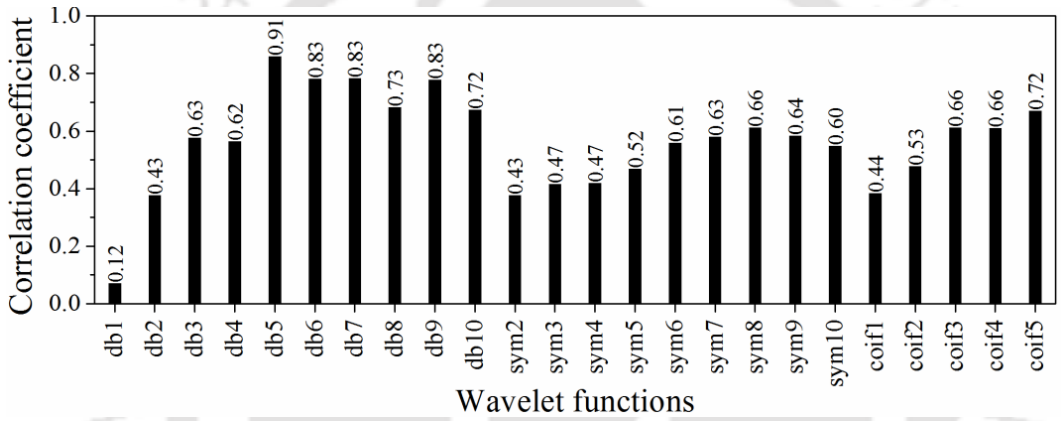

Fig. 5.23 Comparison of wavelet functions for torque signal analysis

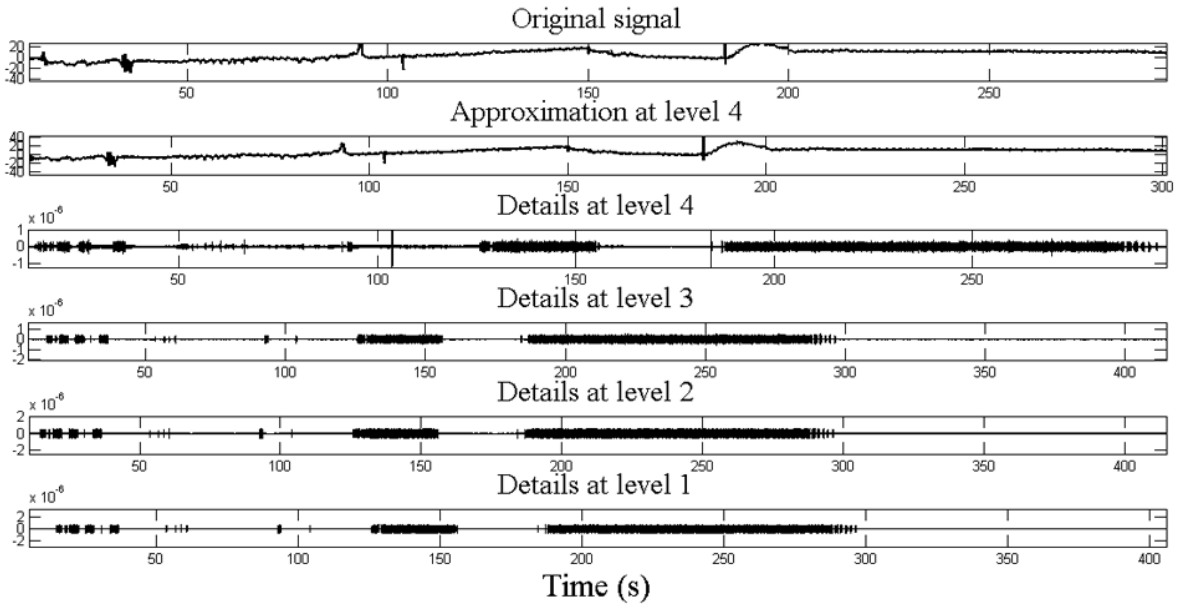

(a)

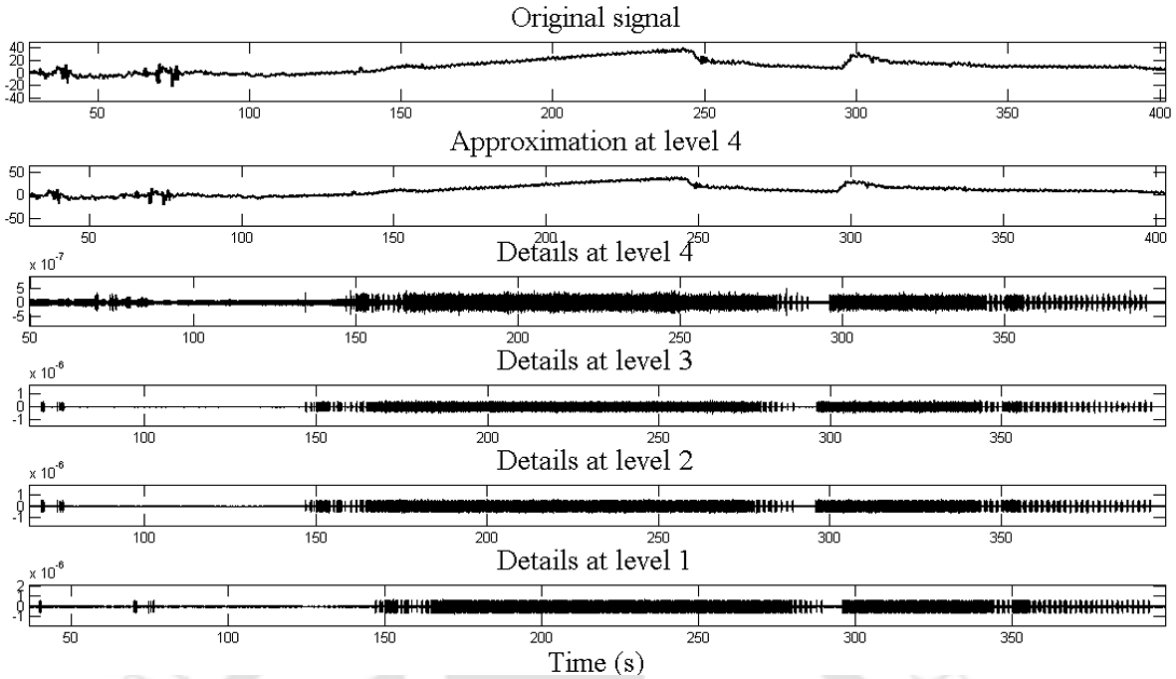

(b)

Fig. 5.24 Discrete wavelet transform of torque signals (a) Exp. No. 45 (b) Exp. No. 36

In this study the approximation part of the decomposed torque signals are further investigated to compute three statistical features D_x, S_x and E_x. For the computation of these three features mathematical expectation (m_x) is required prior hand. The expression for the mathematical expectation of a discrete signal is given in **Eq. 5.40**.

$$m_x = \frac{1}{N}\sum_{n=0}^{N-1} \Upsilon_a \tag{5.40}$$

where, $\Upsilon_a$is the approximation part of the input torque signal processed with wavelet transform and N is the length of the approximation part of the signal.

The dispersion $D_x$characterizes the value dispersion relative to the mathematical expectation m_x. Mathematical expression to represent D_x can be seen in **Eq. 5.40**.

$$D_x = \frac{1}{N-1}\sum_{n=0}^{N-1} (\Upsilon_a - m_x)^2 \tag{5.40}$$

Asymmetry S_x of the signal is defined as shown in **Eq. 5.41**. For the computation of the asymmetry prior knowledge of the mean square deviation of the signal is needed.

The mean square error (σ_x) can be computed from **Eq. 5.42** and the excess E_x is defined as given in **Eq. 8.5**.

$$S_x = \frac{1}{N\sigma_x^4}\sum_{n=0}^{N-1}(\Upsilon_a - m_x)^3 \tag{5.41}$$

$$\sigma_x = \sqrt{D_x} \tag{5.42}$$

$$E_x = \frac{1}{N\sigma_x^4}\sum_{n=0}^{N-1}(\Upsilon_a - m_x)^4 - 3 \tag{5.43}$$

The values of excess and asymmetry define the non-uniformity of the data collection, the asymmetry of the distribution and its fit to the normal law. The computed statistical features are afterwards normalized using the relation shown as **Eq. 5.44**. The features are normalized to eliminate the difference in the range of computed values.

$$Normalizedvalue = \frac{F_i - \min(F)}{\max(F) - \min(F)} \tag{5.44}$$

where, F represents the feature space among D_x, S_x or E_x and i represents the element in the feature space respectively. These normalized features are used for developing the weld quality modelling tool using SVR and ANN modelling techniques.

The modelling of UTS of the joints with torque signal features are attempted through SVR and the performance of SVR is later compared with BPNN. For finding the optimum set of C, range of C is chosen from 1 to 100 in steps of 1 and range of γ is chosen to be 1 to 10 in steps of 0.01 and ε is chosen to be 0.01 to 0.1 in steps of 0.001. Grid search algorithm is implemented for selection of suitable SVR parameters.

To develop methodology for modelling the UTS of the welded component using SVR technique, two models are developed named as Model I and Model II. In Model I, the input space consists of computed normalized statistical signal features and UTS of the joints is the output parameter. On the other hand, in the Model II, the input space consists of the three signal features along with three process parameters considered in this study namely tool rotational speed, welding speed and shoulder diameter. The objective of comparing these two models is to bring out the efficacy of the computed signal features in developing process independent online modelling of UTS in FSW

process. The developed models are trained and tested in the SVR frame work. For modelling both the SVR models, out of 65 patterns, 50 random patterns are chosen to be the training patterns and rest 15 patterns are chosen as the testing patterns used for the evaluation of prediction performance of the models. During the training and testing phases of the models it is ensured that the training patterns and testing patterns contain data from both defective and defect free welds for better generalization of the model. The optimized SVR parameters against each model are listed in **Table 5.6**.

Table 5.6 Optimized SVR parameters for each model

SVR Models	C	γ	ε
Model I	85	1.3	0.006
Model II	60	2.41	0.004

Parameter C, determines the tradeoff between the model complexity and the degree to which deviations larger than ε are tolerated in optimization formulation for SVR. For instance, if C is too large, then the objective is to minimize the empirical risk only, without regard to model complexity part in the optimization formulation. On the other hand parameter ε controls the width of the ε-insensitive zone used to fit the training data. The value of ε can affect the number of support vectors used to construct the regression function. The bigger the ε, the fewer the support vectors are selected. Higher values ε also results in more flat estimates.The parameter γ associated with the kernel function correlates the non-linearity of the estimation. In SVR the input is first mapped onto a feature space using some non-linear mapping function (kernel function) and then a linear model is constructed in this feature space. The parameter γ defines the amount of non-linearity that needs to be handled in the model development. The more is the γ parameter more amount of non-linearity in the input data.

In view of the aforementioned discussion the optimized parameters against both the developed models reflect that Model II shows more non-linear behaviour than Model I. This non-linearity may affect the prediction performance of the developed SVR model. For Model I the optimized cost function associated is larger than that of model II. This implies that the soft margin in Model I is higher than that of Model II. This will result in inclusion of fewer points as the support vectors for the error estimation in SVR than

model II. The same is also observed with the errors shown in **Table 5.7**. Model I yields low training and testing error compared to model II. The explanation made for cost function also holds good for ε parameter for both the models. With the higher value of ε parameter for Model I, fewer support vectors are selected in the optimization problem associated with SVR and this results in low estimation error.

Using the optimized parameters in the SVR models, UTS of the joints are modeled and prediction performances of each of the model are listed in **Table 5.7**. From the table it is seen that Model I gives the better accuracy. This model is comprised of only signal features in the input space of the SVR model. The scattered plots for the developed SVR models can be seen in **Fig. 5.25**. From the figures it is again revealed that Model II is inferior in performance than Model I. In Model II the maximum training and testing error obtained are 2.46 and 1.79 respectively. The same for model I are 0.36 and 1.93, respectively. This indicates that the computed signal features from torque signal can be effective in accurate modelling of UTS of the welded joints in FSW process. The results obtained from SVR are further compared with ANN model.

Table 5.7 Performance of SVR models

	Absolute average percentage error	
SVR Models	**Training patterns**	**Testing patterns**
Model I	0.18	0.53
Model II	0.23	0.58

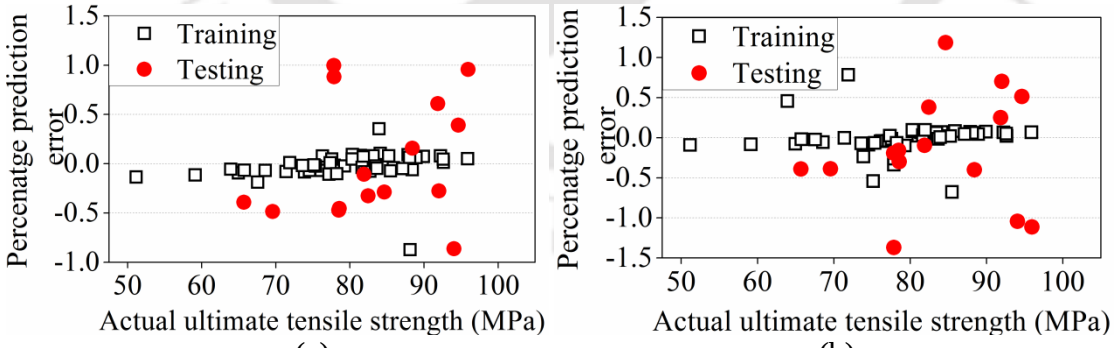

Fig. 5.25 Prediction performance of the SVR with (a) only signal features (b) signal features along with process parameters with torque signal

The performance of SVR model developed for the prediction of UTS of the joints with signal features in the input space (Model I) is compared with model developed using BPNN model. Computer program for ANN model is developed using the C

programming language. As neural networks are prone to overfitting the data, validation datasets are used to monitor the behaviour of the network so that it does not move towards overfitting (Pal et al., 2010). Out of the 65 available patterns, 40 are used for training the ANN model and out of the remaining 25 patterns 10 are used for validation and 15 are used for testing purpose. Prediction capability of BPNN model depends on the architecture of the network, learning rate and momentum coefficient. As the number of inputs and output cannot be changed, the only way to change the network architecture is by changing the number of hidden layers or number of hidden neurons in the respective hidden layers or both. Here, BPNN model was developed using single hidden layer. The number of neurons in the hidden layer is varied from 3 to 30 in steps of 1. Learning rate was varied in between 0.1 to 1 in the steps of 0.1 and momentum coefficient was varied in between 0.01 to 1 in the steps of 0.1. Initial weight values were chosen randomly between ±0.9 and the bias values at the input layer was taken as 0 and that for hidden and output layer as 1.0 respectively. All the inputs and output variables were normalized between 0.1 and 0.9 which ensures that the back propagation algorithm does not drive some of the connections weights to infinity and thus slow down the training. The activation function for hidden and output layers neurons is log-sigmoid. The objective of the training was to minimize the mean square error by updating the weights through gradient descent method. The optimum network architecture obtained is 3-7-1 with learning rate of 0.7 and momentum coefficient of0.51. The performance of BPNN model is shown in the scatter plot in **Fig. 5.26**. **Table 5.8** compares the average absolute percentage error yielded by BPNN model and SVR model in the prediction of UTS of the joints. From the table it is observed that SVR outperforms the modelling of the joint quality compared to BPNN model with an improvement of 90.27%.

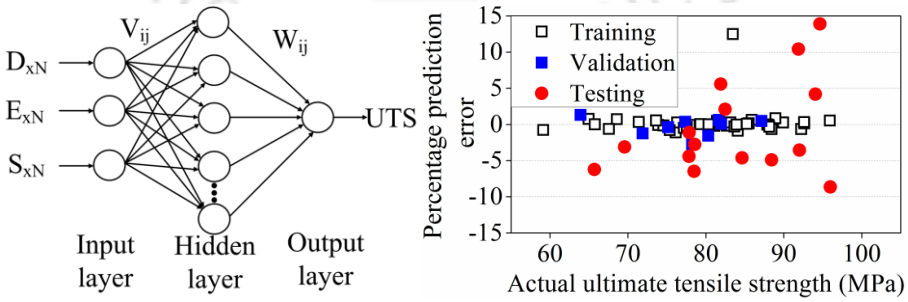

(a) (b)

Fig. 5.26 (a) Schematic of the developed BPNN model and (b) Scatter plot for BPNN prediction performance with torque signal features

Table 5.8 Prediction performance comparison for SVR and ANN with inputs as torque signal features and process parameters

Exp. No.	Actual UTS (MPa)	Predicted UTS (MPa)			
		SVR	% error	BPNN	% error
1	94.05	94.77	-0.76	90.11	4.19
6	84.64	84.18	0.55	88.54	-4.61
42	77.86	77.85	0.02	78.72	-1.10
17	92	92.50	-0.54	95.27	-3.55
24	78.48	78.04	0.56	83.55	-6.46
3	78.56	78.96	-0.51	80.72	-2.75
45	95.95	95.65	0.31	87.67	8.63
21	94.63	95.23	-0.63	81.48	13.89
47	69.56	63.95	-0.06	71.72	-3.10
9	82.45	82.44	0.01	80.73	2.09
4	65.69	66.09	-0.61	69.77	-6.22
5	88.42	86.58	2.08	92.74	-4.88
37	91.86	91.75	0.12	82.30	10.41
32	77.83	78.33	-0.65	81.26	-4.41
14	81.89	81.50	0.48	77.32	5.58
Average absolute percentage error			**0.53**		**5.45**

Real time measurement of torque signal reveals significant variation against the repeated experiments. This implies that relying only with process parameters in prediction of UTS may results in inferior accuracy. In this section a methodology has been developed for prediction of UTS of the joints with SVR and BPNN models with signal features. As like in current signals and force signal analysis SVR performed appreciably in prediction of UTS compared to BPNN model. Moreover, with torque signal also it is observed that inclusion of signal features in the SVR models considerably improves the prediction accuracy. It signifies importance of real time features for accurate modelling compared to modelling only with process parameters. Realizing the importance of signal features in contribution of improvement of quality prediction accuracy a new signal associated with FSW system namely tool rotational

speed signal is tested for development of methodology for accurate prediction of UTS of the joints.

5.9 Prediction of UTS with tool rotational speed signal features

The physics of FSW process confirms that majority (Arora et al., 2012) of heat required for joining materials is achieved through friction between a rotating tool and workpiece material followed by adiabatic heating due to severe plastic deformation. The heat generated in FSW process is responsible for material plasticization and hence joining of the mating surfaces. The most influencing parameter that governs the heat generation is tool rotational speed. Monitoring this parameter in real time through integration of suitable sensor can fetch valuable information regarding the process and any deviation than the desired level can be detected that might influence the process outcome. The monitoring of the process with similar ideology but with other indirect signals such as vertical force and acoustic emission signals has been reported in literature review section. This study is an attempt made to represent tool rotational speed signal which is believed to offer more direct information regarding the process behaviour.

Speed signals acquired during the repeated experiments (Exp. No. 33 and Exp. No. 65) are shown in **Fig. 5.27**. Difference in magnitude as well as trend of these two signals initiates the need to produce the information which not only capture the trend but also the magnitude information. Frequency spectrums of the speed signals do not reveal any notable information to interpret the process variation against the repeated cases. The signals are further processed with WPT, DWT and HHT to extract process information. Interestingly the computed features failed to draw attention in revealing any considerable information regarding the process behaviour and do not correlate to process outcome. This pushes the study to explore another useful signal processing techniques that can offer a direct representation of signal information. The survey of available literature and advantages of fractal theory indicates possible implementation of fractal theory in signal analysis as attempted by many researchers in field of science and engineering. Hence, it is decided to explore possibility of analyzing speed signal with fractal theory for effective monitoring of process behaviour.

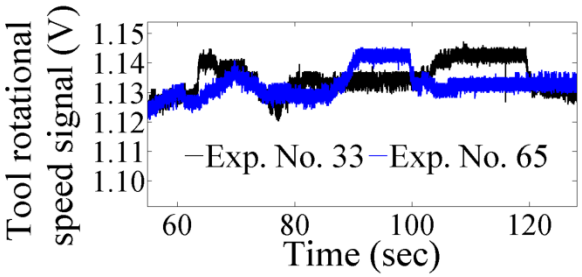

Fig 5.27 Tool rotational speed signal against repeated experiments

Estimation of fractal theory from waveforms is achieved through implementing Higuchi's (Higuchi, 1988) algorithm. The computed FDs against each experimental case can be seen in **Table 5.9**. From the table it is observed that the computed FDs against the repeated experiments show a variation of 4.82% which is quite appreciable for capturing the process anomaly. The variation is the clear indication that fractal theory can extract information regarding the process variation as captured through rotational speed signal. With the disclosure of capability of capturing process variation effect of process parameters on FDs are also investigated observing the variation with tool rotational speed, welding speed and shoulder diameter. Effects of process parameters on the computed fractal dimensions are investigated and the results are graphically represented in **Fig. 5.29**. Interestingly, the variation of fractal dimension with the process parameters shows similar trend as UTS with the process parameters. This invokes a notion that computed FDs can be correlated to UTS of the joints. The correlation of UTS with the fractal dimension shows a nonlinear relation between the two. This leads towards the implementation of nonlinear modeling technique for the correlation of UTS of the joints and FDs of tool rotational speed signal. In the present study, BPNN and SVR are decided to use for the prediction of UTS of the joints with process parameters and FDs.

Table 5.9 Fractal dimension of tool rotational speed signal with Higuchi's algorithm

Exp. No.	Fractal dimension	Exp. No.	Fractal dimension	Exp. No.	Fractal dimension
1	1.841	23	1.858	45	1.863
2	1.864	24	1.887	46	1.810
3	1.855	25	1.853	47	1.352
4	1.866	26	1.871	48	1.722
5	1.800	27	1.802	49	1.682

6	1.867	28	1.749	50	1.826
7	1.859	29	1.825	51	1.587
8	1.736	30	1.818	52	1.745
9	1.819	31	1.765	53	1.813
10	1.891	32	1.570	54	1.691
11	1.834	33	1.869	55	1.796
12	1.682	34	1.882	56	1.834
13	1.945	35	1.719	57	1.864
14	1.775	36	1.828	58	1.692
15	1.858	37	1.865	59	1.772
16	1.761	38	1.925	60	1.894
17	1.924	39	1.925	61	1.846
18	1.878	40	1.528	62	1.653
19	1.904	41	1.829	63	1.804
20	1.848	42	1.807	64	1.798
21	1.923	43	1.366	65	1.787
22	1.891	44	1.778		

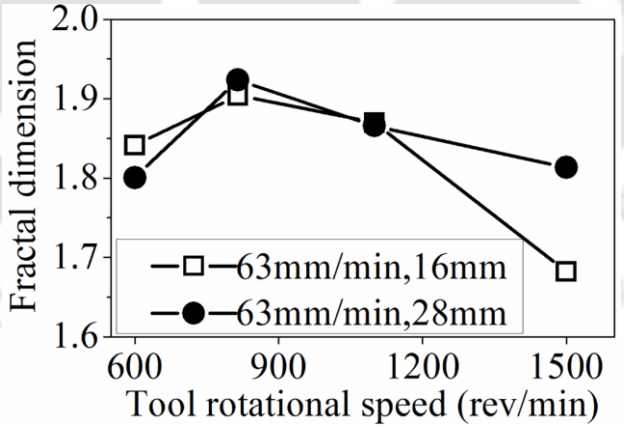

(a)

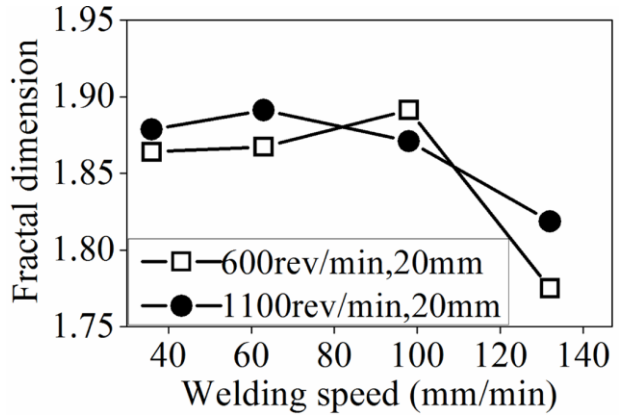

(b)

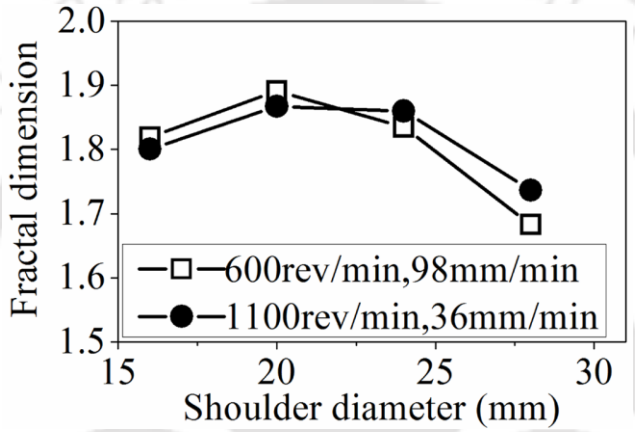

(c)

Fig. 5.28 Variation of fractal dimension with (a) tool rotational speed (b) welding speed (c) shoulder diameter

The prediction of UTS of the joints is attempted with features from tool rotational speed signal. In the models developed for the prediction both the computed FDs and process parameters are used in the input space of the models. SVR parameters C, γ and ε are selected in the range of 1 to 100 in steps of 1, 1 to 10 in steps of 0.01 and 0.01 to 0.1 in steps of 0.001 respectively. Grid search algorithm is applied for the selection of optimum parameters. The optimum parameters are found to be 83, 1.87 and 0.005 for C, γ and ε respectively. A total of 7 patterns are used for testing the developed SVR model with 55 training patterns. For the BPNN model out of 65 patterns, 48 are used for training the network, 10 are used for validation of the network and 7 are used for testing the network. The testing patterns for SVR and BPNN are kept same for comparison purpose. To develop an optimum BPNN model, selection of optimum number of hidden

layer neurons, optimum learning rate (η) and optimum momentum coefficient (α) is important. These three parameters are selected based minimum MSE values. Number of hidden layer neurons is varied in the range of 5 to 30 in the step of 1,η is varied in the range of 0.1 to 0.98 in steps of 0.04 and $\alpha$is varied in the range of 0.01 to 0.97 in steps of 0.04. Optimum BPNN model for the present study is found to be 4-14-1 with η=0.9 and α=0.61.

Prediction performance of BPNN and SVR models are represented in terms of scatter diagram in **Fig. 5.30** and the prediction error against the testing patterns are listed in **Table 5.10**. From the results it is observed that SVR model outperform prediction of UTS of the joints with an absolute average percentage error of 1.23% which is around 84.55% higher than BPNN model.

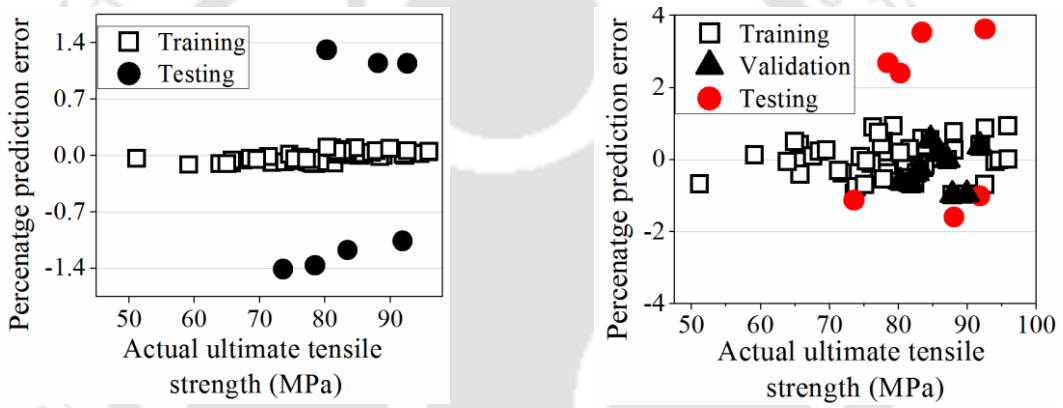

Fig. 5.29 Prediction performance of (a) SVR model and (b) BPNN model with speed signal features

Table 5.10 Comparison of prediction results from BPNN and SVR with speed signal features

Exp. No.	Actual ultimate tensile strength (MPa)	BPNN		SVR	
		Predicted ultimate tensile strength (MPa)	% error	Predicted ultimate tensile strength (MPa)	% error
7	88.12	89.53	-1.60	87.11	1.15
37	91.86	92.79	-1.01	92.84	-1.06

24	78.48	76.38	2.68	79.55	-1.36
31	92.62	89.27	3.62	91.56	1.14
34	83.45	80.51	3.52	84.43	-1.18
11	73.6	74.43	-1.13	74.64	-1.41
61	80.29	78.37	2.39	79.24	1.31
Average absolute percentage error			**2.27**		**1.23**

The FDs computed with Higuchi's algorithm from speed signal effectively represent the process variation confirmed through variation in FDs against repeated experiments. When the FDs are fed to SVR and BPNN models both yields appreciable accuracy in UTS prediction. However, as like in other signals SVR outperform the prediction with an improvement of 84.55% compared to BPNN model. This highlights the successful implementation of rotational speed signal processed with fractal theory as to be competent in developing accurate UTS prediction methodology in FSW process.

The aforementioned sections demonstrate the signal feature extraction and development of models based on machine learning for UTS prediction. The fusion of various features for prediction of UTS of the joints is attempted with BPNN and SVR models. The performance of these two models shows that SVR model is superior with each signal feature compared to BPNN model. The best SVR model for prediction of UTS is obtained with vertical force signal features followed by the SVR model developed with torque signal features with a variation of 0.08% only. The average percentage prediction error with SVR model developed with features from current signals and tool rotational speed signal are 1.85% and 1.23% respectively which can also be appreciated. The study boils down to the conclusion that SVR models are better compared to ANN models in prediction of UTS with signal features. The features against main spindle motor and welding motor current signal, vertical force signal, torque signal and tool rotational speed signal can be used effectively combined with SVR for accurate prediction of UTS of the joints.

5.10 Summary

The present chapter started with introduction and theoretical representation of various signal processing techniques implemented in the present study for efficient feature extraction. Main spindle motor current and welding motor current signals, vertical force signal and tool rotational speed signals are analyzed in order to understand the process behavior. Depending upon the suitability of the signal processing techniques main spindle motor and welding motor current signals are analyzed in time as well as time frequency domain with WPT. On the other hand vertical force signal is analyzed with a modified WPT-HHT proposed in the present study and torque signals are proceed with DWT for extraction of features. The same for tool rotational speed signal is achieved with fractal theory. The features extracted with various techniques for each signal are then fused with SVR and BPNN for developing models for reliable and accurate prediction of UTS of the joints. The findings of the present work are summarized in the following points.

- ✓ A new technique for the selection of suitable mother wavelet function for WPT is proposed. The proposed methodology is free from any process dependency and related only to the signal under consideration.
- ✓ The limitation with HHT of wide frequency band in the first IMF is eliminated by proposing a modified HHT with WPT. The combined WPT-HHT method is capable of generating instantaneous frequency with a narrow frequency band that is useful for observing events in low frequency domain.
- ✓ Two new indicators WPC and CP have been developed with vertical force signal features that shows increasing trend with increase in UTS of the joints.
- ✓ The comparative performance among the BPNN, RBFNN and SVR models for prediction of UTS of the joints showed that SVR models are superior in performance.
- ✓ SVR model developed with vertical force signal features leads to the maximum prediction accuracy of 99.55% with maximum error of -0.85%. The same with BPNN model is found to be 98.42% with maximum error of 2.08% with vertical force signal features. The prediction accuracy of SVR models developed with features from main spindle motor current signals, torque signal and tool rotational speed signal are 98.15%, 99.47% and 98.77% respectively. Similarly with BPNN

models the prediction accuracies are 94.13%, 94.55% and 97.73% respectively for the signals.

Chapter 6

Defect identification in FSW process

6.1 Introduction

The FSW process has a notable advantage of producing welds free from defects those are inevitable in fusion welding processes. However, the process is not free from defects and defects mainly occur due to improper selection of suitable welding parameters (Chen et al., 2003). The process is influenced by many process parameters and deviation of any of these or improper combinations lead to defects in the welded samples. The survey of literature (chapter 2, section 2.6) conveyed that there are mainly three types of defects observed in friction stir welded samples: void defect, tunnel defect (also referred as wormhole defect) and root defect. Void is a discontinuity in the joint and responsible for deteriorating the joint strength as this act as a crack initiation point in the welded samples during testing. In general, it is observed that void is the outcome of improper heat input to the material. In FSW process, improper heat input is the result from low tool rotational speed and shoulder diameter with high welding speed. The amount of heat generated is governed by amount of friction between the shoulder and the workpiece. At low tool rotational speed with low shoulder diameter, the amount of frictional heat generated is less that results in improper plasticization of material around the tool. This affects the flow of material from the leading edge to the trailing edge and results in void without being compensated by the material. From the survey of literature, void are prone to occur in retreating side of the weld (Kim et al., 2006). The tunnel defect is similar to void but exist throughout the length of the weld. This defect is the outcome of both low and high heat input. At low heat input due to insufficient material plasticization and improper material flow around the tool pin results in void towards the trailing edge of the weld and continues length wise with the progression of the tool.

Another aspect of generation of tunnel defect is the high heat input. At high tool rotational speed and shoulder diameter with low tool rotational speed, heat input to the weld is high. At high heat input material in the weld zone gets excessively softens and expelled out of the weld zone in the form of excessive flash. The flash generation in the welding process is considered as a defect and leads to lack of material in the weld zone for compensating the void created by the rotating tool towards the trailing edge in its progression. In the present study tunnel defect is experienced and the cause for formation of tunnel defect is due to the excessive heat input to the weld as indicated by high flash generation. Root defect in FSW process is observed due to improper selection of tool pin length. At low tool pin length the tool cannot reach the bottom of the workpiece and results in hairline defect towards the root of the weld. This defect results in low bending strength and weld strength as it acts as a crack initiation point. Moreover, fatigue life of the welded components is drastically degraded with root defect. Apart from these three defects, few researchers (Cao et al., 2009; Zhang et al., 2006; Zhao et al., 2014) also reported kissing bond defect in welded samples. The cause for formation of this defect is attributed mainly due to formation of oxide layer in the weld zone. These oxide layers distributed over the weld zone and act as a material discontinuity in the weld zone. It is being reported that this defect can act as a crack initiation point for fracture growth within the weld zone (Cao et al., 2006). Among the defects observed in FSW process in terms of severity, void and tunnel defect is maximum as it leads to degradation of joint strength and mitigation of these defects are difficult compared to root defect and kissing bond defect.

Identification of defects in welding processes is a vital task before accepting the joint to ensure desired performance. In FSW process, this becomes more challenging as the defects as referred in the aforementioned paragraph are internal or subsurface. Accordingly, visual testing methods are not applicable for identification of defects in FSW process. Identification of defects in welded samples broadly classified into two categories as destructive and nondestructive testing methods. In destructive testing methods, tests like tensile testing, bend testing, impact testing are implemented (Gibson et al., 2014). Analysis of fracture surfaces can provide an insight to detect presence of defects as these act as crack initiation point. In industrial environment, destructive testing methods are implemented in both test joints and sacrificial joints collected from actual production line. Destructive testing methods are one of the major defect risk

management procedure adopted in industries. However, these processes lead to destruction of welds and the tested piece loses its integrity to be used further. This leads to increase in production cost and demands high time to identify defects. To provide solutions without compromising the integrity of the joints, nondestructive methods are developed in order to identify defects in the welded samples. In FSW process, eddy current testing, radiographic testing and ultrasonic testing methods are widely used for identification of internal defects (Gibson et al., 2014). These techniques offer reliable and accurate means of defect identification but with limitations such as trained operator and high initial cost. The information results from these techniques are difficult to interpret without human intelligence and human presence leads to chances of human error in the process. Machine intelligence is difficult to integrate for interpretation of outcome of these processes for identification of defects.

Apart from the aforementioned techniques real time sensorial data can be used for development of methods for defect identification. Few researchers (Boldsaikhan et al., 2011; Kumari et al., 2016; Kumar et al., 2015) presented methodologies for identification of defects with vertical force signal information. Machine intelligence based methods were implemented to classify defective welds from defect free welds with the help of signal features. However, attempts on defect identification with real time sensorial information is less in FSW process. The advantage of this approach is the ability to develop machine intelligence based methods for interpretation of information for identification and classification of defects in the welded samples. In the present study, defect detection methods are developed with features extracted from vertical force signal, torque signal, tool rotational speed signal and temperature signal.

6.2 Identification of defects

In the present study welding experiments are conducted over wide range of tool rotational speed, welding speed and shoulder diameter as these three mostly influences the heat generation and distribution in FSW process. The complete set of welding experiments can be seen in **Table 3.4** (chapter 3). Among the welding experiments, Exp. No. 35 and Exp. No. 65 results in defective welds (**Fig. 6.1**). The defects are confirmed with mechanical sectioning of the welded samples and it is found that the defect formed is tunnel defect. In addition to the set of experiment as reported in **Table 3.4** (chapter 3) one more set of experiments are performed in order to develop defect detection

methodology with temperature signal. The experiments are listed in **Table 6.1**. In this set of experiments, tool rotational speed and welding speed are kept fixed at 1100 rev/min and 98 mm/min respectively. The tool pin geometry is varied as listed in the respective **Table 6.1**. The mechanical sectioning of the welded samples revealed tunnel defects in E1 and E4 against taper and straight cylindrical tool. From the table it is evidential that welds with threaded pin profile results in defect free welds. This can be attributed due to the fact that with threads the contact surface increases and it leads to more friction between the tool and workpiece material. Moreover, threads in the pin increase the turbulence in the weld material that results in better material flow within the weld zone. During this set of experiments temperature signals are acquired in real time integrating K-type thermocouples in the workpiece material. The configuration of thermocouple arrangement is schematically shown in **Fig. 6.2**. Thermocouples are arranged in both advancing side and retreating side at 1 mm and 4 mm from the shoulder line respectively. In the present study, identification of defects is attempted by developing signal feature based methods as discussed in the following sections.

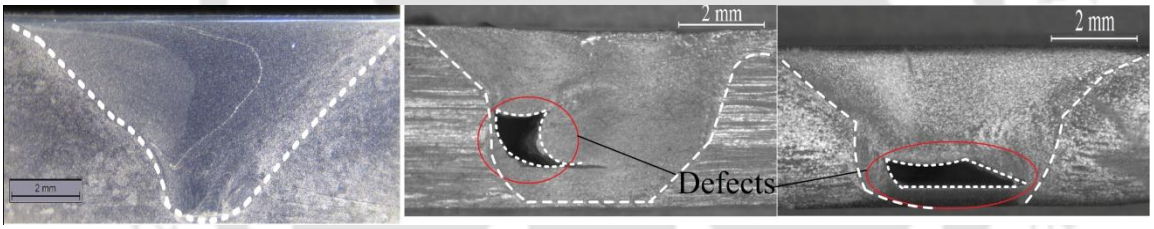

(a) (b) (c)

Fig. 6.1 Defective versus defect free welds (a) defect free weld Exp. No. 45 (b) defective weld Exp. No. 35 (c) defective weld Exp. No. 65

Table 6.1 Welding experiments conducted for defect identification with temperature signal

Exp. No.	Rotational speed (rev/min)	Welding speed (mm/min)	Pin profile	Weld macrographs

E1	1100	98	Taper tool	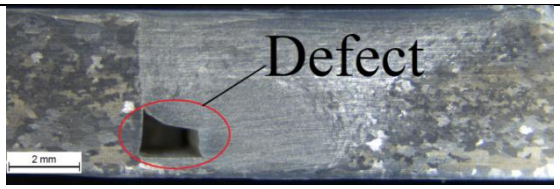
E2	1100	98	Cylindrical tool with taper thread	
E3	1100	98	Taper tool with square thread	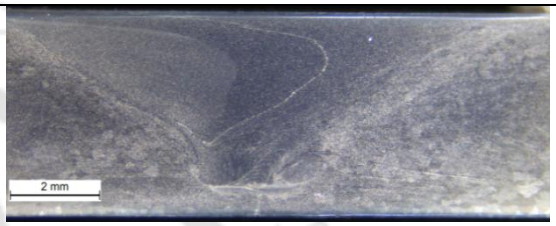
E4	1100	98	Cylindrical	
E5	1100	98	Cylindrical tool with square thread	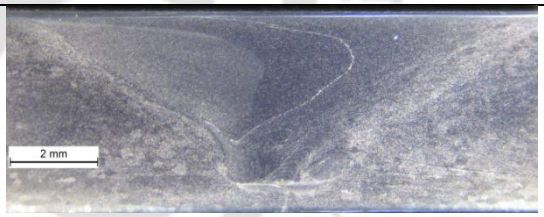

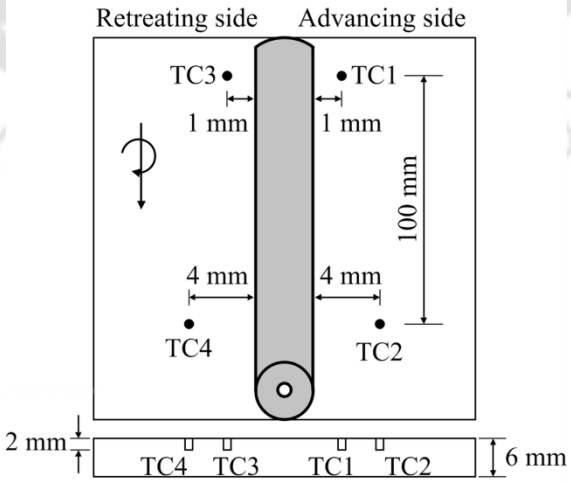

Fig. 6.2 Schematic representation of thermocouple arrangement

6.2.1 Analysis of vertical force signal features

Vertical force or sometimes referred as plunging force is responsible for establishing proper contact between the tool shoulder and the workpiece material. A proper contact leads to proper frictional heat generation resulting in sufficient material heating and in turn material plasticization. Monitoring this parameter in real time would offer information regarding the process. The acquisition of vertical force signal and the related sensor and hard hardware are discussed in chapter 3 (section 3.7). The force signals acquired against Exp. No. 45, Exp. No. 35 and Exp. No. 65 are shown in **Fig. 6.3**.Among these three experiments Exp. No. 45 represent the defect free case with maximum UTS and the other two represents defective cases. From the figure it is evidential that the respective force magnitudes against the defective cases are higher compared to that of defect free case. It is to note that these experimental conditions are having same tool rotational speed of 1100 rev/min. Welding speed for defective cases is 36 mm/min whereas the same for defect free welding case is 132 mm/min. The variation in magnitude as well as trend of the force signals indicate towards anomaly during the process. The undulations in the signals against the defective cases are the indications of abnormal material flow within the weld zone. Abnormal material flow is the outcome of improper heat input that leads to improper material plasticization. The acquired signals can effectively represent the process flow behaviour and can be useful in monitoring the process for the desired outcome. Owing to these revelations the vertical force signals are analyzed for extraction of useful features for correlating to identification of defects.

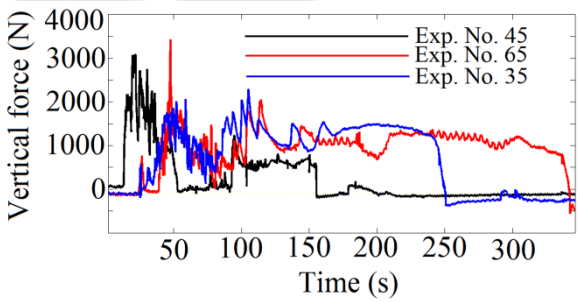

Fig. 6.3 Vertical force signals against defective and defect free welding cases

The vertical force signals acquired during the welding experiments are analyzed with the developed WPT-HHT method as detailed in chapter 5, section 5.7. The method is carried one step further for computation of instantaneous phase and frequency from the IMFs of the force signals. The IMFs computed against Exp. No. 45 and Exp. No. 35 is

shown in **Fig. 6.4**.In the figure C1 to C8 represents the IMFs of the coefficients extracted from WPT of the real-time vertical force signal acquired during FSW process. These functions represent the intrinsic behaviour of the force signals acquired during welding process. As the functions are represented with respect to time, time dependent monitoring of the process is possible. Any anomaly occurred during the process can be detected over time. In signal processing perspective, IMFs represents the fundamental oscillatory behaviour of the signal which represents the physical behaviour of the process from which the signal is acquired. In FSW process, as force signal show appreciable acceptance for monitoring the process behaviour, analyzing the signal through fundamental behaviour of the signal is advantageous for effective monitoring of the process. From the IMFs, it can be observed that the defective and defect free cases have appreciable difference in trend and magnitude. The instantaneous frequency spectra for the defective cases (Exp. No. 35, 65) and defect free welding cases (Exp. No. 45, 3 and 17) are shown in **Fig. 6.5**. From the spectra, it is clearly distinct that defect formation inside the weld increases the frequency of the signal, which can be detected with respect to time. Increase in force signal frequency with defect formation in the weld was also reported by (Boldsaikhan et al., 2011). The above analysis brings the impression that IMFs can be effective in detecting subsurface defects in friction stir welded joints without involving much complicated analysis.

Apart from the instantaneous frequency, instantaneous phase angles obtained from Hilbert transform of the IMFs also give a remarkable notion for detection of defects in the welded samples. Out of the 65 experimental cases, two cases (Exp. No. 35 and 65) were confirmed to have tunnel defect through mechanical cross sectioning method. Rest of the welded samples do not show any evidence of presence of internal defects. The computed instantaneous phase angles for defective and defect free welding cases are displayed in **Fig. 6.6**. In the figure, clear deviation of phase angles can be observed among defective and defect free welding cases. It is to note that, instantaneous phase of defective samples are towards negative scale and that of defect free samples are toward positive scale. The appreciable difference leads to the notion that the proposed approach can be an effective visual method for easy identification of defective welded samples through instantaneous phase angles. From the figure, it is witnessed that there is a distinct phase shift between the defective and defect free weld signals. In theory, accumulated phase shift of a signal can be viewed as the area under the curve between

instantaneous time and instantaneous frequency of the signal. From **Fig. 6.5**, it is seen that area under the time-frequency curve for defective weld signal is higher than the one for defect free weld signal. This possibly introduces a phase shift in the faulty signal that brings deviation as compared with the phase of defect free signal. As it is observed that change in frequency is the outcome of the occurrence of the defect in the weld, which in turn brings the phase shift in the faulty signal. So, it is evidential that presence of defect also brings phase shift in the signal. Although, the physical interpretation of the particular change is difficult and further analysis is desirable in this regard for the generalization of the findings reported herewith.

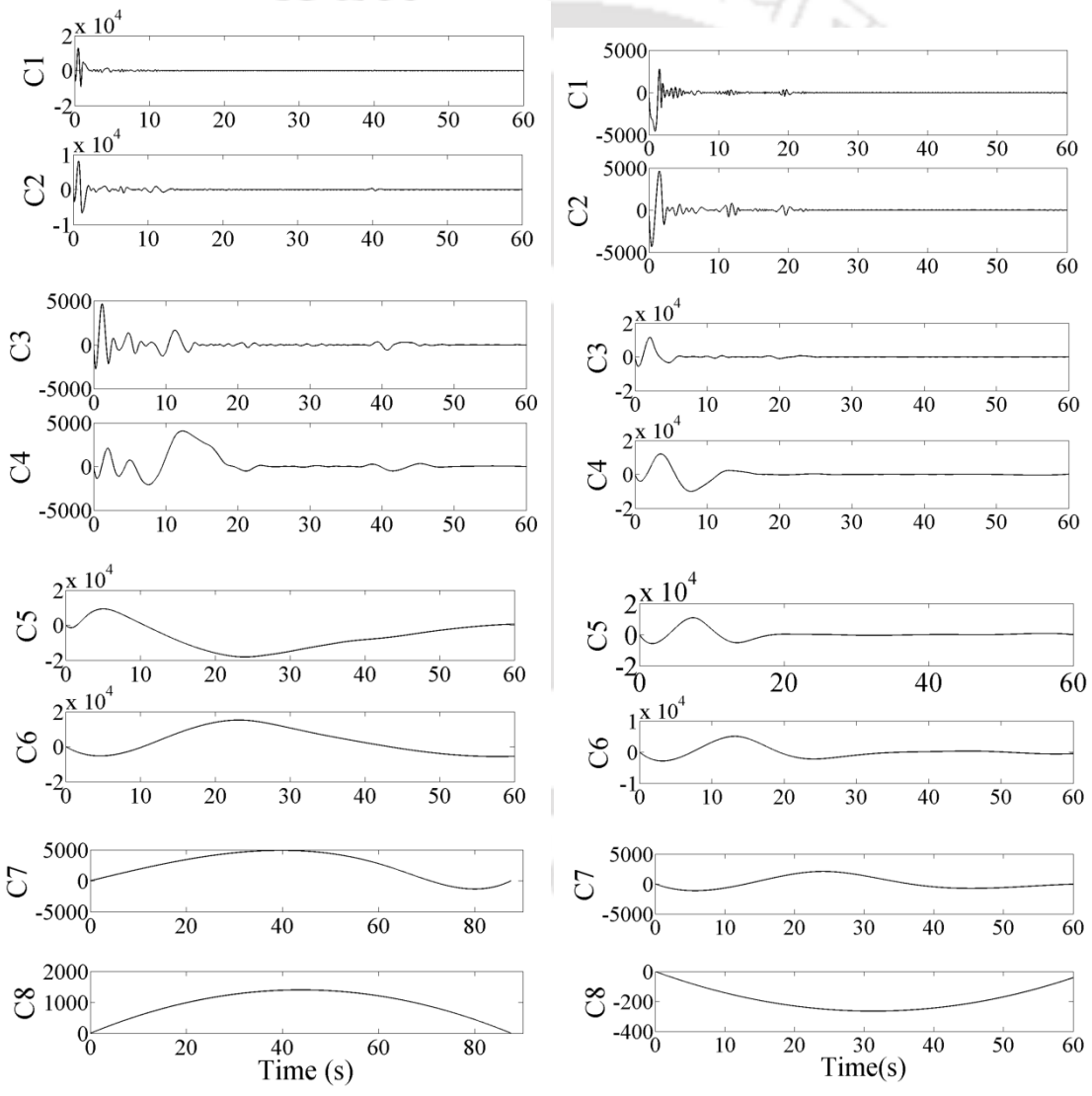

(a) (b)

Fig. 6.4 IMFs computed against (a) Exp. No. 35 and (b) Exp. No. 45

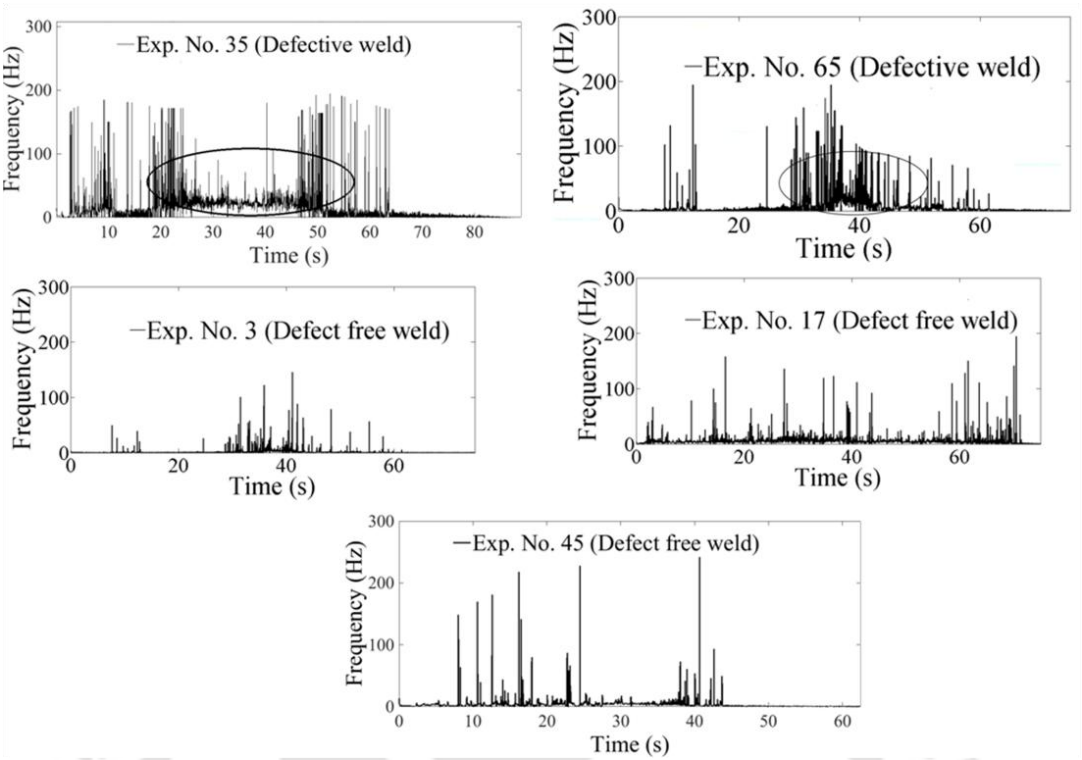

Fig. 6.5 Instantaneous frequency spectra for defective and defect free welds

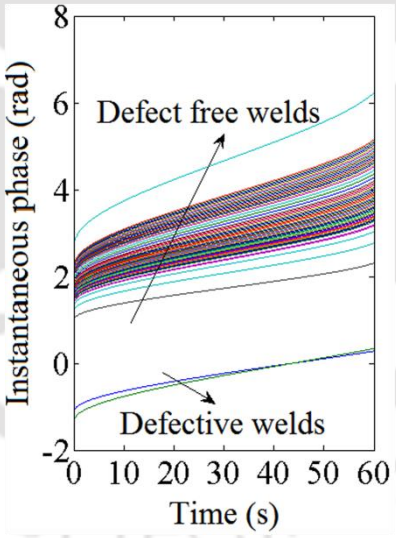

Fig. 6.6 Instantaneous phase angle plot for defective and defect free welds

A simple yet effective methodology has been proposed for identification of internal defects with vertical force signal features. The combined WPT-HHT method offers an accurate method for analyzing the vertical force signal for computation of instantaneous phase and instantaneous frequencies. These two features reveal a direct mean of classification of defective welds from defect free welds that can be regarded as indicators for internal defect detection. The proposed method is suitable for integration

of machine intelligence and human intervention in the process is less making it less prone to human error.

6.2.2 Analysis of torque signal features

As like vertical force control amount of heat generation in FSW process, torque associated with the process also governs the generation of heat in the process. It is the reaction applied by the tool to overcome the material resistance around the welding tool. The resistance of material is proportional to amount of material plasticization which is in turn governed by tool rotational speed and welding speed. Thus, it can inferred that torque is also related to tool rotational speed and welding speed, the two most influencing process parameters in FSW process. In other words it can be justified that torque is a combined effect of these two parameters. Thus, real time monitoring of torque can be useful in monitoring the FSW process as reported by Mehta et al., (2013). In present work apart from vertical force signal; torque signal is also acquired in real time with a measurement setup developed in house. Details of torque signal acquisition can be seen in chapter 3, section 3.7. The survey of available literature revealed no attempts on identification of defect is FSW process with features extracted from torque signal. Hence, identification of internal defects with torque signal can be regarded as an imperative contribution of the present work.

The analysis of torque signal is carried out in time frequency domain with DWT. The approximation part of the decomposed signal are considered further for computation of statistical features namely D_{xN}, E_{xN} and S_{xN}. The details about these features are already discussed in chapter 5, section 5.8. The computed features are then combined to develop a new indicator termed as defect index (DI) as represented by **Eq. 6.1**.

$$DI = \left| \frac{e^{D_{xN}} \log(E_{xN})}{S_{xN}} \right| \tag{6.1}$$

where, DI represents the combined statistical parameter, D_{xN}, E_{xN} and S_{xN} represents the normalized values for D_x, E_x and S_x respectively. The proposed index offers the fidelity to visualize the information related to defect formation in the welds in graphical form since it is one dimensional which would be quite handy for online monitoring. On the other hand realization of the individual signal features collectively in graphical form is difficult since it will require four dimensional space for the representation. Hence, these

features are combined to propose a one dimensional defect indicator for easy realization and interpretation of the process information for identification of defects.The Computed DI values against each experiment are shown in **Fig. 6.7**. The figure reveals that the DI values for defective cases (Exp. No. 35 and Exp. No. 65) are much higher than the rest of the values for other non defective cases. Thus, the proposed DI can be implemented as an indicator for internal defect identification in FSW process.

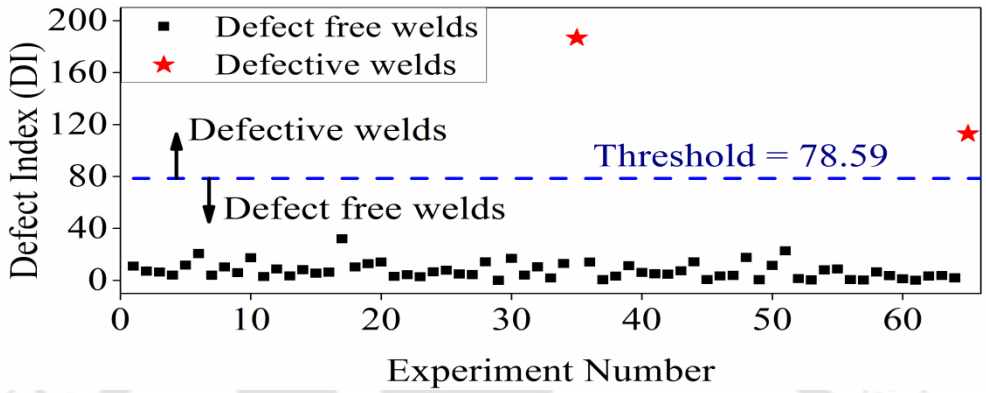

Fig. 6.7 Defect index proposed with torque signal features

To determine the threshold for identifying defective and defect free weld an attempt has been made as given in the following equation.

$$T = \frac{\overline{DI}_{Defective} + \overline{DI}_{Defect\ free}}{2} \quad \textbf{(6.2)}$$

where, T is the computed threshold value, $\overline{DI}_{Defective}$ is the mean of the DIs for defective welded samples and $\overline{DI}_{Defect\ free}$ is the mean of the DIs for defect free welded samples. Form the computed DIs it is observed that the T for the present situation is 78.59. This indicates that above this threshold all the welded samples will be defective and below this threshold limit welded samples will be defect free.

The analysis of torque signals in time frequency domain with DWT leads to an interesting aspect for identification of internal defects. The proposed indicator DI offers single valued information for detecting defective samples and can be used for segregation of defective welds from the defect free welds with the computed threshold value. Inference of human in the proposed methodology is less and the developed methodology is possible to develop further for integration with machine intelligence for developing and automated defect detection system.

6.2.3 Defect identification using fractal theory

Successful development of defect identification methodologies from vertical force as well as torque signals acquired during FSW process motivated this study to test tool rotational speed signal as well for defect identification. This signal is analyzed in time domain with fractal theory and the details are given in chapter 5, section 5.9. Higuchi's algorithm has been used for computation of FDs for development of index for defect identification. As like the earlier methods for defect identification it is also started with observation of the signals in time domain. **Figure 6.8(a)** shows the welding period data for tool rotational speed signal against the defective cases (Exp. No. 35 and Exp. No. 65). The signals show clear deviation when compared with the signal against the defect free welding case as shown in **Fig. 6.8(b)**. The change in the amplitude and trend of the signal for defective cases are clear indication of process anomaly during welding operation. **Figure 6.8(b)** displays the possibility of detecting three characteristic stages of FSW process for a defect-free weld. The figure is intended to prove that the signal acquired during the welding process is actually reflecting the FSW process and is not an outcome of some redundant data or process. The change in the process is tried to identify quantitatively using the measure of fractal dimension in this research work.

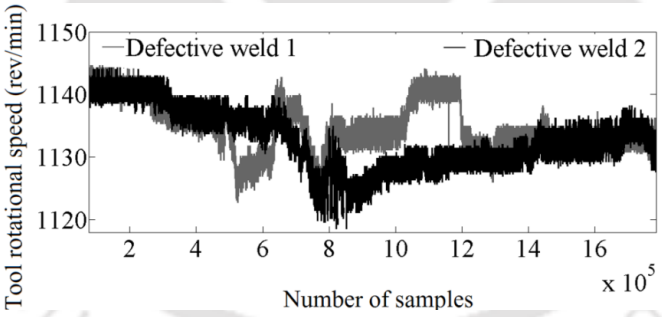

(a)

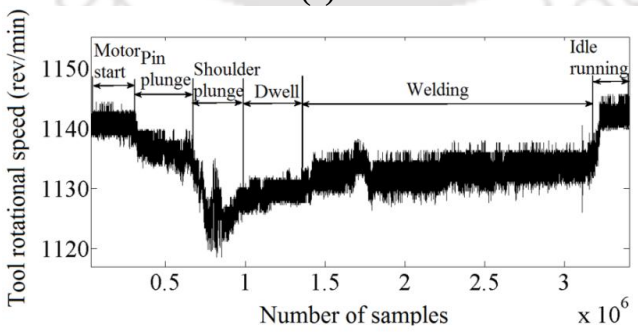

(b)

Fig. 6.8 Tool rotational speed signals for (a) defective welding cases (welding period data only) (b) different salient stages in friction stir welding process for defect free case

Figure 6.9(a) depicts the computed FDs of first two welding stages and there is not much appreciable difference since the plunge depth and dwell time were kept fixed during welding for all the experiments. To correlate the formation of defects, the welding period data is only considered and segmented into several divisions and FDs are computed for each division. For instance defective weld (Exp. No. 35), each division represents 10.4 seconds and it is quite indicative of the self-explanatory characteristic as a part of whole process. The segmentation of whole signals aids to find out any alteration of computed values during scanning through the whole process.

The computed FDs from the segmented data of the welding period are shown in **Fig.6.9(b)**. Very first data point is omitted for all the cases as these are not informative regarding the process behavior since it belongs to very initial stage of welding which may not produce stable signature of the process. It is also very clear that after a certain division *i.e.*, certain point of time, fractal dimension starts decreasing for defective cases. This phenomenon physically correlates to the point of defect formation during welding which is confirmed through visual inspection of the welded sample by post-weld sectioning in several points. Before this point of depression, the FDs do not show any significant variations and the trend can be compared with the defect free welds. It is indicative that up to the point of depression, the welding process was stable, so as the signals and thus the computed FDs are not showing much variation. Ahead of this point, the FDs for both the defective cases drop considerably. This is physically linked with the formation of defects that was captured well by the dynamic behavior of the signals and hence reflected in the computed fractal dimension. Formation of defect is assumed to introduce instability (Kim et al., 2006) in the process and hence a reduction in fractal dimensions is observed. This decrease continues till the point up to which the process is unstable. Once the process becomes stable with the defect inside the weld, an increase in the fractal dimension is observed (**Fig.6.9b**). This analysis helps to find a boundary beyond which defects are formed in the welded samples which is indicated in **Fig. 6.9(b)**.

Defects are identified by sectioning the welded samples and the physical measurements confirm the point from which the defects are visible. **Figure 6.1** indicates the macrograph of the cross-section of welded sample corresponding to welding conditions of **Fig. 6.9**. The tunnel defects are formed in the welds that represents defective welds (Exp. No. 35 and 65). However, present methodology cannot describe

the shape and size of the defect. **Figure 6.10** represents the schematic of defect formation for the case of defective weld against Exp. No. 65. This correlates to the point in time from which the defects started in the weld. This calculated time is in good agreement with the time step corresponding to **Fig. 6.9(b)** in terms of divisions in welding period data where a clear decrease in the fractal dimension of the defective welds observed.This brings the essence of fractal dimension computed from welding period sensor data of tool rotational speed signals may be projected as an independent indicator for the detection of occurrence of defects in the weld.

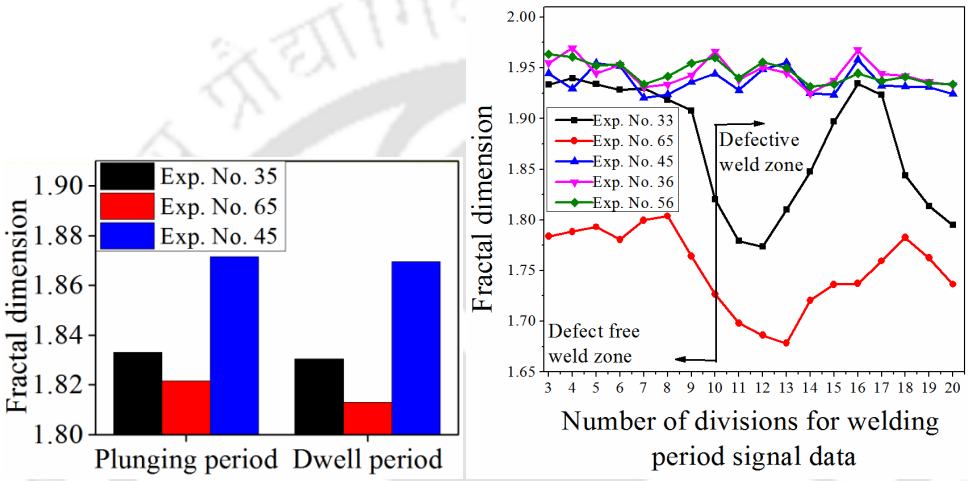

(a) (b)

Fig.6.9 Variation of fractal dimension (a) plunging and dwell period (b) segmented welding period for 20 equal divisions

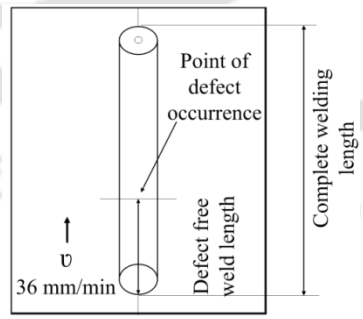

Fig 6.10 Schematic of detection of defects in the welds through sectioningfor defective weld against Exp. No. 65

Fractal dimension computed using Higuchi's method from tool rotational speed signal shows promising direction to identify the formation of defects in FSW process. The defect free weld produces consistent fractal dimension within the tolerance limit of ±

0.025 for all segmented data. Sharp decreasing trend in fractal dimension serves as an indicator to detect the initiation and formation of defects. Appreciable difference in the welding period fractal dimensions (~ 0.13 – 0.15) between the defective cases and defect free welds, reveal that the process outcome can be monitored using the proposed approach. However, the analysis is not tested for characterization of defects for shape and size estimation. The proposed methodology with modification can be adopted for online monitoring of the weld quality in FSW process.

6.2.4 Analysis of temperature signal

In FSW process, local rate of change of temperature greatly influence the mechanical properties of the welded parts (Fuller et al., 2007). Microstructure of the welds that includes grain size, grain boundary character, and coarsening and dissolution of precipitates are influenced by the temperature distribution within and around the stirred zone in FSW process. Hence, it is important to obtain temperature information during FSW process. Apart from the mechanical properties of the welds, temperature distribution is also influenced by the defect formation in FSW process and vice-versa. One of the root causes for formation of defects inside the welded samples is inadequate material flow due to poor material plasticization. Along with the deformation of the material around the rotating tool in FSW process, temperature inside the weld pool is also responsible for inadequate plasticization of material (Shirazu et al., 2015; Chen et al., 2008; Saeid et al., 2008; Morisada et al., 2015). Hence, monitoring the real-time temperature signal in FSW process can lead to alternate perspective for defect identification. Moreover, temperature distribution in the welds is the cumulative outcome of the combination of different input process parameters. Individual monitoring of those parameters may not be cost effective. Thus, analysis of temperature signals in real-time can open new avenues of defect identification in FSW process. Time-temperature profile for experimental cases E1 and E3 (**Table 6.1**) are shown in **Fig. 6.11**. It is to be noted that these two experiments are carried out over same level of process parameters but the weld without threaded pin profile results in internal defect. The temperature signals do not provide any insight that could be an effective indication to reveal the presence of defects inside the weld. In both the cases, maximum temperature is obtained on the advancing side of the weld, which is followed by retreating side (from thermocouples at a distance of 1 mm from the shoulder line).

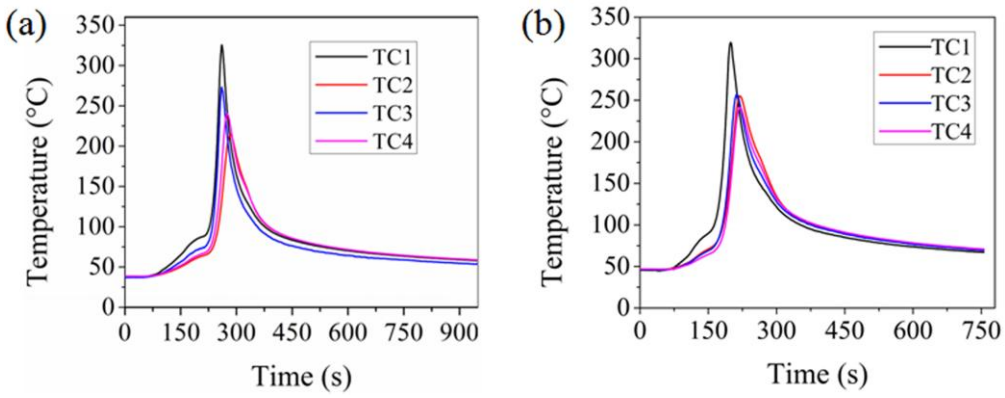

Fig. 6.11 Time-temperature profile of welds from experiments (a) E1 and (b) E3

Inadequacy of fetching valuable information for detection of defects in the welds from time-temperature data motivates this study to investigate rate of change of temperature within the weld. Rate of change of temperature can be treated as a window to observe time-temperature behaviour of the welds which will capture both heating and cooling information during welding process. Mathematically rate of change of temperature can be represented as

$$R_C T = \left| \frac{T_{i+1} - T_i}{t_{i+1} - t_i} \right| \quad \textbf{(6.3)}$$

where, $R_C T$ represents absolute rate of change of temperature, T represents temperature and t represents time and i represents unit step or interval. The mathematical expression of **Eq. 6.3** actually represents the heating rate or cooling rate over fixed space in solution domain. The rate of temperature change links thermal diffusivity which is the ratio of the time derivative of temperature to its curvature and essentially is the measure of thermal inertia. The presence of any discontinuous volume *i.e.*, internal defects obviously alters thermal diffusivity and hence can be detected through rate of temperature change.

In **Fig. 6.12**, absolute rate of change of temperature computed through **Eq. 6.3** is displayed against each thermocouple point and against each experimental case. Remarkably, it can be seen from **Fig. 6.12** that $R_C T$ of defective weld samples are lower than defect free weld samples. The proposed method leads to an effective notion that the indicator proposed can be an efficient alternate for detection of defects in friction stir welded samples.The justification for the low $R_C T$ values for defective welds can be derived from the physics involved in defect formation in FSW process. The defects reported in **Table 6.1** (Exp. No. E1 and E4), are formed due to insufficient material flow

around the pin. Insufficient material flow is the result of inadequate heat generation in the welding processor vice-versa since response (i.e. temperature measurement) is also affected by discontinuity of material volume. The time-temperature information also shows nominal change in maximum temperature for defective and defect free regions. The temperature change indicates the temperature decay in the welds. Lower R_CT signifies that rate of decay is slower and vice-a-versa. This slower decay is attributed due to the fact that the defect region is devoid of continuity. The void formed is possibly filled with air as contamination of other gaseous element in FSW process is negligible (Mishra and Ma, 2005). Thermal conductivity of air (~0.0257 W/m K at 293K) is several times lower than that of aluminium (~205 W/m K at 293 K). Hence, temperature of defect region decreases at much slower rate than defect free region. Slow temperature decay in defective weld is also reported by Saravanan et al. (Saravanan et al., 2014). This effectively justified the lower R_CT for defective welds than defect free welds. Thus, the present approach with real-time temperature data rate of change of temperature can be an effective alternate to existing defect detection methodologies.

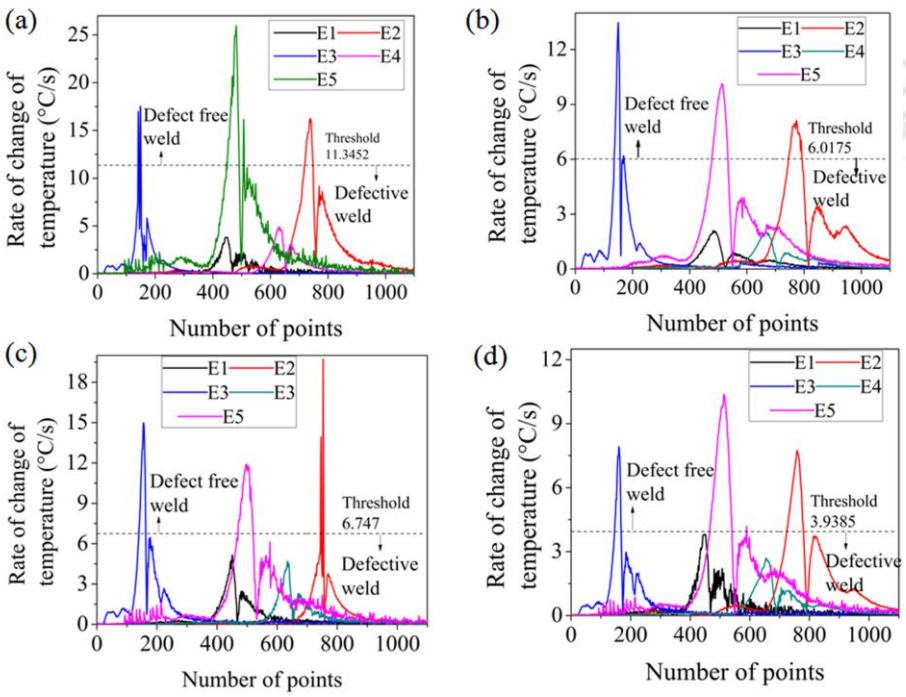

Fig. 6.12 Rate of change of temperature against thermocouples (a) TC1 (b) TC2 (c) TC3 and (d) TC4

The computed absolute R_CT values are further processed to compute the threshold limit for finding the boundary to classify defective welds from defect free

welds. This is achieved by finding the Euclidian distance between the R_CT points using min-max relationship as shown in**Eq. 6.4**. From the analysis, respective threshold limits are computed as shown in **Fig. 6.12**. These threshold values efficiently differentiate the defective region from defect free region.

$$ThL^{R_CT} = dist[min\ (max(R_CT_{DF}))\ , max\ (max\ (R_CT_D))] \quad \textbf{(6.4)}$$

where, ThL^{R_CT} represents threshold limit for R_CT, $dist$ represents Euclidian distance, R_CT_{DF} represents temperature gradient for defect free welding cases and R_CT_D represents temperature gradient against defective welding cases. From the above equation ThL^{R_CT}values against thermocouples TC1, TC2, TC3 and TC4 are found to be 12.45, 6.12, 7.23 and 5.05 respectively.

Another approach based on DWT for the detection of defects using real-time temperature signal is proposed in the present work. DWT is one of the most widely used signal processing techniques. Hence, for a comparative analysis with the proposed approach based on rate of change of temperature, DWT is added in this work. Moreover, DWT is well known for transient detection in signals (Gusap et al., 2008). As defect formation can be correlated to temperature in the weld, any anomaly is expected to detect using discrete wavelet analysis from temperature signal. Temperature signal against each thermocouple and against each experiment is analyzed using DWT at fourth level and using Daubechies fifth order (db5) mother wavelet function. Theoretical illustration of wavelet analysis is available in literature and can be found in relevant technical articles (Pal et al., 2008; Chen et al., 2003). The proposed analysis revolves around computing the detail coefficients of the signals. The detail coefficients are chosen for further analysis as these retain the high frequency components of the signal and defect formation brings increase in frequency of the signal (Boldsaikhan et al., 2011). The detail coefficients are further processed and a new indicator is proposed as given in **Eq. 6.5**.

$$WBI = \sum_{k=1}^{4} [rms(cD_k)] \quad \textbf{(6.5)}$$

where, WBI is the wavelet based indicator, cD_k are the detail coefficients at level k and i is for the total number of detail coeffieicnts at level k and rms stands for the root mean square values of the detail coefficients.

DWT of the temperature signal (against thermocouple TC1, (refer **Fig. 6.2**) acquired during Exp. No. E4 and E5 are shown in **Fig. 6.13**. From the figure it is evidential that detail coefficient have different pattern for defective welding case than defect free welding case. This is further reflected in the proposed indicator computed using **Eq. 6.5**. The values of the proposed indicator are shown in **Fig. 6.14**. The figure displaying the WBI reveals a clear boundary for classifying defective welds from defect free welds. The difference persist in detail coefficients for defective welds and defect free welds are well captured through computing the proposed WBIs. It is observed that the proposed indicator for defect free welding cases are quite low than defective welding cases. This can be justified with the physical illustration of DWT.

In DWT the original signal is decomposed into approximation and detail parts relating to the sampling frequency of the signals, where, approximation part contains the low frequency components of the signal and detail part contains the high frequency components. From the literature it was observed that inclusion of defects in FSW process brings change in signal frequency to higher scales. Moreover, the amplitude of the detail coefficient for defective welding cases is also high as compared to defect free welding cases. This reflects that high frequency components of the signals against defective cases have high spatial distribution than signals against the defect free welding cases. The proposed WBIs are efficient in capturing these change in amplitude values and reflect an efficacious representation of defect conditions within the welds. This non-destructive evaluation approach is simple and free from post-processing steps involved in other available non-destructive evaluation techniques. The computations of the WBIs can be integrated to hardware for less human intervention making the proposed approach to be less dependent on operator skill.

The proposed WBIs can be effectively used for finding threshold values for classifying defective and defect free welds. In this work, threshold value for differentiating the defective weld zone from defect free weld zone is computed from Euclidian distance calculation from the WBIs. The method of threshold computation is given in **Eq. 6.6**.

$$ThL^{W} = dist[max(WBI^{DFW}), min\ (WBI^{DW})] \quad \textbf{(6.6)}$$

where, ThL^{W} represents threshold limit for WBIs, $dist$ is the eucledian distance, WBI^{DFW} represents WBIs for defect free welding cluster, WBI^{DW} represents WBIs for

defective welding cluster. For the present case, ThL^W is found out to be 4.58. This threshold limit sets a clear boundary for the classification of defective welds from defect free welds as shown in **Fig. 6.14**. The discussion and results furnished in this research work is based on the limited range of process parameters and tool geometries. Wide range of process parameters with different tool geometries needs to be considered for the generalization of the results applicable to FSW process which is the future scope of this research work. The proposed approach can be the first level of safeguard regarding the detection of presence of defects in FSW process.

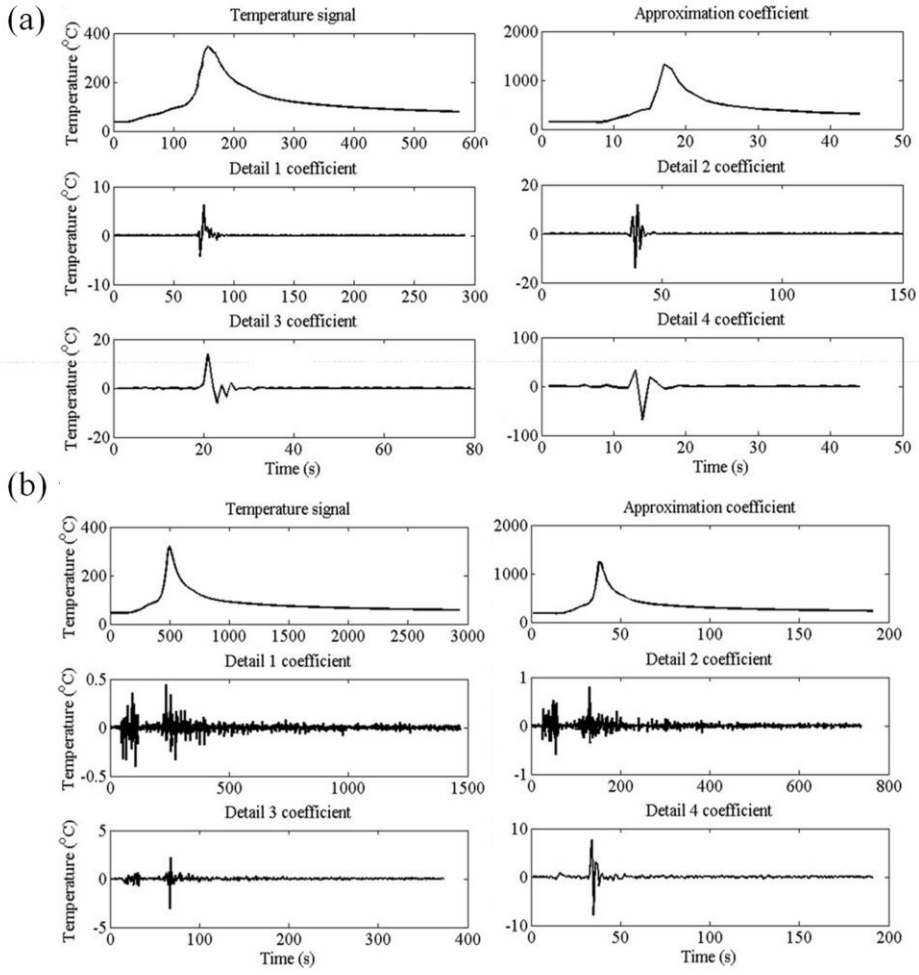

Fig. 6.13 Wavelet decomposition of temperature signal for TC1 against (a) Exp. No. 4 and (b) Exp. No. 5

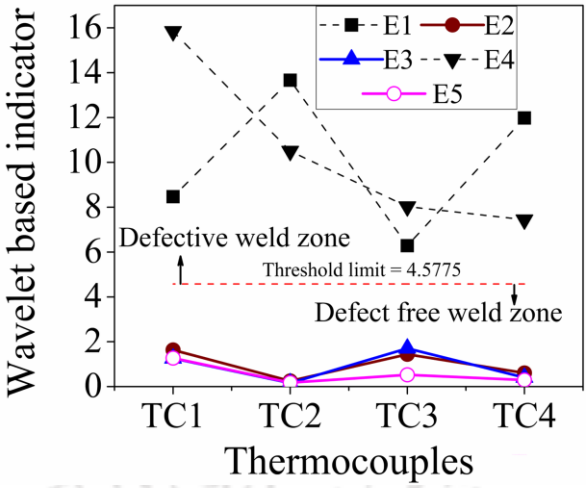

Fig. 6.14 Wavelet based indicator against experiments

Two approaches for detection of internal defects in FSW process are presented using temperature signal. Rate of change of temperature and wavelet based indicator are the two new indicators proposed for effective detection of defects in FSW process. From the analysis it is found that rate of temperature change for defective welds are much lower than the ones for defect free welds. Wavelet based indicator for defective welds are higher than defect free welding cases. Threshold values for rate of change of temperature and wavelet based indicators are computed through Euclidian distance for the respective cases. The computed threshold values effectively sets boundary for the differentiation of defective welds from the defect free welds. These salient findings can be effective for monitoring of FSW process through setting feasible threshold values for detection of defect formation during the process. The approach presented requires less human intervention making it suitable for intelligent systems for decision making regarding the outcome of the process with decision regarding presence of defects in the welded samples.

6.3 Summary

The present study attempted to deliver signal features based nondestructive approaches for identification of internal defects in the welded samples. The same is achieved with vertical force and torque signals, tool rotational speed signal and temperature signal. These signals are processed with different suitable processing techniques for extraction of efficient features and new indicators are developed for segregation of defective welds from defect free welds. The computed threshold values

against the developed indicators provide a margin between the defective and defect free welds. The method proposed with torque signal is comparatively easy to implement and requires less post processing time compared to methods developed with vertical forces signal, tool rotational speed signal and temperature signal.

Chapter 7

Monitoring with weld image information

7.1 Introduction

Top surface of friction stir welded samples carry vital information regarding the process behavior as effectively indicated by Krishnan et al. (2002). However, no investigation reports are available in this aspect. Survey of literature also failed to produce notable contribution in this area, specifically in FSW process. The information contained in top surfaces can be extracted through image features. Fractal theory has already been established for image processing technique (Section 2.4). Other methods that can explore the macro perspective of an image and not limited to describe the local information can reduce the effect of interference information to a greater extent. The core of the fractal theory is to describe the macro perspective of an image in the larger field of vision processing that is more or less similar to human vision processing system. Therefore this study is motivated to extract useful information from top surfaces of the welds through fractal theory. Along with implementation of fractal theory this study will also implement wavelet transform for extraction of useful image features. Advantages like image compression and removal of noise upon reconstruction of images make this process popular in image processing. The top surface images of the welded samples will be preprocessed with various image preprocessing techniques to obtain binary images before applying wavelet transform to the images. The analysis of wavelet transform would act as a comparison base for the results obtained through fractal theory.

7.2 Algorithms for estimation of fractal dimension

Box counting method and Katz's method are the two algorithms used for computation of fractal dimension (FD) from top surface image of friction stir welded samples. Mathematical descriptions of these two algorithms are given in chapter 4 (section 4.5). The algorithms are coded using MATLAB software package (MATLAB 2017b) and the developed codes are verified and validated with benchmark images/signals of known FD. The results are furnished in **Table 7.1**. The percentage error between the theoretical FD and computed FD strengthen the possibility of using the developed codes for the analysis. The computed FDs from images are presented as an indicator to monitoring FSW process through correlation of UTS of the joints.

Table 7.1 Comparison of theoretical and computed fractal dimension

Algorithm	Image/signal	Actual fractal dimension	Calculated fractal dimension	% error
Box counting method	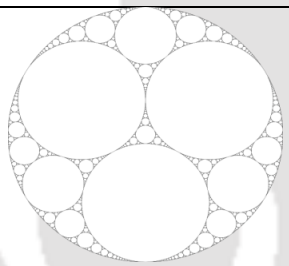 Apollonian gasket	1.328	1.336	-0.60
	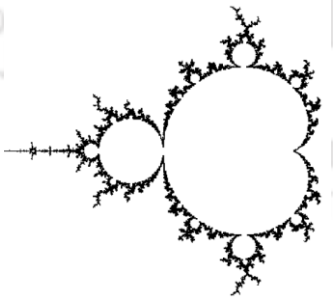 Mandelbrot set	2	2	0
Katz's method	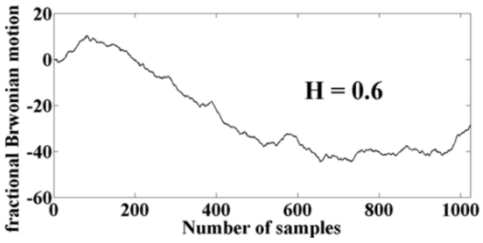	1.4	1.4	0

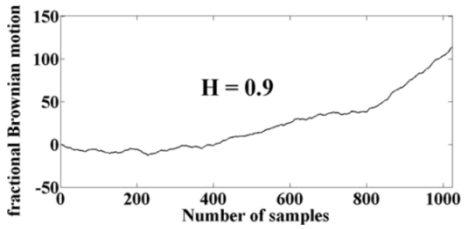	1.1	1.11	-0.90

7.3 Experimental investigation

Tool rotational speed and welding speed are considered in three levels for designing the experimental run matrix and the developed matrix is shown in **Table 7.2**. Welding experiments are performed randomly against each case. After the completion of welding tensile testing specimens as per dimension shown in chapter 3 (section 3.6, Fig. 3.4) are prepared. The values of UTS are reported in **Table 7.2**.

Table 7.2 Design matrix with responses

Exp. No.	Tool rotational speed (rev/min)	Welding speed (mm/min)	Ultimate tensile strength (MPa)
1	815	63	78.59
2	815	98	80.36
3	815	132	83.00
4	1100	63	86.18
5	1100	98	87.46
6	1100	132	84.22
7	1500	63	81.75
8	1500	98	67.67
9	1500	132	79.67
10*	1100	63	84.80

*Exp. No 10 is the repeated case of Exp. No. 4

7.4 Image acquisition and pre-processing

Image from each weld is acquired using a digital camera at fixed resolution and without magnification. **Fig. 7.1a** schematically describes the region of interest of the captured image. The image is captured against the position from which the tensile specimen provides the maximum value among the three specimens prepared from each weld. Top surface images of welds against two different parameter setting are shown in **Fig. 7.1b**. At different process parameter, the semicircular rings on the top surface of the welds are different and it is clearly observed from the captured images. This observation is the key idea of presenting top surface image information to correlate with the weld quality in FSW process.

The semicircular rings on the welds as shown in **Fig. 7.1b** are the outcome of the combined effect of tool rotational speed, welding speed and tool-work piece interaction (Krishnan, 2002).The contact condition between tool and work piece in terms of sliding, sticking and sliding/sticking friction plays an important role for frictional heat generation. The coefficient of friction is strong function of temperature viz. the heat generation between tool shoulder and work piece. Even though, this parameter is not attempted to assess quantitatively, rather it is decided to study the effect of this through the information extracted from the top surface images of the welds in an indirect manner.

Different semicircular rings on the top surface of the welds are the representation of the effects of different combinations of process parameters. In other words, it can be expressed that the semicircular rings formed on the top surface of the weld (parallel to the plane of rotation) bears the cumulative effect of tool rotational speed and welding speed or more precisely forward movement of the tool in one rotation. Forward movement of the tool with continuous rotation extrudes the hot material towards the back of the tool from the front and welding is achieved as this process continues. The semicircular rings formed are the outcome of this typical movement of the tool (Krishnan, 2002). The objective of this study lies in investigating these semicircular rings through the acquired top surface image of the welds to detect process variation(s) under the combined effect of process parameters. It is important for processes like FSW, where too many influencing parameters play a significant role in governing the outcome of the process.

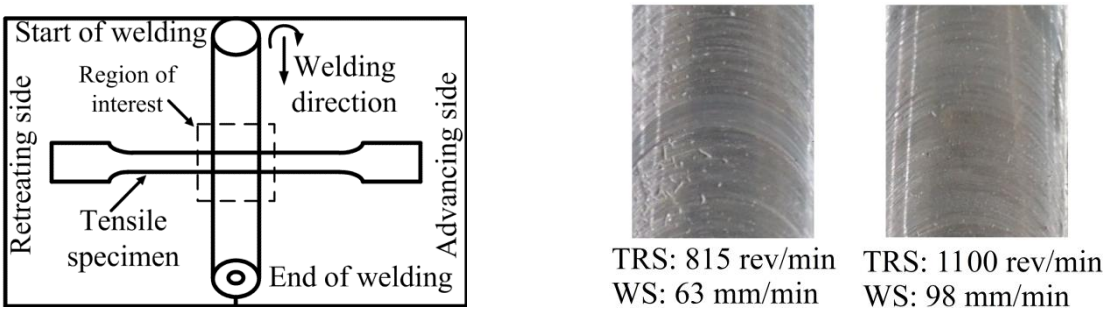

(a) (b)

Fig. 7.1 (a) location on weld for image acquisition (b) semicircular rings at different process conditions

An image is defined as a two dimensional function $f(x, y)$ where x and y are spatial coordinates and the amplitude of 'f 'at any pair of coordinates (x, y) is called the intensity or the grey level of the image at that point or pixel. The captured digital images of the welds are colour (RGB) images. However, the difficulties with colour images are the chances of noise contamination and interference. Converting the image to grey scale will reduce the probability of noise contamination and it will enhance the speed of calculation using grey image. Therefore, all the images are converted to grey image (8-bit) by implementing grey threshold technique using MATLAB software package (MATLAB 2017b). These grey images are used to obtain FD using Katz's method. The next pre-processing applied to the images is the conversion of images to binary images. For the conversion of RGB image to binary image, first the image is converted to a grey image and then to a binary image. These binary images are used to estimate FD using box counting method.

7.5 Image rendering using fractal theory

The box counting method and Katz's method used for estimation for FDs of the images will be referred as Method I and Method II respectively. The details of these two methods are discussed in the following sections.

7.5.1 Method I

In this method, box counting algorithm is applied to binary images to compute the FD. The computed FDs are then correlated to the process parameters and shown in **Fig. 7.2a-b**. With the increase in tool rotational speed, firstly FD decreases and then

gradually follows an increasing trend. Similar trends are not observed for variation of FD with welding speed. FDs reflect the characteristics of the binary image that contains the information of the irregularities due to the formation of semicircular rings on the top surface of the welds. At low tool rotational speed, the irregularities on the top surface of the weld are high and hence, the computed FDs are also high. Similar high FD values are also obtained for the case of high tool rotational speed, which also brings high irregularities in the weld surface. But, at moderate level of tool rotational speed, the irregularities are low and so as the computed FDs against these cases. Experimental observations show that at moderate tool rotational speed, UTS of the joints is better than the rests. It necessitates the need to check the correlation of computed FDs with the UTS values of the joints.

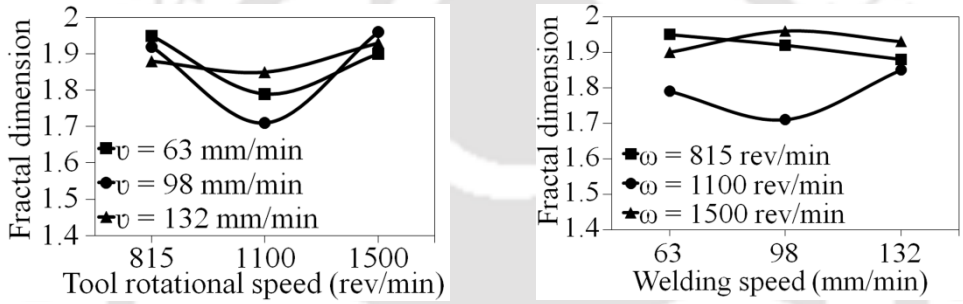

(a) (b)

Fig.7.2 Variation of fractal dimensions computed from Method I with (a) tool rotational speed and (b) welding speed

When the UTS of the joints are correlated with the computed FD, the correlation coefficient obtained is -0.79. Graphically, UTS shows a decreasing trend with the increase in the FD (**Fig. 7.3a**). Whereas, when UTS is correlated to process parameters, the similar decisive conclusion is lacking (**Fig. 7.3b**). Hence, FD of an image (binary) can be an efficient indicator for monitoring weld quality.

7.5.2 Method II

In this method, the algorithm proposed by Katz (1988) is used to estimate the FD. This algorithm applies to 2D waveforms and cannot be applied directly to images. Therefore, the information available in the image is first converted to 2D waveforms in terms of GLD of the image with respective pixel index by converting the RGB images to grey images. Three fixed locations on the top surface of the grey images are selected for

the extraction of grey distributions. Two locations at the two extremities of the weld zone and one at the center of the weld zone are selected. GLDs against each zone are extracted using MATLAB software package (MATLAB 2017b). Among the three locations, grey distributions obtained from the middle of the weld zone show more variations. Hence, these distributions from all the images are considered for this study. **Fig. 7.4** shows a particular case of GLD along the line of extraction on the image. This characteristic distribution is the indicator of the surface irregularities on the top surface of the image and hence reflects the process condition.

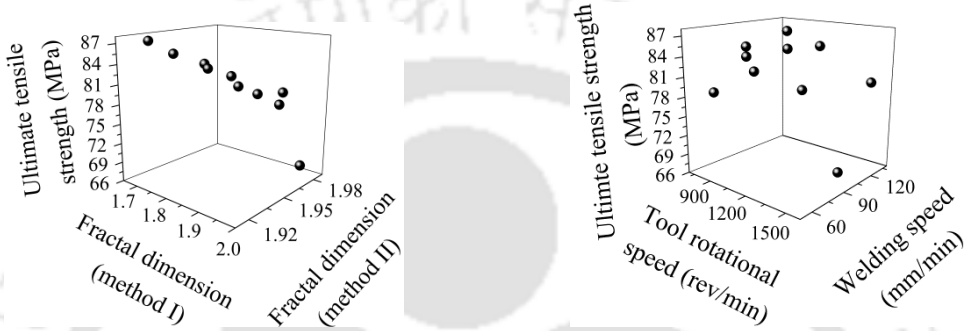

(a) (b)

Fig.7.3 Variation of ultimate tensile strength with (a) computed fractal dimension (b) process parameters

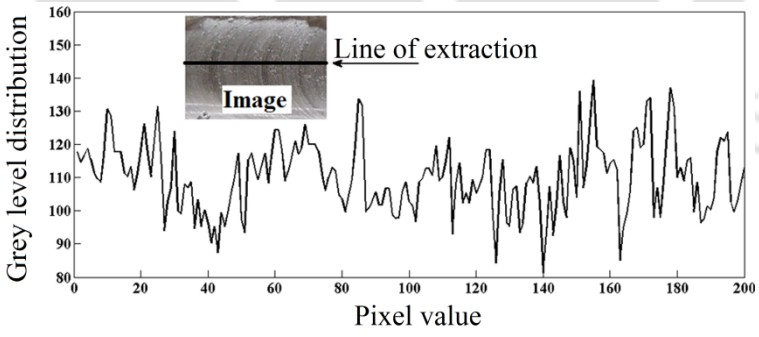

Fig. 7.4 Grey level distribution of image with location of extraction

The computed FD is correlated to the process parameters to investigate the effect of these on the FD. **Fig. 7.5a-b** shows the variation of FD with the process parameters. The trend in the computed FD through this method is the same as observed in the variation of FD computed through Method I. At low tool rotational speed, the irregularities on the surface of the welds are high, which generates more variations in the obtained GLDs of image, resulting in high FD values. The same is again valid for high

tool rotational speed and welding speed values which also generate GLDs with more variations. Whereas, at a moderate level of these two parameters (tool rotational speed and welding speed), GLDs of the images contain fewer variations as compared to other cases and results in less FD. The same conclusions cannot be drawn for the variations of FDs with welding speed as all the data set does not lead to a similar trend. The correlation coefficient between the FDs computed from Method II, and UTS of the joints are found to be -0.91. The variation of computed FDs with UTS of the joints is shown in **Fig. 7.3a**. The clear decreasing trend of UTS with an increase in the FDs from this method is an indication that FDs of GLD of weld images can be a better candidate to monitor process outcome than process parameters.

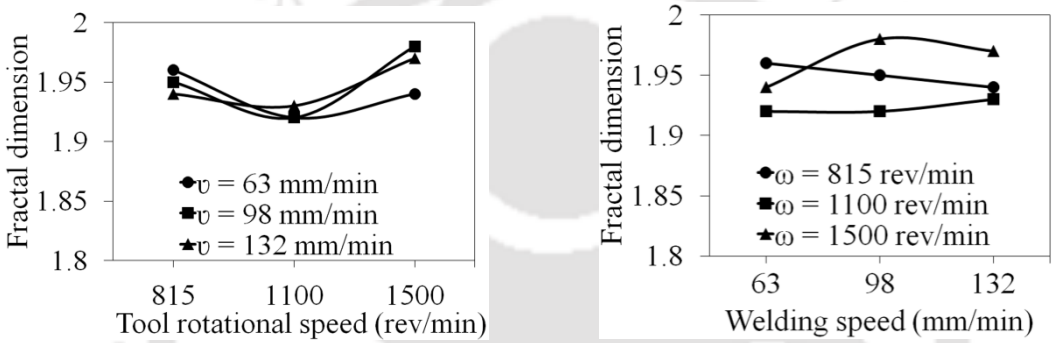

(a) (b)

Fig. 7.5 Variation of fractal dimensions computed from Method II with (a) tool rotational speed and (b) welding speed

Grey values of an image depend on the source, the device used to capture the image and the software used for the conversion of RGB image to grey image. For the present case, the images are captured though a photographic camera keeping the elevation of the image, magnification of the image and light intensity of the image fixed for all the images. The images are captured using a regular photographic camera so that the process can be kept as simple as possible. MATLAB software package (MATLAB 2017b) is used for the conversion of captured RGB image to grey scale image. In this software package, there are dedicated tools available for converting the RGB colour image to grey scale image. For the conversion of the image, the algorithm used weighted values of R, G, B components which is given by **Eq. 7.1** where R_p, G_p and B_p represents intensity levels against at pixel p for red, green and blue components and $GI|_p$ represents grey intensity at the respective pixel p of the image.

$$GI|_p = 0.2989 \times R + 0.5870 \times G + 0.1141 \times B \quad (7.1)$$

The weights for the formulation is fixed and the grey values computed from the image merely depends on the R, G, B components of the individual image. Moreover, in the study, the grey images are not used directly. The intensities from the middle of the grey image along a line are extracted and plotted, where abscissa represents the pixel index and ordinate represents the grey intensities. This plot, as it follows trends, and can be defined as a function of pixel index and intensity content. This idea motivates to treat the intensity distribution as a signal, sampled over different pixel number or index within the same image. This is performed for all the captured images and all the other values, *i.e.*, position of the line of interest against which grey distributions are sampled are fixed for every case. Thus, changes in the images, captured under same environment are bound to yield grey distribution more or less similar to the ones reported in **Fig. 7.4**. The changes in the images are due to the profiles generated in the top surface of the welds due to the combined action of the tool rotation and traversing of the tool over the top surface. At various combinations of tool rotational speed and welding speed the characteristics semicircular rings or profile generated in the top surface will be different from one sample to another. Thus, this will make grey level distributions unique for each image, meaning information contained in the grey distributions plots is unique for a particular set of process parameters. Fractal dimension algorithm is implemented to these plots, to find out the characteristics of the distributions in terms of FDs those are correlated to UTS of the joints. The idea of implementing fractal theory to images is to find the fractal nature of the object (image in this case). The more precise software packages, more sophisticated image acquisition tools obviously lead to more precise information of the image, but this research work is all about to present the concept of weld quality modelling with FD utilizing the available resources and not deviating from the key concept of developing a simple, yet effective modelling technique for the prediction of weld quality. The images are enlarged and the same methodology is implemented to extract the grey level distribution from the grey images. For all the grey distributions from all the images gives the FD consistent up to second decimal point.

7.5.3 Scale invariance of fractal dimension

Rough surfaces and their corresponding profiles are multi scale in nature (Yong et al., 2002). This property is expressed as self-affinity or similarity in fractal theory. It

implies that if the surface is magnified; more and more details will emerge, and the magnified image is statistically similar to the topography of the original image. The above statement should be valid for the acceptance of fractal theory to be applied to images for extracting surface based information. The approach developed with fractal theory for analysis of images needs to be tested for scale dependency before presenting it globally for its acceptance. However, researches in the field of image processing with fractal theory efforts made to investigate scale effect are less or often neglected (Muguthu and Gao, 2013; Kaczor et al., 2012; Takahasi and Nagahama, 2003; Zhong et al., 2003; Ma et al., 1999; Wang et al., 1990). In the present study an attempt has been made to deliver and produce results for images at various magnifications for both Method I and Method II for estimation of FDs from the images. In the Method I, the images are converted to grey scale and grey intensity distributions are obtained using MATLAB software package (MATLAB 2017b). Grey intensity distributions are extracted from three positions from the image, but due to the less variance among these, distributions from the middle section is considered and reported in the present study. Two enlargements are tested apart from the one furnished in the results from Method I. A total of ten images are captured from ten different experimental specimens of the welds. Two magnification levels of 2X and 5X are considered for the results to be presented herewith. Similarly for Method II the same procedures have been adopted for conversion of the images to binary images with the two selected magnification level of 2X and 5X. FDs are computed against the respective images with the Method II and the computed FDs against various scale or magnification have been compared. The computed FDs from images at various magnifications along with no magnification against both Method I and Method II can be seen in **Fig. 7.6**. The results show that the FD does not vary considerably for different scales of enlargement for both the proposed method. So it can be believed that computed FDs were independent of scale of images. The invariance of computed FDs for images at various scales of magnification revealed that the images under consideration behave as fractal images and application of fractal theory is justifiable.

Variation of FDs without magnification against Method I and Method II are compared in **Fig. 7.7**. FDs computed from Method I show less variation than Method II. The possible reason for this lies in the algorithms for the methods. In Method I, box counting method is implemented. The philosophy of this method lies in counting boxes

that covers the object in an image (binary image for the present case) at different resolutions. The size of a box cannot be more than the whole image and also it cannot be less than the single element in the image. *i.e.*, one pixel. Due to these limitations the number of boxes at different resolutions is finite leading to less variation in the computed FD. On the other hand in the Method II, Katz's method is implemented on the one dimensional profiles of the grey intensities of the images. The principle of this approach lies in covering each point in the data set and the more is the variations present in the data points, the more variations will be reflected in the computed FDs. The GLDs of the images shows more variations than the binary images, leads to more variations in computed FDs. It can be said that Method II is more suitable to extract intricate details of an image than Method I.

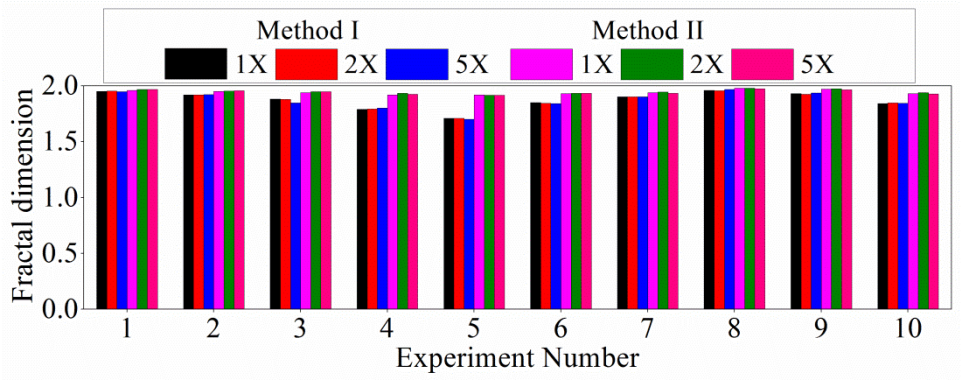

Fig. 7.6 Variation of fractal dimensions under different magnification scales

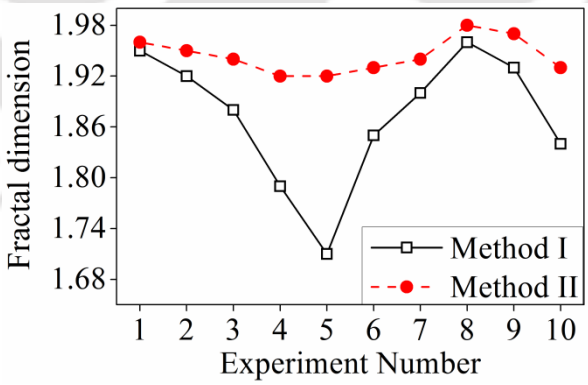

Fig. 7.7 Comparison of fractal dimensions under different scaling of images

7.6 Wavelet analysis of weld images

In signal analysis, wavelet transform has been proved to an effective analyzing tool keeping the characteristics of both time and frequency information. Apart from

signal analysis, wavelet analysis is also capable of extracting information from images (Yajnik et al., 2015; Liu et al., 2015). Using wavelet transform, noise reduction, image compression and enhancement can be performed (Liu et al., 2015). In the present study, the images used for the analysis using fractal theory are also analyzed with 2D wavelet transform to extract information regarding the process outcome.

The acquired images of the top surface of the welds are first converted to grey scale images and then the images are isolated from the background image as backgrounds do not carry any information regarding the process. Once the images are isolated, these are converted to binary images using grey level threshold technique available in MATLAB software package. Different steps involved in image preprocessing are shown in **Fig. 7.8**.

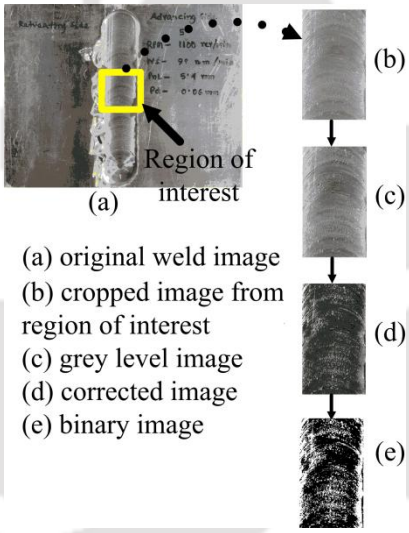

Fig. 7.8 Preprocessing steps applied to original weld images

Binary images of the welds are fed to the developed algorithm in MATLAB environment for performing the 2D wavelet transformation. Wavelet transform is performed at second level of decomposition and suitable mother wavelet is selected based on peak signal to noise ratio (PSNR) as given by **Eq. 7.2**. A total of 53 mother wavelet functions are tested for finding the suitable function and the best one is selected which yields highest PSNR value. PSNR values against the considered mother wavelet functions can be seen in **Fig. 7.9**. From the figure, it is observed that biorthogal2.4 (bior2.4) wavelet attained the maximum PSNR value, hence considered as suitable for this analysis.

$$PSNR = 10\,log_{10}\left(\frac{(maxval)^2}{MSE}\right) \tag{7.2}$$

where, $maxval$ is the maximum value of the approximation coefficient after wavelet decomposition of the image and MSE is the mean square error between the original and reconstructed image.

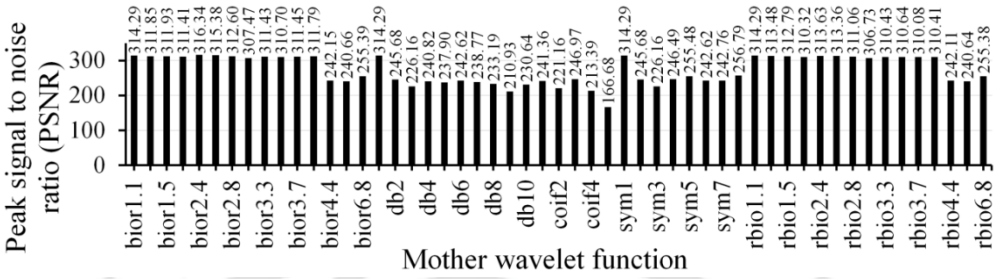

Fig. 7.9 PSNR values against different mother wavelet function

Wavelet transform of the preprocessed images are performed using bior2.4 mother wavelet function and average of approximation coefficients are computed for each image. These computed features when correlated to UTS of the joints, do not reveal any notable correlation. Hence, in this study a new indicator is proposed based on the information acquired using wavelet transform of images. The proposed indicator (CI) is mathematically expressed as given in **Eq. 7.3**.

$$CI = |log_{10}(log_{10}(coeff))| \tag{7.3}$$

where, $coeff$ represent the average root mean square values of the approximation coefficients of the decomposed image. CI values when correlated with UTS of the joints yield a correlation coefficient of -0.93. Graphically, variation of UTS with the proposed CI is shown in **Fig. 7.10**. Decreasing trend of UTS with increase in the CI values is observed from the figure. Moreover, the CI values against the repeated experimental case show appreciable difference which indicates the proposed CI can be an indication towards detection of process variation. This demonstrates that the proposed CI can be effective in monitoring the outcome of the FSW process in terms of UTS of the joints. The results are in accordance with the results obtained from fractal analysis. Features obtained from fractal theory in terms of FDs of images and wavelet transform in terms of CIs reveal its appreciable correlation with the UTS of the joints. In both the cases, UTS

of the joints found to follow a decreasing trend with the increase in the respective features from the images.

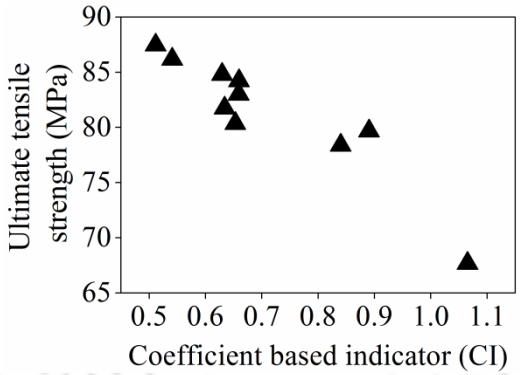

Fig. 7.10 Variation of ultimate tensile strength with CI

The present work demonstrates the avenue of correlating weld top surface image information with quality of the welds. It is considered the variation of weld quality mainly due to variation in the selected process parameters and not due to any appreciable surface or sub-surface defects. The applicability of the proposed approach in defective cases is not evaluated in the current research. Other limitation is with the choice of range of process parameters. In this study, only a narrow range of parameters is selected and analysis is performed over this range. Therefore, wider range of parameters with different tool geometries needs to be tested along with reproducibility of the method has to be evaluated for generalization.

7.7 Summary

The present study demonstrates image based information as an effective indicator to monitor FSW process. Information contained in top surface images of the welded specimens are extracted using well known fractal theory and 2D wavelet packet transform. Following are the conclusions derived from the analysis.

- Ultimate tensile strength of the joints when correlated to tool rotational speed and welding speed: two most influencing process parameters in friction stir welding process do not reveal any notable correlation. This describes inadequacy in relying only in process parameters to monitor the outcome of the process effectively.

- Both methods for the estimation of FDs of images deliver a definite noteworthy trend with ultimate tensile strength of the joints. Moreover, it is also demonstrated that the computed FDs are independent of the scaling of the images. With the increase in FDs of the images, ultimate tensile strength of the welds found to follow a decreasing trend. These manifests that FDs of images can be an effective indicator for monitoring the friction stir welding process. Between the two methods (Method I and Method II), Method I gives more significant difference in FDs against the repeated case, so this method is more effective in detecting process variation.

- Biorthogonal2.4 mother wavelet function is found to be most suitable for the analysis of the weld images at second level of decomposition based on peak signal to noise ratio values. A new indicator (CI) is proposed relating the information extracted from the wavelet transform of images. Ultimate tensile strength of the joints show a decreasing trend with increase in CI revealing its potential to be another effective candidate for monitoring the friction stir welding process. Difference in the computed CI values against the repeated case explores its potential to detect process variation.

- Features obtained from top surface images of the welds whether in terms of FDs or in terms of CIs, show definite trend with ultimate tensile strength of the joints revealing its capability in monitoring the quality outcome of friction stir welding process. These features can be used in the input space of any data driven models for developing predictive models for ultimate tensile strength of the joints.

Chapter 8

Conclusions and future scopes

8.1 Conclusions of the present work

The motivation for the current research work is to develop methodologies that can facilitate monitoring of FSW process with less time, reliability, and appreciable accuracy with less human intervention. With this motive for the present research work is divided in to two main groups. The first one is to develop methodologies for accurate monitoring of weld quality in FSW process and second to develop accurate strategies for identification of internal defects in friction stir welded samples with inconsiderable post processing time. In the first phase of the research work experiments are conducted over wide range of tool rotational speed, welding speed and shoulder diameter. Welding experiments are conducted on AA1100 aluminum alloy in butt joint configuration in a vertical knee type milling machine modified for FSW process. A new forces and torque measurement setup for FSW process is developed in the present study. The welded samples are prepared for mechanical testing as per ASTM E8M standards and tested for measurement of UTS, yield strength and percentage of elongation of the joints. The next phase of research work started with acquisition of main spindle motor current signal, tool rotational speed signal, welding motor current signal, vertical force signal, torque signal and temperature signal during the welding process. The process of acquisition is followed by processing of these signals for effective features extraction. In the processing of acquired signals wavelet transform, Hilbert-Huang transform, and fractal theory have been implemented. Later, extracted signal features are used for developing different methodologies for weld quality monitoring and internal defect identification in FSW process. The salient findings and conclusions of the present research work are highlighted as follows.

- ✓ A strain gauge based force and torque measurement setup has been developed for FSW process. The installation of the developed setup with the existing FSW machine is comparatively easy compared to other force or torque measurement systems. The developed setup can perform to a maximum tool rotational speed of ~11000 rev/min. The developed setup has maximum working limit for vertical force, transverse force and torque are 15 kN, 5kN and 40 N-m with measurement accuracies of 98.73%, 98.94% and 99.04%, respectively.
- ✓ A novel method for selection of suitable mother wavelet function for WPT framework has been developed. Comparison of the developed method with the already published methods revealed that the proposed method is free from process dependencies. The method used a ratio between the energy of the signal and entropy of the wavelet packets for determination of suitable mother wavelet function.
- ✓ The limitation of wide frequency band in the intrinsic mode functions computed from HHT is eliminated by combining the HHT with WPT. The combined WPT-HHT method can offer better visualization of decomposed signals over narrow frequency band which is advantageous for observing sharp events over less duration of time.
- ✓ Features from main spindle motor and welding motor current signals, vertical force and torque signals and tool rotational speed signals are estimated using WPT, WPT-HHT, DWT and fractal theory, respectively. Features are fused with BPNN, RBFNN and SVR models in order to develop models for prediction of UTS of the joints. In all the cases SVR outperform prediction of UTS with maximum accuracy of 99.55% with vertical force signal features and minimum of 97.85% with current signal features. On the other hand maximum and minimum prediction accuracy of BPNN model is found to be 98.42% with vertical force signal features and 94.13% with current signal features.
- ✓ Identification of internal defects in welded specimens has been successfully achieved with features of vertical force signal, torque signal, tool rotational speed signal and temperature signal. Three new indicators namely, defect index (DI), rate of change of temperature (R_cT) and wavelet based indicator (WBI) are developed for identification of defective welds. The indicator DI is

developed from torque signal features, and R_cT and WBI are developed form temperature signal features. Along with these indicators, instantaneous phase and frequency of vertical force signals computed using WPT-HHT are also presented as effective features for identification of internal defects. Fractal dimensions computed from tool rotational speed signal using Higuchi's algorithm also provided an insight for identification of internal defects.

- ✓ The present study also develops a novel method based on top surface images of the welds for monitoring the UTS of the joints. Two methodologies have been proposed for processing of images to extract suitable information using fractal theory. The developed methodologies are compared with 2D wavelet transform and similar results have been obtained. The proposed work delivers a simple yet effective approach for monitoring UTS of the joints with inconsiderably less post processing time.

8.2 Future scopes of the present work

The research work presented in this thesis deals in development of different strategies for monitoring of FSW process. Real time signals are processed with developed methodologies and effective features are extracted from signals and correlated to weld qualities in terms of strength of the joints. Apart from the weld quality monitoring, the current research work also develops methodologies for accurate identification of internal defects in the friction stir welded samples using different signal features. However, the work presented can be extended further and following are the possible future scopes.

- The developed weld quality monitoring methodologies only tested for UTS of friction stir welded joints. However, there are other quality attributes such as yield strength, ductility, hardness and bend strength can be tested with the developed methodologies.
- One of the major contributions of the present research work is the development of strategies for identification of internal defects in friction stir welded samples. These strategies can be extended further for characterization of internal defects for its size estimation, orientation and location of occurrence.

- The image processing methodology developed in the current research work can be extended to test thermographic images of welded samples for monitoring of weld quality and identification of defects in the welded samples.
- Suitable hardware and software integration can be developed so that methodologies developed can be extended towards hardware realization for actual industrial implementation.

APPENDIX I

BPNN Model development steps

Step 1 *Definition*

The architecture of the network is defined in terms of the values for L_I, L_H and L_O. Among the three L_I and L_O are fixed for a particular problem. L_H is an integer value and can be varied. Then values of learning rate η and momentum coefficient α and an activation function (logistic sigmoid in the present work) are assigned. The schematic representation of ANN model is shown in **Fig. A1.1**.

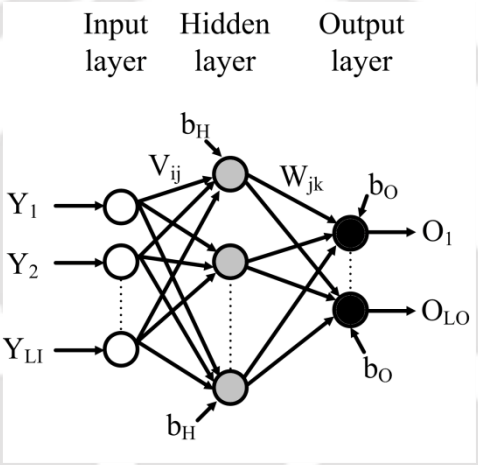

Fig. A1.1 Schematic representation of an ANN model

Step 2 *Initialization*

In this step the weights and biases are initialized. The connections weights V_{ij} and W_{jk} are randomly initialized between ± 0.9 with biases $b_O = b_H = 1$.

Step 3 *Presentation of the training patterns*

The process of network modification by updating its weights, biased and other parameters is known as training. The training may be in sequential mode or batch mode. In the sequential mode the network is modified by utilizing the training patterns sent one after another in a sequence. In batch mode which is used for network training in the present work, the whole training data set consisting of large number of patterns is passed through the network and an average error in predictions is determined. Then it is

propagated back to update the weights and bias values of the network so that the predictions become more accurate.

Step 4 ***Normalization of the data set***

To train a neural network model sometime the raw training data set is required to be scaled in which the range of values is constrained to remain within the range of activation function. In the case of logistic sigmoid function the same is represented as follows.

$$S(y) = \frac{1}{1 + e^{-ay}} \tag{A1.1}$$

where a is constant and y is the input to the activation function S. For a BPNN model with above mentioned activation function the target values must be within [0.1 to 0.9] instead of the usual range [0, 1] as it maps the range of y as $[-\infty, \infty]$. It prevents the training algorithm to drive the connections weights to infinity and thus slowing down the training process. The range of each input is linearly scaled to the range of the activation function. This allows the connections weights to have the same magnitude. Hence, the input and output parameters for all the data set are normalized in the range of 0.1 to 0.9 as follows.

$$y_{norm} = 0.1 + 0.8\frac{y - y_{max}}{y_{max} - y_{min}} \tag{A1.2}$$

where, y_{max} and y_{min} are the maximum and minimum values of any parameter in the data set under consideration, y is the actual value of the parameter and y_{norm} are the normalized values of the parameters.

Step 5 ***Forward Pass***

After applying the activation function to the weighted sum from a neuron the output from it can be calculated and this becomes the input for the next layer. The same process can be carried out for each hidden node and then output node. The output from the j^{th} hidden neuron and k^{th} output neuron for p^{th} pattern is calculated as follows.

$$O_{jH}^{p}(n) = \frac{1}{1 + e^{\left\{-\left(\sum_{i=1}^{L_I} V_{ij}(n) Y_i^p + b_H\right)\right\}}} \tag{A1.3}$$

$$O_{kO}^{p}(n) = \frac{1}{1 + e^{\left\{-\left(\sum_{j=1}^{L_H} O_{jH}^{p}(n) Y_i^p + b_O\right)\right\}}} \quad \textbf{(A1.4)}$$

where, $O_{jH}^{p}(n)$ is the output of the j^{th} hidden neuron for the p^{th} pattern at the n^{th}iteration. $O_{kO}^{p}(n)$ is the output from the output k^{th} neuron for p^{th} pattern at the n^{th} iteration. $V_{ij}(n)$ is the connection weight between i^{th} input neuron and j^{th} hidden neuron at n^{th} iterations. $W_{jk}(n)$ is the connection weight between j^{th} hidden neuron and k^{th} output neuron at n^{th} iterations. Y_i^p is the value of the i^{th} input neuron at the p^{th} pattern.

Step 6 ***Error calculation***

By calculating the output from the k^{th} output neuron $O_{kO}^{p}(n)$, with the target output T_k^p for the p^{th} pattern at the n^{th} iterations the error value can be calculated as follows.

$$E_k^p(n) = \frac{1}{2}\left(O_{kO}^{p}(n) - T_k^p\right)^2 \quad \textbf{(A1.5)}$$

Step 7 ***Setting the stopping criteria for training***

The aim of the training of the BPNN model is to reach where mean square error (MSE) for all training patterns declines to a sufficiently small value. The MSE can be determined by the following.

$$MSE(n) = \frac{1}{2PL_O}\sum_{p=1}^{P}\sum_{k=1}^{L_O}\left(O_{kO}^{p}(n) - T_k^p\right)^2 \quad \textbf{(A1.6)}$$

Where, $MSE(n)$ is the calculated mean square error at the n^{th} iteration, P is the total number of training patterns. The training is stopped when the MSE of the testing data set keeps on increasing while training data set follow a decreasing trend.

Step 8 ***Backward pass***

The updation of all connection weights is as per the gradient descent algorithm that can be expressed mathematically as follows.

$$\Delta V_{ij}(n) = \frac{1}{2PL_O}\sum_{p=1}^{P}\sum_{k=1}^{L_O}\eta\left(T_k - O_{kO}^{p}(n)\right)O_{kO}^{p}(n)\left(1 - O_{kO}^{p}(n)\right)O_{jH}^{p}(n)\left(1 - O_{jH}^{p}(n)\right)V_{jk}(n-1)Y_i + \left\{\alpha\Delta V_{jk}(n-1)\right\} \quad \textbf{(A1.7)}$$

$$\Delta W_{jk}(n) = \frac{1}{2PL_O}\sum_{p=1}^{P}\sum_{k=1}^{L_O}\eta\left(T_k - O_{kO}^{p}(n)\right)O_{kO}^{p}(n)\left(1 - O_{kO}^{p}(n)\right)O_{jH}^{p}(n)\left(1 - O_{jH}^{p}(n)\right) + \{\alpha\Delta V_{jk}(n-1)\} \quad \textbf{(A1.8)}$$

Step 9 ***Iteration***

Till the stopping criterion for learning is reached steps 4 to 7 are repeated. The steps are summarizes in the flowchart shown in **Fig. A1.2**.

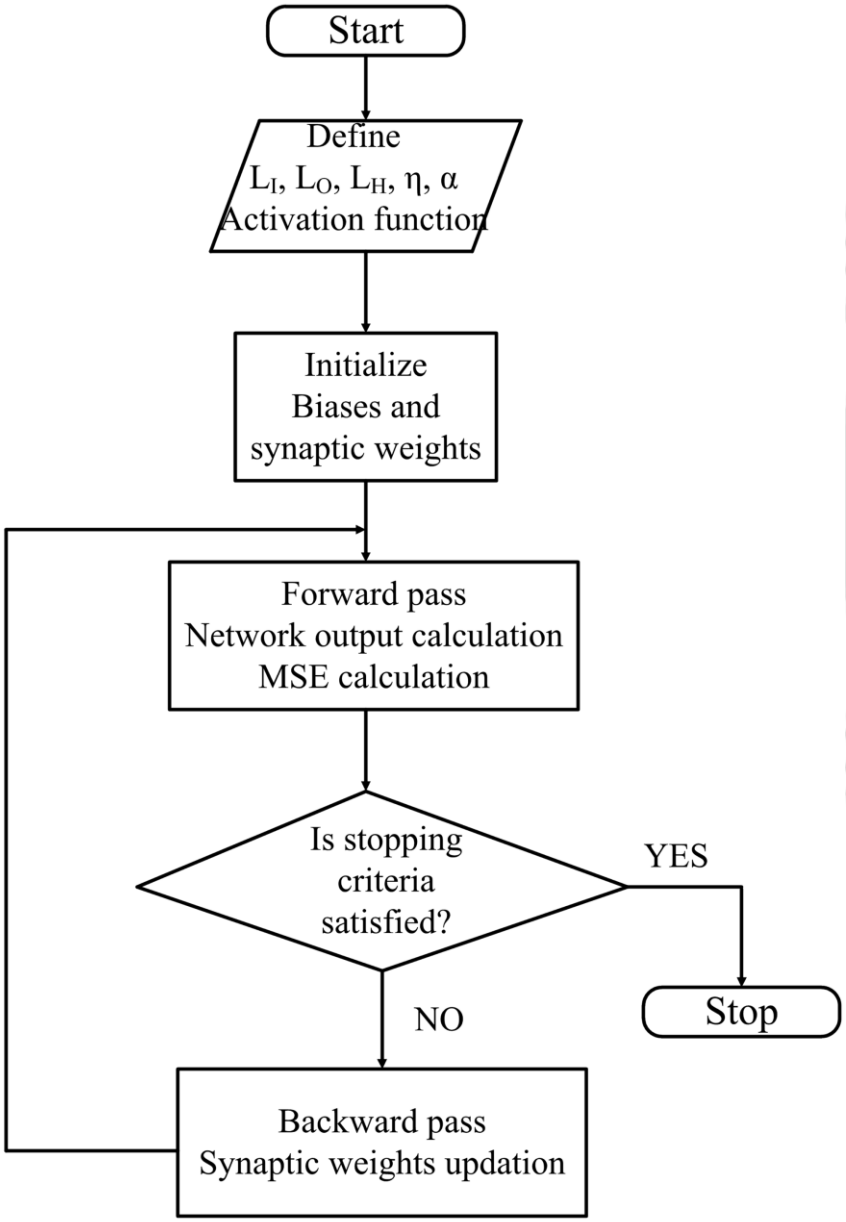

Fig. A1.2 Flowchart from BPNN model development

RBFNN model development steps

Step 1 ***Definition***

The RBFNN architecture is defined, i.e., values for input and output neurons are selected, which depend on the given problem. **Figure A1.3** shows a schematic representation of a RBFNN model.

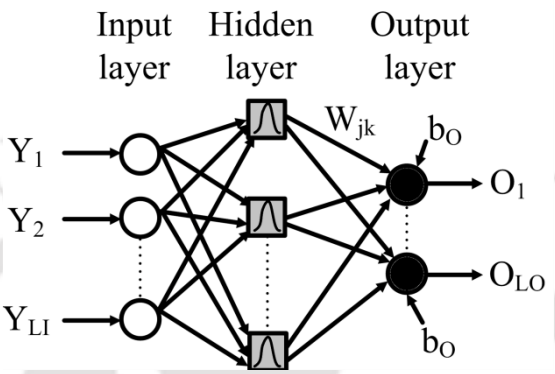

Fig. A1.3 Schematic representation of RBFNN model

Step 2 ***Initialization***

Initially centers of radial basis functions are chosen randomly from the input space. The connections weights V_{jk} between hidden and output layers are randomly initialized between ± 0.9.

Step 3 ***Presentation of the training patterns***

Similar to that of BPNN model the training patterns are normalized in the range of 0.1 to 0.9 and presented to the network in batch mode.

Step 4 ***Forward pass calculations***

The output from the j^{th} hidden neuron and k^{th} output neuron for p^{th} patterns are calculated as given below.

Output of the j^{th} hidden neuron is gen by

$$R_j^i(n) = e^{-\left(\frac{\|Y_i - C_j(n)\|^2}{2(\sigma_j(n))^2}\right)} \quad \textbf{(A1.9)}$$

where, $R_j^i(n)$ is the output of the j^{th} hidden neuron of Y_i input pattern at the n_{th} iteration, $C_j(n)$ is the j^{th} canter at the Gaussian function at the n^{th} iteration, $\|Y_i - C_j(n)\|^2$ is a Euclidean norm and $\sigma_j(n)$ is the width of the Gaussian function at the n^{th} iteration given by the following relation.

$$\sigma(n) = \frac{d_{max}(n)}{\sqrt{2H}} \quad \textbf{(A1.10)}$$

Where, $d_{max}(n)$ is the maximum distance between the chosen centers at the n^{th} iteration.

Output of k^{th} output for i^{th} input pattern at the n^{th} iteration was calculated using the sigmoid activation function

$$O_{kO}^i(n) = \frac{1}{\left(1 + e^{-S_{kO}^i(n)}\right)} \quad \textbf{(A1.11)}$$

$$S_{kO}^i(n) = \sum_{j=0}^{H} V_{jk}(n) R_j^i(n) \quad \textbf{(A1.12)}$$

Where, $O_{kO}^i(n)$ is the output from the k^{th} output neuron with i^{th} input pattern in the n^{th} iteration, $S_{kO}^i(n)$ is the weighted sum of the k^{th} output neuron with i^{th} input patterns at the n^{th} iteration, $V_{jk}(n)$ is the connection weight between the j^{th} hidden neuron and the k^{th} output neuron at the n^{th} iteration.

Step 5 ***Training algorithms***

The network training for RBFNN is done by updating center of the RBF, width of the Gaussian function and the weight between hidden and output neurons of the network. In the present full training algorithm is used in which all the above parameters were updated through back propagation algorithm and at same time scale. The updation of centers is as follows.

$$C_j(n) = C_j(n) - \eta_1 \frac{\partial \xi(n)}{\partial C_j(n)} \quad \textbf{(A1.13)}$$

The spread of the Gaussian function is updated using

$$\sigma_j(n) = \sigma_j(n) - \eta_2 \frac{\partial \xi(n)}{\partial \sigma_j(n)} \quad \textbf{(A1.14)}$$

And weights are updated using

$$V_{jk}(n) = V_{jk} - \eta_3 \frac{\partial \xi(n)}{\partial V_{jk}(n)} \quad \textbf{(A1.15)}$$

Step 6 ***Setting the stopping criteria for training***

All the parameters of the RBFNN model are updated at the same time. If MSE for all the training patterns as given in **Eq. A1.16** reaches to a sufficiently small value the training of the network stops.

$$MSE(n) = \xi(n) = \frac{1}{2NL_O} \sum_{i}^{N} \sum_{k}^{L_O} \left(T_k^i - O_{kO}^i(n)\right)^2 \quad \textbf{(A1.16)}$$

Step 7 ***Iteration***

Till the stopping criterion for learning is met Steps 4 to Steps 6 are replaced. The flowchart for the RBFNN model development is shown in Fig. **A1.4**.

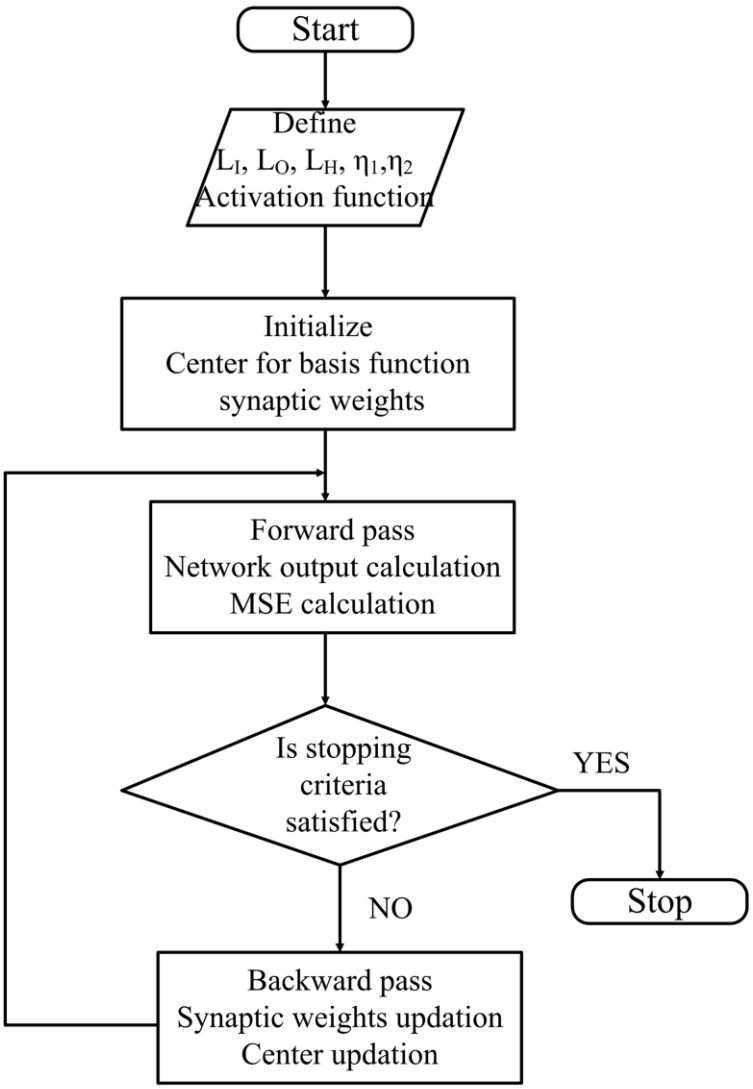

Fig.A1.4 Flowchart for RBFNN model development

APPENDIX II

Support vector regression

Support vector machine (SVM) is a popular machine learning method developed by Vapnik et al. (Cortes and Vapnik, 1995) based on statistical learning with succinct mathematical terms. Compared with other artificial intelligence methods, the rationale of SVM is more complete and the parameters needed are comparatively less and it can better avoid getting stuck in local minima. As a machine learning method, SVM is based on statistical learning and can be divided into support vector classifier and SVR. The aim of SVR is to achieve the mapping approximate $f(.)$, i.e., SVR network $\hat{f}(.)$, according to the given training data set. It can be formulated in parameterized formation as:

$$\hat{f}(.) = C_k k(x, x_k) \tag{A2.1}$$

where,C_k is the parameter that need to be optimized and $k(.,.)$ is the kernel function. According to the principle of structural risk minimization, **Eq. A2.1** is the solution of the regularization problem described by **Eq. A2.2**.

$$\min_{f \in F} J_o(f) = C \sum_{k=1}^{N} L\big(y_k, f(x_k)\big) + \frac{1}{2}\langle f, f\rangle_F \tag{A2.2}$$

where, F is the reproducing Hilbert space defined by $k(.,.)$ and the loss function is estimated as **Eq. A2.3**.

$$L\big(y, f(x)\big) = f(x) = \begin{cases} 0 & |y - f(x)| < \epsilon \\ |y - f(x)| & otherwise \end{cases} \tag{A2.3}$$

where, $L(y, f(x))$ is the error of y obtained by measuring function $f(.)$ at x. The parameter C is used to balance the accuracy of approximation and complexity of mapping.

The above mentioned regularization problem can be equally described as optimization one with certain restraints. And the optimization problem can be transformed into quadratic programming through solving the coefficients $C = [C_1, C_2, \dots\dots, C_N]^T$ by Lagrange multiplier.

$$\min_{c} J_2(c) = \frac{1}{2}\sum_{k,i=1}^{N} C_k C_i (x_k, x_i) - \sum_{k=1}^{N} C_k y_k + \varepsilon \sum_{K=1}^{N} |C_k| \qquad \textbf{(A2.4)}$$

To meet the restraints,

$$|C_k| < C \sum_{k=1}^{N} C_k = 0$$

The training error is estimated by the **Eq. A2.2** and the results show the solution of the above mentioned quadratic programming question in sparse, i.e., only a few C_k are not zero. The corresponding non zero C_k is called as the support vectors. The **Eq. A2.2** in support vector network form can be written as shown in **Eq. 11.15**. The schematic of SVR network can be seen in **Fig. A2.1**.

$$\hat{f}(x) = \sum_{j=1}^{N} \alpha_j \emptyset_j(x) \qquad \textbf{(A2.5)}$$

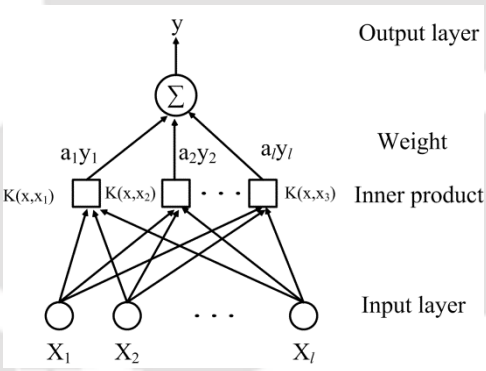

Fig. A2.1 Schematic of support vector regression model

References

Abd El-Hafez H, Mechanical properties and welding power of friction stirred AA2024-T35 joints, Journal of Materials Engineering and Performance, 2011; **20**:836-845.

Abeykoon C, McAfee M, Li K, Martin PJ, Kelly AL, The inferential monitoring of screw load torque to predict process fluctuations in polymer extrusion, Journal of Materials Processing Technology, 2011; **211(12)**:1907-1918.

Abhishekh HA, Thirthali J, Manjegowda A, Phutane VH, Muralidharan K, Gangadhar BN, Ictal EEG fractal dimension in ECT predicts outcome at 2 weeks in schizophrenia, Psychiatry Research, 2013; **209**:155-159.

Abu-Zahra NH, Lange JH, Tool chatter monitoring in turning operations using wavelet analysis of ultrasound waves, international Journal of Advanced Manufacturing Technology, 2002; **20**:248-254.

Ahammer H, Higuchi Dimension of Digital Images, PLoS ONE, 2011; **6(9)**:1-8.

Al-Jarrah JA, Swalha S, Mansour TA, Ibrahim M, Al-Rashdan M, Al-Quahsi DA, Welding equality and mechanical properties of aluminum alloy joints prepared by friction stir welding, Materials and Design, 2014; **56**:926-936.

Amirat Y, Benbouzid MEH, Al-Ahmar E, Bensaker B, Turri S, A brief status on condition monitoring and fault diagnosis in wind energy conversion systems, Renewable and Sustainable energy reviews, 2009; **13**:2629-2636.

Antoni J, Randall RB, Differential diagnosis of gear and bearing faults, Journal of Vibration and Acoustics, 2002; **124**:165-171.

Ao Y, Qiao G, Prognostics for drilling process with wavelet packet decomposition, International Journal of Advanced Manufacturing Technology, 2010; **50**:47-52.

Arora A, Mehta M, De A, DebRoy T, Load bearing capacity of tool pin during friction stir welding, International Journal of Advanced Manufacturing Technology, 2012; **61**:911-920.

Arora KS, Pandey S, Schaper M, Kumar R, Effect of process parameters on friction stir welding of aluminum alloy 2219-T87, International Journal of Advanced Manufacturing Technology, 2010; **50**:941-952.

Astarita A, Squillace A, Carrino L, Experimental study of the forces acting on the tool in the friction stir welding of AA2024 T3 sheets, Journal of Materials Engineering and Performance, 2014; **23(10):**3754-3761.

Aval HJ, Microstructure and residual stress distributions in friction stir welding of dissimilar aluminium alloys, Materials and Design, 2015; **87**:405-413

Axinte DA, Kong MC, An integrated monitoring method to supervise water jet machining, CIRP-Annals Manufacturing Technology, 2009; **58**:303-306.

Aydin H, Tutar M, Durmus A, Bayram A, Sayaca T, Effect of welding parameters on tensile properties and fatigue behaviour of friction stir welded 2014-T6 aluminum alloy, Transactions of Indian Institute of Metals, 2012; **65(1)**:21-30.

Azimzadegan T, Serajzadeh S, An investigation into microstructures and mechanical properties of AA7075-T6 during friction stir welding at relatively high rotational speeds, Journal of Materials Engineering and Performance, 2010; **19**:1256-1263.

Bahrami M, Givi MKB, Dehghani K, Parvin N, On the role of pin geometry in microstructure and mechanical properties of AA7075/SiC nano-composite fabricated by friction stir welding technique, Materials and Design, 2014; **53**:519-527.

Bakker OJ, Gibson C, Wilson P, Lohse N, Popov AA, Linear friction weld process monitoring of fixture cassette deformations using empirical mode decomposition, Mechanical Systems and Signal Processing, 2015; **62**:395-414.

Balasubramanian N, Gattu B, Mishra RS, Process forces during friction stir welding of aluminumalloys, Science and Technology of Welding and Joining, 2009; **14(2)**:141-145.

Bao Y, Hu Z, Xiong T, A PSO and pattern search based memetic algorithm for SVMs parameters optimization, Neurocomputing, 2013; **117**:98-106.

Beer FP, Johnston ER Jr, De-wolf JT, Mazurek DF, Mechanics of Materials, Tata McGraw Hill, Fifth Edition, 2010.

Benbouzid M, A review of induction motors signature as a medium for faults detection, IEEE Transactions on Industrial Electronics, 2000; **47(5)**:984-993.

Bergstra J, Bengio Y, Random search for hyper parameter optimization, Journal of Machine Learning and Research, 2014; **13**:281-305.

Bhatt NN, Kumari K, Dutta S, Friction stir weld classification by applying wavelet analysis and support vector machine on weld surface images, Journal of Manufacturing Processes, 2015; **20(1)**:274-281.

Bin GF, Gao JJ, Li XJ, Dhillon BS, Early fault diagnosis of rotating machinery based on wavelet packets—Empirical mode decomposition feature extraction and neural network, Mechanical Systems and Signal Processing, 2012; **27**:696-711.

Bisadi H, Tavakoli A, Sangsaraki MT, Sangsaraki KT, The influences of rotational and welding speeds on microstructures and mechanical properties of friction stir

welded Al5083 and commercially pure copper sheets lap joints, Materials and Design, 2013; **43**:80-88.

Blignault C, Hattingh DG, Kruger GH, Niekerk TI, James MN, Friction stir weld process evaluation by multi-axial transducer, Measurement, 2008; **41**:32–43.

Boldsaikhan E, Corwin EM, Logar AM, Arbegast WJ, The use of neural network and discrete Fourier transform for real-time evaluation of friction stir welding, Applied Soft Computing, 2011; **11**:4846-4893.

Boz M, Kurt A, The influence of stirrer geometry on bonding and mechanical properties in friction stir welding process, Materials and Design, 2004; **25**:343-347.

Buchibabu V, Reddy GM, Kulkarni D, De A, Friction stir welding of a thick Al-Zn-Mg alloy plate, Journal of Materials Engineering and Performance, 2016; **25**:1163-1171.

Buffa G, Fratini L, Micari F, Mechanical and microstructural prediction by artificial neural networks in FSW processes of dual phase titanium alloys, Journal of Manufacturing Processes, 2012; **14(3)**:289-296.

Cam G, Misticoglu S, Recent developments in friction stir welding of Al-alloys, Journal of Materials Engineering and Performance, 2014; **23**:1936-1953.

Cao X, Jahazi M, Effect of welding speed on the quality of friction stir welded butt joints of a magnesium alloy, Materials and Design, 2009; **30**:2033-2042.

Casalino G, Campanelli S, Mortello M, Influence of shoulder geometry and coating of tool on the friction stir welding of aluminum alloy plates, Procedia Engineering, 2014; **69**:1541-1548.

Cavaliere P, Campanile G, Panella F, Sqillace A, Effect of welding parameters on mechanical and microstructural properties of AA6056 joints produced by friction stir welding, Journal of Materials Processing Technology, 2006; **180**:263-270.

Chappard D, Degasne I, Hure G, Legrand E, Audran M, Basle MF, Image analysis measurement of roughness by texture and fractal analysis correlate with contact profilometry, Biomaterials, 2003; **24**:1399-1407.

Chen C, Daponte JS, Fox MD, Fractal Feature Analysis and Classification in Medical Imaging, IEEE Transactions on Medical Imaging, 1989; **8(2)**:133-142.

Chen C, Kovacevic R, Jandgric D, Wavelet transform analysis of acoustic emission in monitoring friction stir welding of 6061 aluminum, International Journal of Machine Tools and Manufacture, 2003; **43**:1383-1390.

Chen J, Heincke B, Jegen M, Moorkamp M, Using empirical mode decomposition to process marine magnetotelluric data, Geophysical Journal International, 2012; **190**:293-309.

Chen J, Ueji R, Fujii H, Double-sided friction-stir welding of magnesium alloy with concave–convex tools for texture control, Materials and Design, 2015; **76**:181-189.

Chen Z, Shi Y, Jiao B, Zhao H, Ultrasonic nondestructive evaluation of spot welds for zinc-coated high strength steel sheet based on wavelet packet analysis, Journal of Materials Processing Technology, 2009; **209**:2329-2337.

Chen ZW, Pasang T, Qi Y, Shear flow and formation of nugget zone during friction stir welding of aluminum alloy 5083-O, Materials Science and Engineering A, 2008; **474**:312-316.

Chen. X, Li B, Acoustic emission method for tool condition monitoring based on wavelet analysis, International Journal of Advanced Manufacturing Technology, 2007; **33**:968-976.

Cioffi F, Ibanez J, Fernandez R, Doncel GG, The effect of lateral off-set on the tensile strength and fracture of dissimilar friction stir welds, 2024Al alloy and 17%SiC/2124Al composite, Materials and Design, 2015; **65**:438-446.

Cooley JW, Lewis PAW, Welch PD, Historical notes on the fast Fourier transform, IEEE Transactions on Audio and Electroacoustics, 1967; **15(2)**:76–79.

Cortes C, Vapnik V, Support vector networks, Machine Learning, 1995; **20(3)**:273-289.

Cusido J, Romeral L, Ortega JA, Rosero JA, Espinosa AG, Fault detection in induction machines using power spectral density in wavelet decomposition, IEEE Transactions on Industrial Electronics, 2008; **55(2)**:633-643.

Daubechies I, Orthonormal bases of compactly supported wavelets, Communications on Pure and Applied Mathematics, 1988; **41(7)**:909-996.

Dhanunjaya Y, Reddy A, Pratihar DK, Neural network-based expert systems for predictions of temperature distributions in electron beam welding process, International Journal of Advanced Manufacturing Technology, 2011; **55**:535-548.

Dong H, Chen S, Song Y, Guo X, Zhang X, Sun Z, Refilled friction stir spot welding of aluminum alloy to galvanized steel sheets, Materials and Design, 2016; **94**:457-466.

Doukas C, Stavropoulos P, Papacharalampopoulos A, Foteinopoulos P, Vasiliadis E, Chryssolouris G, On the estimation of tool-wear for milling operations based on multi-sensorial data, Procedia CIRP, 2013; **8**:415-420.

Droubi MG, Faisal NH, Orr F, Steel JA, El-Shaib M, Acoustic emission method for defect detection and identification in carbon steel welded joints, Journal of Constructional Steel Research, 2017; **134**:28-37.

Elangovan K, Balasubramanian V, Babu S, Developing an empirical relationship to predict tensile strength of friction stir welded AA2219 aluminumalloy, Journal of Materials Engineering and Performance, 2008; **17(6)**:820-830.

El-Danaf EA, El-Rayes MM, Microstructure and mechanical properties of friction stir welded 6082AA in as welded and post weld heat treated conditions, Materials and Design, 2013; **46**:561-572.

Esteller R, Vachtsevanos G, Echauz J, Litt B, A comparison of waveform fractal dimension algorithms, IEEE Transactions on Circuits and Systems-I: Fundamental Theory and Applications, 2001; **48(2)**:177-183.

Fleming P, Lammlein D, Wilkes D, Fleming K, Bloodworth T, Cook G, Strauss A, DeLapp D, Lienert T, Bement M, Prater T, In-process gap detection in friction stir welding, Sensor Review 2008; **28(1)**:62-67.

Fleming PA, Lammlein DH, Wilkes DM, Misalignment detection and enabling of seam tracking for friction stir welding, Science and Technology of Welding and Joining, 2009; **14(1)**:93-96.

Fortin C, Kumaresan R, Ohley W, Hoefer S, Fractal dimension in the analysis of medical images, IEEE Engineering in Medicine and Biology, 1992; **11(2)**:65-71.

Fratini L, Buffa G, Palmeri D, Using a neural network for predicting the average grain size in friction stir welding processes, Computers and Structures, 2009: **87**:1166-1174.

Fuller MD, Swaminathan S, Zhilyaev AP, McNelley TR, Microstructural transformations and mechanical properties of cast NiAl bronze: Effects of fusion welding and friction stir processing, Materials Science and Engineering A, 2007; **463**: 128-137.

Gang T, Chi DZ, Novel approach to enhancement of ultrasonic TOFD B-scan image for measurement of weld crack, Science and Technology of Welding and Joining, 2007; **12(1)**:87-93.

Gao S, Tang X, Ji S, Yang Z, Prediction of mechanical properties of welded joints based on support vector regression, Procedia Engineering, 2012; **29**:1471-1475.

Garg A, Bhattacharya A, Strength and failure analysis of similar and dissimilar friction stir spot welds: Influence of different tools and pin geometries, Materials and Design, 2017; DOI: https://doi.org/10.1016/j.matdes.2017.04.084

Gayakwad RA, Op-Amps and Linear Integrated Circuits, Pearson, Fourth Edition, 2005.

Gibson BT, Lammlein DH, Prater TJ, Longhurst WJ, Cox CD, Ballun MC, Dharmaraj KJ, Cook GE, Strauss AM, Friction stir welding: process, automation and control, Journal of Manufacturing Processes, 2014; **105**:56-73.

Gilan SS, Jovein HB, Ramezanianpour AA, Hybrid support vector regression – Particle swarm optimization for prediction of compressive strength and RCPT of concretes containing metakaolin, Construction and Building Materials, 2012; **34**:321-329.

Guasp MR, Daviu AA, Sanchez MP, Panadero RP, Cruz JP, A general approach for transient detection of slip-dependent fault components based on the discrete wavelet transform, IEEE Transactions on Industrial Electronics, 2008; **55**:4167-4180.

Guo N, Fu Y, Wang Y, Meng Q, Zhu Y, Microstructure and mechanical properties in friction stir welded 5A06 aluminum alloy thick plate, Materials and Design, 2017; **113**:273-283

Gupta AK, Predictive modelling of turning operations using response surface methodology, artificial neural networks and support vector regression, International Journal of Production Research, 2010; **48(3)**:763-778.

Hammed Z, Hong YS, Cho YM, Ahn SH, Song CK, Condition monitoring and fault detection of wind turbines and related algorithms: a review, Renewable and Sustainable energy reviews, 2009; **13**:1-39.

Hao HL, Ni DR, Huang H, Wang D, Xiao BL, Nie ZR, Ma ZY, Effect of welding parameters on microstructure and mechanical properties of friction stir welded Al-Mg-Er alloy, Materials Science and Engineering A, 2013; **559**:889-896.

Hasan AF, Bennet CJ, Shipway PH, Cater S, Martin J, A numerical methodology for predicting tool wear in friction stir welding, Journal of Materials Processing Technology, 2017; **241**:129-140.

Hassan AA, Prangnell PB, Norman AF, Price DA, Williams SW, Effect of welding parameters on nugget zone microstructure and properties in high strength aluminium alloy friction stir welds, Science and Technology of Welding and Joining, 2003; **8(4)**:257-268.

Haykin S, Neural Networks: a comprehensive foundation, Pearson Education, Delhi, 2003.

He K, Li Q, Chen J, An arc stability evaluation approach for SW AC SAW based on Lyapunov exponent of welding current, Measurement, 2013; **46(1)**:272-278.

He K, Li X, A quantitative estimation technique for welding quality using local mean decomposition and support vector machine, Journal of Intelligent Manufacturing, 2017; **27(3)**:525-533.

He K, Zhang Z, Xiao S, Li X, Feature extraction of AC square wave SAW arc characteristics using improved Hilbert–Huang transformation and energy entropy, Measurement, 2013; **46**:1385-1392.

He K, Zhang Z, Xiao S, Li X, Feature extraction of AC square wave SAW arc characteristics using improved Hilbert-Huang transform and energy entropy, Measurement, 2013; **46(4)**:1385-1392.

Higuchi T, Approach to an irregular time series on the basis of fractal theory, Physica D, 1988; **31**:277-283.

Hou JC, Liu HJ, Zhao YQ, Influence of rotation speed on microstructure and mechanical properties of 6061-T6 aluminum alloy joints fabricated by self-reacting friction stir welding tool, International Journal of Advanced Manufacturing Technology, 2014; **73**:1073-1079.

Hua W, Guanlong C, Ping Z, Zhongqin L, Periodic trend detection from CMM data based on the continuous wavelet transform, International Journal of Advanced Manufacturing Technology, 2006; **27**:733-737.

Huang NE, Shen Z, Long SR, The empirical mode decomposition and the Hilbert spectrum for nonlinear and non-stationary time series analysis. Proceedings of Royal Society of London, 1998; **454**:903-995.

Humberstone M, Wood B, Henkel J, Hines JW, Differentiating between expanded and fault conditions using principal component analysis, Journal of Intelligent Manufacturing, 2012; **23**:179-188.

Hunag PL, Li JF, Sun J, Jia XM, Cutting signals analysis in milling titanium alloy thin-part components and non-thin wall components, International Journal of Advanced Manufacturing Technology, 2016; **84**:2461-2469.

Hwang YM, Kang ZW, Chiou YC, Hsu HH, Experimental Study on temperature distributions within the workpiece during friction stir welding aluminum alloys, International Journal of Machine Tools & Manufacture, 2008; **48**:778-787.

Imam M, Biswas K, Racherla V, Effect of weld morphology on mechanical response and failure of friction stir welds in a naturally aged aluminium alloy, Materials and Design, 2013; **44**:23-34.

Iwaki S, Okada T, Eguchi N, Tanaka S, Namba K, Oiwa N, Imperfections in friction stir welded zones and their precision non-destructive testing. Studies on characteristics of friction stir welded joints in structural thin aluminum alloys, Welding International, 2006; **20(3)**:197-205.

Jang JSR, Sun CT, Mizutani E, Neuro-fuzzy and soft computing, Pearson Education, Delhi, 2004.

Jemielniak K and Arrazola PJ, Application of AE and cutting force signals in tool condition monitoring in micro-milling, CIRP Journals of Manufacturing Science and Technology, 2008; **1(2)**:97-102.

Ji S, Meng X, Liu Z, Huang R, Li Z, Dissimilar friction stir welding of 6061 aluminum alloy and AZ31 magnesium alloy assisted with ultrasonic, Materials Letters, 2017; **201**:173-176.

Kaczor AA, Guixà-González R, Carrió p, Obiol-Pardo C, Pastor M, Selent J, Fractal dimension as a measure of surface roughness of G-protein coupled receptors: Implications for structure and function, Journal of Molecular Modeling, 2012; **18**:4465-4475.

Karabay S, Analysis of drill dynamometer with octagonal ring type transducers for monitoring of cutting forces in drilling and allied process, Materials and Design, 2007a; **28**:673–685.

Karabay S, Design criteria for electro-mechanical transducers and arrangement for measurement of strains due to metal cutting forces acting on dynamometers, Materials and Design, 2007b; **28**:496–506.

Katz JM, Fractal and the analysis of waveforms, Computers in Biology and medicine, 1988; **18(3)**:145-156.

Kaya B, Oysu C, Ertunc HM, Force-torque based online tool wear estimation system for CNC milling of Inconel 718 using neural networks, Advances in Engineering Software, 2011; **42(3)**:76-84.

Khodaverdizadeh H, Mahmoudi A, Heidarzadeh A, Nazari E, Effect of friction stir welding (FSW) parameters on strain hardening behavior of pure copper joints, Materials and Design, 2012; **35**:330-334.

Kim YG, Fujii H, Tsumura T, Komazaki T, Nakata K, Three defect types in friction stir welding of aluminum die casting alloy, Materials Science and Engineering A, 2006; **415**:250-254.

Koo YD, Yoo KH, Na MG, Estimation of residual stress in welding of dissimilar metals at nuclear power plants using cascaded support vector regression, Nuclear Engineering and Technology, 2017; 1-8. DOI: https://doi.org/10.1016/j.net.2017.02.003

Korkut I, A dynamometer design and its construction for milling operation, Materials and Design, 2003; **24**:631-637.

Krishnan KN, On the formation of onion rings in friction stir welds, Materials Science and Engineering *A*, 2002; **327**:246-251.

Krivonosova EA, Gorchakov AI, Fractal analysis of the fatigue fracture surface of metal of welded joints, Welding International, 2013; **27(9)**:690-693.

Kumar K, Kailas SV, The role of friction stir welding tool on material flow and weld formation, Materials Science and Engineering A, 2008; **485**:367-374.

Kumar U, Yadav I, Kumari S, Kumari K, Ranjan N, Kesharwani RK, Jain R, Kumar S, Pal S, Chakravarty D, Pal SK, Defect identification in friction stir welding using discrete wavelet analysis, Advances in Engineering Software, 2015; **85**:43-50.

Kumar U, Yadav I, Kumari S, Kumari K, Ranjan N, Kesharwani RK, Kumar S, Pal S, Chakravarty D, Pal SK, Defect detection in friction stir welding using discrete wavelet analysis, Advances in Engineering Software, 2015; **85**:43-50.

Kumari S, Jain R, Kumar U, Yadav I, Ranjan N, Kumari K, Kesharwani RK, Kumar S, Pal S, Pal SK, Chakravarty D, Defect identification in friction stir welding using continuous wavelet transform, Journal of Intelligent Manufacturing, 2016; DOI: 10.1007/s10845-016-1259-1.

Kupkova M, Kupka M, Rudnayova E, Dusza J, On the use of fractal geometry methods for the wear process characterization, Wear, 2005; **258**:1462-1465.

Kwak JS, Application of wavelet transform technique to detect tool failure in turning operations, International Journal of Advanced Manufacturing Technology, 2006; **28**:1078-1083.

Kwak JS, Ha MK, Detection of dressing time using the grinding force signal based on the discrete wavelet decomposition, International Journal of Advanced Manufacturing Technology, 2004; **23**:87-92.

Lakshminarayanan AK, Balasubramanian V, Comparison of RSM with ANN in predicting tensile strength of friction stir welded AA7039 aluminium alloy joints, Transactions of Nonferrous Metals Society China, 2009; **19**:9-18.

Law LS, Kim JH, Liew WYH, Lee SK, An approach based on wavelet packet decomposition and Hilbert–Huang transform (WPD–HHT) for spindle bearings condition monitoring, Mechanical Systems and Signal Processing, 2012; **33**:197-211.

Leal RM, Sakharova N, Vilaca P, Rodrigues DM, Loureiro A, Effect of shoulder cavity and welding parameters on friction stir welding of thin copper sheets, Science and Technology of Welding and Joining, 2011; **16(2)**:146-152.

Leitao C, Arruti E, Aldanondo E, Rodrigues DM, Aluminium-steel lap joining by multipass friction stir welding, Materials and Design, 2016; **106**:153-160.

Li H, Wang Y, Zhao P, Zhang X, Zhou P, Cutting tool operational reliability prediction based on acoustic emission and logistic regression model, Journal of Intelligent Manufacturing, 2015; **26(5)**:923-931.

Li H, Xiao DY, Fault diagnosis based on power spectral density basis transform, Journal of Vibration and Control, 2013; **21(12)**:2416-2433.

Li H, Yang S, Zhang S, Zhang B, Jiang Z, Feng H, Han P, Li J, Microstructure evolution and mechanical properties of friction stir welding super-austenitic stainless steel S32654, Materials and Design, 2017; **118**:207-217.

Li J, Du Q, Sun C, An improved box-counting method for image fractal dimension estimation, Pattern Recognition, 2009; **42**:2460-2469.

Li J, Hao H, Damage detection of shear connectors under moving loads with relative displacement measurements, Mechanical Systems and Signal Processing, 2015; **60**:124-150.

Li JQ, Effects of tool rotation speed on microstructures and mechanical properties of AA2219-T6 welded by external non-rotational shoulder assisted friction stir welding, Materials and Design, 2013; **43**:299-306.

Li L, Xiao L, Liao H, Liu S, Ye B, Welding quality monitoring of high frequency straight seam pipe based on image feature, Journal of Materials Processing Technology, 2017; **246**:285-290.

Li X, Real-time detection of breakage of small diameter drills with wavelet transform, International Journal of Advanced Manufacturing Technology, 1998; **14**:539-543.

Liebovitch LS, Toth T, A fast algorithm to determine fractal dimensions by box counting, Physics Letters A, 1989; **141**:386-390.

Lienert TJ, Stellwag WL, Grimmett BB, Warke RW, Friction sit r welding studies on mild steel, Welding Journal, 2003; **121**:1-9.

Lim DH, Bae IH, Na MG, Kim JW, Prediction of residual stress in the welding zone of dissimilar metals using data-based models and uncertainty analysis, Nuclear Engineering and Design, 2010; **240**:2555-2564.

Lin L, Chu F, Feature extraction of AE characteristics in offshore structure model using Hilbert–Huang transform, Measurement, 2011; **44**:46-54.

Lin L, Chu F, HHT-based AE characteristics of natural fatigue cracks in rotating shafts, Mechanical Systems and Signal Processing, 2012; **26**:181-189.

Lin PT, Su SF, Lee TT, Support vector regression analysis and systematic parameter selection. Proceedings of International Joint Conference on Neural Networks, Montreal, Canada, July 31-August 4, 2005.

Liu FC, Ma ZY, Influence of tool dimension and welding parameters on microstructure and mechanical properties of friction stir welded 6061-T651 aluminum alloy, Metallurgical and Materials Transactions A, 2008; **39A**:2378-2388.

Liu FC, Nelson TW, In-situ grain structure and texture evolution during friction stir welding of austenite stainless steel, Materials and Design, 2017; **115**:467-478.

Liu H, Zhang H, Pan Q, Lei Y, Effect of friction stir welding parameters on microstructural characteristics and mechanical properties of 2219-T6 aluminum alloy joints, International Journal of Material forming, 2012; **5**:235-241.

Liu HJ, Fujii H, Maeda M, Nogi K, Mechanical properties of friction stir welded joints of 1050-H24 aluminium alloy, Science and Technology of Welding and Joining, 2003; **8(6)**:450-454.

Liu HJ, Fujii H, Nogi K, Microstructure and mechanical properties of friction stir welded joints of AC4A cast aluminum alloy, Materials Science and Technology, 2004; **20**:399-402.

Liu HJ, Hou JC, Guo H, Effect of welding speed on microstructure and mechanical properties of self-reacting friction stir welded 6061-T6 aluminum alloy, Materials and Design, 2013; **50**:872-878.

Liu HJ, Zhang HJ, Yu L, Effect of welding speed on microstructures and mechanical properties of underwater friction stir welded 2219 aluminum alloy, Materials and Design, 2011; **32**:1548-1553.

Liu J, Xu G, Gu X, Zhou G, Ultrasonic test of resistance spot welds based on wavelet package analysis, Ultrasonics, 2015; **56**:557-565.

Liu JZ, Yang Q, Yao B, Brown RW, Yue GH, Linear correlation between fractal dimension of EEG signal and handgrip force, Biological Cybernetics, 2005; **93**:131-140.

Liu JZ, Yang Q, Yao B, Brown RW, Yue GH, Linear correlation between fractal dimension of EEG signal and handgrip force, Biological Cybernetics, 2005; **93**:131-140.

Liu JZ, Yang Q, Yao R, Brown RW, Yue GH, Linear correlation between fractal dimension of EEG signal and handgrip force, Biological Cybernetics, 2005; **93**:131-140.

Liu M, Xia H, Sun L, Li B, Yang Y, Vibration signal analysis of main coolant pump flywheel based on Hilbert-Huang transform, Nuclear Engineering and Technology, 2015; **47**:219-225.

Liu S, Hu Y, Li C, Lu H, Zhang H, Machinery condition prediction based on wavelet and support vector machine, Journal of Intelligent Manufacturing, 2017; **28(4)**:1045-1055.

Liu T, Zhang W, Yan S, A novel image enhancement algorithm based on stationary wavelet transform for infrared thermography to the de-bonding defect in solid rocket motors, Mechanical Systems and Signal Processing, 2015; **62-63**:366-380.

Liu TI, Kumagai A, Wnag YC, Song SD, Fu Z, Lee J, On-line monitoring of boring tools for control of boring operations, Robotics in Computer Integrated Manufacturing, 2010; **26**:230-239.

Lu WC, Ji XB, Li MJ, Liu L, Yue BH, Zhang LM, Using support vector machine for materials design, Advances in Manufacturing, 2013; **1(2)**:151-159.

Ma XQ, Rhyim YM, Jin HW, Park CG, Kim MC, Application of fractal dimension to optimum deposition of NiCrAlY coating by D-Gun spray, Materials and Manufacturing processes, 1999; **14(2)**:195-204.

Mallat SG, A theory for multiresolution signal decomposition: the wavelet representation, IEEE Transactions on Pattern Analysis and Machine Intelligence, 1989; **11(7)**:674-693.

Mandelbrot BB, The fractal geometry of nature, 1982, Freeman, San Francisco.

Manvatkar VD, Arora A, De A, DebRoy T, Neural network models of peak temperature, torque, traverse force, bending stress and maximum shear stress during friction stir welding, Science and Technology of Welding and Joining, 2012; **17(6)**:460-466.

Mao Y, Ke L, Liu F, Huang C, Chen Y, Liu Q, Effect of welding parameters on microstructure and mechanical properties of friction stir welded joints of 2060 aluminum lithium alloy, International Journal of Advanced Manufacturing Technology, 2015; **81(5)**:1419-1431.

MATLAB and Statistics Toolbox Release 2017b, The MathWorks, Inc., Natick, Massachusetts, United States.

Mehta KP, Badheka VJ, Effects of Tool Pin Design on Formation of Defects in Dissimilar Friction Stir Welding, Procedia Technology, 2016; **23**:513-518.

Mehta KP, Badheka VJ, Influence of tool pin design on properties of dissimilar copper to aluminum friction stir welding, Transactions of nonferrous metals society of China, 2017; **27(1)**:36-54.

Mehta M, Chatterjee K, De A, Monitoring torque and traverse force in friction stir welding from input electrical signatures of driving motors, Science and Technology of Welding and Joining, 2013; **18(3)**:191-197.

Mehta M, Reddy GM, Rao AV, De A, Numerical modeling of friction stir welding using the tools with polygonal pins, Defence Technology, 2015; **11**:229-236.

Minton T, Mynors DJ, Utilisation of engineering workshop equipment for friction stir welding, Journal of Materials Processing Technology, 2006; **177(1-3)**:336-339.

Mishra RS and Ma ZY, Friction stir welding and processing, Materials Science and Engineering R, 2005; **50(1-2)**:1-78.

Mitchell JE, The experimental thermo-mechanics of friction stir welding, M.S. Thesis, Vanderbilt University, 2002.

Miura T, Ueji R, Fujii H, Komine H, Yanagimoto J, Stabilization of austenite in low carbon Cr–Mo steel by high speed deformation during friction stir welding, Materials and Design, 2016; **90**:915-921.

Moataz MA, Salem HG, Friction stir welding parameters: a tool for controlling abnormal grain growth during subsequent heat treatment, Materials Science and Engineering A, 2005; **391**:51-59.

Moghadam DG, Farhangdoost K, Influence of welding parameters on fracture toughness and fatigue crack growth rate in friction stir welded nugget of 2024-T351 aluminum alloy joints, Transactions of Nonferrous Metals Society of China, 2016; **26(10)**: 2567-2585.

Mohammadi J, Behnamian Y, Mostafaei A, Izadi H, Saeid T, Kokabi AH, Gerlich AP, Friction stir welding joint of dissimilar materials between AZ31B magnesium and 6061 aluminum alloys: Microstructure studies and mechanical characterizations, Materials Characterization, 2015; **101**:189-207.

Moore G, Bergeron C, Bennett KP, Model selection for primal SVM, Machine Learning, 2011; **85**: 175-208.

Morisada Y, Imaizumi T, Fujii H, Clarification of material flow and defect formation during friction stir welding, Science and Technology of Welding and Joining, 2015; **20(2)**:130-137.

Moura J, What is signal processing? IEEE Signal Processing Magazine, 26(6), 2009.

Movahedi M, Kokabi AH, Reihani S, Najafi H, Effect of tool travel and rotation speeds on weld zone defects and joint strength of aluminum steel lap joints made by friction stir welding, Science and Technology of Welding and Joining, 2012; **17(2)**:162-167.

Muguthu JN, Gao D, Profile fractal dimension and dimensional accuracy analysis in machining metal matrix composites, Materials and Manufacturing Processes, 2013; **28**:1102-1109.

Na MG, Kim JW, Lim DH, Kang YJ, Residual stress prediction of dissimilar metals welding at NPPs using support vector regression, Nuclear Engineering and Design, 2008; **238**:1503-1510.

Nandi S, Toliyat HA, Li X, Condition monitoring and fault diagnosis of electrical motors-a review, IEEE Transactions on energy conservation, 2005; **20(4)**:719-729.

Ng HW, Wey P, Strain Gauge Evaluation with Four-point Bending at Moderate Temperatures, Experimental Mechanics, 1997; **37**:237-244.

Ngui WK, Leong MS, Hee LM, Abdelrhman AM, Wavelet analysis: mother wavelet selection methods, Applied Mechanics and Materials, 2013; **393**:953-958.

Nguyen V, Melkote S, Deshamudre A, Khanna M, Walker D, PVDF sensor based monitoring of single point cutting, Journal of Manufacturing Processes, 2016; **24(2)**:328-337.

Ni DR, Chen DL, Yang J, Ma ZY, Low cycle fatigue properties of friction stir welded joints of a semi-solid processed AZ91D magnesium alloy, Materials and Design, 2014; **56**:1-8.

Okuyucu H, Kurt A, Arcaklioglu E, Artificial neural network application to the friction stir welding of aluminum plates, Materials and Design, 2007; **28**:78-84.

Oliveira JP, Duarte JF, Inacio P, Schell N, Miranda RM, Santos TG, Production of Al/NiTi composites by friction stir welding assisted by electrical current, Materials and Design, 2017; **113**:311-318.

Oppenheim A, Schafer R, Padgett W, Discrete time signal processing, Third Edition, Prentice Hall, 2009.

Pal S, Heyns PS, Freyer BH, Theron NJ, Pal SK, Tool wear monitoring and selection of optimum cutting conditions with progressive tool wear effect and input uncertainties, Journal of Intelligent Manufacturing, 2011; **22(4)**:491-504.

Pal S, Pal SK and Samantaray AK, Neurowavelet packet analysis based on current signature for weld joint strength prediction in pulsed metal inert gas welding process, Science and Technology of Welding and Joining, 2008; **13(7)**:638-645.

Pal S, Pal SK, Samantaray AK, Prediction of the quality of pulsed metal inert gas welding using statistical parameters of arc signals in artificial neural network, International Journal of Computer Integrated Manufacturing, 2010; **23(5)**:453-465.

Palanivel R, Dinaharan I, Laubscher RF, Davim JP, Influence of boron nitride nanoparticles on microstructure and wear behavior of AA6082/TiB_2 hybrid aluminum composites synthesized by friction stir processing, Materials and Design, 2016; **106**:195-204.

Pan F, Xu A, Deng D, Ye J, Jiang X, Tang A, Ran Y, Effects of friction stir welding on microstructure and mechanical properties of magnesium alloy Mg-5Al-3Sn, Materials and Design, 2016; **110**:266-274.

Pan F, Zhu P, Zhang Y, Metamodel-based lightweight design of B-pillar with TWB structure via support vector regression, Computers and Structures, 2010; **88**:36-44.

Papacharalampopoulos A, Stavropoulos P, Doukas C, Foteinopoulos P, Chryssolouris G. Acoustic emission signal through turning tools: A computational study, (CIRP CMMO) Procedia CIRP, 14th CIRP Conference on Modelling of Machining Operations, 13-14 June, Turin, Italy, 2013.

Paramanathan P, Uthayakumar R, Application of fractal theory in analysis human electroencephalographic signals, Computers in Biology and Medicine, 2008; **38**:372-378.

Parida B, Pal S, Fuzzy assisted grey Taguchi approach for optimisation of multiple weld quality properties in friction stir welding process, Science and Technology of Welding and joining, 2015; **20(1)**:35-41.

Parida B, Vishwakarma SD, Pal S, Design and development of fixture and force measuring system for friction stir welding process using strain gauges, Journal of Mechanical Science and Technology, 2015; **29(2)**:739-749.

Park SW, Yoon TJ, Kang CY, Effects of the shoulder diameter and weld pitch on the tensile shear load in friction-stir welding of AA6111/AA5023 aluminum alloys, Journal of Materials Processing Technology, 2017: **241**:112-119.

Parvinnia E, Sabeti M, Jahromi MZ, Boostani R, Classification of EEG Signals using adaptive weighted distance nearest neighbor algorithm, Journal of King Saud University Computer and Information Sciences, 2014; **26**:1-6.

Pena B, Aramendi G, Rivero A, deLacalle LNL, Monitoring of drilling for burr detection using spindle torque, International Journal of Machine Tools and Manufacture, 2005; **45(14)**:1614-1621.

Pend J, Fukumoto S, Brown L, Zhou N, Image analysis of electrode degradation in resistance spot welding of aluminium, Science and Technology of Welding and Joining, 2004; **9(4)**:331-336.

Petrosian A, Kolmogorov complexity of finite sequences and recognition of different preictal EEG patterns, In proceeding of IEEE symposium Computer Based Medical Systems 1995, 212-217.

Pew JW, Nelson TW, Sorensen CD, Torque based weld power model for friction stir welding. -Science and Technology of Welding and Joining, 2007; **12(4)**:341-347.

Praveen A, Vijeyarekha K, Abraham ST, Venkatraman B, Signal quality enhancement using higher order wavelets for ultrasonic TOFD signals from austenitic stainless steel welds, Ultrasonics, 2013; **53**:1288-1292.

Qian JW, Li JL, Xiong JT, Periodic variation of torque and its relations to interfacial sticking and slipping during friction stir welding, Science and Technology of Welding and Joining, 2012; **17(4)**:338-341.

Rado Z, Kane M, An initial attempt to develop an empirical relation between texture and pavement friction using the HHT approach, Wear, 2014; **309**:233-246.

Rajakumar S, Balasubramanian V, Establishing relationships between mechanical properties of aluminium alloys and optimised friction stir welding process parameters, Materials and Design, 2012; **40**:17-35.

Rajamanickam N, Balusamy V, Reddy GM, Natarajan K, Effect of process parameters on thermal history and mechanical properties of friction stir welds, Materials and Design, 2009; **30**:2726-2731.

Ratnam C, Vikram KA, Sen BS, Murthy BSN, Process monitoring and effects of process parameters on responses in turn-milling operations based on SN ratio and ANOVA, Measurement, 2016; **94**:221-232.

Record JH, Covington JL, Nelson TW, Sorensen CD, Webb BW, A look at the statistical identification of critical process parameters in friction stir welding, 2007; **4**:97-103.

Rezai H, Mirbeik MH, Bisadi H, Effect of rotational speed on microstructure and mechanical properties of friction stir welded 7075-T6 aluminum alloy, Proceedings of Institutions of Mechanical Engineers, Part C: Journal of Mechanical Engineering Science, 2011; **225**:1761-1773.

Risovic D, Poljacek SM, Furic K, Gojo M, Inferring fractal dimension of rough/porous surfaces- A comparison of SEM image analysis and electrochemical impedance spectroscopy methods, Applied Surface Science, 2008; **255**:3063-3070.

Rodrigues DM, Leitao C, Louro R, Gouveia H, Loureiro A, High speed friction stir welding of aluminium alloys, Science and Technology of Welding and Joining, 2010; **15(8)**:676-681.

Rosado LS, Santos TG, Piedade M, Advanced technique for non-destructive testing of friction stir welding of metals, Measurement, 2010; **43**:1021-1030.

Roshan SB, Jooibari MB, Teimouri R, Ahmadi GA, Naghibi MF, Sohrabpoor H, Optimization of friction stir welding process of AA7075 aluminum alloy to achieve desirable mechanical properties using ANFIS models and simulated annealing algorithm, International Journal of Advanced Manufacturing Technology, 2013; **69**:1803-1818.

Russel D, Hanson J, Ott E, Dimension of strange attractors, Physical Review Letters, 1980; **45(14)**:1175–1178.

Saeid T, Abdollah-zadeh A, Assadi H, Effect of friction stir welding speed on microstructure and mechanical properties of a duplex stainless steel, Materials Science and Engineering A, 2008; **496**:262-268.

Sahu PK, Pal S, Multi-response optimization of process parameters in friction stir welded AM20 magnesium alloy by Taguchi grey relational analysis, Journal of Magnesium and Alloys, 2015; **3(1)**:36-46.

Sahu PK, Pal S, Pal SK, Jain R, Influence of plate position, tool offset and tool rotational speed on mechanical properties and microstructures of dissimilar Al/Cu friction stir welding joints, Journal of Materials Processing Technology, 2016; **235**:55-67.

Sakthivel T, Sengar GS, Mukhopadhyay J, Effect of welding speed on microstructure and mechanical properties of friction-stir-welded aluminum, International Journal of Advanced Manufacturing Technology, 2009; **43**: 468-473.

Salih OS, Ou H, Sun W, McCartney DG, A review of friction stir welding of aluminium matrix composites, Materials and Design, 2015; **86**:61-71.

Saravanan T, Lahiri BB, Arunmuthu K, Non-destructive evaluation of friction stir welded joints by X-ray radiography and infrared thermography, Procedia Engineering, 2014; **86**:469-475.

Scialpi A, Filippis LAC, Cavaliere P, Influence of shoulder geometry on microstructure and mechanical properties of friction stir welded 6082 aluminum alloy, Journal for Materials Design, 2007; **28**:1124-1129.

Seker U, Kurt A, Cifci I, Design and construction of a dynamometer for measurement of cutting forces during machining with linear motion, Materials and Design, 2003; **23**:355-360.

Shao C, Kim TH, Hu SJ, Jin J, Abell JA, Tool wear monitoring for ultrasonic metal welding of lithium-ion batteries, Journal of Manufacturing Science and Engineering, 2016; **138**:0.51005-1-51005-8.

Shao C, Panyabar K, Kim TH, Jin J, Hu SJ, Spicer JP, Wang H, Abell JA, Feature selection for manufacturing process monitoring using cross-validation, Journal of Manufacturing Systems, 2013; **32**:550-555.

Sharma C, Dwivedy DK, Kumar P, Effect of welding parameters on microstructure and mechanical properties of friction stir welded joints of AA7039 aluminum alloy, Materials and Design, 2012; **36**:379-390.

Shi L, Wu CS, Padhy GK, Gao S, Numerical simulation of ultrasonic field and its acoustoplastic influence on friction stir welding, Materials and Design, 2016; **104**:102-115.

Shirazi H, Kheirandish Sh, Safarkhanian MA, Effect of process parameters on the macrostructure and defect formation in friction stir lap welding of AA5456 aluminum alloy, Measurement, 2015; **76**:62-69.

Shirong, G, Gouan C, Fractal prediction models of sliding wear during the running-in process, Wear, 1999; **231**:249-255.

Shojaeefard MH, Behnagh RA, Akbari M, Givi MKB, Zarhani F, Modelling and Pareto optimization of mechanical properties of friction stir welded AA7075/AA5083 butt joints using neural network and particle swarm algorithm, Materials and Design, 2013; **44**:190-198.

Shoupeng S, Peiwen Q, A Fractal-Dimension-Based Signal-Processing Technique and Its Use for Nondestructive Testing, Russian Journal of Nondestructive testing, 2007; **43(4)**:270-280.

Sick B, Online and indirect tool wear monitoring in turning with artificial neural networks: a review of more than a decade of research, Mechanical Systems and Signal Processing, 2002; **16(4)**:487-546.

Singh KV, Hamilton C, Dymek S, Developing predictive tools for friction stir weld quality assessment, Science and Technology of Welding and Joining, 2010; **15(2)**:142-148.

Soundararajan V, Atharifar H, Kovacevic R, Monitoring and processing the acoustic emission signals from the friction-stir-welding process, Proceedings of Institution

of Mechanical Engineers, Part B: Journal of Engineering Manufacture, 2006; **220**:1673-1685.

Stavropoulos P, Salonitis K, Stournaras A, Pandremenos J, Paralikas J, Chryssolouris G, Advances and Challenges for tool Condition Monitoring in Micro-Milling. (MIM 07) IFAC Workshop on Manufacturing Modelling, Management and Control, Budapest, Hungary, pp. 157-162, 2007.

Ştefanescu DM, Handbook of Force Transducers Principles and Components, Springer, First Edition, 2011.

Su H, Wu CS, Bachmann M, Rethmeier M, Numerical modeling for the effect of pin profiles on thermal and material flow characteristics in friction stir welding, Materials and Design, 2015; **77**:114-125.

Su H, Wu CS, Pittner A, Rethmeier M, Simultaneous measurement of tool torque, traverse force and axial force in friction stir welding, Journal of Manufacturing Processes, 2013; **15(4)**:495-500.

Subramaniam S, Narayan S, Ashok SD, Acoustic emission-based monitoring approach for friction stir welding of aluminum alloy AA6063-T6 with different tool pin profiles, Proceedings of Institution of Mechanical Engineers Part B: Journal of Engineering Manufacture, 2013; **227(3)**:407-416.

Sun T, Roy MJ, Strong D, Withers PJ, Prangnell PB, Comparison of residual stress distributions in conventional and stationary shoulder high-strength aluminum alloy friction stir welds, Journal of Materials Processing Technology, 2017; **242**:92-100.

Sundaram NS, Murugan N, Tensile behaviour of dissimilar friction stir welded joints of aluminum alloys, Materials and Design, 2010; **31**:4184-4193.

Sutton MA, Yang B, Reynolds AP, Yan J, Banded microstructure in 2024-T351 and 2524-T351 aluminum friction stir welds: Part II. Mechanical characterization, Materials Science and Engineering A, 2004; **364(1-2)**:66-74.

Taghi M, Baghmisheh V, Pavesic N, Training RBF networks with selective backpropagation, Neurocomputing, 2004; **62**:39-64.

Takahasi M, Nagahama H, Fractal Dimension of recrystallized quartz grain boundaries and grain fabrics, The Arabian Journal for Science and Engineering, 2003; **28**:215-221

Tanaka M, Komagata M, Tsukada M, Kamiya H, Fractal analysis of the influence of surface roughness of toner particles on their flow properties and adhesion behaviour, Powder Technology, 2008; **186**:1-8.

Tang J, Shen Y, Numerical simulation and experimental investigation of friction stir lap welding between aluminum alloys AA2024 and AA7075, Journal of alloys and compounds, 2016; **666**:493-500.

Tangjitsctcharoen S, Saksri T, Ratanakuakangwan S, Advance in chatter detection in ball end milling process by utilizing wavelet transform, Journal of Intelligent Manufacturing, 2015; **26**:485-499.

Tansel IN, Demetgul M, Okuyucu H, Yapici A, Optimizations of friction stir welding of aluminum alloy by using genetically optimized neural network, International Journal of Advanced Manufacturing Technology, 2010; **48**:95-101.

Taralunga DD, Gussi I, Strungaru R, Fetal ECG enhancement: Adaptive power line interference cancellation based on Hilbert Huang Transform, Biomedical Signal Processing and Control, 2015; **19**:77-84.

Thomas WM, Nicholas ED, Needhman JC, Murch MG, Temple-Smith P, Dawes CJ, International Patent Application PCT/GB92/02203 and GB Patent Application 9125978.8, UK Patent Office, London, December 6, 1991.

Tian Z, Zuo MJ, Wu S, Crack propagation assessment for spur gears using model based analysis and simulation, Journal of Intelligent Manufacturing, 2012; **23**:239-253.

Toktas A, Toktas G, Effect of welding parameters and aging process on the mechanical properties of friction stir welded 6063-T4 Al alloy, Journal of Materials Engineering Performance, 2012; **21**:936-945.

Tozaki Y, Uematsu Y, Tokaji K, Effect of tool geometry on microstructure and static strength in friction stir spot welded aluminum alloys, International Journal of Machine Tools & Manufacture, 2007; **47**:2230-2236.

Trimble D, Monaghan J, Donnell GE, Force generation during friction stir welding of AA2024-T3, CIRP Annals: Manufacturing Technology, 2012; **61**:9-12.

Trummera VR, SuzanoE, BeltrãoM, RoosA, Santos JF, Castro PMST, Influence of the FSW clamping force on the final distortion and residual stress field, Materials Science and Engineering A, 2012; **538**:81-88.

Unsaçar F, Yaldiz S, A dynamometer design for measurement the cutting forces on turning, Measurement, 2006; **39**:80–89.

Valavanis I, Kosmopoulos D, Multiclass defect detection and classification in weld radiographic images using geometric and texture features, Expert Systems with Applications, 2010; **37**:7606-7614.

Vieira AP, Moura EP, Goncalves LL, Rebello JMA, Characterization of welding defects by fractal analysis of ultrasonic signals, Chaos, Solitons and Fractals, 2008; **38(3)**:748-754.

Wang X, Dong L, Xiong L, The change of fractal dimensionality in the recovery and recrystallization process, Journal of Physics: Condensed Matter, 1990; **2**:3879-3884.

Wang X, Wang W, Huang Y, Nguyen N, Krishnakumar K, Design of neural network based estimator for tool wear monitoring in hard turning, Journal of Intelligent Manufacturing, 2008; **19(4)**:383-.

Wang Y, Sun Y, Lv P, Wang H, Detection of line weld defects based on multiple thresholds and support vector machine, NDT&E International, 2008; **41(7)**:517-524.

Wen YF, Cai CZ, Liu XH, Pei JF, Zhu XJ, Xiao TT, Corrosion rate prediction of 3C steel under different sea water environment by using support vector regression, Corrosion Science, 2009; **51**:349-355.

Wu CH, Ho JM, Lee DT, Travel-time prediction with support vector regression, IEEE Transactions on Intelligent Transportation systems, 2004; **5(4)**:276-281.

Xiao Y, Zhan H, Gu Y, Li Q, Modeling heat transfer during friction stir welding using a meshless particle method, International Journal of heat and Mass Transfer, 2017; **104**:288-300.

Xiong JT, Zhang XC, Li P, Characterisation of periodic variation in torque occurred in friction stir welding process, Science and Technology of Welding and Joining, 2014; **19(4)**:350-354.

Yajnik A, Novel technique of oversampling the broken images using wavelet transform, Applied and Computational Harmonic Analysis, 2015; **39**:357-368.

Yaldız S, Unsaçar F, Saglam H, Işık H, Design, development and testing of a four-component milling dynamometer for the measurement of cutting force and torque, Mechanical Systems and Signal Processing, 2007; **21**:1499–1511.

Yang C, Liu P, Yin G, Jiang H, Li X, Defect detection in magnetic tile images based on stationary wavelet transform, NDT&E International, 2016; **83**:78-87.

Yang J, Zhang Y, Zhu Y, Intelligent fault diagnosis of rolling element bearing based on SVMs and fractal dimension, Mechanical Systems and Signal Processing, 2007; **21**:2012-2024.

Yang Y, Kalya P, Landers RG, Krishnamurthy K, Automatic gap detection in friction stir butt welding operations, International Journal of Machine Tools and Manufacture, 2008; **48**:1161-1169.

Yang Y, Kalya P, Landers RG, Krishnamurthy K, Automatic gap detection in friction stir butt welding operations, International Journal of Machine Tools and Manufacture, 2008; **48(10)**:1161-1169.

Yong X, Qiang C, Zhenguo S, Application of fractal theory in welding image processing, Journal of Image and Graphics, 2002; **7(1)**:86-90.

Younis NT, Kang B, Averaging effects of a strain gauge, Journal of Mechanical Science and Technology, 2011; **25**:163-169.

Yu G, Li C, Kamarthi S, Machine fault diagnosis using cluster-based wavelet feature extraction and probabilistic neural network, International Journal of Advanced Manufacturing Technology, 2009; **42**:145:151.

Zaidi S, Development of support vector regression (SVR)-based model for prediction of circulation rate in a vertical tube thermosiphon reboiler, Chemical Engineering Science, 2012; **69**:514-521.

Zapata J, Toro M, Lopez D, Residual stresses in friction stir dissimilar welding of aluminum alloys, Journal of Materials Processing Technology, 2016; **229**:121-127.

Zeng WM, Wu HL, Zhang J, Effects of tool wear on microstructure, mechanical properties and acoustic emission of friction stir welding of 6061 aluminium alloy, ACTA Metallurgica Sinica (English Letters), 2006; **19**:9-19.

Zhanfeng H, Pei W, Jing X, Jingyu H, Application of fractal theory in examination of resistance spot welding quality, In Proceedinigs of International Conference on Advanced Technology of Design and Manufacture, Beijing, China, 2010; 422-424.

Zhang B, Yuan S, Wang X, Friction stir welding of AZ31 magnesium alloys processed by equal channel angular pressing, Rare Metals, 2008; **27(4)**:393-399.

Zhang F, Su X, Chen Z, Nie Z, Effect of welding parameters on microstructure and mechanical properties of friction stir welded joints of a super high strength Al-Zn-Mg-Cu aluminum alloy, Materials and Design, 2015; **67**:483-491.

Zhang H, Lin SB, Wu L, Feng JC, Ma SL, Defects formation procedure and mathematic model for defect free friction stir welding of magnesium alloy, Materials and Design, 2006; **27**:805-809.

Zhang HJ, Wang FJ, Gao WG, Hou YY, Quality assessment for resistance spot welding based on binary image of electrode displacement signal and probabilistic neural network, Science and Technology of Welding and Joining, 2014, **19(3)**, 242-249.

Zhang J, Shen Y, Yao X, Xu H, Li Bo, Investigation on dissimilar underwater friction stir lap welding of 6061-T6 aluminum alloy to pure copper, Materials and Design, 2014; **64**:74-80.

Zhang Z, Chen S, Real-time seam penetration identification in arc welding based on fusion of sound, voltage and spectrum signals, Journal of Intelligent Manufacturing, 2014; **28(1)**:207-218

Zhang Z, Wang Y, Wang K, Fault diagnosis and prognosis using wavelet packet decomposition, Fourier transform and artificial neural network, Journal of Intelligent Manufacturing, 2013; **24**:1213-1227.

Zhang Z, Xiao BL, Ma ZY, Effect of welding parameters on microstructure and mechanical properties of friction stir welded 2219Al-T6 joints, Journal of Materials Science, 2012; **47**:40754086.

Zhang Z, Zhang HW, Numerical studies on controlling of process parameters in friction stir welding, Journal of Materials Processing Technology, 2009; **209(1)**:241-270.

Zhao Y, Lu Z, Yan K, Huang L, Microstructural characterizations and mechanical properties in underwater friction stir welding of aluminum and magnesium dissimilar alloys, Materials and Design, 2015; **65**:675-681.

Zhehe Y, Deqing M, Chen Z, On-line chatter detection and identification based on wavelet and support vector machine, Journal of Materials Processing Technology, 2010; **210(5)**:713-719.

Zhen L, Dong A, Ping S, Xing Z, Analysis of acoustic emission signal by fractal theory in Aluminium alloy spot welding, Transactions of Tianjin University, 2007; **13**:186-190.

Zhen L, Dong A, Shan P, Xing Z, Analysis of acoustic emission signal by fractal theory in aluminum alloy spot welding, Transactions of Tianjin University, 2007; **13(3)**:186-190.

Zhigang F, Hongwei Z, Computing method of fractal dimension of image and its application, Journal of Jiangsu Science and Technology, 2001; **22(6)**:92-95.

Zhong ZW, Lu YG, Fractal roughness structure of diamond-turned copper mirrors, Materials and Manufacturing Processes, 2003; **18(2)**:219-227.

Zhu H, Ge S, Cao X, Tang W, The changes of fractal dimensions of frictional signals in the running-in wear process, 2007; **263**:1502-1507.

Zhu K, Yu X, The monitoring of micro milling tool wear conditions by wear area estimation, Mechanical Systems and Signal Processing, 2017; **93**:80-91.

Zhu Y, Chen G, Chen Q, Zhang G, Shi Q, Simulation of material plastic flow driven by non-uniform friction force during friction stir welding and related defect prediction, Materials and Design, 2016; **108**:400-410.

Bibliography

Bose T, Digital signal and image processing, 2004, John Wiley & Sons, Singapore.

George B, Narici L, Beckenstein E, Fourier and wavelet analysis, 2000, Springer Verlag, New York.

Givi MKB, Asadi P, Advances in friction stir welding and processing, 2014, Elsevier, Amsterdam.

Gonzalez RC, Woods RE, Eddins SL, Digital image processing using MATLAB, 2010, Tata McGraw Hill, New Delhi, India.

Mishra RS, De PS, Kumar N, Friction stir welding and processing: science and engineering, 2014; Springer, New York.

Mitra SK, Kaiser JF, Handbook for digital signal processing, 1993, John Wiley & Sons, New York.

Oppenheim AV, Schafer RW, Digital signal processing, 1975, Prentice Hall of India, New Delhi, India.

Prasad L, Iyenger SS, Wavelet analysis with applications to image processing, 1997, CRC Press, Boca Raton, Florida.

Pratap R, Getting started with MATLAB: a quick introduction for scientists and engineers, 2006, Oxford University Press, New Delhi, India.

Pratihar DK, Soft Computing, 2008, Narosa, New Delhi, India.

Proakis JG, Digital signal processing: principles, algorithms and applications, 1995, Second Edition, Prentice Hall of India, New Delhi, India.

Rao RM, Bopardikar AS, Wavelet transforms: introduction to theory and applications, 1998, Pearson Addison Wesley, New Delhi, India.

Sivanandam SN, Deepa SN, Principles of soft computing, 2011, Wiley (India), New Delhi, India.

List of Publications

A. International Journal

1. **Bipul Das**, Sukhomay Pal, Swarup Bag, Weld quality prediction in friction stir welding using wavelet analysis. ***International Journal of Advanced Manufacturing Technology***, 89, 711-725, 2017.

2. **Bipul Das**, Sukhomay Pal, Swarup Bag, Torque based defect detection and weld quality modelling in friction stir welding process, ***Journal of Manufacturing Processes***, 27, 8-17, 2017.

3. **Bipul Das**, Sukhomay Pal, Swarup Bag, Design and development of force and torque measurement setup for real time monitoring of friction stir welding process, ***Measurement***, 103, 186-198, 2017.

4. **Bipul Das**, Swarup Bag, Sukhomay Pal, Probing weld quality monitoring in friction stir welding through characterization of signals by fractal theory. ***Journal of Mechanical Science and Technology***, 2017, 31(5), 2459-2465.

5. **Bipul Das**, Sukhomay Pal, Swarup Bag, Monitoring of friction stir welding process using main spindle motor current. ***Journal of The Institution of Engineers (India): Series C***, 2017, DOI 10.1007/s40032-017-0371-0.

6. **Bipul Das**, Sukhomay Pal, Swarup Bag, Monitoring of friction stir welding process using weld image information. ***Science and Technology of Welding and Joining***, 21(4), 317-324, 2016.

7. **Bipul Das**, Sukhomay Pal, Swarup Bag, A combined wavelet packet and Hilbert-Huang transform for defect detection and modelling of weld strength in friction stir welding process. ***Journal of Manufacturing Processes***, 22, 260-268, 2016.

8. **Bipul Das**, Sukhomay Pal, Swarup Bag, Defect detection in friction stir welding process through characterization of signals by fractal dimension. ***Manufacturing***

Letters, 7, 6-10, 2016.

9. **Bipul Das**, Sukhomay Pal, Swarup Bag, Defect detection in friction stir welding process using signal information and fractal theory. ***Procedia Engineering***, 144, 172-178, 2016.

10. **Bipul Das,** Sukhomay Pal, Swarup Bag, Probing defects in friction stir welding process using temperature profile. (*Under review*)

B. International Conference

11. **Bipul Das**, Sukhomay Pal, Swarup Bag, Machine vision system based monitoring approach for friction stir welding process. *IEEE First International Conference on Control, Measurement and Instrumentation (CMI)*, 8-10 January 2016. DOI: 10.1109/CMI.2016.7413715

12. **Bipul Das**, Sukhomay Pal, Swarup Bag, Wavelet transform based defect identification in friction stir welding process. *6TH International and 27TH All India Manufacturing Technology, Design and Research Conference*, 16-18 December, 2016.

13. **Bipul Das**, Sukhomay Pal, Swarup Bag, Neurofractal modelling of weld quality in friction stir welding. *2nd International Conference on Advances in Cutting, Welding and Surfacing (CWS)*, 05-07 August 2015.

14. **Bipul Das**, Sukhomay Pal, Swarup Bag, Monitoring of friction stir welding process through signals acquired during the welding. *5TH International and 26TH All India Manufacturing Technology, Design and Research Conference*, 12-14 December, 2014.

C. Chapter in Edited Book

15. **Bipul Das**, Sukhomay Pal, Swarup Bag, Monitoring of weld quality in friction stir welding based on spindle speed and motor current signals. ***Advances in Material Forming and Joining***, Editors: R. G. Narayanan and U. S. Dixit, Springer India, 2015.